Mathematical Problems in Engineering

Advanced Control for Singular Systems with Applications

Special Issue Editor in Chief: Wanquan Liu
Guest Editors: Xinggang Yan, Shoudong Huang, Chunyu Yang, and Guoliang Wang

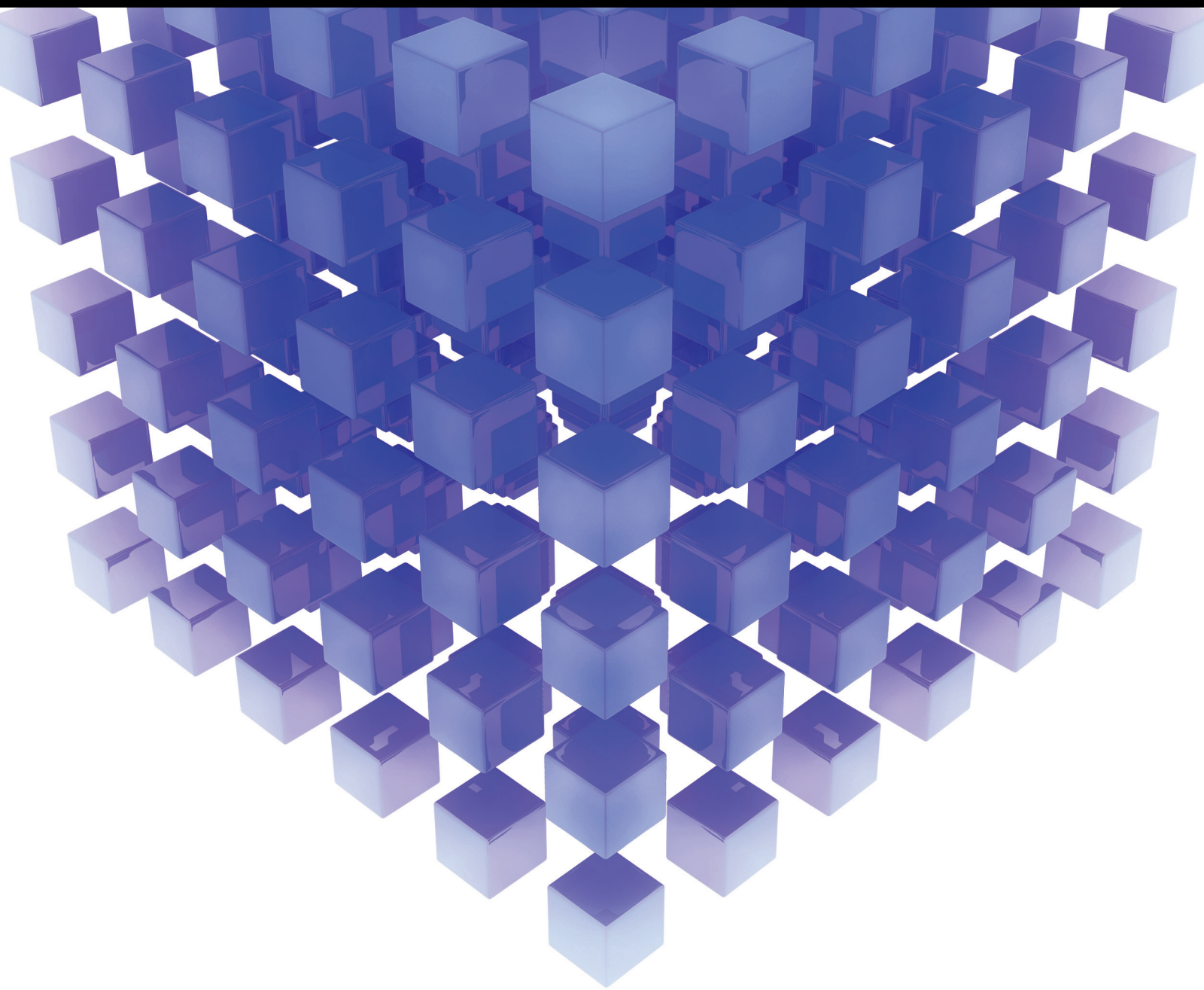

Advanced Control for Singular Systems with Applications

Mathematical Problems in Engineering

Advanced Control for Singular Systems with Applications

Special Issue Editor in Chief: Wanquan Liu
Guest Editors: Xinggang Yan, Shoudong Huang, Chunyu Yang, and Guoliang Wang

Editorial Board

Contents

Advanced Control for Singular Systems with Applications
Wanquan Liu, Xinggang Yan, Shoudong Huang, Chunyu Yang, and Guoliang Wang
Editorial (2 pages), Article ID 1819540, Volume 2018 (2018)

Analysis and Control of the Singular System Model of Aphid Ecosystems
Jingna Liu, Tie Zhang, Lichun Zhao, Bing Liu, and Xueying Wei
Research Article (10 pages), Article ID 3030723, Volume 2018 (2018)

No-Tension Sensor Closed-Loop Control Method with Adaptive PI Parameters for Two-Motor Winding System
Zhiqiang Wang, Haibao Nan, Tingna Shi, Qiang Geng, and Changliang Xia
Research Article (14 pages), Article ID 1851845, Volume 2018 (2018)

H_∞ Tracking Control of Fuzzy Dynamic Output for Nonlinear Networked System with Packet Dropouts
Yang Wang, Jinna Li, and Xiaolei Ji
Research Article (10 pages), Article ID 5149518, Volume 2018 (2018)

Trajectory Optimization of Spray Painting Robot for Complex Curved Surface Based on Exponential Mean Bézier Method
Wei Chen, Junjie Liu, Yang Tang, Jian Huan, and Hao Liu
Research Article (10 pages), Article ID 4259869, Volume 2017 (2018)

Data-Driven Fault Diagnosis Method for Power Transformers Using Modified Kriging Model
Yu Ding and Qiang Liu
Research Article (5 pages), Article ID 3068548, Volume 2017 (2018)

H_∞ Control for T-S Fuzzy Singularly Perturbed Switched Systems
Qianjin Wang, Linna Zhou, Wei Dai, and Xiaoping Ma
Research Article (13 pages), Article ID 2597071, Volume 2017 (2018)

Data-Driven Incipient Sensor Fault Estimation with Application in Inverter of High-Speed Railway
Hongtian Chen, Bin Jiang, and Ningyun Lu
Research Article (13 pages), Article ID 8937356, Volume 2017 (2018)

Robust Course Keeping Control of a Fully Submerged Hydrofoil Vessel with Actuator Dynamics: A Singular Perturbation Approach
Sheng Liu, Changkui Xu, and Lanyong Zhang
Research Article (14 pages), Article ID 6402012, Volume 2017 (2018)

Robust H_∞ Fault Detection for Networked Markov Jump Systems with Random Time-Delay
Yanfeng Wang, Zuxin Li, Peiliang Wang, and Zhe Zhou
Research Article (9 pages), Article ID 2608140, Volume 2017 (2018)

Robust Fault Detection and Estimation in Nonlinear Systems with Unknown Constant Time-Delays
Wenxu Yan, Dezhi Xu, and Qikun Shen
Research Article (14 pages), Article ID 4324370, Volume 2017 (2018)

Optimization of Multiresonant Wireless Power Transfer Network Based on Generalized Coupled Matrix
Qiang Zhao and Anna Wang
Research Article (9 pages), Article ID 6803530, Volume 2017 (2018)

$\mathscr{H}_\infty$ Filtering for Discrete-Time Nonlinear Singular Systems with Quantization
Yifu Feng, Zhi-Min Li, and Xiao-Heng Chang
Research Article (9 pages), Article ID 9548407, Volume 2017 (2018)

Stabilization of Continuous-Time Random Switching Systems via a Fault-Tolerant Controller
Guoliang Wang and Zhiqiang Li
Research Article (8 pages), Article ID 4840859, Volume 2017 (2018)

Disordered Stabilization of Stochastic Delay Systems: The Disorder-Dependent Approach
Guoliang Wang and Hongyang Cai
Research Article (13 pages), Article ID 7057628, Volume 2017 (2018)

Hindawi
Mathematical Problems in Engineering
Volume 2018, Article ID 1819540, 2 pages
https://doi.org/10.1155/2018/1819540

Editorial

Advanced Control for Singular Systems with Applications

Wanquan Liu,[1] **Xinggang Yan**,[2] **Shoudong Huang**,[3] **Chunyu Yang**,[4] **and Guoliang Wang**[5]

[1]*Curtin University, Perth, WA, Australia*
[2]*University of Kent, Canterbury, UK*
[3]*University of Technology Sydney, Sydney, NSW, Australia*
[4]*China University of Mining and Technology, Xuzhou, China*
[5]*Liaoning Shihua University, Fushun, China*

Correspondence should be addressed to Wanquan Liu; wanquan@cs.curtin.edu.au

Received 7 February 2018; Accepted 11 February 2018; Published 5 June 2018

1. Introduction

Singular systems, also referred to as descriptor systems, semistate systems, differential-algebraic systems, or generalized state-space systems, have been one of the main research topics in control theory for nearly half a century as such systems have broad applications in different areas, for example, in the Leontief dynamic model, electrical systems, and mechanical systems.

Many classical control theories and new concepts have been developed for singular systems in the last twenty years such as controllability, impulsive control, and optimal control. In recent years, with the development of communication systems, computer network, and biological systems, some new trends in optimization and control theory for singular systems have emerged and evolved [1–4], which motivated this special issue.

Control systems are developing fast with the advancement of new technologies as well as new systems such as network control, biological systems, and quantum control systems. As we know singular systems can be used to model dynamic systems in a more general framework and more attention should be paid to the development of singular systems with currently occurring applications. Recently, notable advances in biological systems, communication systems, and computer network have increasingly promoted some important new directions in the study of singular systems.

This special issue is intended to present and discuss the new development in singular systems and their applications in different engineering areas. The focuses of this special issue are on the analysis and control of singularly perturbed systems, robust control of singular systems, stability analysis of nonlinear singular systems, singular Markovian systems, and applications of singular systems.

2. The Special Issue

For this special issue, we solicited high quality, original research articles on singular system, theory, and applications. There are 28 submissions in total, and 14 of them are published after a fair and rigorous review process organized by the guest editorial team with the help of the journal editorial office. The accepted papers are more oriented on the robust control of singular systems and the applications of singular systems.

Seven accepted papers are on robust estimation and robust control of singular systems. The paper by Y. Feng et al. investigated the problem of H^∞ filtering for a class of discrete-time Lipschitz nonlinear singular systems with measurement quantization. Y. Wang et al. presented their work on the dynamic output-feedback H^∞ tracking control for fuzzy networked systems, in which each system is discrete-time nonlinear and missing measurable data. The paper by Y. Wang et al. considered the robust H^∞ fault detection for

networked Markov jump systems with random time-delay. The random time-delay is modeled as a Markov process, and the networked Markov jump systems are modeled as control systems containing two Markov chains. The delay-dependent fault detection filter is constructed. Q. Wang et al. presented their work on the design of fuzzy controller with guaranteed H^{∞} performance for a class of the Takagi-Sugeno fuzzy singularly perturbed switched systems. The paper by W. Yan et al. designed a fault detection and estimation algorithm for the robust fault detection and estimation in nonlinear systems with unknown inputs and unknown constant time-delays. G. Wang and Z. Li presented their work on the stabilization of continuous-time random switching systems via exploiting a fault-tolerant controller, where the dwell time of each subsystem consists of a fixed part and random part. In the paper by G. Wang and H. Cai, a general stabilization problem of stochastic delay systems is realized by a disordered controller and studied by exploiting the disorder-dependent approach.

Seven accepted papers are on the different applications of singular systems. J. Liu et al. proposed a singular system model of the aphid ecosystems by considering the change of the parameter related to the natural enemy population and the impact on the aphid populations in the fold catastrophe manifold. They also performed qualitative analysis and control of the singular system model of aphid ecosystems. Q. Zhao and A. Wang considered the problem of optimization of multiresonant wireless power transfer network based on generalized coupled matrix. Z. Wang et al. considered the problem of tension control in a two-motor winding system; a sensorless tension control method with PI parameters of speed controllers adaptive is proposed. H. Chen et al. considered the application of sensor fault estimation in the inverter of high-speed railway. They proposed a data-driven incipient sensor fault estimation methodology under multivariate statistics frame, which incorporates the Kullback–Leibler divergence in information domain and neural network approximation in machine learning. Y. Ding and Q. Liu proposed a data-driven fault diagnosis method which combines the Kriging model and neural network with applications to power transformers. W. Chen et al. presented an automated tool trajectory planning of spray painting robot for complex curved surface based on exponential mean Bézier method. Finally, S. Liu et al. applied a singular perturbation approach to the robust course keeping control of a fully submerged hydrofoil vessel. A two-time scale model is established so that the controllers of the fast and slow subsystems can be designed separately.

Although the selected topics and published papers may not represent all of the recent development in the area, the guest editorial team hope that readers find the special issue helpful and useful.

Acknowledgments

The guest editors of this special issue would like to thank all authors for their submitted papers as well as all reviewers for their hard work and detailed reviews, which led to the 14 accepted papers and the publication of the special issue.

Wanquan Liu
Xinggang Yan
Shoudong Huang
Chunyu Yang
Guoliang Wang

References

[1] Z. Feng and P. Shi, "Sliding mode control of singular stochastic Markov jump systems," *Institute of Electrical and Electronics Engineers Transactions on Automatic Control*, vol. 62, no. 8, pp. 4266–4273, 2017.

[2] M. Chadli and M. Darouach, "Further Enhancement on Robust H$^{\infty}$ Control Design for Discrete-Time Singular Systems," *Institute of Electrical and Electronics Engineers Transactions on Automatic Control*, vol. 59, no. 2, pp. 494–499, 2014.

[3] G. Wang, Q. Zhang, and X. Yan, "Analysis and design of singular Markovian jump systems," *Analysis and Design of Singular Markovian Jump Systems*, pp. 1–284, 2015.

[4] G. Zhang and W. Liu, "Impulsive mode elimination for descriptor systems by a structured P-D feedback," *Institute of Electrical and Electronics Engineers Transactions on Automatic Control*, vol. 56, no. 12, pp. 2968–2973, 2011.

Hindawi
Mathematical Problems in Engineering
Volume 2018, Article ID 3030723, 10 pages
https://doi.org/10.1155/2018/3030723

Research Article

Analysis and Control of the Singular System Model of Aphid Ecosystems

Jingna Liu,[1,2] Tie Zhang,[1] Lichun Zhao,[2] Bing Liu,[2] and Xueying Wei[3]

[1]*Department of Mathematics, Northeastern University, Shenyang 110006, China*
[2]*School of Mathematics and Information Science, Anshan Normal University, Anshan 114007, China*
[3]*Department of Mathematics, Liaoning Normal University, Dalian 116029, China*

Correspondence should be addressed to Tie Zhang; tiezhang1956@163.com

Received 26 May 2017; Revised 14 November 2017; Accepted 28 December 2017; Published 19 February 2018

Academic Editor: Shoudong Huang

Considering the change of the parameter related to the natural enemy population and the impact on the aphid populations in the fold catastrophe manifold, the singular system model of aphid ecosystems is proposed. Combining singular system theory with catastrophe theory, the corresponding dynamics behaviors and the existence conditions of the impasse points are given by using the qualitative analysis. The biological significance of the analytical results is also discussed. The controllers are designed to make the aphid populations stabilize the refuge level by releasing natural enemy. Some numerical simulations are carried out to prove the results.

1. Introduction

Aphid populations are serious pests of wheat and many crops in the world. In some environment and physiography, aphid populations may lead to yield and economic losses [1–4]. Due to the fact that the fast reproduction of the aphid populations and the outbreak is always happening, insecticides are usually used to manage aphid pests. However, insecticides cause environment pollution and the lower quality of agricultural products. To avoid adverse effects of total reliance on insecticides and to ensure the well balanced ecosystems, there is a need to have ecofriendly management measures like releasing natural enemy [5]. Thus it is important to reveal the outbreak of aphid populations using mathematical models. In [6], the characteristics of catastrophe model are first used to describe and explain the phenomena of the population outbreak. In [7], a fold catastrophe model is proposed to explain the outbreak mechanism of the aphid populations by taking the proportion of winged aphid for the state variable and the effective leaf area for a control variable. In [8], on the basis of the Logistic model, a fold catastrophe model is built to show the complex dynamics behaviors of the aphid populations by taking the density of the aphid population for the state variable and the environmental factor for the main parameter. In [9], based on the fold catastrophe model, a new model is proposed by applying the Allee effect to the logistic equation and the corresponding ecological interpretations are provided. According to the model above, Zhao et al. explain the sudden decrease of the aphid populations after spraying pesticides by means of real data and predict the outbreak of the aphid populations by determining catastrophe regions [10, 11]. The results above show the application of catastrophe theory in aphid ecosystems. In fact, catastrophe theory is the theory related to the bifurcation theory, singularity theory, and structure stability [11].

Catastrophe is a widespread phenomenon in various fields, which frequently appears in engineering systems (such as the voltage load jump phenomenon in power systems). Some singular system models are usually used to describe the jump phenomenon in power systems and some results are obtained. Based on the singularity induced bifurcation of singular system, the complex dynamics behavior of power systems is studied and jump mechanisms are investigated [12–14]. According to the theory related to impasse points, the structure stability of power systems is analyzed and the impasse points in a circuit system are used to show the voltage load jump phenomenon [15, 16].

What is the similarity between aphid populations' outbreak or sudden decrease and the voltage load jump phenomenon in power systems? Can the singular system models be used to describe the outbreak or sudden decrease phenomenon of aphid populations? It is what we are thinking about the focus of the paper.

The paper is organized as follows: In Section 2, the singular system model of aphid ecosystems is proposed. In Section 3, the dynamics behavior of aphid populations is discussed and the existence conditions of the impasse point are obtained by using qualitative analyses. In Section 4, the controllers are designed to keep aphid populations at refuge level and some numerical simulations are carried out to prove the results.

2. Modelling

Consider the following fold catastrophe manifold of the aphid populations [11]:

$$0 = r_N N(t)\left(1 - \frac{N(t)}{k_N}\right) - \frac{mPN(t)}{N(t) + d}, \tag{1}$$

where $N(t)$ is the density of the aphid population; P is the parameter related to the natural enemy population; r_N, k_N represent the intrinsic rate and the environmental carrying capacity of the aphid population, respectively; m, d represent the predation rate of the natural enemy population and the half saturation coefficient, respectively.

In model (1), P is the parameter related to the natural enemy population. Without loss of generality, let it be the density of the natural enemy population and change as follows:

$$\frac{dP(t)}{dt} = r_P P(t)\left(1 - \frac{P(t)}{cN(t) + k_{p'}}\right), \tag{2}$$

where r_P is the intrinsic rate of the natural enemy population; $cN(t)$ is the carrying capacity of the natural enemy population related to the density of the aphid population; and $k_{p'}$ is the carrying capacity of the natural enemy population related to other environmental factor, such as crop and prey (except aphid) populations and so on, and it is the maximum density of the natural enemy population when the aphid population is absented.

Coupling the algebraic equation (1) with the differential equation (2), the singular system model for the aphid ecosystem is got:

$$\begin{aligned} \frac{dP(t)}{dt} &= r_P P(t)\left(1 - \frac{P(t)}{cN(t) + k_{p'}}\right), \\ 0 &= r_N N(t)\left(1 - \frac{N(t)}{k_N}\right) - \frac{mP(t)N(t)}{N(t) + d}, \end{aligned} \tag{3}$$

where r_N, r_P, m, d, k_N, c, and $k_{p'}$ are defined as the above.

For model (3), let

$$\begin{aligned} x &= hP, \\ y &= gN, \\ \tau &= qt; \end{aligned} \tag{4}$$

applying transformation (4) to model (3), the following model is got:

$$\begin{aligned} \frac{dx(\tau)}{d\tau} &= x(\tau)\left(\frac{r_N}{q} - \frac{(gr_P/cqh)\,x(\tau)}{y(\tau) + k_{p'}g/c}\right), \\ 0 &= y(\tau)\left(\frac{r_N}{g} - \frac{r_N}{g^2 k_N}y(\tau) - \frac{(m/h)\,x(\tau)}{y(\tau) + gd}\right). \end{aligned} \tag{5}$$

Let

$$\begin{aligned} \frac{r_N}{g^2 k_N} &= 1, \\ \frac{m}{h} &= 1, \\ \frac{gr_P}{cqh} &= 1; \end{aligned} \tag{6}$$

the following are given:

$$\begin{aligned} g &= \sqrt{\frac{r_N}{k_N}} > 0, \\ h &= m > 0, \\ q &= \frac{gr_P}{ch} > 0. \end{aligned} \tag{7}$$

In model (5), let

$$\begin{aligned} a &= \frac{r_P}{g}, \\ b &= \frac{k_{P'}g}{c}, \\ l &= \frac{r_N}{g}, \\ n &= gd. \end{aligned} \tag{8}$$

It becomes

$$\begin{aligned} \frac{dx(\tau)}{d\tau} &= x(\tau)\left(a - \frac{x(\tau)}{y(\tau) + b}\right), \\ 0 &= y\left(l - y(\tau) - \frac{x(\tau)}{y(\tau) + n}\right). \end{aligned} \tag{9}$$

Model (9) is discussed on the domain D, where D is

$$D = \left\{\left(x(\tau), y(\tau)\right) \mid x(\tau) \geq 0,\ \ y(\tau) \geq 0\right\}. \tag{10}$$

3. Qualitative Analysis

3.1. Impasse Points. Consider the following model:

$$\begin{aligned} \frac{dx(t)}{dt} &= f(x(t), y(t)), \\ 0 &= g(x(t), y(t)). \end{aligned} \tag{11}$$

According to literature [17], the equilibria and singular points of model (11) are defined as follows:

$$\begin{aligned} &\mathrm{EQ} \triangleq \{(x_0, y_0) \mid f(x_0, y_0) = 0,\ g(x_0, y_0) = 0\}, \\ &S \triangleq \left\{(x_0, y_0) \mid g(x_0, y_0) = 0,\ \det \frac{\partial g(x_0, y_0)}{\partial y} = 0\right\}. \end{aligned} \tag{12}$$

Lemma 1. *For model (9),*

(1) *there may exist five equilibria* $M_1(0,0)$, $M_2(0,l)$, $M_3(ab,0)$, $M_1^*(x_1^*, y_1^*)$, *and* $M_2^*(x_2^* y_2^*)$, *where* $y_1^* < y_2^*$ *and* x_i^*, y_i^*, $i = 1,2$ *satisfy the following equation set:*

$$\begin{aligned} y(\tau) &= \frac{x(\tau)}{a} - b, \\ x(\tau) &= (l - y(\tau))(y(\tau) + n); \end{aligned} \tag{13}$$

(2) *there exist two singular points* $S_1(x_{S_1}, y_{S_1})$ *and* $S_2(x_{S_2}, y_{S_2})$, *where* $x_{S_1} = (l+n)^2/4$, $y_{S_1} = (l-n)/2$, $x_{S_2} = ln$, *and* $y_{S_2} = 0$.

According to literature [16], let $\Psi = \{y \mid h(y_0, \lambda) = g(x_0 + \lambda f(x_0, y_0), y) = 0\}$ be the induced solution curve, then the limit points and impasse points are defined as follows.

Definition 2. For model (11), for any $\lambda^+ > \lambda_0$ (resp., $\lambda^- < \lambda_0$), there exists a neighbourhood N_0 of (y_0, λ_0) such that $\Psi^+ \cap N = \varnothing$ (resp., $\Psi^- \cap N = \varnothing$), then the point (y_0, λ_0) is called right (resp., left) limit point of the induced solution curve Ψ at $\lambda = \lambda_0$, where N is any of subsets of N_0 and

$$\begin{aligned} \Psi^+ &= \{(y, \lambda) \mid h(y, \lambda) = 0,\ \lambda_0 < \lambda < \lambda^+\}, \\ \Psi^- &= \{(y, \lambda) \mid h(y, \lambda) = 0,\ \lambda^- < \lambda < \lambda_0\}. \end{aligned} \tag{14}$$

Definition 3. For model (11), the point $Q(x_0, y_0)$ is forward (resp., backward) point, if $(y_0, 0)$ is a right (resp., left) limit point of the induced solution curve Ψ.

According to the definitions above, in order to find the impasse points, the following conditions are given:

(1) The impasse points must be the singular points.

(2) The corresponding limit point must be the solution to $h(y, \lambda) = 0$.

(3) The corresponding limit point must be the solution to $\partial h(y, \lambda)/\partial y = 0$.

(4) The linear coefficient for λ must not be zero in the Taylor expansion of the $h(y, \lambda)$ at the point $(y_{S_1}, 0)$.

In fact, for singular points of model (9),

$$\begin{aligned} h(y, \lambda)\big|_{(y_{S_1}, 0)} &= y_{S_1}\left(l - y_{S_1} - \frac{x_{S_1}}{y_{S_1} + n}\right) = 0, \\ h(y, \lambda)\big|_{(y_{S_2}, 0)} &= y_{S_2}\left(l - y_{S_2} - \frac{x_{S_2}}{y_{S_2} + n}\right) = 0; \end{aligned} \tag{15}$$

thus, $(y_{S_1}, 0)$ and $(y_{S_2}, 0)$ are the solution to $h(y, \lambda) = 0$.

Since

$$\begin{aligned} \left.\frac{\partial h(y, \lambda)}{\partial y}\right|_{(y_{S_1}, 0)} &= l - y_{S_1} - \frac{x_{S_1}}{y_{S_1} + n} \\ &\quad + y_{S_1}\left(-1 + \frac{x_{S_1}}{(y_{S_1} + n)^2}\right) = 0, \end{aligned} \tag{16}$$

one has

$$\begin{aligned} \left.\frac{\partial h(y, \lambda)}{\partial y}\right|_{(y_{S_2}, 0)} &= l - y_{S_2} - \frac{x_{S_2}}{y_{S_2} + n} \\ &\quad + y_{S_2}\left(-1 + \frac{x_{S_2}}{(y_{S_2} + n)^2}\right) \\ &= l + \frac{(l+n)^2}{4n} \neq 0; \end{aligned} \tag{17}$$

thus, $(y_{S_1}, 0)$ is the solution to $\partial h(y, \lambda)/\partial y = 0$, but $(y_{S_2}, 0)$ is not.

And the Taylor expansion of the $h(y, \lambda)$ at the point $(y_{S_1}, 0)$ is

$$\begin{aligned} h(y, \lambda) &= h(y_{S_1}, 0) + \left.\frac{\partial h(y, \lambda)}{\partial \lambda}\right|_{(y_{S_1}, 0)} (\lambda - 0) \\ &\quad + \left.\frac{\partial h(y, \lambda)}{\partial y}\right|_{(y_{S_1}, 0)} (y - y_{S_1}) \\ &\quad + \left.\frac{\partial^2 h(y, \lambda)}{\partial \lambda^2}\right|_{(y_{S_1}, 0)} (\lambda - 0)^2 \\ &\quad + \left.\frac{\partial^2 h(y, \lambda)}{\partial y^2}\right|_{(y_{S_1}, 0)} (y - y_{S_1})^2 + o(\varepsilon^3) \\ &= -\frac{l^2 - n^2}{4}\left(a - \frac{(l+n)^2}{2(l - n + 2b)}\right)\lambda \\ &\quad - \frac{l-n}{l+n}\left(y - \frac{l-n}{2}\right) + o(\varepsilon^3); \end{aligned} \tag{18}$$

thus, the following result is got.

Theorem 4. *For model (9),*

(1) *if* $a < (l+n)^2/2(l - n + 2b)$, *then the point* $(y_{S_1}, 0)$ *is a left limit point of the induced solution curve* Ψ, *and the point* S_1 *is a backward impasse point;*

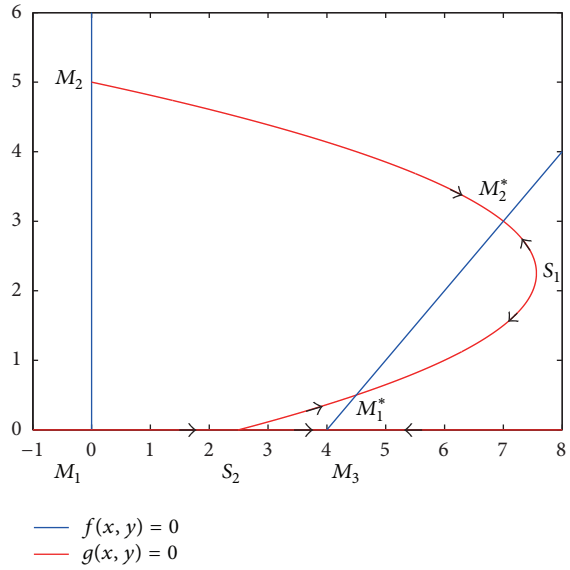

Figure 1: $l > n$, $ab > ln$ and $a = 1$.

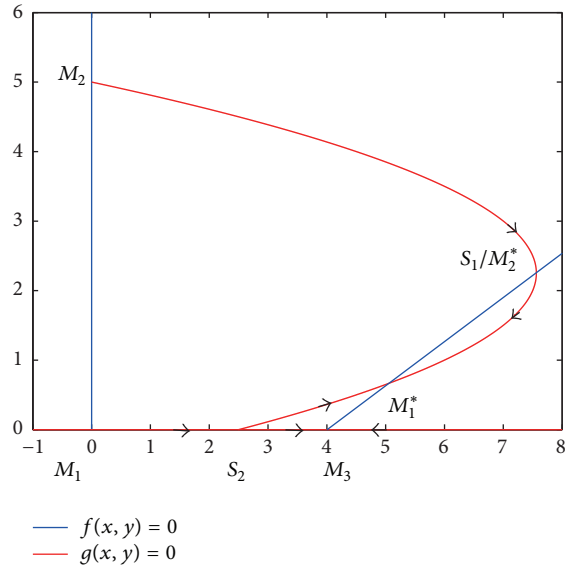

Figure 2: $l > n$, $ab > ln$ and $a = 1.2$.

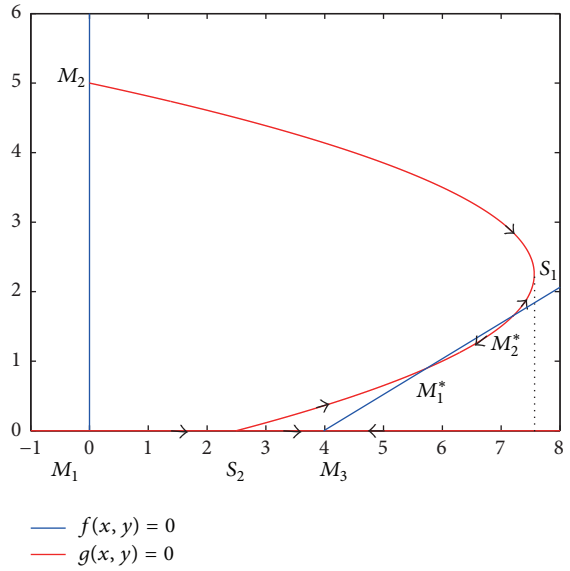

Figure 3: $l > n$, $ab > ln$ and $a = 1.5$.

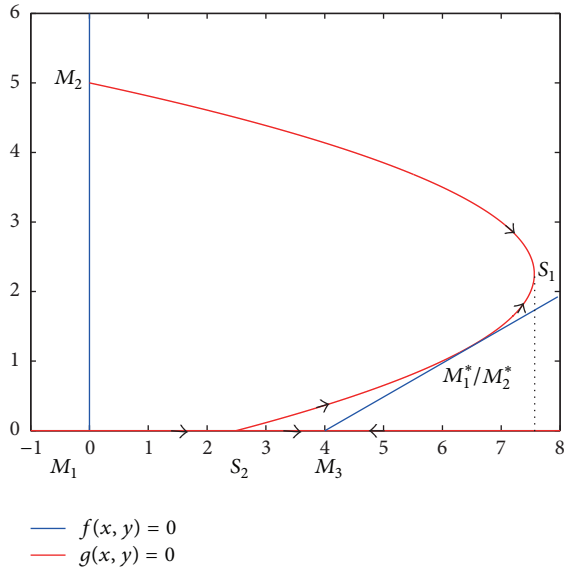

Figure 4: $l > n$, $ab > ln$ and $a = 2$.

(2) *if* $a > (l + n)^2/2(l - n + 2b)$, *then the point* $(y_{S_1}, 0)$ *is a right limit point of the induced solution curve* Ψ, *and the point* S_1 *is a forward impasse point;*

(3) *if* $a = (l + n)^2/2(l - n + 2b)$, *then there is no limit point or impasse point.*

3.2. Qualitative Analysis Results. Based on the characteristics of the equilibria, singular points, and impasse points, using the geometrical analysis method, the qualitative analysis results of the singular system model (9) are obtained.

Theorem 5. *The equilibria* M_1, M_2 *are both unstable nodes, and the equilibrium* M_3 *is a stable node.*

Theorem 6. *For model (9), if* $l > n$ *and* $ab > ln$, *the qualitative analysis results are as follows:*

(1) If the points M_1^* *and* M_2^* *are on either side of point* S_1, *respectively, then they are both stable nodes and the point* S_1 *is a backward impasse point (see Figure 1).*

(2) If the points M_2^* *and* S_1 *coincide, then that is a saddle point; the point* M_1^* *is a stable node; and there is no impasse point (see Figure 2).*

(3) If the points M_1^* *and* M_2^* *locate below the point* S_1, *then the point* M_1^* *is a stable node; the point* M_2^* *is a saddle point; and the point* S_1 *is a forward impasse point (see Figure 3).*

(4) If the points M_1^* *and* M_2^* *coincide, then that is a saddle point and the point* S_1 *is a forward impasse point (see Figure 4).*

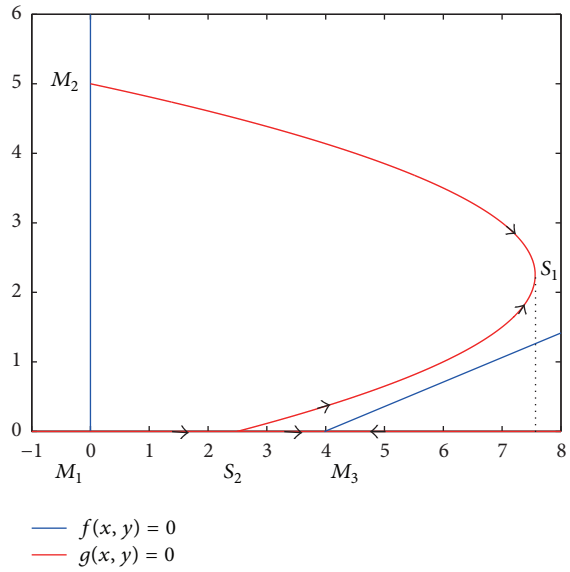

Figure 5: $l > n$, $ab > ln$ and $a = 3$.

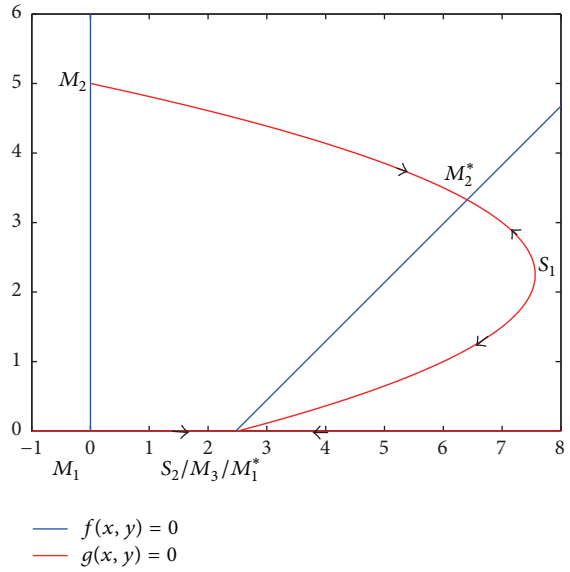

Figure 6: $l > n$, $ab = ln$ and $a = 1.25$.

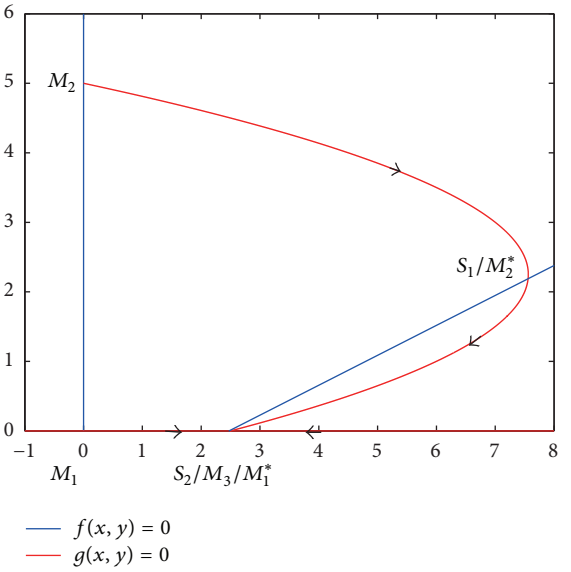

Figure 7: $l > n$, $ab = ln$ and $a = 2.2$.

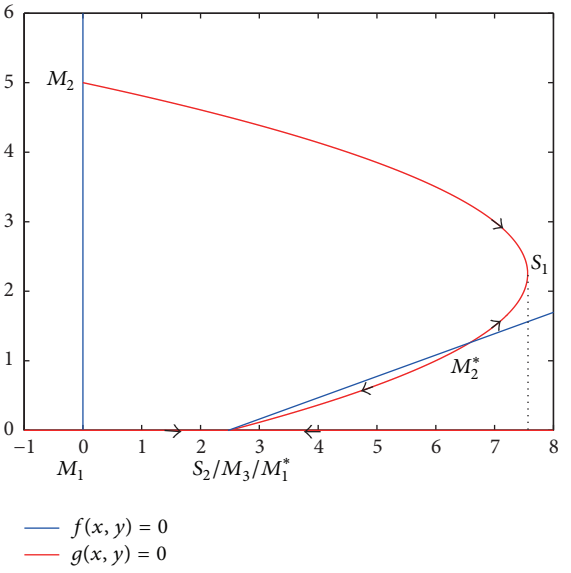

Figure 8: $l > n$, $ab = ln$ and $a = 3.5$.

(5) If the points M_1^* and M_2^* disappear, then the point S_1 is a forward impasse point (see Figure 5).

Theorem 7. *For model (9), if $l > n$ and $ab = ln$, the points M_1^*, M_1, and S_2 and the qualitative analysis results are as follows:*

(1) If the point M_2^* locates above the point S_1, then it is a stable node; the point M_1^* is a stable node; and the point S_1 is a backward impasse point (see Figure 6).

(2) If the points M_2^* and S_1 coincide, then that is a saddle point; the point M_1^* is a stable node; and there is no impasse point for this case (see Figure 7).

(3) If the point M_2^* locate below the point S_1, then it is a unstable node; the point M_1^* is a stable node; the point M_2^* is a saddle point; and the point S_1 is a forward impasse point (see Figure 8).

(4) If the points M_2^* disappear, then the point M_1^* is a saddle point and the point S_1 is a forward impasse point (see Figure 9).

Theorem 8. *For model (9), if $l > n$ and $ab < ln$, the point M_1^* disappears and the qualitative analysis results are as follows:*

(1) If the point M_2^* locates above the point S_1, then it is a stable node and the point S_1 is a backward impasse point (see Figure 10).

(2) If the points M_2^* and S_1 coincide, then that is a saddle point and there is no impasse point for this case (see Figure 11).

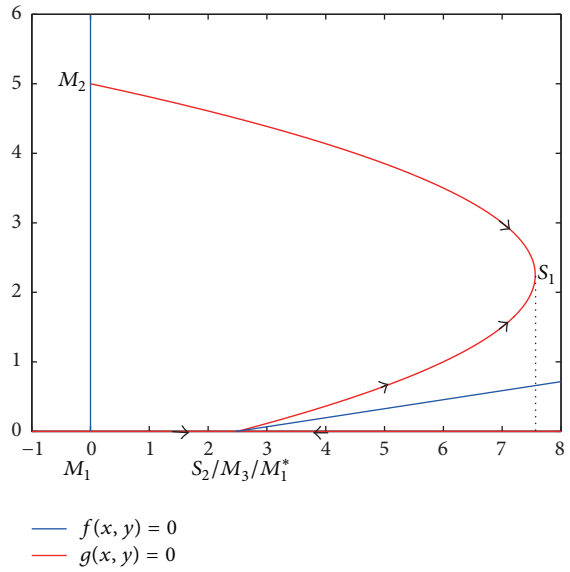

Figure 9: $l > n$, $ab = ln$ and $a = 5.5$.

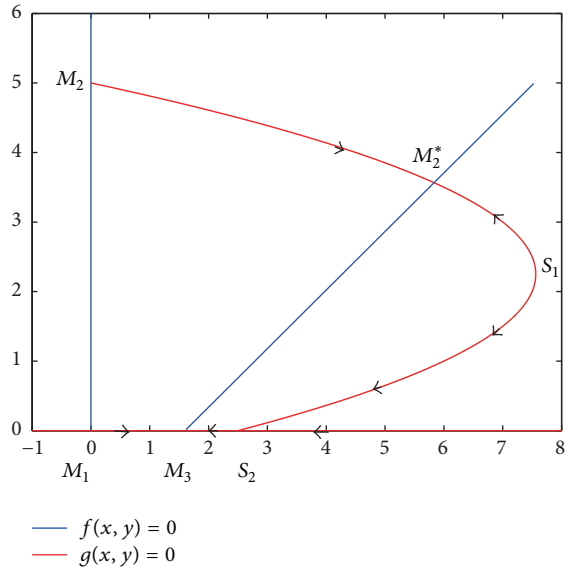

Figure 10: $l > n$, $ab < ln$ and $a = 1.5$.

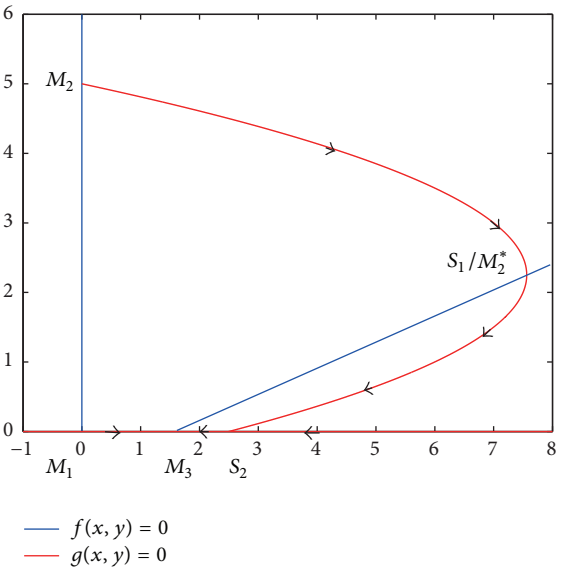

Figure 11: $l > n$, $ab < ln$, and $a = 2.5$.

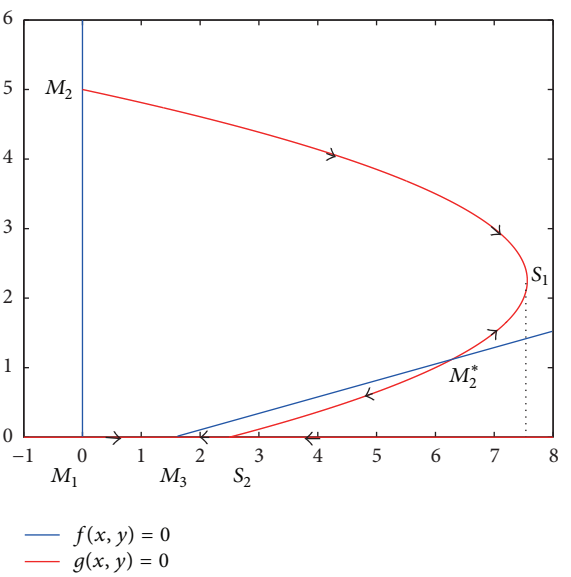

Figure 12: $l > n$, $ab < ln$, and $a = 3$.

(3) If the point M_2^* locate below the point S_1, then it is a unstable node and the point S_1 is a forward impasse point (see Figure 12).

Theorem 9. *For model (9), if $l \leq n$, the points M_1^*, S_1 and S_2 disappear and the qualitative analysis results are as follows:*

(1) If $ab < ln$, then the point M_2^* disappears, too (see Figure 13).

(2) If $ab = ln$, then the points M_2^* and M_3 coincide and that is a stable node (see Figure 14).

(3) If $ab > ln$, then the point M_2^* is a stable node (see Figure 15).

Remark 10. For model (9), if the point S_1 is the forward impasse point, then there is catastrophe, that is, the aphid population outbreak or sudden decrease (see Figures 3, 4, 5, 8, 9, and 12).

3.3. Biological Significance. According to the qualitative analysis and the corresponding figures, a is an important parameter, which has a positive correlation with the intrinsic rate of the natural enemy population and the environmental carrying capacity of the aphid population and negative correlation with the intrinsic rate of the aphid population. The stable state of the aphid ecosystems will change over the increase of the parameter a. Moreover, for different initial states, the corresponding change process will be different.

In fact, all the qualitative analysis results can be divided into two categories: the first one is that the lower part of the

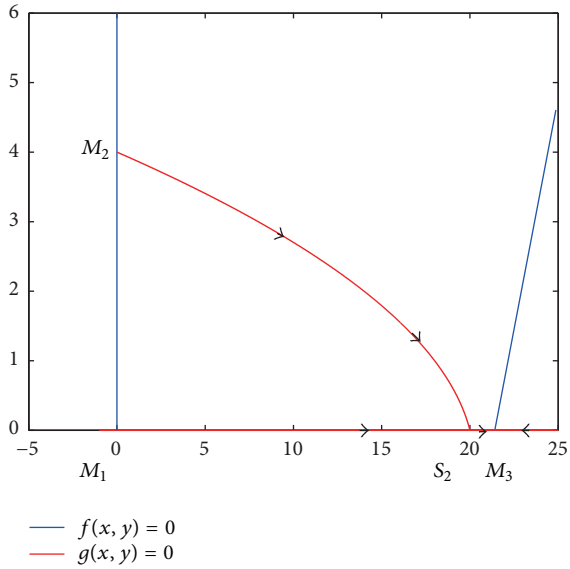

Figure 13: $l \leq n$, $ab > ln$, and $a = 1.5$.

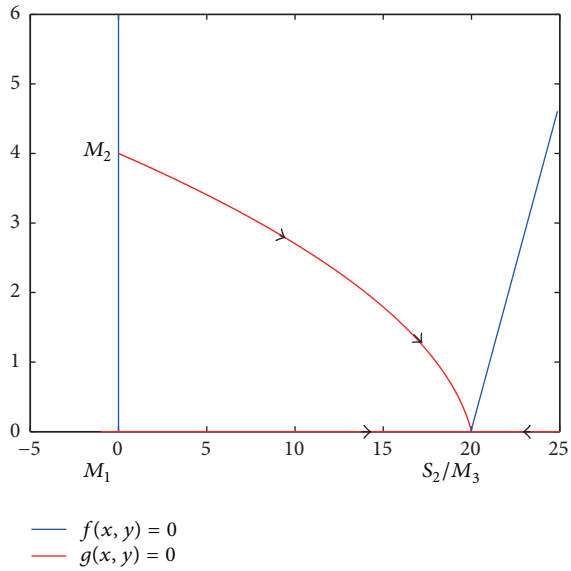

Figure 14: $l \leq n$, $ab = ln$, and $a = 2.5$.

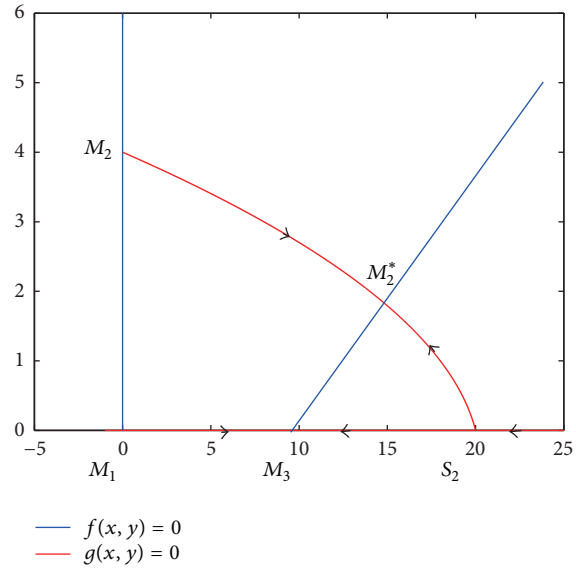

Figure 15: $l \leq n$, $ab < ln$, and $a = 3$.

parabola $x(\tau) = (l - y(\tau))(y(\tau) + n)$ intersects with the x-axis and the corresponding results are Theorems 6–8. The second one is that the upper part of the parabola intersects with the x-axis and the corresponding result is Theorem 9. And the following biological significance is discussed to the two categories.

For the first category, one has the following:

(1) If the environmental carrying capacity of the natural enemy population is larger than x_{S_2}, the following biological significance is got: when the density of the aphid population of the initial state is higher than y_{S_1}, with gradual increase of the parameter a, the system state is changed from the final state with the high aphid population density to the occurrence of the beneficial catastrophe; that is, the aphid population density is suddenly decreased and the aphid ecosystem finally stays in the state of the aphid population absence. When the density of the aphid population of the initial state is lower than y_{S_1}, with gradual increase of the parameter a, the density of the aphid population in the stable state of the aphid ecosystem is gradually increased until the catastrophe occurs.

(2) If the environmental carrying capacity of the natural enemy population is equal to x_{S_2} or smaller than x_{S_2}, the following biological significance is got: when the density of the aphid population of the initial state is higher than y_{S_1}, with gradual increase of the parameter a, the aphid ecosystem state is changed from the final state with the high aphid population density to the state of the aphid population absence, then to the beneficial catastrophe occurs. When the density of the aphid population of the initial state is lower than y_{S_1}, with gradual increase of the parameter a, the aphid ecosystem state is changed from the final state with the aphid population absence to the occurrence of catastrophe.

For the second category, with gradual increase of the parameter a, the aphid ecosystem state is changed from the state of the aphid population absence to the state with the high aphid population density.

According to the qualitative analysis and the biological significance above, the following two important results are got:

(1) If the point M_2^* appears above the point S_1, then it must be a stable node. In this case, the solution to any initial state above the point S_1 will be stable at the point M_2^*, which represents the high density of the aphid population. This phenomenon is not what people want and the control is needed to reduce the density of the aphid population.

(2) For model (9), the curve segment S_1S_2 of the catastrophe manifold is in the refuge level of the aphid ecosystem, and once the system reaches the curve segment S_1S_2, it either becomes stable at the point M_3 or M_1^* (that is, the aphid

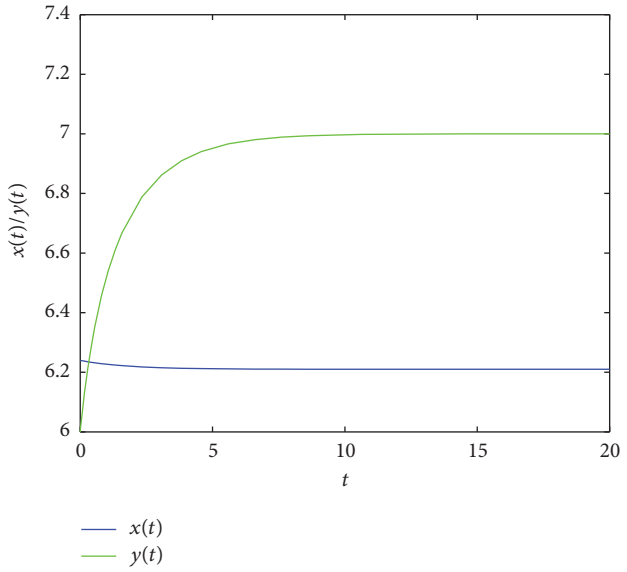

Figure 16: Time response before control.

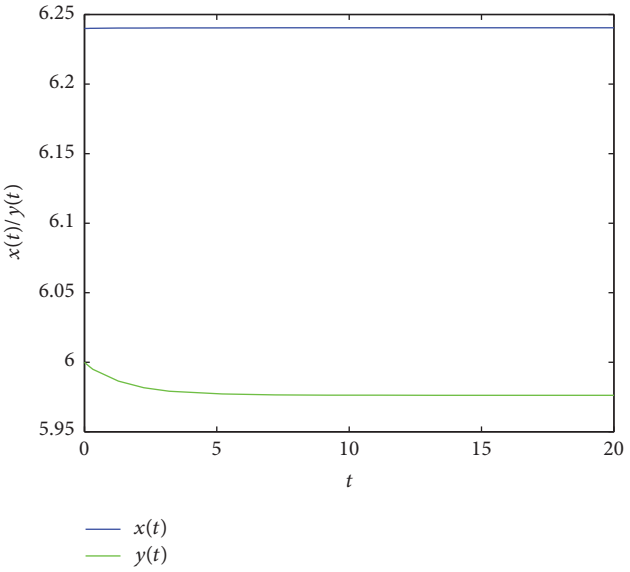

Figure 17: Time response after Controller 11 (stability).

systems stabilize at the low density of the aphid population) or causes a beneficial catastrophe to the x-axis after reaching the impasse point S_1.

The controllers are designed to manage the aphid ecosystems in the next section.

4. Controller Design

Taking releasing natural enemy as the control means, the corresponding control model of model (9) is proposed,

$$\begin{aligned} \frac{dx(\tau)}{d\tau} &= x(\tau)\left(a - \frac{x(\tau)}{y(\tau)+b}\right) + u(\tau), \\ 0 &= y\left(l - y(\tau) - \frac{x(\tau)}{y(\tau)+n}\right), \end{aligned} \tag{19}$$

where $u(\tau)$ is the releasing amount of the natural enemy population and $u(\tau) \geq 0$.

Controller 11. The controller $u(\tau)$ is only related to the density of the natural enemy population, then $u(\tau) = F_1(x(\tau))$.

Controller 12. The controller $u(\tau)$ is related to both the density of the natural enemy population and the density of the aphid population, then $u(\tau) = F_2(x(\tau), y(\tau))$.

Without loss of generality, for Controller 11, take

$$F_1(x(\tau)) = c_1 x(\tau), \quad c_1 > 0, \tag{20}$$

and for Controller 12, take

$$F_2(x(\tau), y(\tau)) = x(\tau)\left(c_2 - \frac{c_3 x(\tau)}{y(\tau)+b}\right), \quad c_2, c_3 > 0, \tag{21}$$

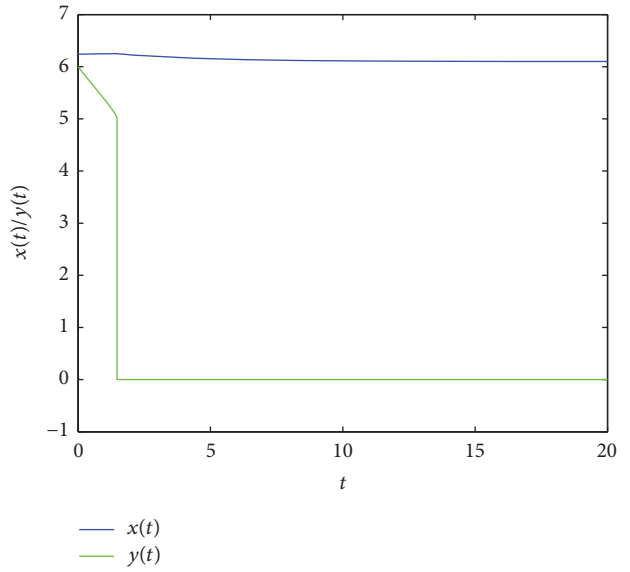

Figure 18: Time response after Controller 11 (catastrophe).

then the point M_2^* does not appear above the point S_1 and either the aphid ecosystem stabilizes in the low density of the aphid population or a beneficial catastrophe occurs (see Figures 17–20).

Figure 16 shows the phenomenon that the system stabilizes in high density of the aphid population before control. For the phenomenon, Figures 17 and 19 verify Controllers 11 and 12 can make the system stable in low density of the aphids populations. Figures 18 and 20 show the catastrophe after control implementation, namely, the extinction of the aphids population, which is not ideal from the perspective of ecological diversity. So aiming at this situation, the controller parameters should continue to be adjusted to make the system stable in the low density of aphids population. Because

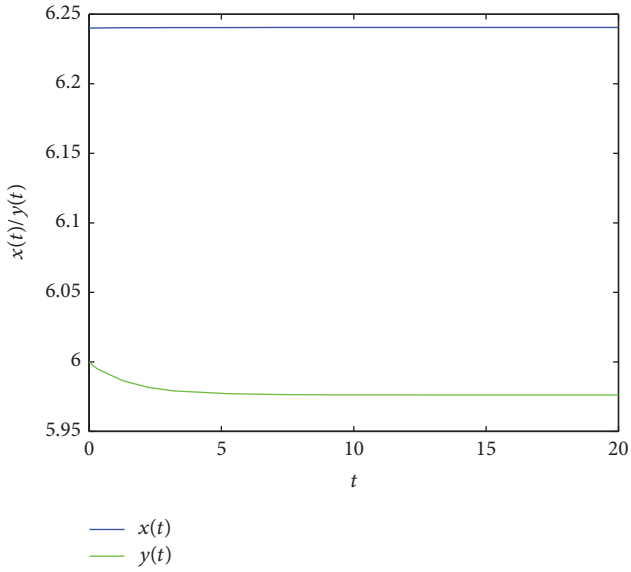

Figure 19: Time response after Controller 12 (stability).

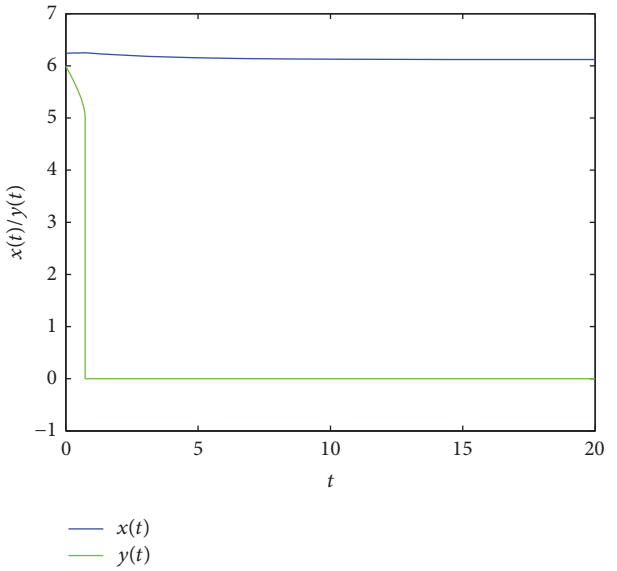

Figure 20: Time response after Controller 12 (catastrophe).

the controlled quantity can be determined by monitoring the density of the natural enemy population in the aphid ecosystem, it is easy to implement Controller 11. Although it is relatively complex to implement Controller 12, it can effectively avoid using too many natural enemies in the state with low density of natural enemy population and density of the aphid population, so as to avoid unessential economic input.

Conflicts of Interest

The authors declare that they have no conflicts of interest.

Acknowledgments

This work is supported by the National Natural Science Foundation of China (11371081 and 11371030).

References

[1] S. Chander, L. R. Ahuja, F. B. Peairs, P. K. Aggarwal, and N. Kalra, "Modelling the effect of Russian wheat aphid Diuraphis noxia (Mordvilko) and weeds in winter wheat as guide to management," *Agricultural Systems*, vol. 88, pp. 494–513, 2006.

[2] M. K. D. K. Piyaratne, H. Y. Zhao, and Q. X. Meng, "Catastrophic behavior of aphid population dynamics: An analysis of swallowtail model," *Computational Ecology and Software*, vol. 5, pp. 775–788, 2014.

[3] D. Morgan, "Population dynamics of the bird cherry-oat aphid, Rhopalosiphum padi (L.), during the autumn and winter: A modelling approach," *Agricultural and Forest Entomology*, vol. 2, no. 4, pp. 297–304, 2000.

[4] H. R. Parry, A. J. Evans, and D. Morgan, "Aphid population response to agricultural landscape change: A spatially explicit, individual-based model," *Ecological Modelling*, vol. 199, no. 4, pp. 451–463, 2006.

[5] M. K. D. K. Piyaratne, H. Zhao, and Q. Meng, "APHIDSim: A population dynamics model for wheat aphids based on swallowtail catastrophe theory," *Ecological Modelling*, vol. 253, pp. 9–16, 2013.

[6] D. D. Jones, "Catastrophe theory applied to ecological systems," *Simulation Transactions of the Society for Modeling and Simulation International*, vol. 29, pp. 1–15, 1977.

[7] H. B. Wang and C. Jin, "Application of catastrophe theory in interspecies eology," *Journal of Ecology*, vol. 7, pp. 41–45, 1988.

[8] l. R. Zhai, "Application of Spatial Analysis Technique in Pest Population Management," *Journal of Applied Ecology*, vol. 5, pp. 314–318, 1997.

[9] H. Y. Zhao and S. Z. Wang, "Apply catastrophe theory to study control strategy of aphid ecosystem," *Chinese Science Bulletin*, vol. 3422, pp. 1445–1949, 1989.

[10] X. D. Zhao, L. G. Zhu, H. Y. Zhao, and L. F. Zheng, "Prey under nature enemy model parameter grey estimattion," *Journal of Northwest A F University (NatSciEd)*, vol. 36, pp. 185–188, 2008.

[11] D. M. Li, Z. Zhang, Z. F. Ma, and B. Y. Xie, "Allee effect and a catastrophe model of population dynamics," *Discrete and Continuous Dynamical Systems-Series B*, vol. 4, pp. 629–634, 2012.

[12] M. Yue and R. Schlueter, "Bifurcation subsystem and its application in power system analysis," *IEEE Transactions on Power System*, vol. 19, no. 4, pp. 1885–1893, 2004.

[13] S. Ayasun, C. O. Nwankpa, and H. G. Kwatny, "Computation of singular and singularity induced bifurcation points of differential-algebraic power system model," *IEEE Transactions on Circuits System*, vol. 5, pp. 1525–1537, 2004.

[14] W. Marszalek and Z. W. Trzaska, "Singularity-induced bifurcations in electrical power system," *IEEE Transaction on Power System*, vol. 20, pp. 302–310, 2005.

[15] I. O. Chua and A. Deng, "Impasse points. part I: numerrcal aspects," *International Journal of Circuit Theory and Applications*, vol. 17, pp. 213–225, 1989.

[16] I. O. Chua and A. Deng, "Impasse points. part II: numerrcal aspects," *International Journal of Circuit Theory and Applications*, vol. 17, pp. 271–282, 1989.

[17] L. Dai, *Singular Control System*, Springer, New York, NY, USA, 1989.

Hindawi
Mathematical Problems in Engineering
Volume 2018, Article ID 1851845, 14 pages
https://doi.org/10.1155/2018/1851845

Research Article

No-Tension Sensor Closed-Loop Control Method with Adaptive PI Parameters for Two-Motor Winding System

Zhiqiang Wang[1], **Haibao Nan**[2], **Tingna Shi**[2], **Qiang Geng**[1] and **Changliang Xia**[1,2]

[1] *Tianjin Key Laboratory of Advanced Technology of Electrical Engineering and Energy, Tianjin Polytechnic University, Tianjin 300387, China*
[2] *School of Electrical Engineering and Automation, Tianjin University, Tianjin 300072, China*

Correspondence should be addressed to Zhiqiang Wang; wangzhq@tju.edu.cn

Received 7 February 2017; Revised 13 July 2017; Accepted 9 August 2017; Published 16 January 2018

Academic Editor: Xinggang Yan

In a winding system, it is very important to control the tension precisely. Based on the process of rewinding and unwinding, a sensorless tension control method with PI parameters of adaptive speed controllers is proposed in this paper. According to the principle of torque balance, a tension observer is designed to replace the tension sensor, and the observed value instead of the measured value of tension is used as feedback. Then the measurement delay caused by tension sensor is reduced. For the time-variable inertia, Landau discrete-time recursive algorithm is used to estimate the inertias of the rewind and unwind motors. Moreover, the estimated inertias are used to adjust the PI parameters of the speed controllers. As the tension control system has the ability to adapt to the change of inertia, its dynamic performance is improved to some extent. In addition, the proposed sensorless tension control method is simple and easy to implement, which only uses the current and speed signals of the motors without any additional hardware needed. At last, the feasibility and effectiveness of the proposed method are verified by the experimental results.

1. Introduction

Tension control system is widely applied in industrial fields where high precision and productivity are required, including printing, textile, chemical fiber, and metallurgy. Improper control of tension will result in the winding material fracture, wrinkle, deviation, and so on [1–3]. Currently, there are three ways to control the tension in industrial application: open-loop control, direct closed-loop control, and indirect closed-loop control [4–7]. Since the precision is lower in open-loop control method, the direct closed-loop control methods are commonly used in actual industry. However, tension sensors need to be installed in direct closed-loop control method. Besides the high price and the existing delay, the signal of the tension sensor is also very weak, which is easily interfered by the environment, so this method cannot be applied in some special occasions. Therefore, if a tension observer can be designed to replace the tension sensor and the same control performance can be obtained compared with the direct closed-loop control method, it will be of great significance in tension control field.

Domestic and foreign scholars have put forward a variety of implementations about tension control without tension sensor in winding systems. Valenzuela et al. at the University of Concepcion, Chile, proposed a control scheme without tension sensor in papermaking system. Two new tension estimators are developed for a two-drum electric-braking-generator production winder that are based on unwinding and rewinding variables, respectively, with the essential dynamic, friction, and inertial variation effects considered in the scheme [8–11]. Lynch from the University of Alberta in Canada exploited linear time-varying error dynamics to design a reduced-order, nonlinear tension observer. Exponential stability of the error dynamics is also demonstrated in this method, and the performance of the estimator is experimentally compared with two competing designs on real web-handing machine [12]. Song and Sul proposed a tension control method with tension observer, which is used

in continuous strip processing line, including the acceleration torque. As this scheme directly controls torque current of motors, faster dynamic response can be obtained in case of linear speed acceleration or deceleration [13, 14]. In [15], a sliding-mode (SM) feedback linearization control system is designed for a multimotor web-winding system. This method consists of a SM velocity controller and two SM tension controllers. Two tension observers are suggested to eliminate the need of tension sensors in a web-winding system. Moreover, the effectiveness and capability of the proposed control strategy are verified by simulation. In the field of multimotor control, sliding-mode variable structure control method is a very effective control algorithm. In [16, 17], the basic principle of the SM method is introduced in detail, and some of the unique problems in the motor control and multimotor control are introduced. In [18], to filter out the measurement noises of velocities and estimate the load torque of motors, an augmented observer is proposed. In [19], a novel data-based hybrid tension estimation and fault diagnosis method is proposed to estimate the unmeasured tension between two neighbouring rolls. The tension error compensation model is designed by applying neural networks principal component regression, and the corresponding tension fault diagnosis method is designed using the estimated tensions. Moreover, the proposed tension estimation and fault diagnosis method is applied to a real continuous annealing process line in a steel-making company.

There are many factors that influence the tension control performance in actual industrial production, among which one of the most important is the time-varying inertia [20, 21]. The moment of inertia will change with the radii of the rewind and unwind rolls, which will change with the operation of the system. The performance may further deteriorate if controller parameters are not adjusted properly according to the time-varying inertia. The traditional solution is to estimate the moment of inertia based on speed, thickness, and density of the winding material and correct the controller parameters using the estimated inertia to achieve the desired control performance. However, in some instances the density and thickness are unknown or vary with the humidity, temperature, and other external environment changes. Therefore, the traditional method of estimating the inertia cannot be used in some special occasions.

This paper is organized as follows. In Section 2, the dynamic model is set up, and the traditional tension control structure is analyzed. In Section 3, a new tension control strategy without tension sensor is proposed. For the identification of tension, a reduced-order observer is designed to observe the tension, which eliminates the use of tension sensor. For the time-varying inertia, Landau discrete-time recursive algorithm is adopted to estimate the inertia, and the estimated inertias are used to correct the PI parameters of speed controllers, so that the tension control system can still have good dynamic performance even if the inertia changes substantially. At last, a series of comparative experiments are conducted, and the feasibility and effectiveness of the proposed method are verified by the experimental results.

2. The Description and Modelling of the Winding System

The tension control system that contains only one tension zone is shown in Figure 1(a). This is the simplest unit of tension control system of multispan. This structure mainly contains rewind roll, unwind roll, tension sensor, controllers, and so on. Then, the changes of radii and inertia of the rewind and unwind rolls are analyzed. According to the relationship of the volume diameter, thickness of the winding material, and the rotation angle, the following equation can be obtained:

$$\begin{aligned} R_{\mathrm{r}}(t) &\approx R_{\mathrm{ro}} + \frac{\theta_{\mathrm{r}}}{2\pi}h, \\ R_{\mathrm{u}}(t) &\approx R_{\mathrm{uo}} - \frac{\theta_{\mathrm{u}}}{2\pi}h, \end{aligned} \tag{1}$$

where R_{r} and R_{u} are the radii of rewind and unwind rolls, respectively; R_{ro} and R_{uo} are the initial radii of rewind and unwind rolls, respectively; θ_{r} and θ_{u} represent the rotation angles of rewind and unwind rolls, respectively; and h represents the thickness of the winding material.

After differentiation of (1), the change rates of the volume diameters of rewind and unwind rolls are obtained

$$\begin{aligned} \frac{\mathrm{d}R_{\mathrm{r}}(t)}{\mathrm{d}t} &= \frac{\omega_{\mathrm{r}}h}{2\pi}, \\ \frac{\mathrm{d}R_{\mathrm{u}}(t)}{\mathrm{d}t} &= -\frac{\omega_{\mathrm{u}}h}{2\pi}, \end{aligned} \tag{2}$$

where ω_{r} and ω_{u} are the angular velocity of rewind and unwind rolls, respectively. The inertia of rewind and unwind rolls can be expressed as follows [19]:

$$\begin{aligned} J_{\mathrm{r}}(t) &= J_{\mathrm{ro}} + \frac{\pi}{2}\rho b\left(R_{\mathrm{r}}^4 - R_{\mathrm{ro}}^4\right), \\ J_{\mathrm{u}}(t) &= J_{\mathrm{uo}} + \frac{\pi}{2}\rho b\left(R_{\mathrm{u}}^4 - R_{\mathrm{uo}}^4\right). \end{aligned} \tag{3}$$

In (3), $J_{\mathrm{r}}(t)$ and $J_{\mathrm{u}}(t)$ represent the inertias of rewind and unwind rolls, respectively; J_{ro} and J_{uo} represent the inertias when the rewind and unwind rolls are empty; ρ is the density of the winding material; and b is the width of the winding material. After differentiation of (3), the change rate of the inertias of rewind and unwind rolls are obtained

$$\begin{aligned} \frac{\mathrm{d}J_{\mathrm{r}}(t)}{\mathrm{d}t} &= 2\pi\rho b R_{\mathrm{r}}^3 \frac{\mathrm{d}R_{\mathrm{r}}(t)}{\mathrm{d}t}, \\ \frac{\mathrm{d}J_{\mathrm{u}}(t)}{\mathrm{d}t} &= 2\pi\rho b R_{\mathrm{u}}^3 \frac{\mathrm{d}R_{\mathrm{u}}(t)}{\mathrm{d}t}. \end{aligned} \tag{4}$$

According to the torque balance principle and the Karnopp friction model used in this manuscript [22], then the dynamic equations can be expressed as

$$\begin{aligned} \frac{\mathrm{d}}{\mathrm{d}t}\left(J_{\mathrm{r}}\omega_{\mathrm{r}}\right) &= T_{\mathrm{er}} - FR_{\mathrm{r}} - T_{\mathrm{fr}} - B_{\mathrm{r}}\omega_{\mathrm{r}}, \\ \frac{\mathrm{d}}{\mathrm{d}t}\left(J_{\mathrm{u}}\omega_{\mathrm{u}}\right) &= T_{\mathrm{eu}} + FR_{\mathrm{u}} - T_{\mathrm{fu}} - B_{\mathrm{u}}\omega_{\mathrm{u}}, \end{aligned} \tag{5}$$

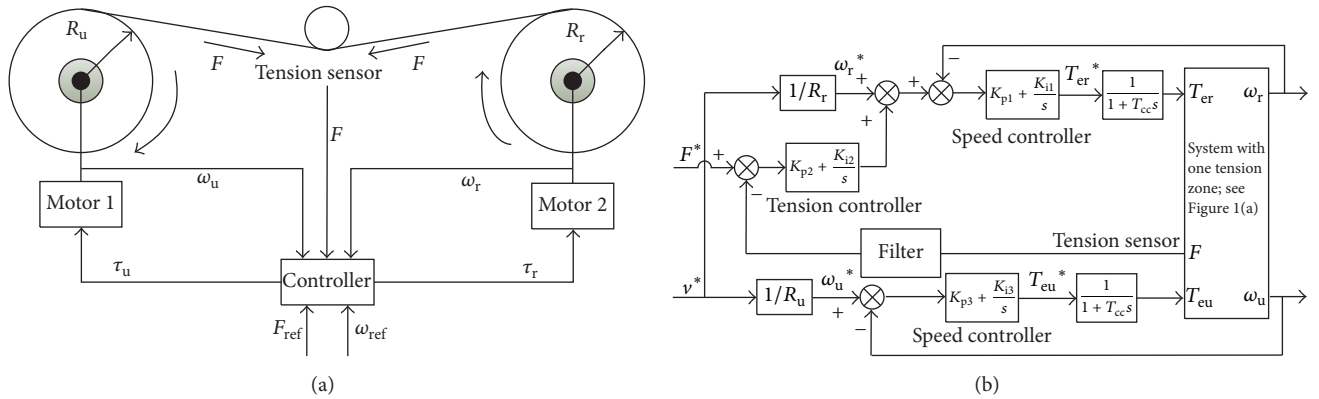

Figure 1: Winding system with two motors. (a) Tension control system with two motors; (b) tension controller with tension sensor.

where T_{er} and T_{eu} are the output torque of the rewind and unwind rolls, respectively; F is the tension of the system; B_r and B_u are viscous friction coefficients; and T_{fr} and T_{fu} are coulomb friction. The viscous friction coefficients and coulomb friction are obtained by measurements in experiment at the offline state. During the operation, the friction torque changes over time, with degradation of bearings, lubrication, and so on. Accurate estimation or online measurement of the friction is actually very difficult and is impossible in real-world industrial winders. However, the change of the friction with degradation of bearings and lubrication is small and very slow, so viscous friction coefficients and coulomb friction can be considered constant value during the operation.

Substituting (1)~(4) into (5) and rearranging (5), the following equation can be obtained:

$$\begin{aligned} F \cdot \left(R_{ro} + \frac{\theta_r}{2\pi} h\right) &= T_{er} - T_{fr} - B_r \omega_r \\ &\quad - 2\pi \omega_r \rho b R_r^3 \frac{dR_r(t)}{dt} \\ &\quad - \left[J_{ro} + \frac{\pi}{2} \rho b \left(R_r^4 - R_{ro}^4\right)\right] \\ &\quad \cdot \frac{d\omega_r}{dt}, \\ F \cdot \left(R_{uo} - \frac{\theta_u}{2\pi} h\right) &= -T_{eu} + T_{fu} + B_r \omega_u \\ &\quad + 2\pi \omega_u \rho b R_u^3 \frac{dR_u(t)}{dt} \\ &\quad + \left[J_{uo} + \frac{\pi}{2} \rho b \left(R_u^4 - R_{uo}^4\right)\right] \\ &\quad \cdot \frac{d\omega_u}{dt}. \end{aligned} \tag{6}$$

According to the analysis above, the size of the tension is influenced by many factors, such as the density and width of the winding material, volume diameter, friction coefficient, and velocity. Variation in any of the aforementioned factors will impose a certain effect on the tension. Therefore, tension control system is a multivariable, nonlinear, strong coupling control system. To accurately control the tension, the impact of various factors must be considered.

Presently, tension sensor is commonly used in direct closed-loop tension control structure among the actual industrial production. The structure is shown in Figure 1(b). The unwind motor is used to control the entire system speed and the rewind motor is used to control the tension. In Figure 1(b), v^* represents the reference velocity and T_{cc} corresponds to the time constant of the first-order delay of the current controller.

3. The Design of No-Tension Sensor Control System with Adaptive PI Parameters

3.1. The Design of the Tension Observer. From the dynamic equations of rewind and unwind motors, it is easy to find that the change of tension is reflected in the torque elements of the rewind and unwind rolls. Therefore, a tension observer can be implemented based on the drive torque components that is related to the tension zone. The tension could be obtained through analyzing the dynamic equation of the rewind motor or unwind motor, and they should be equal in theory. The rewind roll is taken as an example in the following analysis.

Taking the tension F as a state variable, as the change rate of tension is far less than the sampling frequency of the controller, the tension can be considered as a constant value in a control period; that is to say,

$$\frac{dF}{dt} = 0. \tag{7}$$

Since the change rate of inertia is much less than the change rate of angular velocity in the tension control system, (5) can be approximated by

$$\begin{aligned} \frac{d}{dt}\left(J_r \omega_r\right) &\approx J_r \frac{d\omega_r}{dt} \approx T_{er} - FR_r - T_{fr} - B_r \omega_r, \\ \frac{d}{dt}\left(J_u \omega_u\right) &\approx J_u \frac{d\omega_u}{dt} \approx T_{eu} + FR_u - T_{fu} - B_u \omega_u. \end{aligned} \tag{8}$$

According to (7) and the first equation of (8), the dynamic state equation of the rewind motor can be obtained as

$$\begin{aligned} \dot{\mathbf{x}} &= \mathbf{A}\mathbf{x} + \mathbf{B}\mathbf{u}, \\ \mathbf{y} &= \mathbf{C}\mathbf{x}, \end{aligned} \tag{9}$$

where $\mathbf{x} = \begin{bmatrix} \omega_r & F \end{bmatrix}^T$ is state variable; $\mathbf{u} = [T_{er} - T_{fr}]$ is input signal; $\mathbf{y} = [\omega_r]$ is the output signal; $\mathbf{A} = \begin{bmatrix} -B_r/J_r & -R_r/J_r \\ 0 & 0 \end{bmatrix}$; $\mathbf{B} = \begin{bmatrix} 1/J_r \\ 0 \end{bmatrix}$; and $\mathbf{C} = \begin{bmatrix} 1 & 0 \end{bmatrix}$.

The necessary and sufficient condition for system (9) to have an observer and be able to choose the observer poles arbitrarily is the observability of system (9). The observability matrix of (9) is

$$\mathbf{Q} = \begin{bmatrix} \mathbf{C} \\ \mathbf{CA} \end{bmatrix} = \begin{bmatrix} 1 & 0 \\ -\dfrac{B_r}{J_r} & -\dfrac{R_r}{J_r} \end{bmatrix}. \tag{10}$$

As $|\mathbf{Q}| = -R_r/J_r \neq 0$, the matrix rank of $\mathbf{Q}$ is rank $\mathbf{Q} = 2$, so system (9) is observable.

According to the idea of reduced-order state observer in modern control theory [23], if we take the angular velocity of the rewind motor as a correction variable in the tension observer, the tension observer can be expressed as

$$\begin{aligned} \dot{\hat{\mathbf{x}}} &= \mathbf{A}\hat{\mathbf{x}} + \mathbf{B}\mathbf{u} + \mathbf{K}\left(\mathbf{y} - \hat{\mathbf{y}}\right), \\ \hat{\mathbf{y}} &= \mathbf{C}\hat{\mathbf{x}}, \end{aligned} \tag{11}$$

where $\hat{\mathbf{x}} = \begin{bmatrix} \hat{\omega}_r & \hat{F} \end{bmatrix}^T$ is the state variable of the observer; $\hat{\mathbf{y}} = [\hat{\omega}_r]$ is the output of the observer; and $\mathbf{K} = [k_1 \ k_2]^T$ is the feedback gain.

From (9) and (11), the observation error can be obtained as

$$\begin{aligned} \dot{\mathbf{x}} - \dot{\hat{\mathbf{x}}} &= \mathbf{A}\mathbf{x} + \mathbf{B}\mathbf{u} - \left[\left(\mathbf{A} - \mathbf{KC}\right)\hat{\mathbf{x}} + \mathbf{B}\mathbf{u} + \mathbf{K}\mathbf{y}\right] \\ &= \left(\mathbf{A} - \mathbf{KC}\right)\left(\mathbf{x} - \hat{\mathbf{x}}\right). \end{aligned} \tag{12}$$

The characteristic of (12) can be expressed as follows:

$$\det\left[s\mathbf{I} - \left(\mathbf{A} - \mathbf{KC}\right)\right] = s^2 + \left(\frac{B_r}{J_r} + k_1\right)s - \frac{R_r}{J_r}k_2 = 0. \tag{13}$$

Through the stability conditions of state observer, it is known that if an appropriate matrix $\mathbf{K}$ is selected to make all roots of the characteristic equation have negative real parts, the following equation is obtained:

$$\lim_{t\to\infty}\left(\mathbf{x} - \hat{\mathbf{x}}\right) = 0. \tag{14}$$

The key to observe the state variables accurately is the selection of $\mathbf{K}$ matrix, which is independent of the state variable $\mathbf{x}$ and the input $\mathbf{u}$. Assuming that the desired two observer eigenvalues are α and β, the expected characteristic equation can be obtained as

$$s^2 - \left(\alpha + \beta\right)s + \alpha \cdot \beta = 0. \tag{15}$$

According to (13) and (15), the $\mathbf{K}$ matrix can be selected as

$$\begin{aligned} k_1 &= -\left(\alpha + \beta\right) - \frac{B_r}{J_r}, \\ k_2 &= -\alpha\beta\frac{J_r}{R_r}. \end{aligned} \tag{16}$$

The positions of the poles α and β should be chosen according to the desired characteristics of the system. The tension observer will be asymptotically stable as long as the poles α and β have negative real parts. $\alpha = \beta = -6$ is adopted in this paper.

The observer input signal coulomb friction T_{fr} is obtained by repeated measurements in experiment at the offline state; the electromagnetic torque is obtained by the current of q-axis; it can be expressed as follows:

$$T_{er} = K_T \cdot i_{qr}, \tag{17}$$

where K_T is the torque coefficient of rewind motor and i_{qr} is the q-axis current of rewind motor.

3.2. Identification of the Inertia. The moment of inertia will change with the radii of the rewind and unwind rolls, which will change with the operation of the system. Therefore, if the controller parameters are not corrected according to the inertia, the dynamic performance of the tension control system will deteriorate. The conventional method is to use (3) to estimate the inertia approximately, for which the knowledge of the density, thickness, and other variables of the winding material is required. However, these variables are unknown or difficult to obtain by measurement in some cases. In this paper, Landau discrete-time recursive algorithm is used to observe the inertias [24]. The main idea of Landau algorithm is to use the equation with the unknown parameter as the reference model and the equation without the unknown parameter as the adjustable model. The two models have the same physical input and output. Then, the parameters of the adjustable model are adjusted in real time by the error of the output of the two models until the difference between the two is no longer further reduced, thus realizing the output of the adjustable model's output tracking control object [25]. Thus the inertias can be obtained accurately even under the condition that the density, thickness, and other parameters of the winding material are unknown. Taking rewind roll as an example for analysis and ignoring friction coefficient, (8) can be described as follows:

$$\begin{aligned} \omega_r(k) &= \omega_r(k-1) \\ &\quad + \frac{T_s}{J_r}\left[T_{er}(k-1) - R_r(k-1)F(k-1)\right], \\ \omega_r(k-1) &= \omega_r(k-2) \\ &\quad + \frac{T_s}{J_r}\left[T_{er}(k-2) - R_r(k-2)F(k-2)\right]. \end{aligned} \tag{18}$$

In (18), T_s is the control period. Since the sampling time is very short, it can be assumed that the change periods of

tension and radii are much greater than the speed calculation period; then the following equation can be obtained:

$$R_r(k-1)F(k-1) \approx R_r(k-2)F(k-2). \quad (19)$$

By the subtraction of the two equations in (18), the following equation is obtained:

$$\omega_r(k) = 2\omega_r(k-1) - \omega_r(k-2) + bU(k-1). \quad (20)$$

In (20), $U(k-1) = T_{er}(k-1) - T_{er}(k-2)$; $b = T_s/J_r$; if we take (20) as the reference model, the adjustable model expressed in the a priori form can be described as follows, namely, the estimated angular speed in the kth control cycle.

$$\hat{\omega}_r^0(k) = 2\omega_r(k-1) - \omega_r(k-2) + \hat{b}(k-1)U(k-1). \quad (21)$$

In (21), $\hat{b}(k-1) = T_s/\hat{J}_r$ is the variable to be identified and $\hat{\omega}_r^0(k)$ is the adjustable model expressed in the a priori form; the priori error can be expressed as follows:

$$e_0(k) = \omega_r(k) - \hat{\omega}_r^0(k). \quad (22)$$

According to Landau discrete-time recursive algorithm, the adaptive rate of inertia can be expressed as

$$\hat{b}(k) = \hat{b}(k-1) + \gamma \frac{U(k-1)}{1+\gamma U^2(k-1)} e_0(k). \quad (23)$$

In (23), γ represents the adaptive gain; since T_s is a constant value, the inertia $\hat{J}_r$ can be calculated through the observed value $\hat{b}(k)$.

According to the basic principle of Landau algorithm, it can be seen that changing the value of γ can change the convergence speed and precision of $\hat{b}(k)$. And the higher the adaptive gain, the smaller the convergence time of Landau algorithm. But the jitter amplitude of the result of the moment of inertia identification increases with the increase of the adaptive gain γ value. When the value of the adaptive gain is too large, the chattering of the moment of inertia is too severe to be unrecognizable, and the magnitude of the adaptive gain γ needs to be compromised between the convergence time and the recognition accuracy. Therefore, the value of the adaptive gain γ needs to be compromised between the convergence time and the identification accuracy.

3.3. Structure Diagram of the Proposed Tension Control Method. The control block diagram of the tension control method proposed in this paper is shown in Figure 2(a). It mainly consists of a rewind motor, an unwind motor, a tension observer, and two inertia observers. The rewind and unwind motors are used to drive the winding rolls. The two motors are both surface mounted permanent magnet synchronous motors. Double-closed-loop vector control structure with inner current loop and outer speed loop is adopted in this system. The controllers of current loop, velocity loop, and tension loop are all integral isolated PI regulators. The PI parameters of speed controllers are designed according to the bandwidth related in [26, 27].

And the speed signal is obtained by incremental encoder. The tension observer is used to observe the tension, which eliminates the application of tension sensor. The inertia observers are used to observe the inertias of the rewind and unwind motors. Moreover, the observed inertias are used to correct the parameters of speed controllers. Therefore, the tension control system can still have a good dynamic performance even if the inertia changes dramatically.

Then the methods of how to set the PI parameters and how to revise the PI parameters are described. Taking the rewind motor as an example, as can be seen from (8), the inertia of the motor can affect system dynamic performance. The response time of electromagnetic torque is much less than the response time of the mechanical system as to the PMSM Vector Control System. So the dynamic process of the current loop can be ignored when analyzing the speed tracking performance and the disturbance rejection performance. Figure 3 shows the simplified control block diagram of the velocity loop.

In Figure 3, ω_{ref} is the reference speed, $T_L = FR_r + T_{fr}$ is the load torque, and e_ω is the tracking error.

Considering that the friction factor B_r is generally much smaller, therefore, the friction factor B_r is ignored in the subsequent analyses. In this case, the closed-loop transfer function from ω_{ref} to ω_r can be expressed as

$$G_{io}(s) = \frac{\omega_r(s)}{\omega_{ref}(s)} = \frac{k_{vp}}{J_r} \frac{s + k_{vi}/k_{vp}}{s^2 + \left(k_{vp}/J_r\right)s + k_{vi}/J_r}, \quad (24)$$

where k_{vp} is the proportional gain of the PI controller and k_{vi} is the integral gain of the PI controller; $k_{vp} > 0$, $k_{vi} > 0$.

The closed-loop transfer function from T_L to ω_r can be expressed as

$$G_{do}(s) = \frac{\omega_r(s)}{T_L(s)} = -\frac{1}{J_r} \frac{s}{s^2 + \left(k_{vp}/J_r\right)s + k_{vi}/J_r}. \quad (25)$$

The speed tracking performance and the disturbance rejection performance are good or bad when using PI controller depends on the pole-zero distribution of the transfer function (24) and (25), respectively. As can be seen from (24) and (25), the pole-zero distributions are closely related to k_{vp} and k_{vi}. The parameters k_{vp} and k_{vi} are mainly determined by the dynamic performance index of tension control system. The bandwidth of speed loop can be determined through the speed loop rise time t_{rc}.

$$\alpha_s = \frac{\ln 9}{t_{rc}} \approx \frac{2.2}{t_{rc}}. \quad (26)$$

If the proportionality coefficient k_{vp} is set as follows, it can guarantee that the speed loop rise time is less than t_{rc}.

$$k_{vp} = \alpha_s J_0, \quad (27)$$

where J_0 is the default value of the inertia.

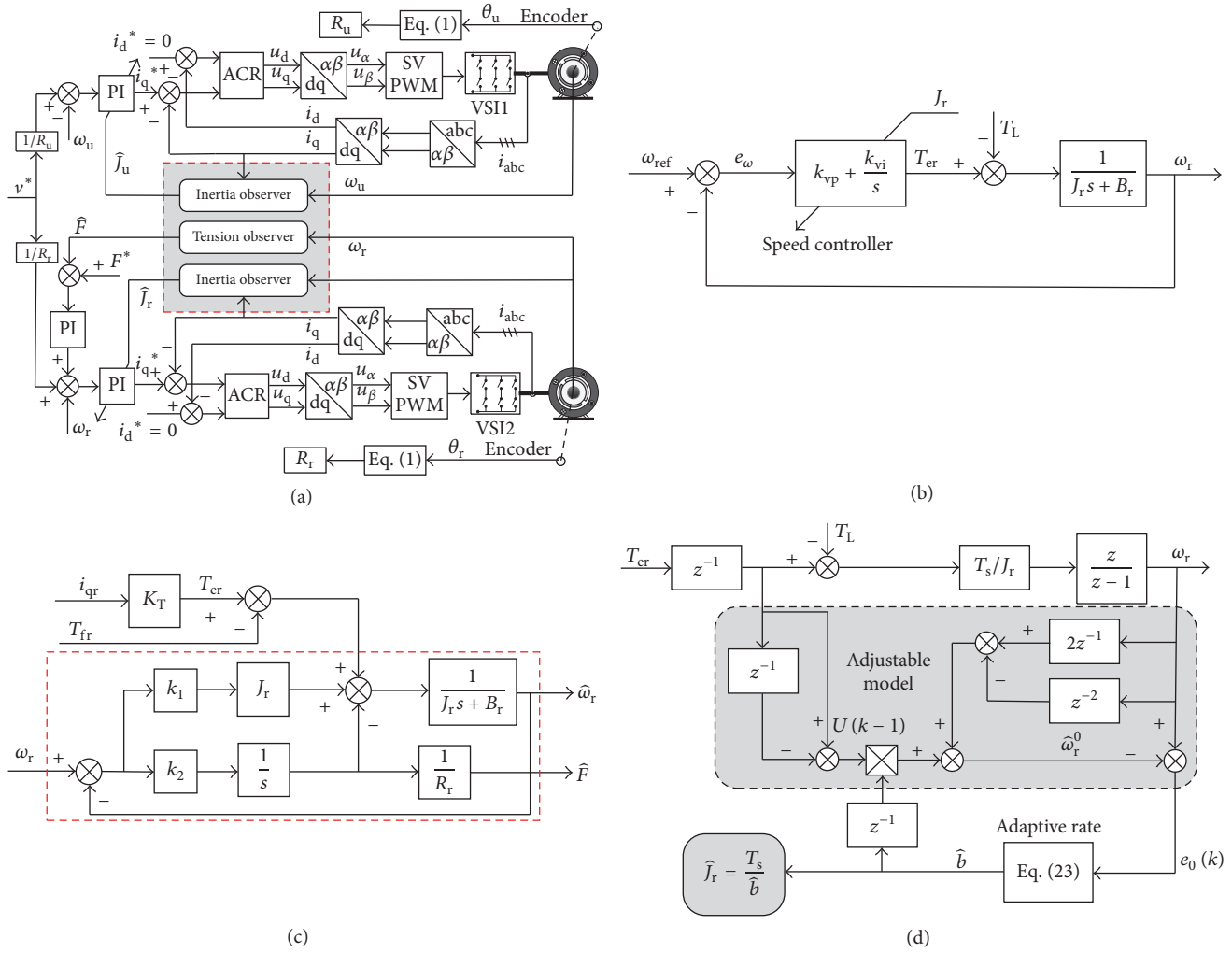

Figure 2: Structure diagram of the proposed tension control method. (a) Structure diagram of the proposed tension control method; (b) simplified control block diagram of the rewind motor velocity loop; (c) block diagram of the tension observer; (d) block diagram of the inertia observer.

The integral coefficient k_{vi} can be set as

$$k_{vi} = \left(\frac{\alpha_s}{2\zeta}\right)^2 J_0, \tag{28}$$

where ζ is the damping ratio.

Substitute (27) and (28) into (24) and (25); then the following equations are obtained:

$$\begin{aligned} G_{io}(s) &= \frac{\omega_r(s)}{\omega_{ref}(s)} \\ &= \frac{J_0}{J_r} \frac{\alpha_s\left(s + \alpha_s/4\zeta^2\right)}{s^2 + \left(J_0/J_r\right)\alpha_s s + \left(J_0/J_r\right)\left(\alpha_s/2\zeta\right)^2}, \\ G_{do}(s) &= \frac{\omega_r(s)}{T_L(s)} \\ &= -\frac{1}{J_r} \frac{s}{s^2 + \left(J_0/J_r\right)\alpha_s s + \left(J_0/J_r\right)\left(\alpha_s/2\zeta\right)^2}. \end{aligned} \tag{29}$$

As can be seen from (29), the above two equations have the same characteristic equation.

$$s^2 + 2\frac{J_0}{J_r}\zeta\omega_0 s + \frac{J_0}{J_r}\omega_0^2 = 0, \tag{30}$$

where $\omega_0 = \alpha_s/2\zeta$; it is the natural angular frequency of the speed loop.

When the system robustness is analyzed, it is necessary to evaluate the performance of the maximum drop value ω_{tm} of the motor speed as the sudden load is applied and the speed error integral value IE in the recovery process.

When there is load disturbance, there are

$$\begin{aligned} \omega_{tm} &\le \frac{T_L}{k_{vp}}, \\ IE &= \lim_{t\to\infty} \int_0^t \mathcal{L}^{-1}\left(\frac{s}{J_r s^2 + k_{vp}s + k_{vi}} \cdot \frac{T_L}{s}\right) \\ &= \lim_{s\to 0} s \cdot \frac{1}{s} \cdot \frac{s}{J_r s^2 + k_{vp}s + k_{vi}} \cdot \frac{T_L}{s} = \frac{T_L}{k_{vi}}. \end{aligned} \tag{31}$$

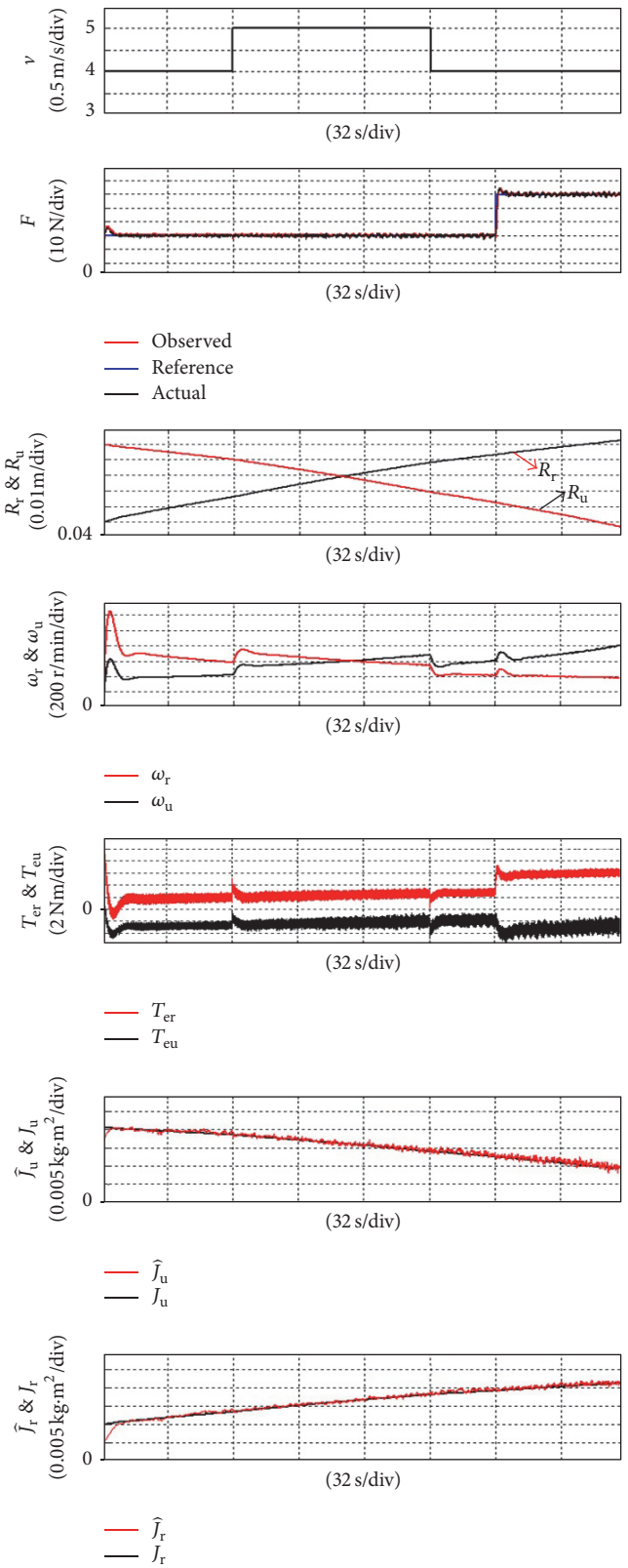

Figure 3: The simulation wave of the whole process of rewinding with all characteristics.

It can be seen from (31) that maximum speed drop value will reduce by improving k_{vp} and the integral value of speed error in the process of recovery can be lowered by increasing k_{vi}. However, the improvement of k_{vi} corresponds to the decrease of ζ. This will reduce the robustness of the permanent magnet synchronous motor control system and oscillation can occur in severe cases. Therefore, it is generally necessary to constrain the value of the parameter by the phase margin of the system. The open-loop transfer function of the system $G_{open}(s)$ is

$$G_{open}(s) = \frac{sk_{vp} + k_{vi}}{s} \cdot \frac{1}{sJ_r}. \tag{32}$$

Let $|G_{open}(s)| = 1$; we can get the shear frequency ω_c of the system as follows:

$$\omega_c = \frac{\alpha_s}{2\zeta}\sqrt{2\zeta^2 + \sqrt{4\zeta^4 + 1}}. \tag{33}$$

Furthermore, the phase margin ϕ_m of the system is as follows:

$$\begin{aligned}\phi_m &= \pi + \arg G_{open}(j\omega_c) \\ &= \arctan\left(2\zeta\sqrt{2\zeta^2 + \sqrt{4\zeta^4 + 1}}\right).\end{aligned} \tag{34}$$

In order to ensure the robustness of the permanent magnet synchronous motor control system, we should take $\phi_m \geq 60^\circ$; then we can obtain $0.61 \leq \zeta \leq 1$. In this paper, we take $\zeta = 0.707$.

Through the analysis above, the following can be obtained: the PI parameter tuning strategy has good adaptability to the permanent closed-loop control system of permanent magnet synchronous motor. The range of ζ will be determined according to the range of the phase margin firstly and then the speed loop bandwidth value of the speed control system is determined according to the actual needs, for permanent magnet synchronous motor with different moment of inertia. The PI parameter can be set by the magnitude of its moment of inertia. Meanwhile, the PI parameter tuning method above is also applicable to the current loop PI parameter tuning. The derivation process will not be repeated in this paper.

4. Simulation and Experimental Results Analysis

4.1. Simulation Results Analysis. In addition, the effectiveness of the observer is also simulated analysis. The simulation parameters are shown in Table 1 except the material inertia. We simulated the larger density material as the motor load, while employing a longer observation time. Figure 3 shows the simulation waveforms of the whole process of the tension control system. The simulation parameters are basically the same as the experimental ones. Only the empty volumes inertia and the full volumes inertia are different, and they are 0.01 kg·m^2 and 0.022 kg·m^2, respectively. The figures from top to bottom in turn are line speed of reference values, tense values (reference value and actual value, observed value), winding and rewinding roller radius, winding and rewinding motor angular speed, winding and rewinding motor electromagnetic torque, and winding and rewinding roll moment of inertia (actual value and observed value). In simulation, the system linear velocity changed from 4 m/s to 5 m/s and then to 4 m/s, and the tension reference value changed from 30 N to 60 N suddenly.

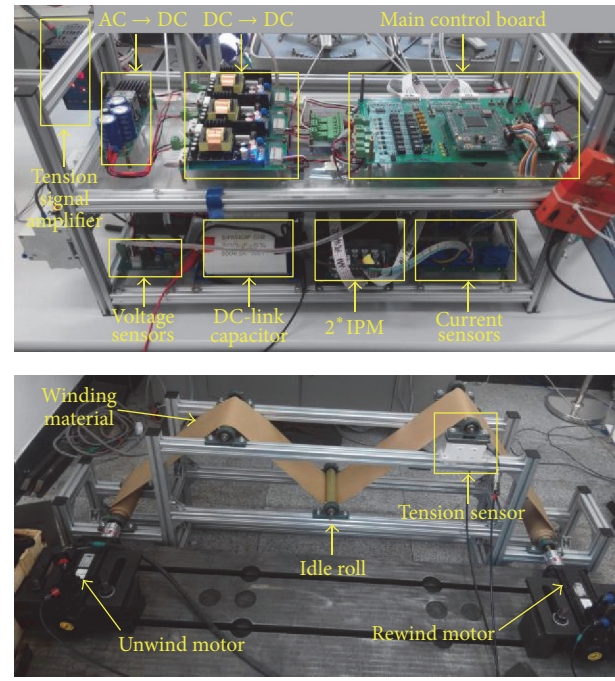

Figure 4: Experimental platform.

It can be seen from the figure that when the linear velocity of the system is constant, with the operation of the system, the winding roller radius increases gradually and roll radius decreases. As the winding and rewinding roll radius changes continuously, the winding of the motor angular velocity decreases and rolling motor angular velocity increases gradually. We can see from the 6th and 7th picture, with the operation of the system, the rotational inertia of the rewinding motor increases gradually, rolling moment of inertia of the motor decreases, and the inertia observer proposed in this paper can estimate the moment of inertia in real time. The analysis results have been added to the revised manuscript.

4.2. Experimental Platform. In order to verify the correctness of the proposed strategy, an experimental platform of tension control system is established shown in Figure 4. The experimental platform consists of a main control board, power circuit, drive circuit, current sensor, voltage sensor, winding material, unwinding motor, rewinding motor, idle rollers, and so on. The DSP applied in the system is TMS320F28335 produced by TI, and the Intelligent Power Module (IPM) is PS21867 produced by Mitsubishi. The

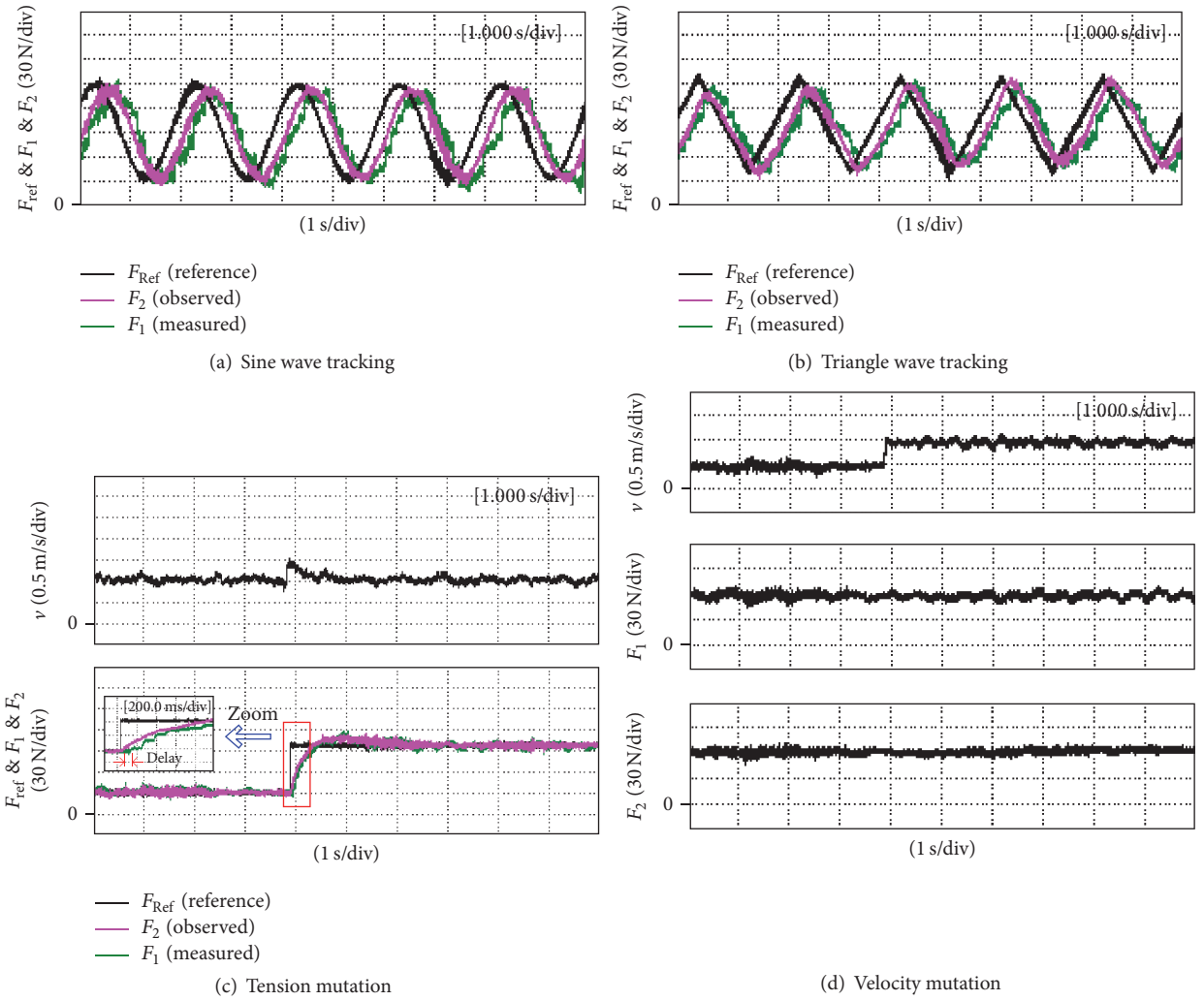

Figure 5: Closed-loop control method with tension sensor.

switching frequency of the inverter is 5 kHz. Two identical permanent magnet synchronous motors (PMSM) are applied as the rewind and unwind motors in the experiment. The winding material applied in the system is kraft paper. In order to do comparison experiment, a tension sensor is installed, the tension sensor applied in this system is LX-015-TD produced by Mitsubishi, and the tension signal amplifier applied in this system is KTC820. The size of the experimental prototype is 2.5 m × 0.6 m, and the detailed mechanical parameters of experimental platform are shown in Table 1.

4.3. Verification Experiment of Tension Identification. Figure 5 shows the experimental waveforms of the direct closed-loop control method with tension sensor and Figure 6 shows the method proposed in this paper. Figures 5 and 6 show, respectively, the experimental waveforms under the circumstance that the reference linear velocity remains 1.0 m/s and the reference tension changes in the sinusoidal manner, the experimental waveforms under the circumstance that the reference linear velocity remains 1.0 m/s and the reference tension changes in the triangular manner, the experimental waveforms under the circumstance that the reference linear velocity remains 1.0 m/s and the reference tension changes from 30 N to 100 N abruptly, and the experimental waveforms under the same circumstance that the reference tension remains 60 N and the reference linear velocity changes from 0.5 m/s to 1.0 m/s abruptly. In the experimental waveforms, v represents the linear velocity and F_{ref}, F_1, and F_2 are, respectively, the reference tension, the tension measured by tension sensor, and the tension observed by the proposed method.

Due to the characteristics of the tension sensor, its output signal is very weak, generally only 200 mV. Therefore, usually it takes an amplifier circuit and a filter circuit to process the output signal. The filter time constant used in this experiment is 100 ms. However, some delay of tension sensor signal will be caused inevitably.

As can be seen from Figures 5(a)~5(b) compared to the reference tension F_{ref}, in the tension F_1 measured by the tension sensor, there exists a delay. And F_2 is the observed value by the proposed method in the paper. Because tension

Table 1: Mechanical parameters of experimental prototype.

PMSM (rewind motor and unwind motor)		
Rated power P_N	kW	2.3
Rated speed n	r/min	1500
Inertia J	kg·m^2	0.00272
Resistance R	Ω	0.635
Inductance L	mH	4.025
Coulomb friction torque (T_{fr}/T_{fu})	N·m	0.06/0.06
Viscous friction coefficient (B_r/B_u)	N·m/(rad/s)	0.0004/0.0004
Number of poles p		4
Winding rolls and winding material		
Radii (empty volumes/full volumes)	m	0.05/0.1
Inertia (empty volumes/full volumes)	kg·m^2	0.00138/0.00348
Width b	m	0.18
Thickness h	mm	0.15
Specification (kraft paper)	g	120
Tension sensor (LX-015-TD) and signal amplifier (KTC820)		
Rated capacity	N	150
Output voltage	V	3
Filter time	ms	100

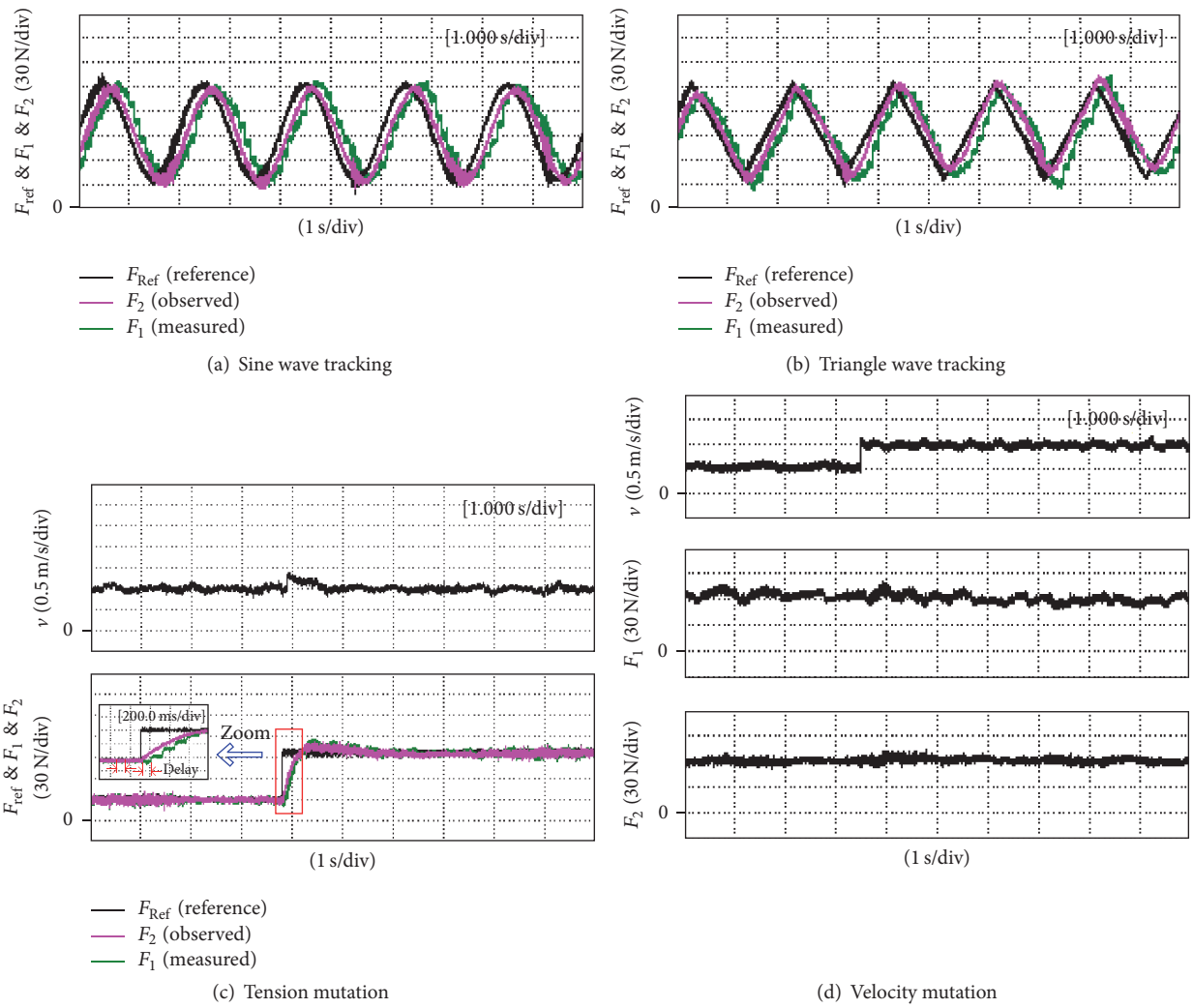

Figure 6: Closed-loop control method without tension sensor.

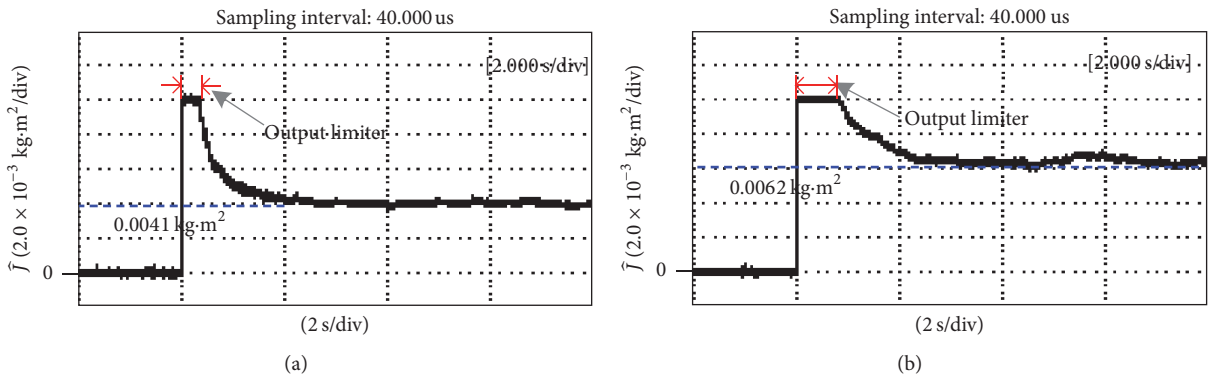

Figure 7: Inertia identification results. (a) Empty volumes; (b) full volumes.

sensor method is used at this time, there is a bigger delay between F_{ref} and F_2. For the tension system, it can be seen that control method with tension sensor will be difficult to meet the requirements for many high-speed applications. However, from Figures 6(a)~6(b), there is a smaller delay between F_{ref} and F_2, compared to Figures 5(a)~5(b).

Thus, from Figures 5(c) and 6(c), when the reference tension changes from 30 N to 100 N abruptly (tension mutation), the linear velocity change without tension sensor control method is smaller than that with tension sensor. And the tension observed by the proposed method can track the reference tension excellently. From Figures 5(d) and 6(d), when the reference linear velocity changes from 0.5 m/s to 1.0 m/s abruptly (velocity mutation), it can be seen that the observed tension by the proposed method can track the reference tension precisely even if the linear velocity changes abruptly. In summary, the proposed method can achieve nearly the same control performance as the direct closed-loop control method with tension sensor.

4.4. Verification Experiments of Inertia Identification and Adaptive Parameter of the Controller. The total inertia on the rewind motor side consists of the inertia of motor armature, driving shaft, the winding material, and so on. Among them, the inertias of motor armature and driving shaft are constants, while the inertia of winding material is time-varying, because the material is continuously released into the process. After calculation, the theoretical values of inertia when the rewind roll is empty and full are 0.0041 kg·m^2 and 0.0062 kg·m^2, respectively. Landau algorithm adaptive gain γ is 0.05 in the experiment. Because the identification process of inertia involves the division calculation, to prevent the arithmetic overflow in the early operation, the output limiter is adopted. As can be seen from Figure 7, the proposed identification method can converge to the theoretical value of inertia within two seconds.

In order to verify the parameters self-adaptive function of the proposed method, a series of comparative experiments are conducted. In some large industrial applications such as the steel rolling production line, the inertia changes generally substantially. It is necessary to correct the parameters of speed controllers based on the inertia. However, due to the limitations of the experimental platform in this paper, the inertia changes very slowly, and the effect is difficult to observe in one set of experiments. Therefore, in order to observe the effect of the algorithm clearly, the experiments are carried out in two stages that the unwind roll is empty and full, respectively. In the two cases of unchanged parameters and adaptive parameters, the reference linear velocity remains 1.0 m/s and the reference tension changes from 30 N to 110 N. Moreover, the reference tension remains 60 N, and the reference linear velocity changes from 0.5 m/s to 1.0 m/s. Experimental waveforms are shown in Figure 6. Since the observed inertias have yet to converge to the actual value during the start-up phase of the motor, the algorithm of adaptive parameters is not applied until the system goes through the start-up phase and reaches the steady state.

Figure 8(a) shows that since the PI parameters of speed controller are not self-adaptive in case of inertia variation, when the parameters are unchanged, a slight overshoot is generated when the unwind roll is in full volume. However, in Figure 8(b), because the parameters adapt themselves to the inertia variation, the waveform is basically the same whether the rewind roll is empty or full. Figures 8(c) and 8(d) show that when the unwind roll is empty, the changes of velocity have the same influence on tension whether the speed controller parameters are unchanged or adaptive. However, when the unwind roll is full, velocity changes have greater influence on the tension when the controller parameters are unchanged than when the controller parameters are adaptive, which demonstrates the effectiveness of the proposed method.

5. Conclusion

This paper proposes a novel tension control strategy which needs no additional hardware. A sensorless tension control strategy only using the speed signal obtained by the encoder and the current signal of the rewind motor is realized. The unwind motor is used to set the linear velocity, and the rewind motor is used to control the tension. With respect to the variation of the inertias caused by the radii of rewind and unwind rolls, Landau discrete adaptive algorithm is adopted in this paper, which overcomes the shortcomings of the conventional method to estimate the inertia that the

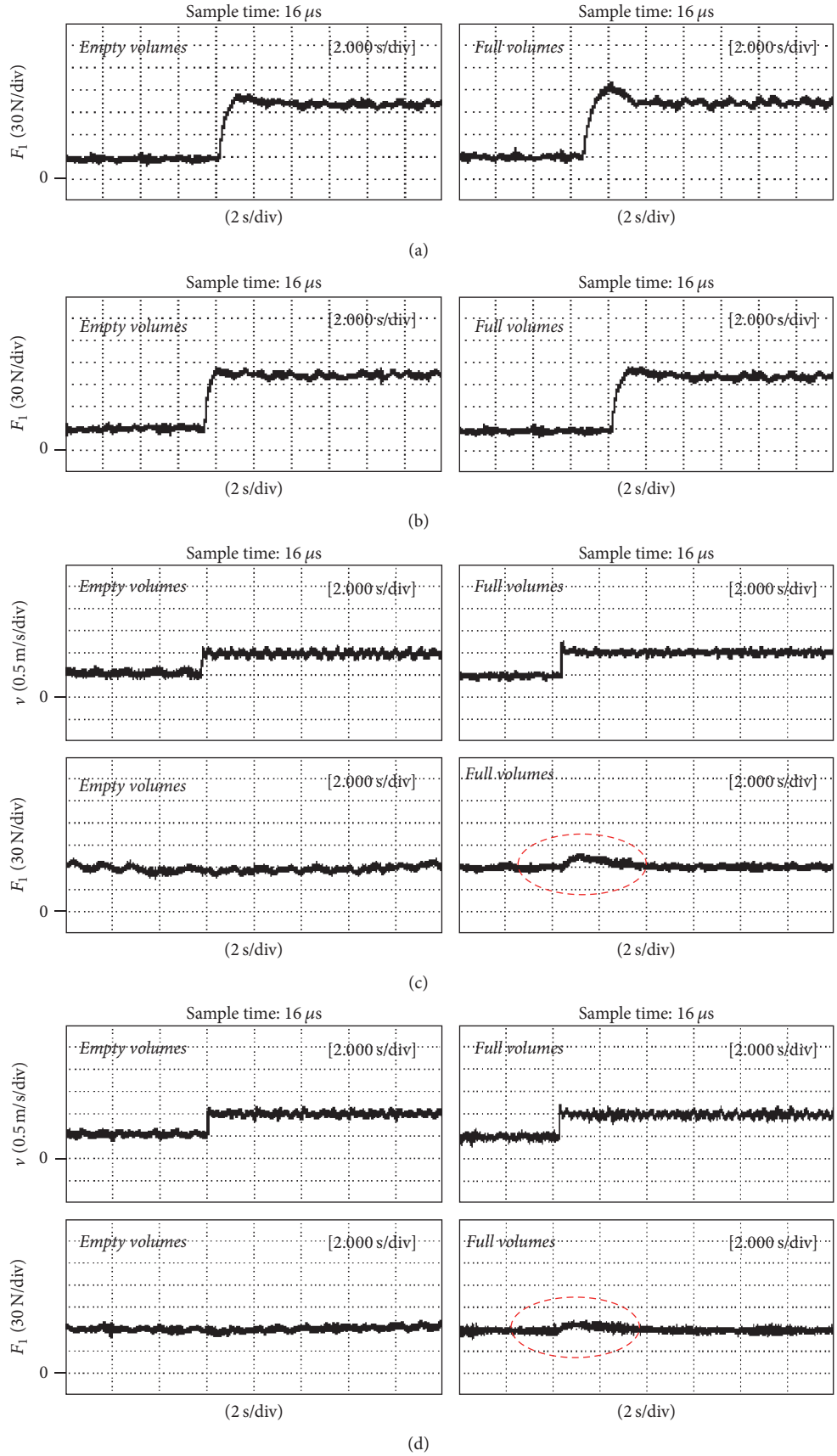

Figure 8: Adaptive controller parameters experiment when the tension and velocity mutation. (a) Tension mutation, parameters unchanged; (b) tension mutation, adaptive parameters; (c) velocity mutation, parameters unchanged; (d) velocity mutation, adaptive parameters.

knowledge of the density, thickness, and other information of the winding material is required. Moreover, the observed inertia is used to adjust the parameters of speed controllers online, which enables the tension control system to still maintain good dynamic performance even if the inertia changes dramatically. Experimental results demonstrate the feasibility of the program. The tension sensor is replaced by a tension observer in this paper, which reduces the cost, solves the problems that tension sensor cannot be ins f matalled in some special occasions, and avoids the quality degradation caused by the delay of sensors. In addition, the structure of the method is simple and easy to implement. Therefore, the proposed method proves to be of practical value in industrial applications.

Conflicts of Interest

The authors declare that there are no conflicts of interest regarding the publication of this paper.

Acknowledgments

This work was partially supported by National Natural Science Foundation of China (no. 51377121 and no. 51407127).

References

[1] N. Nevaranta, M. Niemela, J. Pyrhonen, O. Pyrhonen, and T. Lindh, "Indirect tension control method for an intermittent web transport system," in *Proceedings of the 15th International Power Electronics and Motion Control Conference and Exposition, EPE-PEMC 2012 ECCE Europe*, Novi Sad, Serbia, September 2012.

[2] C. Wang, Y. Wang, R. Yang, and H. Lu, "Research on precision tension control system based on neural network," *IEEE Transactions on Industrial Electronics*, vol. 51, no. 2, pp. 381–386, 2004.

[3] T. Shi, H. Liu, Q. Geng, and C. Xia, "Improved relative coupling control structure for multi-motor speed synchronous driving system," *IET Electric Power Applications*, vol. 10, no. 6, pp. 451–457, 2016.

[4] H. Koç, D. Knittel, M. De Mathelin, and G. Abba, "Modeling and robust control of winding systems for elastic webs," *IEEE Transactions on Control Systems Technology*, vol. 10, no. 2, pp. 197–208, 2002.

[5] C. Lee and K. Shin, "A Study on the Taper Tension Control Considering Telescoping in the Winding System," in *Proceedings of the 2007 IEEE Industry Applications Annual Meeting*, pp. 398–403, New Orleans, LA, USA, September 2007.

[6] F. He and Q. Wang, "Compensation and fuzzy control of tension in strip winding control system," in *Proceedings of the 2012 7th IEEE Conference on Industrial Electronics and Applications, ICIEA 2012*, pp. 22–27, Singapore, July 2012.

[7] S. Zhang, W. He, and S. Sam Ge, "Modeling and control of a nonuniform vibrating string under spatiotemporally varying tension and disturbance," *IEEE/ASME Transactions on Mechatronics*, vol. 17, no. 6, pp. 1196–1203, 2012.

[8] M. A. Valenzuela, J. M. Bentley, and R. D. Lorenz, "Sensorless tension control in paper machines," *IEEE Transactions on Industry Applications*, vol. 39, no. 2, pp. 294–304, 2003.

[9] R. Carrasco and M. A. Valenzuela, "Tension control of a two-drum winder using paper tension estimation," *IEEE Transactions on Industry Applications*, vol. 42, no. 2, pp. 618–628, 2006.

[10] M. A. Valenzuela, R. Carrasco, and D. Sbarbaro, "Robust sheet tension estimation for paper winders," *IEEE Transactions on Industry Applications*, vol. 44, no. 6, pp. 1937–1949, 2008.

[11] G. Ramírez, R. D. Lorenz, and M. A. Valenzuela, "Observer-based estimation of modulus of elasticity for papermaking process," *IEEE Transactions on Industry Applications*, vol. 50, no. 3, pp. 1678–1686, 2014.

[12] A. F. Lynch, S. A. Bortoff, and K. Röbenack, "Nonlinear tension observers for web machines," *Automatica*, vol. 40, no. 9, pp. 1517–1524, 2004.

[13] S.-H. Song and S.-K. Sul, "A new tension controller for continuous strip processing line," *IEEE Transactions on Industry Applications*, vol. 36, no. 2, pp. 633–639, 2000.

[14] S.-H. Song and S.-K. Sul, "Design and control of multispan tension simulator," *IEEE Transactions on Industry Applications*, vol. 36, no. 2, pp. 640–648, 2000.

[15] N. R. Abjadi, J. Soltani, J. Askari, and G. R. Arab Markadeh, "Nonlinear sliding-mode control of a multi-motor web-winding system without tension sensor," *IET Control Theory & Applications*, vol. 3, no. 4, pp. 419–427, 2009.

[16] K. Zhang, B. Jiang, X.-G. Yan, and Z. Mao, "Sliding mode observer based incipient sensor fault detection with application to high-speed railway traction device," *ISA Transactions®*, vol. 63, pp. 49–59, 2016.

[17] M. Mohamed, X.-G. Yan, S. K. Spurgeon, and B. Jiang, "Robust sliding-mode observers for large-scale systems with application to a multimachine power system," *IET Control Theory & Applications*, vol. 11, no. 8, pp. 1307–1315, 2017.

[18] D. Shin, W. Kim, and Y. Lee, "Observer based nonlinear tension control for multi motor wire winding system," in *Proceedings of the in Proceeds of 12th International Conference on Automation and Systems (ICCAS)*, pp. 1333–1336, JeJu Island, Oct 2012.

[19] Q. Liu, T. Chai, H. Wang, and S.-Z. J. Qin, "Data-based hybrid tension estimation and fault diagnosis of cold rolling continuous annealing processes," *IEEE Transactions on Neural Networks and Learning Systems*, vol. 22, no. 12, pp. 2284–2295, 2011.

[20] P. R. Pagilla, R. V. Dwivedula, and N. B. Siraskar, "A decentralized model reference adaptive controller for large-scale systems," *IEEE/ASME Transactions on Mechatronics*, vol. 12, no. 2, pp. 154–163, 2007.

[21] P. R. Pagilla, N. B. Siraskar, and R. V. Dwivedula, "Decentralized control of web processing lines," *IEEE Transactions on Control Systems Technology*, vol. 15, no. 1, pp. 106–117, 2005.

[22] R. Bettendorf, "Winder software testing with real-time dynamic simulation," *IEEE Transactions on Industrial Electronics*, vol. 52, no. 2, pp. 489–498, 2005.

[23] B. Zhou and G. Duan, "Solutions to the positive real control problem for linear systems via reduced-order observer," in *Proceedings of the 7th World Congress on Intelligent Control and Automation, WCICA'08*, pp. 4623–4627, Chongqing, China, June 2008.

[24] Y. Guo, L. Huang, and M. Muramatsu, "Research on inertia identification and auto-tuning of speed controller for AC servo system," in *Proceedings of the Power Conversion Conference-Osaka 2002, PCC-Osaka 2002*, pp. 896–901, Osaka, Japan, April 2002.

[25] I. D. Landau, *Adaptive Control*, Springer, Berlin, Germany, 1998.

[26] L. Harnefors, S. E. Saarakkala, and M. Hinkkanen, "Speed control of electrical drives using classical control methods," *IEEE Transactions on Industry Applications*, vol. 49, no. 2, pp. 889–898, 2013.

[27] C. Xia, B. Ji, T. Shi, and Y. Yan, "Two-degree-of-freedom proportional integral speed control of electrical drives with Kalman-filter-based speed estimation," *IET Electric Power Applications*, vol. 10, no. 1, pp. 18–24, 2015.

Hindawi
Mathematical Problems in Engineering
Volume 2018, Article ID 5149518, 10 pages
https://doi.org/10.1155/2018/5149518

Research Article

H_∞ Tracking Control of Fuzzy Dynamic Output for Nonlinear Networked System with Packet Dropouts

Yang Wang,[1] **Jinna Li**,[2] **and Xiaolei Ji**[1]

[1]*Department of Mathematics and Physics, Shenyang University of Chemical Technology, Shenyang, Liaoning 110142, China*
[2]*College of Information Engineering, Shenyang University of Chemical Technology, Shenyang, Liaoning 110142, China*

Correspondence should be addressed to Jinna Li; lijinna_721@126.com

Received 21 May 2017; Accepted 13 December 2017; Published 10 January 2018

Academic Editor: Wanquan Liu

The tracking control of H_∞ dynamic output feedback is proposed for the fuzzy networked systems of the same category, in which each system is discrete-time nonlinear and is missing measurable data. In other words, the loss of data packet occurs randomly in both the uplink and the downlink. The independent variables that are called the Bernoulli random variables are considered to design the loss of data packets. The method of parallel distributed compensation (PDC) in terms of the T-S fuzzy model is applied to investigate the dynamic controller of tracking control on the systems. Then, it is presented that the analytical H_∞ performance of the output error between the reference model and the fuzzy model for the closed-loop system containing dynamic output feedback controller is proven. Furthermore, the achieved sufficient conditions in terms of LMIs ensure that the closed-loop system is stochastically stable in the H_∞ sense. Finally, a numerical system is offered to show the effectiveness of the established technique.

1. Introduction

The fundamental problem of control application and its theory is the problem of control tracking [1, 2]. With the development of modern science and technology, the tracking control of network control systems (NCSs) has witnessed significant achievements in the past twenty years [3–6]. The problems of synthesis, analysis, and modeling of NCSs become more and more difficult with the introduction of communication networks. To tackle these challenges, for the singular systems of the same category in which the input and state were quantitated, the plan of an event-based H_∞ control was supposed in [7].

The tracking control of output, playing an important role in the industrial, economic, and biological control processes, which is known as the control of reference model, can approximate the reference output of a given model. In some fields, the tracking control of output is employed far and wide, such as motors [8, 9], robots [10], and flights [11]. Based on the tracking control of output, many preliminary studies have been produced [12–15]. Papers [6, 16–18] proposed some questions about stability, and some scholars proposed some thinking about H_∞ control [19] as well as the problem of designing about the filter in the literature [20]. As a result of the increased complicacies of the systems, nonlinear characteristics occur randomly in reality. Furthermore, the aforementioned methods for linear networked control systems cannot be used more directly. In the light of nonlinear characteristics, a few classes of advanced techniques containing sliding mode control [21], adaptive control [22, 23], and fuzzy control [24, 25] were applied. The tracking control of network control system involves some nonlinear factors, such as bandwidth constraints, packet dropouts, and network delays. Then, the designing and analysis of the system become more difficult and complex. In general, T-S [26] fuzzy model can approximate to the smooth nonlinear system as much as possible and in fuzzy system theories we can use the developed technology to research nonlinear systems. It can be seen that the T-S fuzzy model has been successfully applied in a large number of realistic nonlinear systems from literature [27–29]. Between the controlled output and external input, literatures [30–32] describe that the H_∞ control minimizes the gain of energy. In the tracking control of H_∞ output, the system that contains nonlinear perturbations and time-varying delay is studied by Zhang and Yu [33]. In the case of packet loss and time delay, at home and abroad, the scholars

are researching the problem about the performance analysis of the network control system with H_∞ output tracking and the design issues of controller [34]. In literatures [35, 36], the faulty links of communication are often described by the Markov chain and the distribution of Bernoulli random variables. In literature [37], under the links of imperfect communication, the feedback control of H_∞ output has been studied for the systems of the same category. However, it should be pointed out that the above researches do not take fully into account the links of faulty communication and a complete message of the state vector, which is the critical shortcoming of the state-feedback controller when put into effect in reality. In [38], the design of tracking control is investigated by applying IT2 T-S method and it is employed to a classical practical application which is called mass-spring-damping system. Moreover, the authors researched the presented issue for nonlinear structures in view of the fuzzy observer as well as the influence of unknown state variables and data loss in Ethernet transmission. However, they did not take into account the dynamic output feedback controller in the systems. Therefore, our idea is that for the nonlinear tracking systems of discrete time with packet loss consisting in both the downlink and the uplink a dynamic output feedback controller is designed and the parallel distributed compensation (PDC) using T-S fuzzy model is constructed to tackle nonlinearity.

In this paper, the tracking control of H_∞ dynamic output feedback is suggested for the fuzzy networked systems with missing data. The independent variables which are called the Bernoulli random variables are considered to design the loss of data packets when it occurs randomly in both the uplink and the downlink. The method of parallel distributed compensation (PDC) in terms of the T-S fuzzy model is employed to plan the dynamic output controller of tracking control. Then, the analysis of H_∞ performance for the closed-loop system containing dynamic controller is presented. Furthermore, the sufficient conditions in terms of LMIs guarantee that the closed-loop system is stochastically stable in the sense of H_∞ performance.

The rest of this article is as follows. Under data missing, the researched problem of H_∞ tracking control for the fuzzy networked systems of the same species is formulated in Section 2. It is presented that the designing of fuzzy dynamic output controller and the performance analysis of H_∞ output tracking are the main results in Section 3. Section 4 gives a numerical example and in Section 5 we put forward the conclusion of paper.

Notation. In this paper, the notation applied is comparatively standard. The matrix transposition is stood for by superscript "T" and the space of n-dimensional Euclidean is denoted by R^n. Zero matrix and the identity matrix are signified by 0 and I, respectively. The symbol $*$ is employed to denote the symmetry term in the expressions of complex matrix and symmetric block matrices, and $P \geq 0$ stands for P being real symmetric and positive definite (semidefinite). The space of square-integrable vector over $[0, \infty)$ is suggested by $l2[0, \infty)$. $\|M\| = \sqrt{\mathrm{tr}(M^T M)}$ shows matrix norm. $|\cdot|$ shows the norm of Euclidean vector and the norm of $l2[0, \infty)$ is defined by $\|\cdot\|_2$. The notation $E\{\alpha\}$ indicates the expectation of the event α. $E\{\alpha/\beta\}$ indicates the expectation of the event α conditional on the event β. It is assumed that the matrices in this paper have compatible dimensions if the dimensions are not demonstrably prescribed.

2. Problem Formulation

Firstly, we consider the T-S fuzzy model. It is a discrete-time nonlinear system with data missing. The overall fuzzy model is described by fuzzy aggregation of the linear models.

2.1. T-S Fuzzy Model. The i-th rule of the T-S is the following:

Model Rule i:

$$\begin{aligned} \text{If} \quad & z_1(t) \text{ is } M_{i1}, \ldots, z_g(t) \text{ is } M_{ig} \\ \text{Then} \quad & x(t+1) = A_i x(t) + B_i u(t) + E_i \varpi(t), \\ & r(t) = C_{1i} x(t) + D_i u(t) + F_i \varpi(t), \\ & y(t) = C_{2i} x(t), \\ & \qquad (i = 1, 2, \ldots, r), \end{aligned} \tag{1}$$

where M_{id} $(d = 1, 2, \ldots, g)$ is the fuzzy set associated with the i-th model rule and d-th premise variable component; $x(t) \in R^{n_x \times 1}$ denotes the state vector; $u(t) \in R^{n_u \times 1}$ denotes the control input vector; $y(t) \in R^{n_y \times 1}$ denotes the vector of measured output; $r(t) \in R^{n_r \times 1}$ denotes the vector of controlled output; $\varpi(t) \in l2[0, \infty)$ are external disturbances and $\varpi(t) \in R^{n_\varpi \times 1}$. A_i, B_i, E_i, D_i, F_i, C_{1i}, and C_{2i} are local system matrices with appropriate dimensions. $z(t) = [z_1(t) \cdots z_g(t)]^T$ are known premise variables. The scalar r is the number of rules. The final fuzzy system is listed:

$$\begin{aligned} x(t+1) &= \sum_{i=1}^{r} h_i \left[A_i x(t) + B_i u(t) + E_i \varpi(t) \right], \\ r(t) &= \sum_{i=1}^{r} h_i \left[C_{1i} x(t) + D_i u(t) + F_i \varpi(t) \right], \\ y(t) &= \sum_{i=1}^{r} h_i C_{2i} x(t), \end{aligned} \tag{2}$$

where for all t we suppose the following: $h_i(z(t)) = \omega_i(z(t)) / \sum_{i=1}^{r} \omega_i(z(t))$, $\omega_i(z(t)) = \prod_{d=1}^{g} M_{id}(z_d(t))$, $\omega_i(z(t)) \geq 0$, $\sum_{i=1}^{r} \omega_i(z(t)) > 0$, $\sum_{i=1}^{r} h_i(z(t)) = 1$, and $h_i(z(t)) \geq 0$ $(i = 1, 2, \ldots, r)$. In what follows, we write $h_i \triangleq h_i(z(t))$ for brevity.

The designing of fuzzy dynamic output controller is our objective. In this way, the output $r(t)$ of the controlled model can track the signal $r_r(t)$ of reference model to satisfy the performance of the required tracking. Assume the reference model as follows:

$$\begin{aligned} x_r(t+1) &= \sum_{i=1}^{r} h_i \left[G_i^r x_r(t) + B_i^r \sigma(t) \right], \\ r_r(t) &= \sum_{i=1}^{r} h_i \left[H_i^r x_r(t) + L_i^r \sigma(t) \right], \end{aligned}$$

$$y_r(t) = \sum_{i=1}^{r} h_i M_i^r x(t), \tag{3}$$

where $x_r(t) \in R^{n_x \times 1}$ is the state of reference model; $r_r(t) \in R^{n_r \times 1}$ is the controlled output of reference model; $y_r(t) \in R^{n_y \times 1}$ is the measured output of reference model; $\sigma(t) \in R^{n_\varpi \times 1}$ is the input of bounded reference energy; G_i^r (Hurwitz), B_i^r, H_i^r, L_i^r, and M_i^r are constant matrices with appropriate dimensions.

From (2) and (3), the augmented error system is as follows:

$$\begin{aligned}
\xi(t+1) &= \sum_{i=1}^{r} h_i \left[\widetilde{A}_i \xi(t) + \widetilde{B}_i u(t) + \widetilde{E}_i \nu(t)\right], \\
e(t) &= r(t) - r_r(t) \\
&= \sum_{i=1}^{r} h_i \left[\widetilde{C}_{1i} \xi(t) + \widetilde{D}_i u(t) + \widetilde{F}_i \nu(t)\right], \\
\overline{e}(t) &= y(t) - y_r(t) = \sum_{i=1}^{r} h_i \widetilde{C}_{2i} \xi(t),
\end{aligned} \tag{4}$$

where

$$\begin{aligned}
\xi(t) &= \begin{bmatrix} x(t) \\ x_r(t) \end{bmatrix}, \\
\nu(t) &= \begin{bmatrix} \varpi(t) \\ \sigma(t) \end{bmatrix}, \\
\widetilde{A}_i &= \begin{bmatrix} A_i & 0 \\ 0 & G_i^r \end{bmatrix}, \\
\widetilde{B}_i &= \begin{bmatrix} B_i \\ 0 \end{bmatrix}, \\
\widetilde{E}_i &= \begin{bmatrix} E_i & 0 \\ 0 & B_i^r \end{bmatrix}, \\
\widetilde{C}_{1i} &= \begin{bmatrix} C_{1i} & -H_i^r \end{bmatrix}, \\
\widetilde{D}_i &= D_i, \\
\widetilde{F}_i &= \begin{bmatrix} F_i & -L_i^r \end{bmatrix}, \\
\widetilde{C}_{2i} &= \begin{bmatrix} C_{2i} & -M_i^r \end{bmatrix}.
\end{aligned} \tag{5}$$

2.2. Fuzzy Dynamic Output Feedback Controller Design. Based on the T-S fuzzy model (4), in this paper, we construct the following dynamical output feedback controller:

Rule C_i:

$$\begin{aligned}
&\text{If} \quad z_1(t) \text{ is } M_{i1}, \ldots, z_g(t) \text{ is } M_{ig} \\
&\text{Then} \quad \eta_c(t+1) = A_i^c \eta_c(t) + B_i^c e^c(t), \\
&\qquad\quad u^c(t) = C_i^c \eta_c(t),
\end{aligned} \tag{6}$$

where $\eta_c(k) \in R^{n_\eta \times 1}$ is the state vector of the controller; $e^c(t) \in R^{n_e \times 1}$ is the input vector of the controller; $u^c(t) \in R^{n_u \times 1}$ is the output vector of the controller; A_i^c, B_i^c, and C_i^c are matrices with appropriate dimensions. Then

$$\begin{aligned}
\eta_c(t+1) &= \sum_{i=1}^{r} h_i \left[A_i^c \eta_c(t) + B_i^c e^c(t)\right], \\
u^c(t) &= \sum_{i=1}^{r} h_i C_i^c \eta_c(t).
\end{aligned} \tag{7}$$

2.3. Unreliable Communication Links. It can be seen that the model is with the links of communication network from Figure 1. In this paper, we consider that a few elements are introduced via network and the loss of data packets occurs randomly in both the uplink and the downlink. Thus $\overline{e}(t) \neq e^c(t)$ and $u^c(t) \neq u(t)$. We represent the above phenomenon by applying a stochastic method and it is described as follows:

$$\begin{aligned}
e^c(t) &= \alpha(t)\, \overline{e}(t), \\
u(t) &= \beta(t)\, u^c(t),
\end{aligned} \tag{8}$$

where $\{\alpha(t)\}$ and $\{\beta(t)\}$ satisfy the process of Bernoulli random distribution. $\{\alpha(t)\}$ presents the downlink of unreliable communication and $\{\beta(t)\}$ describes the uplink. Assume $\{\alpha(t)\}$ and $\{\beta(t)\}$ as follows:

$$\begin{aligned}
&\text{prob}\{\alpha(t) = 1\} = E\{\alpha(t)\} = \overline{\alpha}, \\
&\text{prob}\{\alpha(t) = 0\} = 1 - \overline{\alpha}, \\
&\text{prob}\{\beta(t) = 1\} = E\{\beta(t)\} = \overline{\beta}, \\
&\text{prob}\{\beta(t) = 0\} = 1 - \overline{\beta}.
\end{aligned} \tag{9}$$

According to (8), we obtain

$$\begin{aligned}
\eta_c(t+1) &= \sum_{i=1}^{r} h_i \left[A_i^c \eta_c(t) + \alpha(t) B_i^c \overline{e}(t)\right], \\
u^c(t) &= \sum_{i=1}^{r} h_i C_i^c \eta_c(t).
\end{aligned} \tag{10}$$

Combining (4) and (10), one has the augmented closed-loop system:

$$\begin{aligned}
\overline{\xi}(t+1) &= \sum_{i=1}^{r} \sum_{j=1}^{r} h_i h_j \left[A_{ij} \overline{\xi}(t) + \Xi_i \nu(t)\right], \\
e(t) &= \sum_{i=1}^{r} \sum_{j=1}^{r} h_i h_j \left[C_{ij} \overline{\xi}(t) + \widetilde{F}_i \nu(t)\right],
\end{aligned} \tag{11}$$

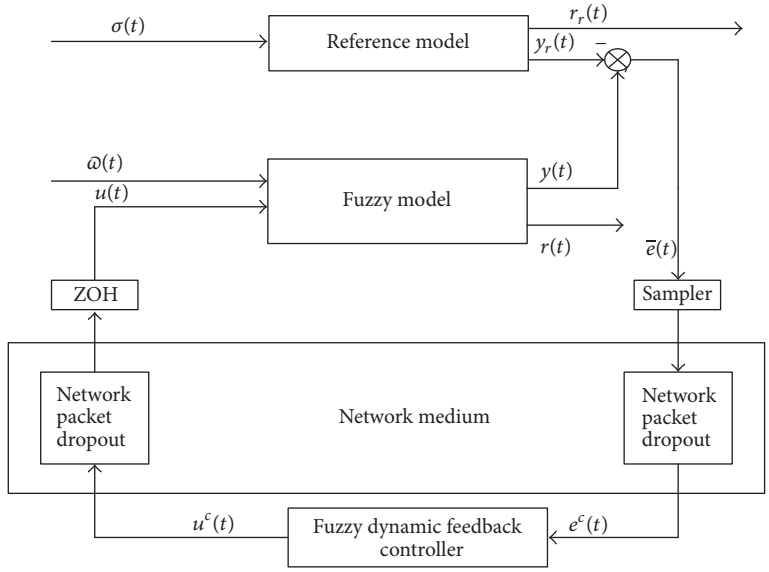

Figure 1: Plant flow chart.

where

$$A_{ij} = \begin{bmatrix} \widetilde{A}_i & \beta(t)\widetilde{B}_i C_j^c \\ \alpha(t) B_j^c \widetilde{C}_{2i} & A_j^c \end{bmatrix},$$
$$\Xi_i = \begin{bmatrix} \widetilde{E}_i \\ 0 \end{bmatrix},$$
$$C_{ij} = \begin{bmatrix} \widetilde{C}_{1i} & \beta(k)\widetilde{D}_i C_j^c \end{bmatrix}, \tag{12}$$
$$\overline{\xi}(t) = \begin{bmatrix} \xi(t) \\ \eta_c(t) \end{bmatrix}.$$

Assume that

$$\alpha(t) = \overline{\alpha} + \widetilde{\alpha}(t),$$
$$\beta(t) = \overline{\beta} + \widetilde{\beta}(t); \tag{13}$$

then

$$E\{\widetilde{\alpha}(t)\widetilde{\alpha}(t)\} = \overline{\alpha}(1-\overline{\alpha}),$$
$$E\left\{\widetilde{\beta}(t)\widetilde{\beta}(t)\right\} = \overline{\beta}\left(1-\overline{\beta}\right). \tag{14}$$

In this paper, we design the output feedback controller to ensure the stochastic stability of closed-loop system which fulfills the performance of external disturbance attenuation. Therefore, the definition is as follows.

Definition 1 (see [39]). Any initial condition is considered $\overline{\xi}(0)$. Under $\nu(t) \equiv 0$, if there exists a matrix $W > 0$, then $E\{\sum_{t=0}^{\infty} |\overline{\xi}(t)|^2|_{\overline{\xi}(0)}\} < \overline{\xi}^T(0) W \overline{\xi}(0)$, and the closed-loop system (11) is stochastically stable.

Then, in this paper, the problem that is dealt with is drawn up as follows: the augmented system in (11) is asymptotically stable with $\nu(t) \equiv 0$ and satisfies

$$E\left\{\sum_{t=0}^{\infty} |e(t)|^2\right\} \le \gamma^2 \|\nu\|_2^2, \tag{15}$$

where $\gamma > 0$; then the H_∞ performance γ of output tracking is obtained.

3. Main Results

Two parts of results are included in this section, containing the conditions of designing controller and the criteria of sufficient stability.

Theorem 2. *Consider the model of the augmented fuzzy system (11). With the supposed matrices A_j^c, B_j^c, and C_j^c ($j = 1, \ldots, r$) of the controller gain, the system of closed-loop fuzzy model in (11) is stochastically stable and fulfills H_∞ performance γ of external disturbance attenuation, if there exist matrices p_l ($l = 1, \ldots, r$), fulfilling the following inequality:*

$$\left(A_{ij}^1\right)^T P_l A_{ij}^1 + \left(A_{ij}^2\right)^T P_l A_{ij}^2 - P_i < 0, \tag{16}$$

$$\begin{bmatrix} -I & 0 & 0 & 0 & C_{ij}^1 & \widetilde{F}_i \\ 0 & -I & 0 & 0 & C_{ij}^2 & 0 \\ 0 & 0 & -P_l^{-1} & 0 & A_{ij}^1 & \Xi_i \\ 0 & 0 & 0 & -P_l^{-1} & A_{ij}^2 & 0 \\ * & * & * & * & -P_i & 0 \\ * & * & * & * & 0 & -\gamma^2 I \end{bmatrix} < 0, \tag{17}$$

where

$$A_{ij}^{1}=\begin{bmatrix}\widetilde{A}_i & \overline{\beta}\widetilde{B}_iC_j^c\\ \overline{\alpha}B_j^c\widetilde{C}_{2i} & A_j^c\end{bmatrix},$$
$$A_{ij}^{2}=\begin{bmatrix}0 & \sqrt{\overline{\beta}\left(1-\overline{\beta}\right)}\widetilde{B}_iC_j^c\\ \sqrt{\overline{\alpha}\left(1-\overline{\alpha}\right)}B_j^c\widetilde{C}_{2i} & 0\end{bmatrix},\quad (18)$$
$$C_{ij}^{1}=\left[\widetilde{C}_{1i}\ \ \overline{\beta}\widetilde{D}_iC_j^c\right],$$
$$C_{ij}^{2}=\left[0\ \ \sqrt{\overline{\beta}\left(1-\overline{\beta}\right)}\widetilde{D}_iC_j^c\right].$$

Proof. Defining $\nu(t)\equiv 0$, the stochastic stability of system (11) is proven. For system (11), the following Lyapunov function is chosen:

$$V(t)=\overline{\xi}^{T}(t)\left[\sum_{i=1}^{r}h_iP_i\right]\overline{\xi}(t),\quad (19)$$

where $P_i>0$; supposing that $h_l^{+}=h_l^{+}(z(t+1))$, we have

$$\begin{aligned}E\{\Delta V(t)\}&=E\left\{V(t+1)|\,\overline{\xi}(t)\right\}-V(t)=E\left\{\overline{\xi}^{T}(t)\right.\\&\cdot\sum_{l=1}^{r}h_l^{+}\left[\sum_{i=1}^{r}\sum_{j=1}^{r}\sum_{s=1}^{r}\sum_{t=1}^{r}h_ih_jh_sh_t\left(A_{ij}{}^{T}P_lA_{st}\right)\right]\overline{\xi}(t)\Bigg\}\\&-\overline{\xi}^{T}(t)\left[\sum_{i=1}^{r}h_iP_i\right]\overline{\xi}(t)\le\overline{\xi}^{T}(t)\sum_{l=1}^{r}h_l^{+}\\&\cdot\sum_{i=1}^{r}\sum_{j=1}^{r}h_ih_j\left[\left(A_{ij}^{1}\right)^{T}P_lA_{ij}^{1}+\left(A_{ij}^{2}\right)^{T}P_lA_{ij}^{2}\right]\overline{\xi}(t)\\&-\overline{\xi}^{T}(t)\left[\sum_{i=1}^{r}h_iP_i\right]\overline{\xi}(t)=\overline{\xi}^{T}(t)\sum_{l=1}^{r}h_l^{+}\\&\cdot\sum_{i=1}^{r}\sum_{j=1}^{r}h_ih_j\left[\left(A_{ij}^{1}\right)^{T}P_lA_{ij}^{1}+\left(A_{ij}^{2}\right)^{T}P_lA_{ij}^{2}-P_i\right]\overline{\xi}(t).\end{aligned}\quad (20)$$

Let

$$\begin{aligned}&\Psi\\&=\sum_{l=1}^{r}h_l^{+}\sum_{i=1}^{r}\sum_{j=1}^{r}h_ih_j\left[\left(A_{ij}^{1}\right)^{T}P_lA_{ij}^{1}+\left(A_{ij}^{2}\right)^{T}P_lA_{ij}^{2}-P_i\right].\end{aligned}\quad (21)$$

From

$$\begin{aligned}\lambda_{\min}(-\Psi)\left|\overline{\xi}(t)\right|^{2}&\le\overline{\xi}^{T}(t)(-\Psi)\overline{\xi}(t)\\&\le\lambda_{\max}(-\Psi)\left|\overline{\xi}(t)\right|^{2}\end{aligned}\quad (22)$$

we obtain

$$\begin{aligned}&E\left\{\overline{\xi}^{T}(t+1)\left[\sum_{l=1}^{r}h_l^{+}P_l\right]\overline{\xi}(t+1)\right\}\\&-\overline{\xi}^{T}(t)\left[\sum_{i=1}^{r}h_iP_i\right]\overline{\xi}(t)\\&\le-\lambda_{\min}(-\Psi)\overline{\xi}^{T}(t)\overline{\xi}(t).\end{aligned}\quad (23)$$

From $t=0,1,\ldots,k$ and $k\ge 1$, for the above inequality, calculating and summing mathematical expectation, we can have

$$\begin{aligned}&E\left\{\overline{\xi}^{T}(k+1)\left[\sum_{l=1}^{r}h_l^{+}P_l\right]\overline{\xi}(k+1)\right\}\\&-\overline{\xi}^{T}(0)\left[\sum_{i=1}^{r}h_iP_i\right]\overline{\xi}(0)\\&\le-\lambda_{\min}(-\Psi)E\left\{\sum_{t=0}^{k}\left|\overline{\xi}(t)\right|^{2}\right\}.\end{aligned}\quad (24)$$

Then, when $k=1,\ldots,\infty$ and given $E\{\overline{\xi}^{T}(\infty)[\sum_{l=1}^{r}h_l^{+}P_l]\overline{\xi}(\infty)\}\ge 0$, we obtain

$$\begin{aligned}E\left\{\sum_{t=0}^{k}\left|\overline{\xi}(t)\right|^{2}\right\}&\le\left(\lambda_{\min}(-\Psi)\right)^{-1}\\&\cdot\left\{\overline{\xi}^{T}(0)\left[\sum_{i=1}^{r}h_iP_i\right]\overline{\xi}(0)\right.\\&\left.-E\left\{\overline{\xi}^{T}(k+1)\left[\sum_{l=1}^{r}h_l^{+}P_l\right]\overline{\xi}(k+1)\right\}\right\}\\&\le\left(\lambda_{\min}(-\Psi)\right)^{-1}\overline{\xi}^{T}(0)\left[\sum_{i=1}^{r}h_iP_i\right]\overline{\xi}(0)=\overline{\xi}^{T}(0)\\&\cdot\left[\left(\lambda_{\min}(-\Psi)\right)^{-1}\sum_{i=1}^{r}h_iP_i\right]\overline{\xi}(0).\end{aligned}\quad (25)$$

Let $W\triangleq(\lambda_{\min}(-\Psi))^{-1}\sum_{i=1}^{r}h_iP_i$; we obtain $\Psi<0$ and $W>0$. Therefore, we acquire that system (11) is stochastically stable in terms of Definition 1.

The following section will introduce the H_∞ performance of external disturbance attenuation when the initial condition is zero. The H_∞ index is as follows:

$$\begin{aligned}J&\triangleq E\left\{e^{T}(t)\,e(t)\big|_{\Theta(t)}\right\}-\gamma^{2}\nu^{T}(t)\,\nu(t)\\&+E\left\{V(t+1)|_{\Theta(t)}\right\}-V(t).\end{aligned}\quad (26)$$

Let $\Theta(k)=\left[\begin{smallmatrix}\overline{\xi}(k)\\ \nu(k)\end{smallmatrix}\right]$; then, we obtain

$$
\begin{aligned}
J &\triangleq E\left\{V(t+1)|_{\Theta(t)}\right\} - V(t) + E\left\{e^T(t)\,e(t)\Big|_{\Theta(t)}\right\} - \gamma^2\nu^T(t)\,\nu(t) = E\left\{\Theta^T(t)\sum_{l=1}^{r}h_l^+\right.\\
&\left.\cdot\sum_{i=1}^{r}\sum_{j=1}^{r}\sum_{s=1}^{r}\sum_{t=1}^{r}h_ih_jh_sh_t\left(\begin{bmatrix}A_{ij} & \Xi_i\end{bmatrix}^T P_l\begin{bmatrix}A_{st} & \Xi_s\end{bmatrix}\right)\Theta(t)\right\} - \gamma^2\nu^T(t)\,\nu(t) - \bar{\xi}^T(t)\left[\sum_{i=1}^{r}h_iP_i\right]\bar{\xi}(t) + E\left\{\Theta^T(t)\right.\\
&\left.\cdot\sum_{i=1}^{r}\sum_{j=1}^{r}\sum_{s=1}^{r}\sum_{t=1}^{r}h_ih_jh_sh_t\left(\begin{bmatrix}C_{ij} & \widetilde{F}_i\end{bmatrix}^T\begin{bmatrix}C_{st} & \widetilde{F}_s\end{bmatrix}\right)\Theta(t)\right\} = \Theta^T(t)\sum_{l=1}^{r}h_l^+\\
&\cdot\sum_{i=1}^{r}\sum_{j=1}^{r}\sum_{s=1}^{r}\sum_{t=1}^{r}h_ih_jh_sh_t\begin{bmatrix}\left(A_{ij}^1\right)^T P_lA_{st}^1 + \left(A_{ij}^2\right)^T P_lA_{st}^2 & \left(A_{ij}^1\right)^T P_l\Xi_s\\ \Xi_i^TP_lA_{st}^1 & \Xi_i^TP_l\Xi_s\end{bmatrix}\Theta(t) - \Theta^T(t)\sum_{i=1}^{r}h_i\begin{bmatrix}P_i & 0\\ 0 & \gamma^2I\end{bmatrix}\Theta(t) + \Theta^T(t)\sum_{l=1}^{r}h_l^+\\
&\cdot\sum_{i=1}^{r}\sum_{j=1}^{r}\sum_{s=1}^{r}\sum_{t=1}^{r}h_ih_jh_sh_t\begin{bmatrix}\left(C_{ij}^1\right)^T C_{st}^1 + \left(C_{ij}^2\right)^T C_{st}^2 & \left(C_{ij}^1\right)^T\widetilde{F}_s\\ \widetilde{F}_i^TC_{st}^1 & \widetilde{F}_i^T\widetilde{F}_s\end{bmatrix}\Theta(t) \le \Theta^T(t)\sum_{l=1}^{r}h_l^+ \qquad (27)\\
&\cdot\sum_{i=1}^{r}\sum_{j=1}^{r}h_ih_j\begin{bmatrix}\left(A_{ij}^1\right)^T P_lA_{ij}^1 + \left(A_{ij}^2\right)^T P_lA_{ij}^2 & \left(A_{ij}^1\right)^T P_l\Xi_i\\ \Xi_i^TP_lA_{ij}^1 & \Xi_i^TP_l\Xi_i\end{bmatrix}\Theta(t) - \Theta^T(t)\sum_{i=1}^{r}h_i\begin{bmatrix}P_i & 0\\ 0 & \gamma^2I\end{bmatrix}\Theta(t) + \Theta^T(t)\sum_{l=1}^{r}h_l^+\\
&\cdot\sum_{i=1}^{r}\sum_{j=1}^{r}h_ih_j\begin{bmatrix}\left(C_{ij}^1\right)^T C_{ij}^1 + \left(C_{ij}^2\right)^T C_{ij}^2 & \left(C_{ij}^1\right)^T\widetilde{F}_i\\ \widetilde{F}_i^TC_{ij}^1 & \widetilde{F}_i^T\widetilde{F}_i\end{bmatrix}\Theta(t) = \Theta^T(t)\sum_{l=1}^{r}h_l^+\\
&\cdot\sum_{i=1}^{r}\sum_{j=1}^{r}h_ih_j\left\{\begin{bmatrix}\left(A_{ij}^1\right)^T P_lA_{ij}^1 + \left(A_{ij}^2\right)^T P_lA_{ij}^2 & \left(A_{ij}^1\right)^T P_l\Xi_i\\ \Xi_i^TP_lA_{ij}^1 & \Xi_i^TP_l\Xi_i\end{bmatrix} + \begin{bmatrix}\left(C_{ij}^1\right)^T C_{ij}^1 + \left(C_{ij}^2\right)^T C_{ij}^2 & \left(C_{ij}^1\right)^T\widetilde{F}_i\\ \widetilde{F}_i^TC_{ij}^1 & \widetilde{F}_i^T\widetilde{F}_i\end{bmatrix} - \begin{bmatrix}P_i & 0\\ 0 & \gamma^2I\end{bmatrix}\right\}\\
&\cdot\Theta(t) = \Theta^T(t)\sum_{l=1}^{r}h_l^+\sum_{i=1}^{r}\sum_{j=1}^{r}h_ih_j\left\{\begin{bmatrix}C_{ij}^1 & \widetilde{F}_i\\ C_{ij}^2 & 0\end{bmatrix}^T\begin{bmatrix}C_{ij}^1 & \widetilde{F}_i\\ C_{ij}^2 & 0\end{bmatrix} + \begin{bmatrix}A_{ij}^1 & \Xi_i\\ A_{ij}^2 & 0\end{bmatrix}^T\begin{bmatrix}P_l & 0\\ 0 & P_l\end{bmatrix}\begin{bmatrix}A_{ij}^1 & \Xi_i\\ A_{ij}^2 & 0\end{bmatrix} - \begin{bmatrix}P_i & 0\\ 0 & \gamma^2I\end{bmatrix}\right\}\Theta(t).
\end{aligned}
$$

From Schur complement, according to (17), we can obtain $J \le 0$ and $E\{\sum_{t=0}^{\infty}|e(t)|^2\} \le \gamma^2\|\nu\|_2^2$.

The proof is finished. □

4. Simulation Results

A numerical example is applied to explain the validity of the proposed method in the following section of this paper. Consider the following systems:

Model Rule i:

$$
\begin{aligned}
&\text{If} \quad x_i(t) \text{ is } h_i\left(x_i(t)\right) \quad i = 1, 2.\\
&\text{Then} \quad x(t+1) = A_ix(t) + B_iu(t) + E_i\varpi(t),\\
&\qquad r(t) = C_{1i}x(t) + D_iu(t) + F_i\varpi(t),\\
&\qquad y(t) = C_{2i}x(t),
\end{aligned} \qquad (28)
$$

where

$$
\begin{aligned}
A_1 &= \begin{bmatrix}-0.4618 & 0.8913;\ -0.6137 & 1.2153\end{bmatrix};\\
A_2 &= \begin{bmatrix}-0.0146 & -1.1552;\ 1.0101 & 0.3005\end{bmatrix};\\
B_1 &= \begin{bmatrix}0.5857 & 1.5251\end{bmatrix};\\
B_2 &= \begin{bmatrix}2.2415 & 2.9953\end{bmatrix};\\
E_1 &= \begin{bmatrix}-0.0099 & 0.0258\end{bmatrix};\\
E_2 &= \begin{bmatrix}-0.0623 & 0.0774\end{bmatrix};\\
F_1 &= 0.0023;\\
F_2 &= 0.0290;\\
C_{11} &= \begin{bmatrix}-1.0789 & 0\end{bmatrix};\\
C_{21} &= \begin{bmatrix}0.9962 & 0\end{bmatrix};\\
D_1 &= -1;\\
C_{12} &= \begin{bmatrix}0.0585 & 0\end{bmatrix};\\
C_{22} &= \begin{bmatrix}0.4795 & 0\end{bmatrix};\\
D_2 &= 1.
\end{aligned} \qquad (29)
$$

The corresponding reference model is assumed as follows:

$$\begin{aligned} x_r(t+1) &= G_i^r x_r(t) + B_i^r \sigma(t), \\ r_r(t) &= H_i^r x_r(t) + L_i^r \sigma(t), \\ y_r(t) &= M_i^r x(t), \end{aligned} \tag{30}$$

where

$$\begin{aligned} G_1^r &= -0.02; \\ B_1^r &= 0.5; \\ H_1^r &= -0.3; \\ L_1^r &= 0.5; \\ M_1^r &= -0.15; \\ G_2^r &= 0.1; \\ B_2^r &= 0.2; \\ H_2^r &= 0.03; \\ L_2^r &= -0.35; \\ M_2^r &= 0.135. \end{aligned} \tag{31}$$

The corresponding form of controller is expressed as follows:

$$\begin{aligned} \eta_c(t+1) &= A_i^c \eta_c(t) + B_i^c e^c(t), \\ u^c(t) &= C_i^c \eta_c(t). \end{aligned} \tag{32}$$

When the minimum value of γ is $\gamma = 0.6039$, $\text{prob}\{\alpha(t) = 1\} = 0.95$, and $\text{prob}\{\beta(t) = 1\} = 0.85$, the gains of controller are as follows:

$$\begin{aligned} A_1^C &= \begin{bmatrix} 0.0144 & 0.0452 & -0.0090 \\ 0.0461 & 0.1613 & -0.0242 \\ 0.0066 & -0.0245 & -0.0159 \end{bmatrix}, \\ A_2^C &= \begin{bmatrix} -0.0023 & -0.0180 & 0.0019 \\ 0.0022 & -0.0423 & -0.0004 \\ -0.0039 & 0.0156 & 0.0021 \end{bmatrix}, \\ B_1^C &= \begin{bmatrix} 0.0518 \\ 0.2082 \\ -0.0842 \end{bmatrix}, \\ B_2^C &= \begin{bmatrix} 0.1035 \\ 0.2613 \\ 0.0835 \end{bmatrix}, \\ C_1^C &= \begin{bmatrix} 0.0045 & 0.0133 & -0.0037 \end{bmatrix}, \\ C_2^C &= \begin{bmatrix} -0.0016 & -0.0043 & 0.0014 \end{bmatrix}. \end{aligned} \tag{33}$$

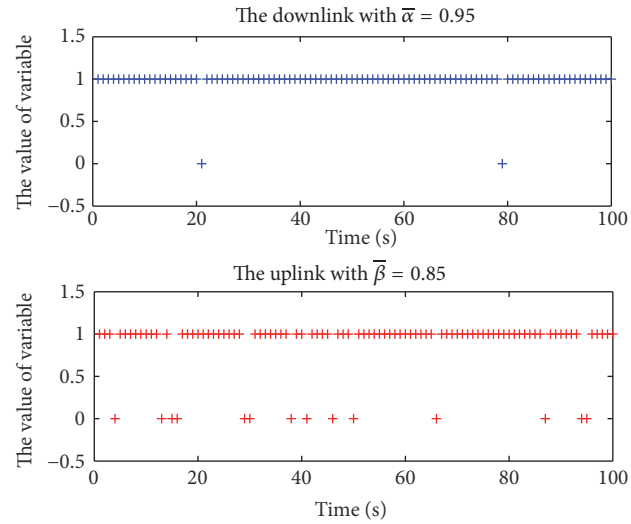

Figure 2: Random packet dropouts.

The Membership functions are as follows:

$$\begin{aligned} h_1(x_1(t)) &= \begin{cases} \dfrac{(x_1(t)+3)}{3}, & -3 \le x_1(t) \le 0, \\ \dfrac{(3-x_1(t))}{3}, & 0 \le x_1(t) \le 3, \\ 0, & \text{else}, \end{cases} \\ h_2(x_1(t)) &= 1 - h_1(x_1(t)). \end{aligned} \tag{34}$$

In Figure 2, the dropouts of random data packet are displayed, in which it contains both the uplink and the downlink. Furthermore, it is assumed that the initial value of the model is $[-1 \ \ 4]^T$ and the initial value of the reference system is 1. The external disturbance of the model is assumed as follows: $\varpi(t) = 1/(2+t)$; and the disturbance term of the reference system is $\sigma(t) = \sin(1/0.5 * (t))$; in Figure 3, output $r_r(t)$ of the reference model and the output $r(t)$ of the system are opened up before our eyes, in which $r_r(t)$ is tracked well by the output $r(t)$, despite the fact that the initial values are not equal to zero. The initial value of the controller is $[-2 \ \ 1 \ \ 0]^T$. Figure 4 draws up the state of dynamic output feedback controller. Figure 5 illustrates that the dynamical output feedback controller can make the error system tend towards stability. In this simulation, the external disturbances are added to characterize the fluctuation of system. In Figure 6, under the action of the dynamical output feedback controller, the controlled output result of the closed-loop system is shown. At each sampling time, as a result of the controller, the error $e(t)$ is gradually approaching 0 and the steady states of the closed-loop system are finally reached by continuously adjusting. Therefore, in this paper, the plan of dynamic output feedback controller can ensure that H_∞ performance is satisfied and the required stochastic stability is obtained.

Based on the above survey, the simulation outcome may certify that the project of dynamic output feedback controller satisfies the defined requirements of designing. It can be seen

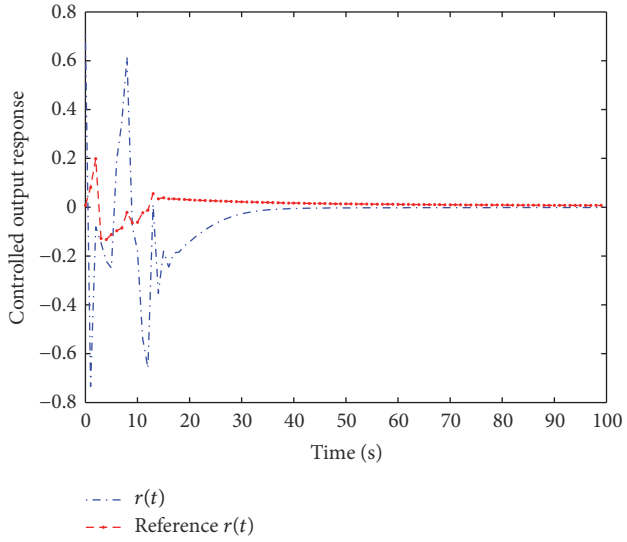

Figure 3: Output tracking response of the system.

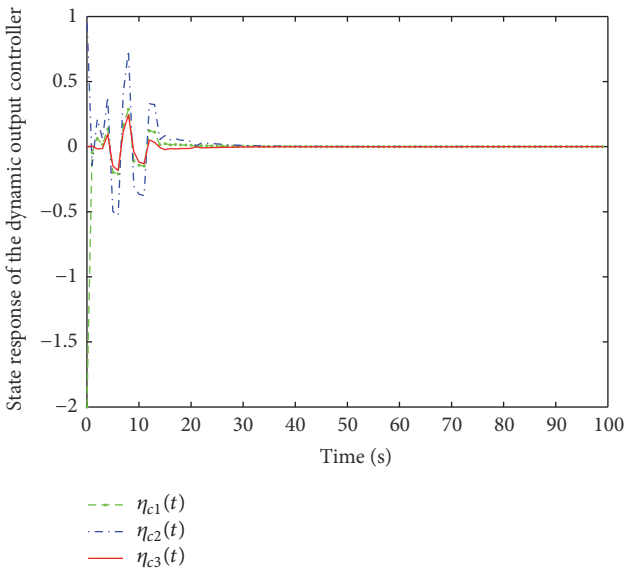

Figure 4: State response of the dynamic output feedback controller.

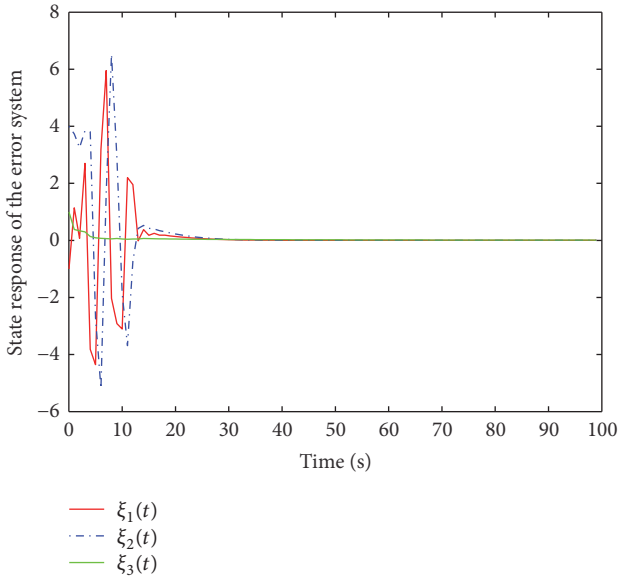

Figure 5: State response of the error system.

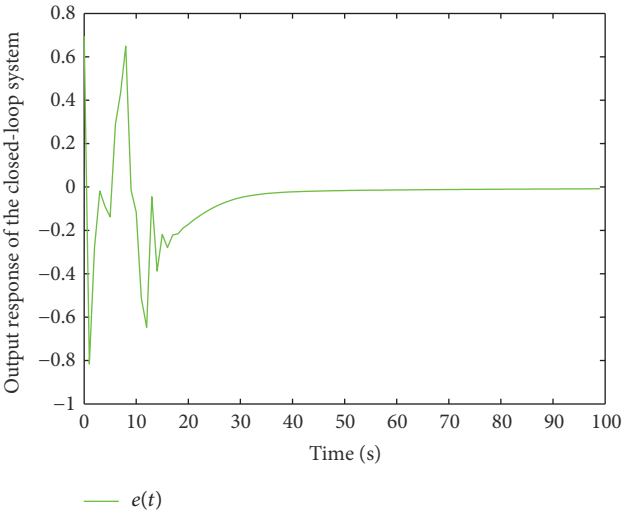

Figure 6: Output response of the closed-loop system.

that under the circumstances of questionable communication links the method [27] of state-feedback control is not valid for the nonlinear tracking systems when the state variables of the tracking systems are unmeasured or undiscovered. In this paper, the proposed plan results of dynamic output feedback controller can finish off the above questionable system in which the measurements are missing.

5. Conclusions

In this paper, the tracking control of H_∞ dynamic output feedback is suggested for the fuzzy networked systems with missing data. When the loss of data packets occurs randomly in both the uplink and the downlink, the Bernoulli random variables are considered to design it. The method of planning the dynamic output controller is employed to achieve the stability of tracking control systems. Then, the analysis of H_∞ performance for the closed-loop system is shown. Furthermore, the achieved sufficient conditions in terms of LMIs ensure that the closed-loop system is stochastically stable in the H_∞ sense.

We will devote ourselves to the more realistic and practical output feedback framework for tracking control. We will consider unknown state variables and data loss. In view of T-S fuzzy model, the problem of tracking control with the observer is proposed for uncertain nonlinear networked control systems. The unmeasurable state variables are estimated by the fuzzy observer rather than the model, which may bring about more precise results. The controller of fuzzy tracking control is proposed in terms of the fuzzy observer. The applied

controller designing method may cut down complexity and strengthen the flexibility.

Conflicts of Interest

The authors declare that there are no conflicts of interest regarding the publication of this paper.

Acknowledgments

This work is supported by the National Natural Science Foundation of China (61673280).

References

[1] H. Zhang, Y. Shi, and A. S. Mehr, "Robust static output feedback control and remote PID design for networked motor systems," *IEEE Transactions on Industrial Electronics*, vol. 58, no. 12, pp. 5396–5405, 2011.

[2] J. Qiu, H. Gao, and S. X. Ding, "Recent advances on fuzzy-model-based nonlinear networked control systems: a survey," *IEEE Transactions on Industrial Electronics*, vol. 63, no. 2, pp. 1207–1217, 2016.

[3] R. A. Gupta and M. Y. Chow, "Networked control system: overview and research trends," *IEEE Transactions on Industrial Electronics*, vol. 57, no. 7, pp. 2527–2535, 2010.

[4] J. Xiong and J. Lam, "Stabilization of networked control systems with a logic ZOH," *Institute of Electrical and Electronics Engineers Transactions on Automatic Control*, vol. 54, no. 2, pp. 358–363, 2009.

[5] J. Zhang, J. Lam, and Y. Xia, "Output feedback sliding mode control under networked environment," *International Journal of Systems Science*, vol. 44, no. 4, pp. 750–759, 2013.

[6] W. Zhang, M. S. Branicky, and S. M. Phillips, "Stability of networked control systems," *IEEE Control Systems Magazine*, vol. 21, no. 1, pp. 84–97, 2001.

[7] P. Shi, H. Wang, and C.-C. Lim, "Network-based event-triggered control for singular systems with quantizations," *IEEE Transactions on Industrial Electronics*, vol. 63, no. 2, pp. 1230–1238, 2016.

[8] J. Hu, D. M. Dawson, and Y. Qian, "Position tracking control of an induction motor via partial state feedback," *Automatica*, vol. 31, no. 7, pp. 989–1000, 1995.

[9] N. C. Shieh, P. C. Tung, and C. L. Lin, "Robust output tracking control of a linear brushless DC motor with time-varying disturbances," *IEE Proceedings Electric Power Applications*, vol. 149, no. 1, pp. 39–45, 2002.

[10] D. M. Dawson, Z. Qu, and J. J. Carroll, "Tracking control of rigid-link electrically-driven robot manipulators," *International Journal of Control*, vol. 56, no. 5, pp. 991–1006, 1992.

[11] L. Benvenuti, M. D. Di Benedetto, and J. W. Grizzle, "Approximate output tracking for nonlinear nonminimum phase systems with an application to flight control," *International Journal of Robust and Nonlinear Control*, vol. 4, no. 3, pp. 397–414, 1994.

[12] Y. M. Li, S. C. Tong, and T. S. Li, "Adaptive fuzzy output feedback dynamic surface control of interconnected nonlinear pure-feedback systems," *IEEE Transactions on Cybernetics*, vol. 45, no. 1, pp. 138–149, 2015.

[13] C. Chen, Z. Liu, Y. Zhang, C. L. P. Chen, and S. Xie, "Asymptotic fuzzy tracking control for a class of stochastic strict-feedback systems," *IEEE Transactions on Fuzzy Systems*, vol. 25, no. 3, pp. 556–568, 2017.

[14] Y. Li, S. Tong, and T. Li, "Composite adaptive fuzzy output feedback control design for uncertain nonlinear strict-feedback systems with input saturation," *IEEE Transactions on Cybernetics*, vol. 45, no. 10, pp. 2299–2308, 2015.

[15] M. Kamali, J. Askari, and F. Sheikholeslam, "An output-feedback adaptive actuator failure compensation controller for systems with unknown state delays," *Nonlinear Dynamics*, vol. 67, no. 4, pp. 2397–2410, 2012.

[16] H. Gao, X. Meng, and T. Chen, "Stabilization of networked control systems with a new delay characterization," *Institute of Electrical and Electronics Engineers Transactions on Automatic Control*, vol. 53, no. 9, pp. 2142–2148, 2008.

[17] O. C. Imer, S. Yüksel, and T. Başar, "Optimal control of LTI systems over unreliable communication links," *Automatica*, vol. 42, no. 9, pp. 1429–1439, 2006.

[18] M. Liu, D. W. C. Ho, and Y. Niu, "Stabilization of Markovian jump linear system over networks with random communication delay," *Automatica*, vol. 45, no. 2, pp. 416–421, 2009.

[19] H. Gao, T. Chen, and J. Lam, "A new delay system approach to network-based control," *Automatica*, vol. 44, no. 1, pp. 39–52, 2008.

[20] B. Jiang, Z. Mao, and P. Shi, "H_∞-filter design for a class of networked control systems via T-S fuzzy-model approach," *IEEE Transactions on Fuzzy Systems*, vol. 18, no. 1, pp. 201–208, 2010.

[21] J. Liu, W. Luo, X. Yang, and L. Wu, "Robust model-based fault diagnosis for pem fuel cell air-feed system," *IEEE Transactions on Industrial Electronics*, vol. 63, no. 5, pp. 3261–3270, 2016.

[22] W. He, Y. Chen, and Z. Yin, "Adaptive neural network control of an uncertain robot with full-state constraints," *IEEE Transactions on Cybernetics*, vol. 46, no. 3, pp. 620–629, 2016.

[23] Y.-J. Liu, Y. Gao, S. Tong, and Y. Li, "Fuzzy approximation-based adaptive backstepping optimal control for a class of nonlinear discrete-time systems with dead-zone," *IEEE Transactions on Fuzzy Systems*, vol. 24, no. 1, pp. 16–28, 2016.

[24] R. Lu, H. Cheng, and J. Bai, "Fuzzy-model-based quantized guaranteed cost control of nonlinear networked systems," *IEEE Transactions on Fuzzy Systems*, vol. 23, no. 3, pp. 567–575, 2015.

[25] Y. Yi, W. X. Zheng, C. Sun, and L. Guo, "DOB fuzzy controller design for non-gaussian stochastic distribution systems using two-step fuzzy identification," *IEEE Transactions on Fuzzy Systems*, vol. 24, no. 2, pp. 401–418, 2016.

[26] X. Xie, D. Yue, H. Zhang, and C. Peng, "Control synthesis of discrete-time T-S Fuzzy systems: reducing the conservatism whilst alleviating the computational burden," *IEEE Transactions on Cybernetics*, vol. 47, no. 9, pp. 2480–2491, 2017.

[27] H. Gao, Y. Zhao, and T. Chen, "H∞ fuzzy control of nonlinear systems under unreliable communication links," *IEEE Transactions on Fuzzy Systems*, vol. 17, no. 2, pp. 265–278, 2009.

[28] K. Tanaka and H. O. Wang, *Fuzzy Control Systems Design and Analysis: A Linear Matrix Inequality Approach*, John Wiley & Sons, New York, NY, USA, 2001.

[29] C. Lin, Q.-G. Wang, and T. H. Lee, "H_∞ output tracking control for nonlinear systems via T-S fuzzy model approach," *IEEE Transactions on Systems, Man and Cybernetics, Part B (Cybernetics)*, vol. 36, no. 2, pp. 450–457, 2006.

[30] A. Elsayed and M. J. Grimble, "A new approach to the H_∞ design of optimal digital linear filters," *IMA Journal of Mathematical Control and Information*, vol. 6, no. 2, pp. 233–251, 1989.

[31] H. Zhang, Y. Shi, and A. Saadat Mehr, "On H_∞ filtering for discrete-time takagi-sugeno fuzzy systems," *IEEE Transactions on Fuzzy Systems*, vol. 20, no. 2, pp. 396–401, 2012.

[32] W. M. McEneaney, "Robust H_∞ filtering for nonlinear systems," *Systems & Control Letters*, vol. 33, no. 5, pp. 315–325, 1998.

[33] D. Zhang and L. Yu, "H_∞ output tracking control for neutral systems with time-varying delay and nonlinear perturbations," *Communications in Nonlinear Science and Numerical Simulation*, vol. 15, no. 11, pp. 3284–3292, 2010.

[34] Y.-L. Wang and G.-H. Yang, "Output tracking control for networked control systems with time delay and packet dropout," *International Journal of Control*, vol. 81, no. 11, pp. 1709–1719, 2008.

[35] M. S. Mahmoud and G. D. Khan, "Dynamic output feedback of networked control systems with partially known Markov chain packet dropouts," *Optimal Control Applications and Methods*, vol. 36, no. 1, pp. 29–44, 2015.

[36] L. Wu, X. Yao, and W. X. Zheng, "Generalized H_2 fault detection for two-dimensional Markovian jump systems," *Automatica*, vol. 48, no. 8, pp. 1741–1750, 2012.

[37] J. Qiu, G. Feng, and H. Gao, "Fuzzy-model-based piecewise H_∞ static-output-feedback controller design for networked nonlinear systems," *IEEE Transactions on Fuzzy Systems*, vol. 18, no. 5, pp. 919–934, 2010.

[38] H. Li, C. Wu, X. Jing, and L. Wu, "Fuzzy tracking control for nonlinear networked systems," *IEEE Transactions on Cybernetics*, vol. 47, no. 8, pp. 2020–2031, 2017.

[39] L. Wang, H. Du, C. Wu, and H. Li, "A new compensation for fuzzy static output-feedback control of nonlinear networked discrete-time systems," *Signal Processing*, vol. 120, pp. 255–265, 2016.

Hindawi
Mathematical Problems in Engineering
Volume 2017, Article ID 4259869, 10 pages
https://doi.org/10.1155/2017/4259869

Research Article

Trajectory Optimization of Spray Painting Robot for Complex Curved Surface Based on Exponential Mean Bézier Method

Wei Chen,[1,2] Junjie Liu,[1] Yang Tang,[3] Jian Huan,[1] and Hao Liu[1]

[1]*School of Electronics and Information, Jiangsu University of Science and Technology, Zhenjiang 212003, China*
[2]*School of Automation, Southeast University, Nanjing 210096, China*
[3]*School of Science, Jiangsu University, Zhenjiang 212013, China*

Correspondence should be addressed to Yang Tang; ty800117@ujs.edu.cn

Received 22 May 2017; Revised 24 August 2017; Accepted 11 September 2017; Published 20 November 2017

Academic Editor: Shoudong Huang

Automated tool trajectory planning for spray painting robots is still a challenging problem, especially for a large complex curved surface. This paper presents a new method of trajectory optimization for spray painting robot based on exponential mean Bézier method. The definition and the three theorems of exponential mean Bézier curves are discussed. Then a spatial painting path generation method based on exponential mean Bézier curves is developed. A new simple algorithm for trajectory optimization on complex curved surfaces is introduced. A golden section method is adopted to calculate the values. The experimental results illustrate that the exponential mean Bézier curves enhanced flexibility of the path planning, and the trajectory optimization algorithm achieved satisfactory performance. This method can also be extended to other applications.

1. Introduction

Spray painting robot is an important advanced paint production equipment, which is widely used in the paint production line of automotive. The complex shape of the workpiece in the actual industrial production is often encountered. The basic steps of the existing method in the trajectory optimization for spray painting on this kind of complex curved surface are as follows:

(1) After obtaining the CAD (Computer Aided Design) data of the workpiece surface, triangulation is directly performed on the surface. And the surface is modeled by the corresponding method.

(2) After patching the complex curved surface according to the surface topology, each patch is approximated as a plane. Then the spray painting trajectory is optimized on each patch.

(3) The spray painting trajectory at the junction between patches is optimized. It needs to be optimized according to the geometric position relation of the painting path on every two patches: PA-PA (parallel-parallel), PA-PE (parallel-perpendicular), and PE-PE (perpendicular-perpendicular) [1–3].

(4) Perform the tool trajectory optimal integration on each patch. Specifically, we can use ant colony algorithm or genetic algorithm.

In general, such trajectory optimization method for spray painting on a complex curved surface can basically meet the requirement of spray painting. However, this method has many steps to perform, and it needs to undergo three optimization operations such as the trajectory optimization on patch, optimization for spray painting trajectory at the junction of every two patches, and the tool trajectory optimal integration on each patch in actual process [4–6]. The operation will be more troublesome, and a lot of system time will be consumed. In addition, when the area of complex curved surface is larger or with more patches, the following two problems will occur:

(1) It is necessary to combine the optimized trajectories at the junction between the patches after the optimization for the painting path. The error will be larger, which will make the uniformity of the paint thickness at the junction of the patches worse. What is more, a lot of system execution time will be consumed in this process [7].

(2) When the number of patches is large, the population size (this is the concept of ant colony algorithm) will increase when performing the tool trajectory optimal integration on each patch. In this case, the convergence speed of genetic algorithm or ant colony algorithm is slow, and the algorithm is easy to fall into different local optimum fields, which leads to poor spray painting effect and lower spray painting efficiency [8–10].

Because of the existence of the problems above, the spray painting effect of the complex workpiece surface is still not very satisfactory in the current spray painting operations. Under this background, a new trajectory optimization method on curved surface based on Bézier surface is proposed in this paper. The specific idea for this method is after modeling the complex curved surface by using the Bézier triangular surface modeling technique, the discrete point array on the equidistant surface of the complex curved surface is found by the calculation method for discrete point array on equidistant surface of Bézier surface. Then the spatial painting path generation method based on the exponential mean Bézier curve is used to obtain the spatial painting path on the complex curved surface. According to the new trajectory optimization method on the complex curved surface, the spray painting trajectory is optimized along the specified spatial path, and the complete optimized trajectory for spray painting on the complex curved surface is obtained. The advantage of this method is that it does not need to split the complex curved surface but makes the full use of the flexible regulatory property of exponential mean Bézier curve to plan for the spatial painting path. This method not only increases the flexibility in the optimization process, but also greatly simplifies the steps of spray painting operations on complex curved surfaces.

2. Path Planning

Trajectory optimization of the spray painting robot consists of two parts, one is the path planning and the other is the spray speed optimization. The effect of spray painting on the complex curved surface workpiece is still not very satisfactory in the current spray painting operation. In the spray painting operation, the curvature of the workpiece surface is likely to be large due to the complexity of curved surface and the shape of the workpiece surface, which makes it more difficult to optimize the spray painting trajectory. In the first part of the description, the existing method is curved triangulation. In this method, Cubic Cardinal spline curves are used to connect the discrete point arrays on the equidistant surface of the Bézier surface, and each adjacent Cardinal spline curve is connected by Hermite spline curve [11–13]. Since both Cardinal and Hermite curves are parametric cubic polynomials, the local control properties for the curves are particularly poor and it is difficult to make a direct and geometric intuitionistic estimate of the geometry of the curve under normal circumstances.

In the current surface modeling technology of CAGD (Computer Aided Geometric Design) for free-form curved surface, Bézier theory and method have been widely used in the CAM/CAD system as a set of mature algorithm theories, which shows a strong vitality and practical value. The main reason is that Bézier method is easy to operate and it has good geometric properties. The traditional Bézier curve is defined as a convex combination of spatial position vector with the Bernstein basis function as weight, which is also a kind of average value. But the traditional Bézier curve has great limitations on describing the geometry of the entity, and its rational and polynomial form also have many shortcomings. Therefore, it is of vital importance to find the new basis functions of Bézier curves. In this section, Bézier curves are evenly combined with exponential mean, and the definition of exponential mean Bézier curves with parameter is put forward [14, 15]. The three basic properties of this kind of curves are given, such as the elevation, de Casteljau algorithm, and segmentation theorem which are applied to the method for generating the painting path in complicated surface. Finally, better results can be obtained.

2.1. Definition and Properties of Exponential Mean Bézier Curves. The traditional arithmetic weighted Bézier curve is defined as follows:

$$B_n(t) = \sum_{i=0}^{n} B_{i,n}(t) V_i, \quad 0 \le t \le 1, \tag{1}$$

where basis Bernstein function $B_{i,n}(t) = C_n^i t^i (1-t)^{n-i}$, $0 \le t \le 1$. V_i $(i = 0, 1, \ldots, n)$ is the control vertices. Since $\sum_{i=0}^{n} B_{i,n}(t) = 1$, $B_n(t)$ can be seen as the weighted average of control vertices $V_0, V_1, \ldots, V_n$.

Make the exponential mean of control vertices $V_0, V_1, \ldots, V_n$ on this basis; we can get the definition of exponential mean Bézier curve.

Definition 1. Define

$$L_n^s(t) = \begin{cases} \log_s \sum_{i=0}^{n} B_{i,n}(t) s^{V_i}, & s \in R_+^* \\ \sum_{i=0}^{n} B_{i,n}(t) V_i, & s = 1 \end{cases} \qquad 0 \le t \le 1 \tag{2}$$

for $\forall s \in R_+$; $L_n^s(t)$ is called the n-time s-order exponential mean Bézier curve.

Obviously, n-time first-order exponential mean Bézier curve is the Bézier curve in traditional sense. After introducing the displacement operator E, difference operator Δ, and unit operator I motioned above, then we have

$$\begin{aligned} \log_s \sum_{i=0}^{n} B_{i,n}(t) s^{V_i} &= \log_s \left((1-t) I + tE\right)^n s^{V_0} \\ &= \log_s (I + t\Delta)^n s^{V_0} \end{aligned} \tag{3}$$

so, $L_n^s(t)$ has the following operator representation:

$$L_n^s(t) = \begin{cases} \log_s (I + t\Delta)^n s^{V_0}, & s \in R_+^* \\ (I + t\Delta)^n V_0, & s = 1. \end{cases} \tag{4}$$

The derivative formula of $L_n^s(t)$ is given as follows:

$$\left(L_n^s(t)\right)' = \begin{cases} \dfrac{n(I+t\Delta)^{n-1}\,\Delta s^{V_0}}{(I+t\Delta)^n s^{V_0}\ln s}, & s \in R_+^* \\ n(I+t\Delta)^{n-1}\,\Delta V_0, & s = 1; \end{cases} \tag{5}$$

obviously,

$$\left(L_n^s(0)\right)' = \begin{cases} \dfrac{n}{\ln s}\dfrac{s^{V_1}-s^{V_0}}{s^{V_0}}, & s \in R_+^* \\ n\left(V_1 - V_0\right), & s = 1, \end{cases}$$

$$\left(L_n^s(1)\right)' = \begin{cases} \dfrac{n}{\ln s}\dfrac{s^{V_n}-s^{V_{n-1}}}{s^{V_n}}, & s \in R_+^* \\ n\left(V_n - V_{n-1}\right), & s = 1. \end{cases} \tag{6}$$

Note the exponential mean Bézier curves determined by the control vertices $V_0, V_1, \ldots, V_n$ as $L_n^s(V_0, V_1, \ldots, V_n; t)$. Then, it satisfies the interpolation properties at the endpoints, which is

$$\begin{aligned} L_n^s\left(V_0, V_1, \ldots, V_n; 0\right) &= V_0, \\ L_n^s\left(V_0, V_1, \ldots, V_n; 1\right) &= V_n \end{aligned} \tag{7}$$

and when $s \in R_+^*$, from $B_{i,n}(t) = B_{n-i,n}(1-t)$, we can obtain

$$\begin{aligned} L_n^s\left(V_n, V_{n-1}, \ldots, V_0; t\right) &= \log_s \sum_{i=0}^{n} B_{n-i,n}(1-t)\, s^{V_{n-i}} \\ &= \log_s \sum_{i=0}^{n} B_{i,n}(1-t)\, s^{V_i} = L_n^s\left(V_0, V_1, \ldots, V_n; 1-t\right) \end{aligned} \tag{8}$$

and when $s = 1$, similarly we can obtain

$$\begin{aligned} L_n^s\left(V_n, V_{n-1}, \ldots, V_0; t\right) &= \sum_{i=0}^{n} B_{i,n}(t)\, V_{n-i} \\ &= \sum_{i=0}^{n} B_{n-i,n}(1-t)\, V_{n-i} = \sum_{i=0}^{n} B_{i,n}(1-t)\, V_i \\ &= L_n^s\left(V_0, V_1, \ldots, V_n; 1-t\right). \end{aligned} \tag{9}$$

It can be seen that the exponential mean Bézier curve defined by the same control polygon is unique. The parametric cubic Hermite interpolation does not have the symmetry represented by the formula above.

In the Bézier curve design, the flexibility of curve designing can be improved by increasing the number of control vertices while keeping the curve shape unchanged, which is called elevation. The exponential mean Bézier curve is also a parametric polynomial curve segment with global properties. In the discrete point arrays on the equidistant surface of a complex curved surface, it is possible that the control vertices cannot reach the ideal curve (path) shape no matter how we adjust them. That is, the "rigidity" of the curve (path) is adequate while the "flexibility" is insufficient. The control vertices are added by elevation, which reduces the "rigidity" of the painting path on the complex curved surface, increases its "flexibility," and enhances the potential flexibility of controlling the shape of the painting path on complex curved surfaces.

Theorem 2. *When $s \in R_+^*$, suppose a n-time s-order exponential mean Bézier curve is expressed as*

$$L_n^s(t) = \log_s \sum_{i=0}^{n} B_{i,n}(t)\, s^{V_{i,n}}. \tag{10}$$

The control vertices are $V_{0,n}, V_{1,n}, \ldots, V_{n,n}$; n + m-time s-order exponential mean Bézier curve is expressed as

$$L_{n+m}^s(t) = \log_s \sum_{i=0}^{n+m} B_{i,n+m}(t)\, s^{V_{i,n+m}} \tag{11}$$

and the control vertices are $V_{0,n+m}, V_{1,n+m}, \ldots, V_{n+m,n+m}$, and then n-time curve $L_n^s(t)$ can be elevated to n + m-time curve $L_{n+m}^s(t)$ and satisfies

$$s^{V_{i,n+m}} = \sum_{j=0}^{m} \frac{C_n^{i-j} C_m^j}{C_{n+m}^i} s^{V_{i-j,m}}, \quad i = 0, 1, \ldots, n+m. \tag{12}$$

Proof.

$$\begin{aligned} L_n^s(t) &= \log_s \sum_{i=0}^{n} B_{i,n}(t)\, s^{V_{i,n}} \\ &= \log_s \sum_{i=0}^{n} C_n^i t^i (1-t)^{n-i} (1-t+t)^m\, s^{V_{i,n}} \\ &= \log_s \sum_{j=0}^{m} \sum_{i=0}^{n} \frac{C_n^i C_m^j C_{n+m}^{i+j}}{C_{n+m}^{i+j}} t^{i+j} (1-t)^{n+m-(i+j)}\, s^{V_{i,n}} \\ &= \log_s \sum_{j=0}^{m} \sum_{k=j}^{n+j} \frac{C_n^{k-j} C_m^j C_{n+m}^k}{C_{n+m}^k} t^k (1-t)^{n+m-k}\, s^{V_{k-j,n}} \\ &= \log_s \sum_{i=0}^{n+m} B_{i,n+m}(t) \sum_{j=0}^{m} \frac{C_n^{i-j} C_m^j C_{n+m}^i}{C_{n+m}^i} s^{V_{i-j,n}} \end{aligned} \tag{13}$$

and $L_{n+m}^s(t) = \log_s \sum_{i=0}^{n+m} B_{i,n+m}(t) s^{V_{i,n+m}}$; thus

$$s^{V_{i,n+m}} = \sum_{j=0}^{m} \frac{C_n^{i-j} C_m^j}{C_{n+m}^i} s^{V_{i-j,m}}, \quad i = 0, 1, \ldots, n+m \tag{14}$$

and when $s = 1$, n-time first-order exponential mean Bézier curve

$$L_n^s(t) = \sum_{i=0}^{n} B_{i,n}(t)\, V_{i,n} \tag{15}$$

can be also elevated to $n + m$-time first-order exponential mean Bézier curve $L_{n+m}^s(t) = \sum_{i=0}^{n+m} B_{i,n+m}(t) V_{i,n+m}$.

In particular, when $m = 1$ and $s \in R_+^*$,

$$s^{V_{i,n+1}} = \frac{i}{n+1} s^{V_{i-1,n}} + \left(1 - \frac{i}{n+1}\right) s^{V_{i,n}}, \quad i = 0, 1, \ldots, n+1 \tag{16}$$

and when $s = 1$,

$$V_{i,n+1} = \frac{i}{n+1} V_{i-1,n} + \left(1 - \frac{i}{n+1}\right) V_{i,n}, \quad i = 0, 1, \ldots, n+1, \tag{17}$$

where $V_{i,n}$ is the control point of the n-time s-order exponential mean Bézier curve $L_n^s(t)$ and $V_{i,n+1}$ is the control point of the $(n+1)$-time s-order exponential mean Bézier curve $L_{n+1}^s(t)$ after elevation. □

In the process of selecting the control vertices according to the discrete point arrays on the equidistant surface of the complex curved surface, the geometric properties of the complex curved surfaces themselves determine that the geometrical properties of the Bézier curves obtained from these control vertices are also complex. The process of each intermediate vertex generated by the de Casteljau algorithm is linear interpolation. This algorithm can resolve a complex geometric computation problem into a series of linear operations. The algorithm is easy to program and the speed is quite fast. Also, it facilitates the rapid generation of spatial painting path on complex curved surface.

Theorem 3 (de Casteljau algorithm theorem). *$L_n^s(t)$ is the n-time s-order exponential mean Bézier curve. Suppose that the control vertex $\{V_i\}_{i=0}^n$ and parameter $t \in [0,1]$ are given. Then $V_i^{[r]}$ is defined as follows:*

$$V_i^{[r]} = \begin{cases} \log_s\left((1-t)\, s^{V_i^{[r-1]}} + t s^{V_{i+1}^{[r-1]}}\right), & s \in R_+^* \\ (1-t)\, V_i^{[r-1]} + t V_{i+1}^{[r-1]}, & s = 1,\ r = 1, 2, L, n-r \\ V_i^{[0]} = V_i, \end{cases} \tag{18}$$

and this satisfies $L_n^s(t) = V_0^{[n]}$, $s \in R_+$.

Proof. When $s = 1$,

$$L_n^s(t) = \sum_{i=0}^{n} B_{i,n}(t)\, V_i = ((1-t)\, I + tE)^n V_0 \tag{19}$$

while

$$V_i^{[r]} = (1-t)\, V_i^{[r-1]} + t V_{i+1}^{[r-1]} = ((1-t)\, I + tE)\, V_i^{[r-1]} = ((1-t)\, I + tE)^r V_i^{[0]} = ((1-t)\, I + tE)^r V_0. \tag{20}$$

Let $i = 0$ and $r = n$; then we have

$$V_0^{[n]} = ((1-t)\, I + tE)^n V_0 = L_n^s(t). \tag{21}$$

When $s \in R_+^*$,

$$L_n^s(t) = \log_s \sum_{i=0}^{n} B_{i,n}(t)\, s^{V_i} = \log_s ((1-t)\, I + tE)^n s^{V_0} \tag{22}$$

while

$$V_i^{[r]} = \log_s\left((1-t)\, s^{V_i^{[r-1]}} + t s^{V_{i+1}^{[r-1]}}\right) = \log_s ((1-t)\, I + tE)\, s^{V_i^{[r-1]}} \tag{23}$$

and thereby

$$V_i^{[r]} = ((1-t)\, I + tE)\, s^{V_i^{[r-1]}} = \cdots = ((1-t)\, I + tE)^r s^{V_i^{[0]}} = ((1-t)\, I + tE)^r s^{V_i}; \tag{24}$$

thus

$$V_i^{[r]} = \log_s ((1-t)\, I + tE)^r s^{V_i}. \tag{25}$$

Let $i = 0$ and $r = n$; then we have

$$V_0^{[n]} = \log_s ((1-t)\, I + tE)^n s^{V_0} = L_n^s(t). \tag{26}$$

de Casteljau's algorithm theorem improves the rapidity of generating the spatial paths on complex curved surfaces. However, since the curvature of the complex curved surface itself changes greatly, in the actual spray painting operations, sometimes the entire painting path needs to be processed by segment. That is, the entire path curve needs to be divided into two subpath curve segments. The de Casteljau algorithm can not only determine a point on the path curve, but also introduce the path curve segmentation problem. There are two vertices sets $V_0, V_0^{[1]}, \ldots, V_0^{[n]}$ and $V_0^{[n]}, V_1^{[n-1]}, \ldots, V_n$ in the de Casteljau algorithm. We can get the two subcurve segments divided from the entire exponential mean Bézier curve by using the exponential mean Bézier curve determined by these two vertices sets as the control vertex. □

Theorem 4 (path curve segmentation theorem). *Suppose $t \in [0,1]$ and $u \in [0,1]$, for $\forall s \in R_+$; we have*

$$\begin{aligned} &L_n^s\left(V_0, V_0^{[1]}, \ldots, V_0^{[n]}; u\right) = L_n^s\left(V_0, V_1, \ldots, V_n; ut\right), \\ &L_n^s\left(V_0^{[n]}, V_1^{[n-1]}, \ldots, V_n; u\right) \\ &\quad = L_n^s\left(V_0, V_1, \ldots, V_n; 1 - (1-u)(1-t)\right). \end{aligned} \tag{27}$$

Proof. When $s \in R_+^*$,

$$\begin{aligned} L_n^s(V_0, V_1, \ldots, V_n; ut) &= \log_s \sum_{i=0}^{n} B_{i,n}(ut)\, s^{V_i} \\ &= \log_s ((1-ut)\, I + utE)^n s^{V_0} \\ &= \log_s [(1-u)\, I + u((1-t)\, I + tE)]^n s^{V_0} \\ &= \log_s \sum_{i=0}^{n} C_n^i (1-u)^{n-i} u^i ((1-t)\, I + tE)^i s^{V_0} \\ &= \log_s \sum_{i=0}^{n} B_{i,n}(u)\, s^{V_0^{[i]}} = L_n^s\left(V_0, V_0^{[1]}, \ldots, V_0^{[n]}; u\right), \end{aligned}$$

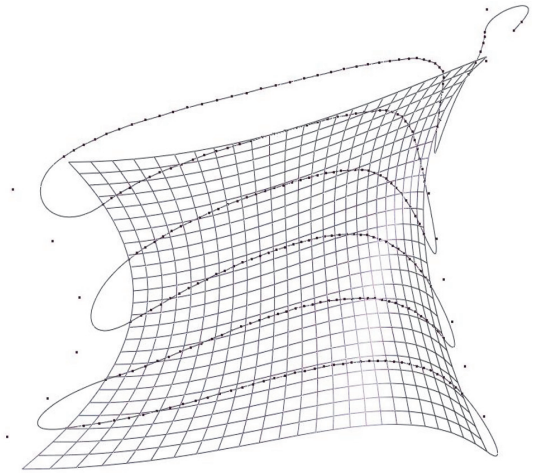

Figure 1: The U-direction spatial path of the surface.

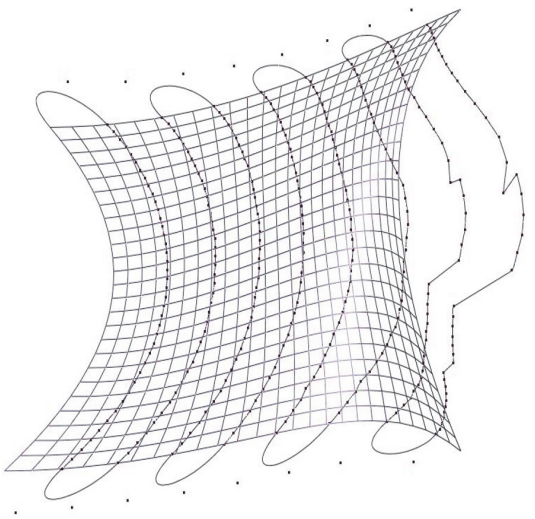

Figure 2: The V-direction spatial path of the surface.

$$
\begin{aligned}
&L_n^s\left(V_0, V_1, \ldots, V_n; 1-(1-u)(1-t)\right)\\
&= \log_s\left[(1-u)(1-t)I + (1-(1-u)(1-t))E\right]^n s^{V_0}\\
&= \log_s\left[uE + (1-u)\left[(1-t)I + tE\right]\right]^n s^{V_0}\\
&= \log_s \sum_{i=0}^{n} C_n^i u^i (1-u)^{n-i}\left[(1-t)I + tE\right]^{n-i} s^{V_i}\\
&= \log_s \sum_{i=0}^{n} B_{i,n}(u)\, s^{V_i^{[n-i]}} = L_n^s\left(V_0^{[n]}, V_1^{[n-1]}, \ldots, V_n; u\right).
\end{aligned}
\tag{28}
$$

When $s = 1$, it can be proved as the same token.

The aim of the segmentation theorem is actually to find the two control vertices on the subcurve segment of the painting path in order to get the two small control polygons, which are closer to the curve than the original control polygon. □

2.2. Spatial Path Generation of Exponential Mean Bézier Curves. Due to the large curvature changes of the complex curved surface studied in this paper, the Cardinal splines and the parametric polynomial expressions of the Hermite splines themselves determine that the local control is relatively poor. Therefore, the exponential mean Bézier curves with parameter are used in order to overcome these shortcomings. The discrete point arrays (U-direction or V-direction) are regarded as the experimental data point arrays, and an exponential mean Bézier curve is used to fit the data points. Then the control vertices of the curves are inverted to generate the spatial painting path, where the U-direction spatial path of the surface is shown in Figure 1 and the V-direction spatial path of the surface is shown in Figure 2.

In the following, we will make the following first-order ($s = 1$) exponential mean Bézier curve as an example.

Take the U-direction as an example; the discrete point array is represented as a set of data points:

$$P_i \quad (i = 0, 1, \ldots, m). \tag{29}$$

Obtain an exponential menial Bézier curve

$$L_n^1(t) = \sum_{i=0}^{n} B_{i,n}(t)\, V_i, \quad 0 \le t \le 1,\ n < m; \tag{30}$$

these data points are fitted, and the control vertex V_i is to be determined. The curve is obtained by using the least-squares approximation method.

First, P_i $(i = 0, 1, \ldots, m)$ is parameterized. The parameter sequence is determined by using the specification accumulation chord length parameterization: $0 = t_0 < t_1 < \cdots < t_m = 1$, so we have

$$L_n^1(t_i) = \sum_{i=0}^{n} B_{i,n}(t_i)\, V_i = P_i, \quad i = 0, 1, \ldots, m. \tag{31}$$

The problem is transformed into solving the least-squares solution of the equation set. The problem can be solved by solving the following regularization equation:

$$\Phi^T \Phi \begin{pmatrix} V_0 \\ V_1 \\ \vdots \\ V_n \end{pmatrix} = \Phi^T \begin{pmatrix} P_0 \\ P_1 \\ \vdots \\ P_n \end{pmatrix}, \tag{32}$$

where

$$\Phi = \begin{pmatrix} B_{0,n}(t_0) & B_{1,n}(t_0) & \cdots & B_{n,n}(t_0) \\ B_{0,n}(t_1) & B_{1,n}(t_1) & \cdots & B_{n,n}(t_1) \\ \vdots & \vdots & \ddots & \vdots \\ B_{0,n}(t_n) & B_{1,n}(t_n) & \cdots & B_{n,n}(t_n) \end{pmatrix}. \tag{33}$$

In practical problems, we often hope that $V_0 = P_0, V_n = P_m$. That is, the two ends of the curve coincide with the first and last points of the data point. Then (32) becomes the following equation:

$$\sum_{j=1}^{n-1} B_{j,n}(t_i) V_i = P_i - \left[B_{0,n}(t_i) P_0 + B_{n,n}(t_i) P_m\right], \quad i = 1, 2, \ldots, m-1; \tag{34}$$

then its least-squares solution V_j $(i = 1, 2, \ldots, n-1)$ together with the two endpoints P_0, P_m forms the control vertices of the curve.

In the following, the smooth stitching condition of two adjacent curves is obtained by using Beta constraint formula. Suppose that the control vertex of the curve on the left of $L_-(t)$ is $\{V_i^-\}_{i=0}^n$, the control vertex of the curve on the right of $L_+(t)$ is $\{V_i^+\}_{i=0}^m$. In order to obtain a common unit tangent vector and a common curvature vector at the connection point of the two curved segments, we need to meet the following requirements:

$$\begin{aligned} L_+(0) &= L_-(1), \\ L_+'(0) &= \beta_1 L_-'(1), \\ L_+''(0) &= \beta_2 L_-'(1) + \beta_1^2 L_-''(1). \end{aligned} \tag{35}$$

By solving the derivative of $L(t)$, the above condition can be transformed into

$$\begin{aligned} V_o^+ &= V_n^-, \\ m\Delta V_o^+ &= \beta_1 n \Delta V_{n-1}^-. \end{aligned} \tag{36}$$

Then

$$\Delta V_1^+ = \frac{n}{m(m-1)}\beta_2 \Delta V_{n-1}^- + \frac{n(n-1)}{m(m-1)}\beta_1^2 \Delta^2 V_{n-2}^-. \tag{37}$$

At this point, the curve obtained by the smooth stitching of two adjacent curves is the specified spatial painting path.

The application of the three basic properties of exponential mean Bézier curves and their own parameters improves the flexibility of the painting path on complex curved surfaces. And the potential flexibility of shape controlling on the painting path is also enhanced. At the same time, it makes the algorithm very simple, stable, and reliable. The algorithm is easy to program and the speed is quite fast. Also, it facilitates the rapid generation of spatial painting path on complex curved surface.

3. Trajectory Algorithm

After generating the exponential mean Bézier curves according to the method described in Section 2, a new simple algorithm for trajectory optimization on complex curved surfaces is introduced in this section. The method is simple in expression and fast in operation speed, which can meet the requirement of spray painting quality on complex curved surface.

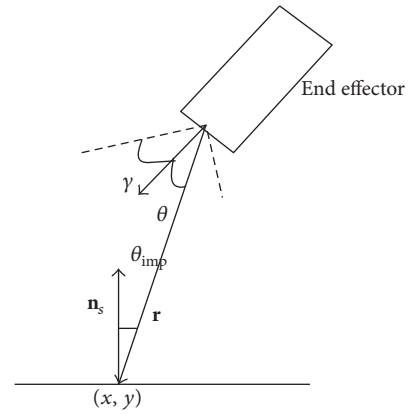

Figure 3: Spray painting model of the system.

When the end effector is in a specific position, the trajectory and position vector $\mathbf{p}(t)$ at a point $(x, y, h(x, y))$ on the surface can be expressed as $f_s(\mathbf{p}(t), x, y)u(t)$, where $f_s(\mathbf{p}(t), x, y)$ is the spray painting trajectory and $u(t)$ is the paint flow which $u(t)$ changes with the movement of the end effector. The spray painting trajectory $f_s(\mathbf{p}(t), x, y)$ is determined by the distance of the end effector and the surface and its spatial position. The spray painting model of the system is shown in Figure 3. Here, an experimental method is used to establish the paint deposition rate model. In the experiment, after a period of time, the paint deposition rate of the end effector is measured at a fixed position, and the paint deposition rate model is determined by the reverse flow distribution method. When the position of the end effector is $\mathbf{p}(t)$, the expression of spray painting trajectory is

$$f_s(\mathbf{p}(t), x, y) = \frac{\cos(\theta_{\text{imp}})\,\Theta(\theta, \gamma)\,\zeta(\theta_{\text{imp}})}{|\mathbf{r}^2|}, \tag{38}$$

where $\mathbf{r}$ denotes the vector of the end effector to point (x, y), θ_{imp} denotes the angle between $\mathbf{r}$ and the normal vector $\mathbf{n}_s$ of point (x, y), and $\Theta(\theta, \gamma)$ represents the droplet distribution of the conical paint stream. The droplet distribution depends on the normal vector of the end effector (it is determined by the position of the end effector), the angle θ between $\mathbf{r}$ and the perpendicular bisector of the end effector, and the inner half-angle γ of the conical paint flow, which can be represented as a regularized Dirac function:

$$\Theta(\theta, \gamma) = \frac{(\gamma^2 - \pi^2)\left[1 + \cos(\pi\theta/\gamma)\right]}{2\pi\left[2\gamma^2 - \pi^2 + \pi^2\cos\gamma\right]}. \tag{39}$$

Through a large number of spray painting experiments, it can be found that $\gamma = 0.32$ rad under normal circumstances. In some spray painting experiments (especially on metal surfaces), a significant portion of the paint is wasted due to

splashing and sticking efficiency $\zeta(\theta_{\text{imp}})$. The expression of sticking efficiency $\zeta(\theta_{\text{imp}})$ is

$$\zeta\left(\theta_{\text{imp}}\right) = \zeta\left(0\right)\left[1 - \alpha\theta_{\text{imp}}^2\left(1 - \frac{2\theta_{\text{imp}}^2}{\pi^2}\right)\right], \quad (40)$$

where $\zeta(0)$ represents the paint efficiency, α represents the fitting parameters in usual case $\zeta(0) = 0.67$, and $\alpha = 0.04$. In fact, it has been assumed in the model of Figure 1 that there is no paint deposition outside the paint cone angle γ. In the actual spray painting operation, there will be a small amount of splash paint falling outside the paint cone angle, but this situation can be ignored.

Assuming that the paint thickness distribution on the curved surface is $m(x, y)$, one of the objectives of the spray painting operation is to achieve the desired paint thickness distribution $m(x, y)$. In practice, the paint thickness distribution $m(x, y)$ varies on the curved surface. However, in the experiment, it is common to predefine an expected value in the system. That is, the paint thickness distribution is a constant. Therefore, for determining the vector $\mathbf{p}(t)$ of the locus and position of the nozzle as well as the flow rate $u(t)$, the minimum difference between the actual paint distribution and the actual paint thickness distribution can be selected as the optimization objective function. That is,

$$\min_{\mathbf{p}(t),u(t)} \quad \iint_S \left| m\left(x, y\right) - \int_0^T f_s\left(\mathbf{p}\left(t\right), x, y\right) u\left(t\right) dt \right|^2 dx\, dy, \quad (41)$$

where S represents a paint curved surface and T indicates the completion time of the spray painting operation. Since the objective function is not a convex function, the optimization problem is difficult to solve. Suppose that $h(x, y)$ is a constant, the distance of the end effector and the curved surface remains constant and is always perpendicular to the curved surface. Then the expression of spray painting trajectory is

$$f_s\left(\mathbf{p}\left(t\right), x, y\right) = f\left(x - x_\alpha\left(t\right), y - y_\alpha\left(t\right)\right), \quad (42)$$

where $f(x - x_\alpha(t), y - y_\alpha(t))$ represents the constant painting path. If the moving speed of end effector remains unchanged while the paint flow can be adjusted in the process of spray painting operation, then the above optimization problem can be transformed into

$$\min_{x_\alpha, y_\alpha, u(t)} \quad \iint_S \left| m\left(x, y\right) - \int_0^T f\left(x - x_\alpha\left(t\right), y - y_\alpha\left(t\right)\right) u\left(t\right) dt \right|^2 dx\, dy. \quad (43)$$

Here, the golden section method in mathematical programming can be used to solve the discrete points on the spray painting trajectory, from which we can get the optimized trajectory on the complex curved surface.

4. Experimental Verification

4.1. Spray Painting Simulation. Taking the automotive body of a brand as the paint objective, we have simulated the feasibility of exponential mean Bézier method. Since the left and right sides are completely symmetrical, only one side is listed. In addition, the car body spraying path is shown in Figure 4.

According to the actual spray painting requirements in the production process of the car, the ideal paint thickness $q_d = 50$ um, the error of the maximum paint thickness $q_w = 10$ um, painting radius $R = 60$ mm, painting distance $h = 80$ mm, and painting speed $V = 389$ mm/s (the optimization speed on the plane). We have collected 200 discrete points at the top, side, and rear of the body. The paint thickness curve of each sampling point on the automobile body is shown in Figure 5. The graph shows that the coating thickness meets the requirements, and the simulation results verify the effectiveness of the trajectory optimization method.

4.2. Spray Painting Experiment. We use FANUC industrial robots in the experiment. According to the characteristics of FANUC industrial robot off-line programming and spraying space trajectory, the method of spraying space trajectory converting to the robot motion trajectory is proposed.

By analyzing the relationship between the workpiece coordinate system and the robot coordinate system, the robot tool coordinate system is calibrated, and then the space trajectory in the workpiece coordinate system is transformed into the robot coordinate system. In the inverse solution of the robot, the optimal model of the shortest joint motion is established, and the inverse solution of the robot is derived [16].

Finally, the best inverse combination is obtained to realize the transformation of the spraying space trajectory to the robot motion trajectory.

The spatial paths obtained from different directions are shown in Figures 6, 7, and 8.

The spray painting experiment will be carried out along the specified painting path. Before the experiment, the following two points need to be explained:

(1) In the literature [12], the experimental results show that the spray painting effect is better with the path planning scheme along the U-direction path, and it is not easy to further improve the effect with the prior technology. As the spray painting effect along the V-direction path is not ideal, we just generate the V-direction path here in order to form a contrast between the two.

(2) The spatial painting path generation method based on the exponential mean Bézier curve is used in the experiment of this paper. As this method is more accurate but the calculation process is more complex, more discrete points of the equidistant surface need to be generated in the calculation. Then the spatial path density in V-direction generated by this

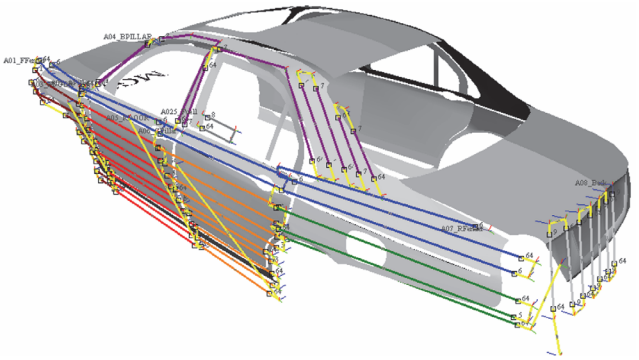

Figure 4: The spraying path for part of car body.

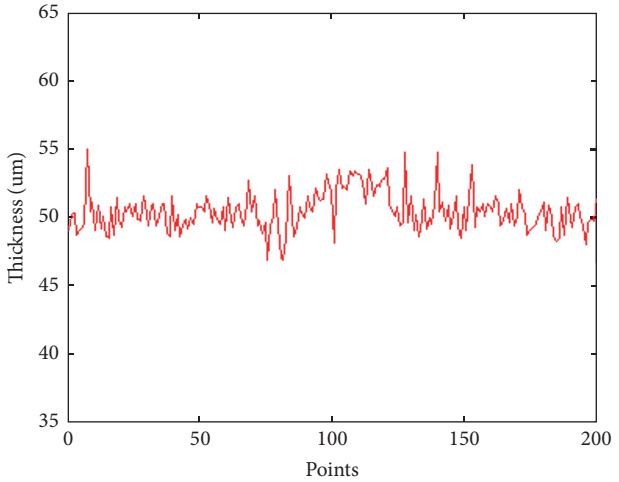

Figure 5: Material thickness of random chosen points on the car body.

method is also large (i.e., the distance between adjacent two paths is small). Therefore, in the spray painting experiment, we no longer need to optimize the spray painting speed. We can only perform uniform spray painting operation along the generated path in the experiment.

Figure 9 shows the robotic spray painting experiment of V-direction path planning for FANUC robot. Because the shape of the workpiece is symmetrical, half of the workpiece is sprayed in the experiment.

In the spray experiment, the ideal paint thickness is q_d = 50 um, maximum allowable error q_w = 10 um, painting radius R = 50 mm, painting distance h = 100 mm, and painting speed V = 256 mm/s (the optimization speed on the plane) when performing uniform spray painting. We take 400 discrete points evenly on the workpiece surface after spray painting operation. The paint thickness curve is shown in Figure 10 after using a paint thickness gauge to measure the paint thickness at the discrete points. The results of the experimental data obtained by using the surface spray painting method are shown in Table 1.

It can be seen from the comparison of the experimental results that the spray painting effect is better when using the

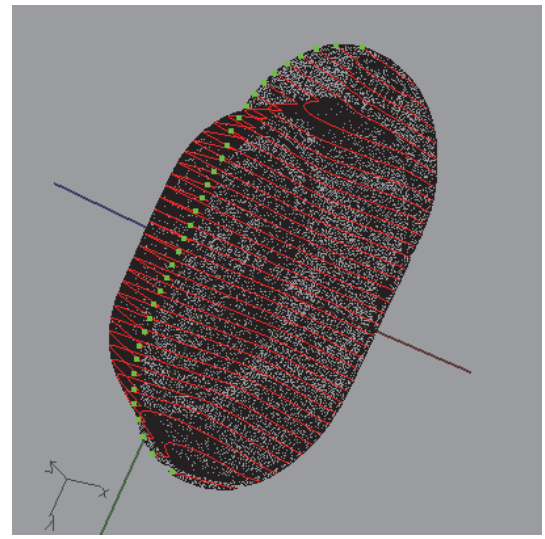

Figure 6: Spray painting path (x-axis direction).

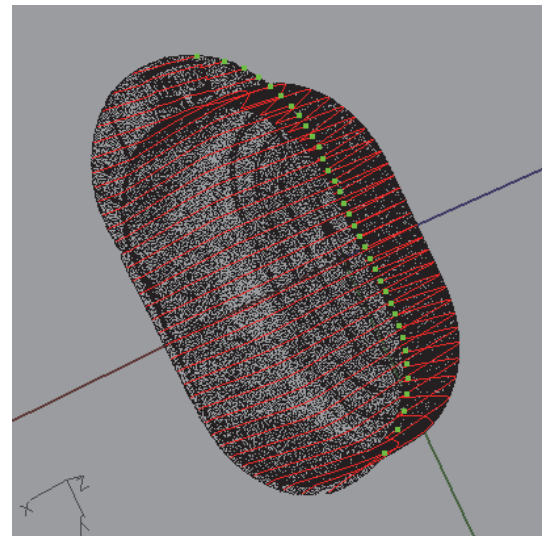

Figure 7: Spray painting path (y-axis direction).

Table 1: Comparison of spray painting experiment.

	Data for this paper	Data for literature [12]
Average (μm)	51.8	52.2
Maximum (μm)	58.1	58.3
Minimum (μm)	44.2	43.1
Painting time (s)	136	99

method proposed in this paper, but the spray painting time is obviously increased. There are two main reasons accounting for this:

(1) The painting path obtained by the spatial painting path generation method based on the exponential mean Bézier curve is longer, which leads to the longer spray painting time.

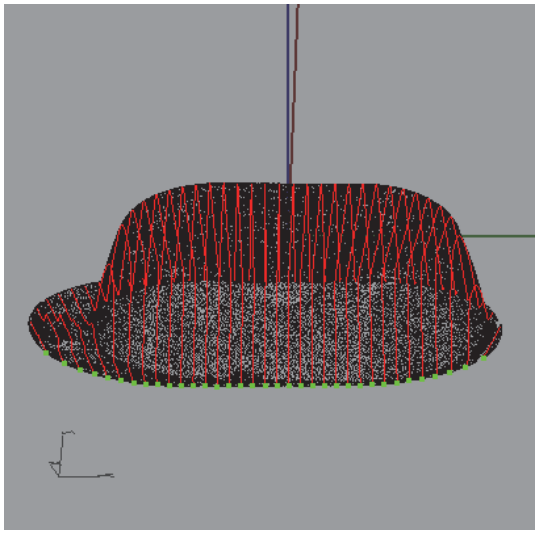

Figure 8: Spray painting path (z-axis direction).

Figure 9: Spray painting experiment of V-direction path planning for FANUC robot.

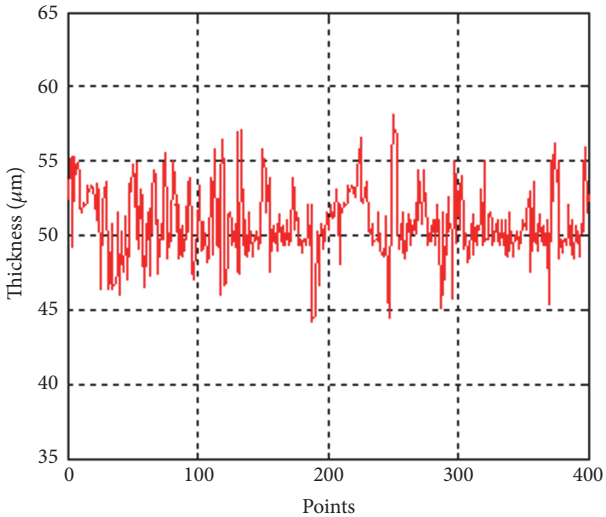

Figure 10: Material thickness of random chosen points for V-direction trajectory.

(2) Since the method is carried out with uniform spray painting, the spray painting speed is not optimized. That is, the robot does not have the acceleration and deceleration process during the spray painting operation. So the spray painting time is longer.

However, it should be noted that although the method in literature [12] can optimize the spray painting speed, it is based on the situation that the workpiece is divided into a number of triangular facets. When the sprayed workpiece is relatively large, the number of triangles will also be very large. In the multiobjective optimization problem with constraints, the two optimization objectives: paint thickness uniformity and spray painting time are coupled and competing with each other, which makes it difficult to solve the exact solution of this multiobjective optimization problem. In this case, for workpiece with large curved surface, the solution will inevitably lead to slower system operation and system real-time deterioration, and the calculation error will become larger. At this point, the spray painting effect should be better when using the method proposed in this chapter for uniform spray painting.

5. Conclusion

In this paper, a new trajectory optimization method based on the Bézier method on complex curved surface is proposed. By using the Bézier triangular surface modeling technique, the complex surface is modeled and the discrete points array on the equidistant surface of the toric surface is found by using the discrete point array calculation method of Bézier surface equidistant surface. Then the spatial painting path generation method based on the exponential mean Bézier curve is used to obtain the spatial painting path on the complex curved surface. And then, according to a new paint thickness algorithm in the spray painting model on complex curved surface, the spray painting trajectory is optimized along the specified spatial path and a complete spray painting trajectory on the complex curved surface is obtained. The biggest advantage of this method is that it does not need to patch the complex curved surface but makes full use of the flexible feature of exponential mean Bézier curves to plan the spatial painting path first. This method enhances the potential flexibility of the shape control on painting path. The experimental results show that it is better to use the method proposed in this paper to make the uniform spraying effect when spraying the large surface workpiece.

Conflicts of Interest

The authors declare that there are no conflicts of interest.

Acknowledgments

This research is supported by the National Natural Science Foundation of China (nos. 51505193 and 61503162), Project Funded by China Postdoctoral Science Foundation (2016M601691), the Major Research and Development Project (Modern Agriculture) of Zhenjiang City (NY2015025), Top-Notch Academic Programs Project of

Jiangsu Higher Education Institutions (PPZY2015C216), and Natural Science Foundation of Jiangsu Province in China (no. BK20150473).

References

[1] Z. Yuan, "Trajectory planning of Bezier curve based on improved genetic algorithm," *Journal of Shanghai Dian Ji University*, vol. 15, no. 4, pp. 237–240, 2012.

[2] Z. Jie, C. Zongyan, L. Tiger, and L. Qingtao, "Optimal path planning for autonomous mobile robot based on Bezier curve," *Journal of Lanzhou University (Natural Science Edition)*, vol. 49, no. 2, pp. 249–254, 2013.

[3] I. Juhász and Á. Róth, "A class of generalized B-spline curves," *Computer Aided Geometric Design*, vol. 30, no. 1, pp. 85–115, 2013.

[4] A. Stentz, "Optimal and efficient path planning for partially-known environments," in *Proceedings of the IEEE International Conference on Robotics and Automation*, vol. 4, pp. 3310–3317, 2002.

[5] N. Toljic, K. Adamiak, G. S. P. Castle, H.-H. Kuo, and H.-T. Fan, "Three-dimensional numerical studies on the effect of the particle charge to mass ratio distribution in the electrostatic coating process," *Journal of Electrostatics*, vol. 69, no. 3, pp. 189–194, 2011.

[6] E. Kolakowska, S. F. Smith, and M. Kristiansen, "Constraint optimization model of a scheduling problem for a robotic arm in automatic systems," *Robotics and Autonomous Systems*, vol. 62, no. 2, pp. 267–280, 2014.

[7] A. Gasparetto, R. Vidoni, D. Pillan, and E. Saccavini, "Automatic path and trajectory planning for robotic spray painting," in *Proceedings of the 7th German Conference on Robotics*, pp. 211–216, Munich, German, 2012.

[8] W. Chen, D. A. Zhao, and X. Y. Ping, "Spraying path planning of spray robot based on ant colony algorithm," *Machinery Design and Manufacture*, vol. 7, pp. 67–69, 2011.

[9] H. Chen and W. Sheng, "Transformative industrial robot programming in surface manufacturing," in *Proceedings of the IEEE International Conference on Robotics and Automation*, pp. 6059–6064, Shanghai, China, May 2011.

[10] M. Posa, C. Cantu, and R. Tedrake, "A direct method for trajectory optimization of rigid bodies through contact," *International Journal of Robotics Research*, vol. 33, no. 1, pp. 69–81, 2014.

[11] Y. Zeng, J. Gong, N. Xu, and N. Wu, "Tool trajectory optimization of spray painting robot for many-times spray painting," *International Journal of Control and Automation*, vol. 7, no. 8, pp. 193–208, 2014.

[12] W. Chen, Y. Tang, and Q. Zhao, "A novel trajectory planning scheme for spray painting robot with Bézier curves," in *Proceedings of the 28th Chinese Control and Decision Conference, CCDC 2016*, pp. 6746–6750, China, May 2016.

[13] W. Chen and D. Zhao, "Path planning for spray painting robot of workpiece surfaces," *Mathematical Problems in Engineering*, vol. 2013, Article ID 659457, 6 pages, 2013.

[14] B. Li and Z. Shao, "Precise trajectory optimization for articulated wheeled vehicles in cluttered environments," *Advances in Engineering Software*, vol. 92, pp. 40–47, 2016.

[15] P. J. From, J. Gunnar, and J. T. Gravdahl, "Optimal paint gun orientation in spray paint applications-experimental results," *IEEE Transactions on Automation Science and Engineering*, vol. 8, no. 2, pp. 438–442, 2011.

[16] F. Nagata, Y. Okada, T. Kusano, and K. Watanabe, "CLS Data Interpolation with Spline Curves and Its Post Processing for Generating a Robot Language," in *Proceedings of the International Conference on Industrial Application Engineering 2017*, pp. 358–363.

Hindawi
Mathematical Problems in Engineering
Volume 2017, Article ID 3068548, 5 pages
https://doi.org/10.1155/2017/3068548

Research Article

Data-Driven Fault Diagnosis Method for Power Transformers Using Modified Kriging Model

Yu Ding and Qiang Liu

School of Information and Control Engineering, Liaoning Shihua University, Fushun, Liaoning 113001, China

Correspondence should be addressed to Qiang Liu; neuliuqiang@163.com

Received 25 May 2017; Accepted 20 September 2017; Published 22 October 2017

Academic Editor: Wanquan Liu

A data-driven fault diagnosis method that combines Kriging model and neural network is presented and is further used for power transformers based on analysis of dissolved gases in oil. In order to improve modeling accuracy of Kriging model, a modified model that replaces the global model of Kriging model with BP neural network is presented and is further extended using linearity weighted aggregation method. The presented method integrates characteristics of the global approximation of the neural network technology and the localized departure of the Kriging model, which improves modeling accuracy. Finally, the validity of this method is demonstrated by several numerical computations of transformer fault diagnosis problems.

1. Introduction

Transformer is one of the most important equipment in power system [1], which is mainly used to transfer electrical energy between two or more circuits through electromagnetic induction. In the course of using this equipment, some factors such as electrical, thermal, and mechanical stresses may lead to irreversible damage to the insulating material [2]. In order to improve the reliability of power supply, fault diagnosis for transformer has drawn much attention from researchers, and many fault diagnosis methods have been widely proposed during the past decades.

At present, Dissolved Gas-in-oil Analysis (DGA) is a commonly used method to identify incipient failures of transformer fault [3]. With the development of artificial intelligence and computer technology, many fault diagnosis algorithms have been proposed based on DGA, such as neural network [4, 5], fuzzy logic [6, 7], expert system [8], support vector machine [2, 9], and rough set theory [10]. Given that existing methods have their own characteristics and some limitations, effective fault diagnosis methods that integrate advantages of existing technologies to improve the modeling accuracy still remain an open area of research.

As a classic modeling technology, Kriging model combines a global model plus localized departures to construct approximation from sample data. It has been widely used in the field of Computer-Aided Engineering (CAE) [11, 12]. On the other hand, neural network technology is a well-known information processing paradigm and has been widely applied in various areas due to its advantages such as adaptive learning. In this paper, a data-driven fault diagnosis model based on Kriging model and BP neural network is constructed and then is used for transformer fault diagnosis problems based on DGA. In order to improve the modeling accuracy of Kriging model, BP neural network is used to modify the global model of Kriging model, where the modified formula is given in detail. The modified Kriging model combines global and adaptive learning abilities of neural network technology and retains the localized departures of the Kriging model in the meantime. It integrates the advantages of both methods, which thus effectively improve the modeling accuracy. Finally, some examples of transformer fault diagnosis show that the proposed method is effective and feasible.

2. Overall Design of Modified Kriging Model: A Hybrid Model

The Kriging model is an unbiased estimation model based on the minimum variance estimation of sample points and their

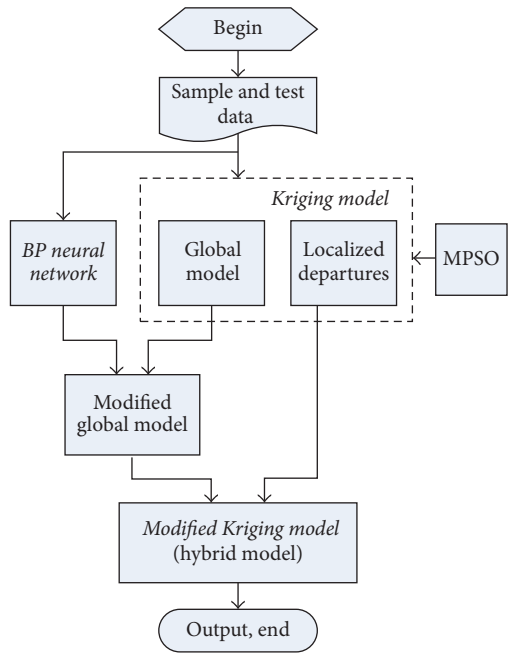

Figure 1: Overall design of hybrid model.

response values. The output can be viewed as a combination of a regression model and a stochastic process [13, 14]. The regression model is equivalent to the global simulation of the sample space, and the stochastic process is equivalent to local deviation.

In order to further improve the accuracy of the Kriging model, this paper proposes a transformer fault diagnosis method that combines Kriging model and neural network technology. The structure of this hybrid model is shown in Figure 1. The main steps for constructing the hybrid model are as follows:

(1) Determine characteristic variables and fault types based on DGA method, and collect sample data and test data.

(2) According to sample data, construct BP network model.

(3) Construct the Kriging model based on sample data.

(4) The global simulation of Kriging model is modified and updated by neural network, and then the hybrid model is constructed.

3. Modeling Method of Hybrid Model

3.1. Kriging Model and Parameter Optimization. The Kriging model contains global simulation plus localized departures, and the basic principles of which can be briefly given as follows [13, 14]: set approximate function as $y(x)$, and the function between the response value and the independent variable of the system can be formulated as follows:

$$y(x) = F(\beta, x) + Z(x), \tag{1}$$

where $y(x)$ is the unknown function of interest, $F(\beta, x)$ is the regression model that is equivalent to the global simulation, and β is regression parameter; $Z(x)$ is a normal stochastic process in which the mean value is 0 and the variance is denoted as σ^2. It reflects the randomness of the response and is equivalent to partial divergence.

The covariance matrix of $Z(x)$ is formulated as follows:

$$\operatorname{cov}\left[Z(x_i), Z(x_j)\right] = \delta^2 \mathbf{R}\left[R(\theta, x_i, x_j)\right], \tag{2}$$

where $\mathbf{R}$ is correlation matrix; the order of matrix is M. $i, j = 1, 2, \ldots, M$; M is the number of sample points; x_i and x_j are the ith and the jth sample points; $R(\theta, x_i, x_j)$ is the correlation function between x_i and x_j. In this paper, we utilize the Gaussian correlation function:

$$R(\theta, x_i, x_j) = \exp\left(-\sum_{k=1}^{N} \boldsymbol{\theta}_k \left|x_i^{(k)} - x_j^{(k)}\right|^2\right), \tag{3}$$

where N is the dimension of the problem; $x_i^{(k)}$ and $x_j^{(k)}$ are the kth dimensional components of the ith and the jth sample points, respectively; $\boldsymbol{\theta}_k$ is the unknown related parameters of the interpolation model.

In general, $\boldsymbol{\theta}_k$ can be replaced with a scalar θ. Thus, formula (3) can be formulated as

$$R(\theta, x_i, x_j) = \exp\left(-\theta \sum_{k=1}^{N} \left|x_i^{(k)} - x_j^{(k)}\right|^2\right). \tag{4}$$

Therefore, the estimated value of test point x can be given by the following equation:

$$\hat{y}(x) = \hat{\beta} + \mathbf{r}^T(x)\, \mathbf{R}^{-1}\left(\mathbf{y} - \mathbf{f}\hat{\beta}\right), \tag{5}$$

where $\hat{\beta}$ is the estimate of the global simulation; $\mathbf{y}$ is sample data response; $\mathbf{f}$ is M column vectors; $\mathbf{r}^T(x)$ is the correlation vector between observation point x and sample data, which can be formulated as follows:

$$\mathbf{r}^T(x) = \left(R(x, x_1), R(x, x_2), \ldots, R(x, x_M)\right)^T. \tag{6}$$

When $f(x)$ is a constant, $\hat{\beta}$ can be simplified and estimated by the following equation:

$$\hat{\beta} = \left(\mathbf{f}^T \mathbf{R}^{-1} \mathbf{f}\right)^{-1} \left(\mathbf{f}^T \mathbf{R}^{-1} \mathbf{y}\right). \tag{7}$$

The parameter θ determines the accuracy of the Kriging model, which can be solved by the following optimization problem:

$$\min \quad L(\theta) = |\mathbf{R}|^{1/M}\, \widehat{\delta^2}, \tag{8}$$

where $\widehat{\delta^2}$ is variance estimation, which can be determined by the following equation:

$$\widehat{\delta^2} = \frac{1}{M}\left(\mathbf{y} - \mathbf{f}\hat{\beta}\right)^T \mathbf{R}^{-1}\left(\mathbf{y} - \mathbf{f}\hat{\beta}\right). \tag{9}$$

To optimize parameter θ, intelligent optimization algorithms are commonly used. In this paper, a modified particle swarm optimization (MPSO) [15] is used to optimize the parameters of Kriging model. The key points of applying

MSPO to perform optimization are threefold: (1) make θ as encoding in real numbers; (2) take (8) as the objective function; and (3) with respect to the constraint condition of $\theta > 0$, the commonly used penalty function method is applied.

The inertia weight and learning factors in MPSO [15] are updated as follows:

$$\omega = (\omega_s - \omega_e)\left(\frac{t}{T}\right) + (\omega_e - \omega_s)\left(\frac{2t}{T}\right) + \omega_s, \tag{10}$$

$$c1 = (c1_s - c1_e)\left(\frac{t}{T}\right) + (c1_e - c1_s)\left(\frac{2t}{T}\right) + c1_s, \tag{11}$$

$$c2 = (c2_s - c2_e)\left(\frac{t}{T}\right) + (c2_e - c2_s)\left(\frac{2t}{T}\right) + c2_s, \tag{12}$$

where ω_s and ω_e are the initial value and the final value of inertia weight ω, respectively; $c1_s$ and $c1_e$ and $c2_s$ and $c2_e$ are the initial value and the final value of learning factors $c1$ and $c2$, respectively; T is the maximum number of iterations; t is the current iteration number.

3.2. Combinations of Neural Network and Kriging Model. The mapping relationship between the characteristic variables and fault types of transformer is very complex, which increases difficulty in improving high accuracy of Kriging model. On the other hand, neural network technology, for example, BP network, is a well-known information processing paradigm with some advantages such as adaptive learning and strong adaptability. The basic principle of BP network can be found in many references such as [4, 5, 16], details of which are not introduced here. In general, the output of BP network can be formulated as follows:

$$o_i = f\left(\sum_{i=0}^{n} \omega_{ij} x_j + q_i\right), \tag{13}$$

where o_i are the outputs of BP network, f is transfer function, ω_{ij} are network weights, q_i are network thresholds, and x_j are the outputs of the upper layer node.

To improve modeling accuracy, a modified Kriging model (hybrid model) is constructed by combining Kriging model and BP neural network technology, and the overall design of which has been shown in Figure 1. More specifically, the global model of Kriging model is replaced with BP neural network, which is given by (14):

$$\widehat{y}(x) = o_i + \mathbf{r}^T(x)\,\mathbf{R}^{-1}\left(\mathbf{y} - \mathbf{f}\widehat{\beta}\right). \tag{14}$$

Further, this modified method can be extended using linearity weighted aggregation method, which is formulated by (15):

$$\lambda = \gamma_1 o_i + \gamma_2 \widehat{\beta}, \tag{15}$$

where λ is the modified global model and γ_1 and γ_2 are weighting coefficients.

Thus, the final output of the hybrid model can be given as follows:

$$\widehat{y}(x) = \lambda + \mathbf{r}^T(x)\,\mathbf{R}^{-1}\left(\mathbf{y} - \mathbf{f}\widehat{\beta}\right). \tag{16}$$

Table 1: Data distribution of each fault type.

Fault type	Coding mode	Sample data	Test data
Normal	Y_1	15	15
High temperature overheating	Y_2	25	25
Medium temperature overheating	Y_3	15	15
Low temperature overheating	Y_4	9	9
Partial discharge	Y_5	9	8
Low energy discharge	Y_6	20	16
High energy discharge	Y_7	20	23

Table 2: Comparisons of diagnostic results.

Test method	Average calculation time	Accuracy rate
BP network	5.06 s	72.07%
SVM	6.21 s	75.67%
Kriging model	2.49 s	81.08%
Hybrid method	7.84 s	91.89%

Obviously, the hybrid model is of generality. When $\gamma_1 = 0$ and $\gamma_2 = 1$, the hybrid model becomes original Kriging model and (16) can be rewritten by (5). When $\gamma_1 = 1$ and $\gamma_2 = 0$, the hybrid model can be formulated by (14), where the global model of Kriging model is replaced with BP neural network.

4. Application of Transformer Fault Diagnosis

4.1. Feature Variable and Fault Type. In general, the concentrations of five gases (H_2, CH_4, C_2H_6, C_2H_4, and C_2H_2) dissolved in transformer oil can be selected as characteristic variables based on DGA data samples. The corresponding fault types of the characteristic variables contain normal, high temperature overheating, medium temperature overheating, low temperature overheating, partial discharge, low energy discharge, and high energy discharge. In this paper, we select some DGA data published in [17, 18]. The distributions and coding of these fault data are shown in Table 1.

4.2. Parameter Setting. In this paper, BP network structure is set as three-layer network. The selected sample data have 5 characteristic variables; thus the number of nodes in the input layer of the network is set as 5; the number of nodes in the output layer is set as 1; the number of hidden layer nodes is set as 8 by trial and error. The initial weights and thresholds of the network are randomly initialized, and Log-sigmoid is selected as function transfer function.

Parameters of MPSO are set as follows: $\omega_s = 0.95$, $\omega_e = 0.55$, $c1_s = c2_e = 2.25$, $c1_e = c2_s = 0.75$, $T = 40$, and population size $P = 20$. Figure 2 shows the MPSO convergence curve of objective function.

4.3. Analysis of Examples. (1) Table 2 shows the comparisons between the proposed method and other methods. As far as these test examples are concerned, the proposed method

Table 3: Some test results (μL/L).

Serial number	H_2	CH_4	C_2H_6	C_2H_4	C_2H_2	Fault type	
						Actual fault	Fault analysis
(1)	93	58	43	37	0	Middle temperature overheating	Middle temperature overheating
(2)	139	52	6.8	63	9.6	Middle and low temperature overheating	Middle temperature overheating
(3)	19.6	320.7	279.2	574.7	0	High temperature overheating	High temperature overheating
(4)	457	79	54	190	2.4	High temperature overheating	High temperature overheating
(5)	279	41	18.1	42	31.8	High energy discharge	High energy discharge
(6)	14.67	3.68	10.54	2.71	0.2	Normal	Normal
(7)	345	112.25	27.5	51.5	58.75	Low energy discharge	Low energy discharge
(8)	217.5	40	4.9	51.8	67.5	High energy discharge	High energy discharge
(9)	181	262	210	528	0	Middle and low temperature overheating	Low temperature overheating
(10)	44.3	17.3	3.6	23.3	10.4	High energy discharge	High energy discharge
(11)	172.9	334.1	172.9	812.5	37.7	Partial discharge	Partial discharge
(12)	12.26	8.86	13.95	18.21	0	Normal	Low energy discharge
(13)	56	78	18	173	0	Low temperature overheating	Low temperature overheating

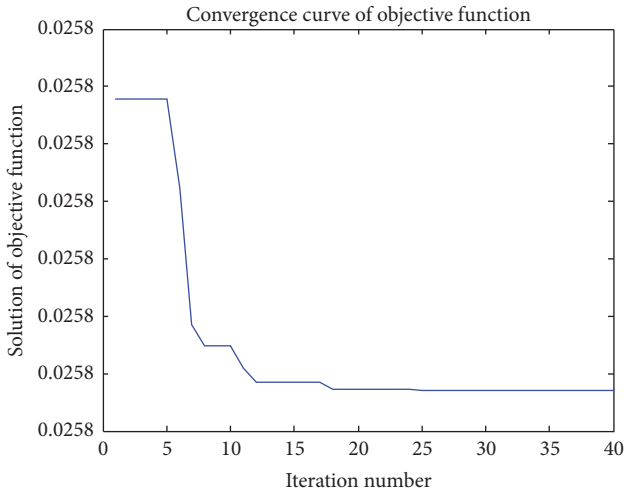

Figure 2: Convergence curve of MPSO.

can effectively improve the accuracy of transformer fault diagnosis.

(2) Tables 2 and 1 also show that the calculation time of presented method is averagely about 7.84 s for test data including 111 sample points (hardware configuration: CPU i5, RAM 4 G; programming software: Matlab), which demonstrates the efficiency of the presented method.

(3) Table 3 lists some test results using the presented method (due to limitation of paper length, the complete results are not listed here). The results show that diagnosis accuracy is basically satisfactory.

5. Conclusions

In this paper, a data-driven fault diagnosis model based on Kriging model and neural network is proposed. The proposed model is based on the Kriging model and integrates neural network technology. Meanwhile, the localized departures of Kriging model are retained.

The presented hybrid model is further used for power transformer fault diagnosis problems based on DGA method. Some numerical computations of transformer fault diagnosis problems are conducted, and the results show the feasibility and efficiency of the proposed method. In addition, the presented modified Kriging model is of some potential application value in other areas such as power system and engineering machinery.

Conflicts of Interest

The authors declare that the mentioned received funding did not lead to any conflicts of interest regarding the publication of this manuscript and there are not any possible conflicts of interest in the manuscript.

Acknowledgments

This study is supported by Program for Liaoning Excellent Talents in University (Grant no. LJQ2014037) and Natural Science Foundation of Liaoning Province of China (Grant no. 20170540589).

References

[1] J. Pleite, C. Gonzalez, J. Vazquez, and A. Lazaro, "Power Transfomer Core Fault Diagnosis Using Frequency Response Analysis," in *Proceedings of the MELECON 2006 - 2006 IEEE Mediterranean Electrotechnical Conference*, pp. 1126–1129, Benalmadena, Spain.

[2] S.-W. Fei and X.-B. Zhang, "Fault diagnosis of power transformer based on support vector machine with genetic algorithm," *Expert Systems with Applications*, vol. 36, no. 8, pp. 11352–11357, 2009.

[3] S. S. M. Ghoneim and I. B. M. Taha, "A new approach of DGA interpretation technique for transformer fault diagnosis," *International Journal of Electrical Power & Energy Systems*, vol. 81, pp. 265–274, 2016.

[4] Y. J. Sun, S. Zhang, C. X. Miao et al., "Improved BP neural network for transformer fault diagnosis," *Journal of China*

University of Mining & Technology, vol. 17, no. 01, pp. 138–142, 2007.

[5] S. Seifeddine, B. Khmais, and C. Abdelkader, "Power transformer fault diagnosis based on dissolved gas analysis by artificial neural network," in *Proceedings of the 2012 1st International Conference on Renewable Energies and Vehicular Technology, REVET 2012*, pp. 230–236, March 2012.

[6] S. M. Islam, T. Wu, and G. Ledwich, "A novel fuzzy logic approach to transformer fault diagnosis," *IEEE Transactions on Dielectrics and Electrical Insulation*, vol. 7, no. 2, pp. 177–186, 2000.

[7] Y.-C. Huang and H.-C. Sun, "Dissolved gas analysis of mineral oil for power transformer fault diagnosis using fuzzy logic," *IEEE Transactions on Dielectrics and Electrical Insulation*, vol. 20, no. 3, pp. 974–981, 2013.

[8] C. E. Lin, J. M. Ling, and C. L. Huang, "An expert system for transformer fault diagnosis using dissolved gas analysis," *IEEE Transactions on Power Delivery*, vol. 8, no. 1, pp. 231–238, 1993.

[9] Y.-C. Xiao, X.-H. Chen, and H.-J. Zhu, "Application of genetic support vector machine in power transformer fault diagnosis," *Shanghai Jiaotong Daxue Xuebao/Journal of Shanghai Jiaotong University*, vol. 41, no. 11, pp. 1878–1886, 2007.

[10] A.-H. Zhou, H. Song, H. Xiao, and X.-H. Zeng, "Power transformer fault diagnosis based on integrated of rough set theory and neural network," in *Proceedings of the 2nd International Conference on Intelligent Systems Design and Engineering Applications, ISDEA 2012*, pp. 1463–1465, January 2012.

[11] S. Jeong, M. Murayama, and K. Yamamoto, "Efficient optimization design method using kriging model," *Journal of Aircraft*, vol. 42, no. 2, pp. 413–420, 2005.

[12] T. W. Simpson, T. M. Mauery, J. J. Korte, and F. Mistree, "Kriging models for global approximation in simulation-based multidisciplinary design optimization," *AIAA Journal*, vol. 39, no. 12, pp. 2233–2241, 2001.

[13] S. Dey, T. Mukhopadhyay, and S. Adhikari, "Stochastic free vibration analyses of composite shallow doubly curved shells - A Kriging model approach," *Composites Part B: Engineering*, vol. 70, no. 5, pp. 99–112, 2015.

[14] Z. Chen, S. Peng, X. Li et al., "An important boundary sampling method for reliability-based design optimization using kriging model," *Structural and Multidisciplinary Optimization*, vol. 52, no. 1, pp. 55–70, 2015.

[15] Q. Liu and C. Wang, "Pipe-assembly approach for aero-engines by modified particle swarm optimization," *Assembly Automation*, vol. 30, no. 4, pp. 365–377, 2010.

[16] H. M. Guo and A. Yang, "Diagnosis of transformer fault based on GA-BP neural network," *Coal Mine Machinery*, vol. 36, no. 7, pp. 318–320, 2015.

[17] Y. B. Tang, *Data-Driven Fault Diagnosis and Prediction for Large-Scale Power Transformer*, Central South University, Changsha, China, 2013.

[18] W. Gao, *Study on Fault Diagnosis for Power Transformer Based on Support Vector Machine of Artificial Immune Algorithm*, Taiyuan University of Technology, Taiyuan, China, 2012.

Hindawi
Mathematical Problems in Engineering
Volume 2017, Article ID 2597071, 13 pages
https://doi.org/10.1155/2017/2597071

Research Article

H_∞ Control for T-S Fuzzy Singularly Perturbed Switched Systems

Qianjin Wang, Linna Zhou, Wei Dai, and Xiaoping Ma

School of Information and Control Engineering, China University of Mining and Technology, Xuzhou 221116, China

Correspondence should be addressed to Linna Zhou; linnazhou@cumt.edu.cn

Received 20 March 2017; Revised 4 August 2017; Accepted 12 September 2017; Published 15 October 2017

Academic Editor: Asier Ibeas

This paper is concerned with the design of fuzzy controller with guaranteed H_∞ performance for a class of Takagi-Sugeno (T-S) fuzzy singularly perturbed switched systems. First, by using the average dwell time approach together with the piecewise Lyapunov function technique, a state feedback controller that depends on the singular perturbation parameter ε is developed. This controller is shown to work well for all $\varepsilon \in (0, \varepsilon_0]$. Then, for sufficiently small ε, an ε-independent controller design method is proposed. Furthermore, under the ε-independent controller, the ε-bound estimation problem of the overall switched closed-loop system is solved. Finally, an inverted pendulum system is used to evaluate the feasibility and effectiveness of the obtained results.

1. Introduction

Many practical systems possess multiple time scale characteristics [1–4]. It is well known that control methods for normal systems can not be directly applied to this class of systems, since these methods may cause ill-conditioned numerical problems. To conquer these problems, singular perturbation methods have been widely used in control design of multiple time scale systems (see [5–9] and the references therein).

Singularly perturbed systems (SPSs), whose partial time derivatives involve a small singular perturbation parameter ε, have been widely investigated by many researchers. It is important to obtain the ε-bound such that stability and other performances of SPSs can be ensured. Studies on ε-bound can be mainly divided into two types: one only presents sufficient conditions for the existence of the ε-bound [10, 11], and the other proposes methods to estimate the ε-bound [9, 12].

Singularly perturbed switched systems (SPSSs) consist of a group of SPSs and a certain switching law, which specifies the active SPS at the switching instance. In practical processes, a great number of control systems, whose behavior is simultaneously determined by multiple time scales and switching, can be modeled as SPSSs [13–15]. The control model of the hot strip mill was treated as a SPSS and an H_2 robust controller was designed in [15]. Recently, SPSSs have attained much attention in the literature (see [16–20]). It has been shown in [17–20] that the stability of fast/slow switched subsystems can not guarantee the stability of the original switched systems. In order to guarantee the system stability under an arbitrary switching signal, a common Lyapunov function for individual SPSs or a dwell time scheme has to be considered. In [19], by combining the multiple Lyapunov functions method with the dwell time scheme, sufficient conditions for ensuring exponential stability of time-delay SPSSs with stable fast switched subsystems were derived. These conditions were described by a few ε-dependent algebraic inequalities, which led to a heavy and tedious calculation. The proposed method in [19] was further extended to time-delay SPSSs with impulsive effects [20]. However, few results on the ε-bound estimation are available for SPSSs. The exceptions were given by [21, 22]. A convex optimization based method was presented to make the best estimate of ε-bound for SPSSs whose fast switched subsystems can not depend on the switching signal in [21]. The ε-dependent stabilization and ε-bound problems were addressed by adopting dwell time switching signal and constructing ε-dependent multiple Lyapunov functions for SPSSs in [22].

Fuzzy control has been widely used for engineering practice [23, 24]. The Takagi-Sugeno (T-S) model, which has elegant ability to approximate a certain class of complex

nonlinear functions, was extensively utilized in control system design [25–27]. Based on T-S fuzzy control, many LMI-based fuzzy control design methods have been developed for SPSs. The stabilization problem was addressed for fuzzy SPSs in [28], and some LMI-based control algorithms were proposed. Over past a few years, H_∞ control for fuzzy SPSs has attained a lot of attention. H_∞ control was addressed for fuzzy SPSs in [11, 29–31], and sufficient conditions independent of ε for the existence of H_∞ controller were presented. The resulting conditions in [11, 28–31] are only applicable to stabilizing the system and being with an H_∞ performance for sufficiently small ε. Hence, some researchers have concentrated on the ε-bound design problem for fuzzy SPSs [32–34].

As an important class of hybrid systems, switched fuzzy systems have been a hot spot of present research. Recently, a great number of theoretical results are available for switched fuzzy systems. By using a common or multiple Lyapunov functions method, stability issues for switched fuzzy systems were considered in [35–39]. However, the existing literature on fuzzy SPSSs is rather limited. An LMI-based dynamic state feedback control method was given and the ε-bound problem of system was solved for nonaffine-in-control SPSSs [40]. This method decomposed the switched system into fast and slow subsystems and can not be suitable for nonstandard fuzzy SPSSs. In our previous paper [41], where the stabilization and ε-bound problems were addressed for T-S fuzzy SPSSs without the external disturbance input by constructing the ε-dependent piecewise Lyapunov function. Moreover, to the authors' best knowledge, H_∞ control for fuzzy SPSSs has not been addressed yet.

In this paper, we will investigate the design of fuzzy controller with guaranteed H_∞ performance for a class of T-S fuzzy SPSSs. The problem is composed of stabilization control, H_∞ control, and ε-bound design. First, for a given upper bound ε_0 for ε and a prespecified H_∞ performance bound $\gamma > 0$, an ε-dependent controller is developed, such that, for any $\varepsilon \in (0, \varepsilon_0]$, the switched system is asymptotically stable and the L_2-gain from the disturbance input to the controlled output is less than or equal to γ. This controller is shown to work well for all $\varepsilon \in (0, \varepsilon_0]$. Then, an ε-independent controller design method is proposed in terms of LMIs. Furthermore, under the ε-independent controller, the ε-bound estimation approach is given. Finally, an inverted pendulum system is used to evaluate the feasibility and effectiveness of the obtained results.

The rest of this paper is organized as follows. In Section 2, the problems to be considered are formulated and preliminaries are presented. The main results are given in Section 3. An example is given in Section 4 to illustrate the obtained methods. And Section 5 concludes the paper. The notations used in this paper are standard. The notations T and $\star$ stand for the matrix transpose and the transpose of the off diagonal element of the LMI, respectively. $\lambda_M(Q)$ and $\lambda_m(Q)$ denote the maximal and minimal eigenvalues of a symmetric matrix Q, respectively. $\|\cdot\|$ denotes Euclidean norm for vectors or the spectral norm of matrices. $He\{\cdot\}$ is defined as $He\{\Theta\} = \Theta + \Theta^T$ for a square matrix Θ.

2. Problem Formulation

Consider a T-S fuzzy SPSS, which involves $r_{\sigma(t)}$ rules of the following form.

The lth rule is

$$\begin{aligned}
&\text{Plant Rule } l\text{:}\\
&\text{IF } \upsilon_1(t) \text{ is } M^l_{\sigma(t)1},\ \upsilon_2(t) \text{ is } M^l_{\sigma(t)2}, \ldots, \upsilon_\phi(t) \text{ is } M^l_{\sigma(t)\phi}\\
&\text{THEN}\\
&E(\varepsilon)\dot{x}(t) = A_{\sigma(t)l}x(t) + B_{\sigma(t)l}u(t) + E_{\sigma(t)l}w(t)\\
&z(t) = C_{\sigma(t)l}x(t)\\
&\text{for } l = 1, 2, \ldots, r_{\sigma(t)},
\end{aligned} \tag{1}$$

where $E(\varepsilon) = \begin{bmatrix} I_{n_1} & 0 \\ 0 & \varepsilon I_{n_2} \end{bmatrix}$, ε is a small positive scalar which represents the singular perturbation parameter. $\sigma(t)$ is a piecewise constant function with respect to time, referred as to a switching signal, which takes its values in the finite set $S = \{1, 2, \ldots, M\}$, M represents the number of individual subsystems. $M^l_{\sigma(t)m}$ ($l = 1, 2, \ldots, r_{\sigma(t)}$, $m = 1, 2, \ldots, \phi$) are fuzzy sets, $r_{\sigma(t)}$ is the number of fuzzy rules, $\upsilon(t) = \left[\upsilon_1(t)\ \upsilon_2(t)\ \cdots\ \upsilon_\phi(t)\right]^T$ is the premise vector that may depend on states in many cases, ϕ is the number of premise variables, $x(t) \in R^n$ is the state vector, $u(t) \in R^m$ is the control input, $w(t) \in R^r$ is the disturbance input that belongs to $L_2[0, \infty]$, and $z(t) \in R^p$ is the controlled output. For any given T_f, a time sequence of $t_1 < \cdots < t_{k+1}$ ($k \geq 1$) is labeled as the switching instants over the interval $(0, T_f)$. It means that the kth T-S fuzzy subsystem is active as $t \in [t_k, t_{k+1})$. And $A_{\sigma(t)l}$, $B_{\sigma(t)l}$, $E_{\sigma(t)l}$, and $C_{\sigma(t)l}$ are of the following form:

$$\begin{aligned}
A_{il} &= \begin{bmatrix} A_{il11} & A_{il12} \\ A_{il21} & A_{il22} \end{bmatrix},\\
B_{il} &= \begin{bmatrix} B_{il1} \\ B_{il2} \end{bmatrix},\\
E_{il} &= \begin{bmatrix} E_{il1} \\ E_{il2} \end{bmatrix},\\
C_{il} &= \begin{bmatrix} C_{il1} & C_{il2} \end{bmatrix},\\
&\qquad i \in S.
\end{aligned} \tag{2}$$

Denote

$$\xi_{\sigma(t)l}(\upsilon(t)) = \prod_{k=1}^{\phi} M^l_{\sigma(t)k}(\upsilon_k(t)), \quad l = 1, 2, \ldots, r_{\sigma(t)}, \tag{3}$$

where $M^l_{\sigma(t)k}(\upsilon_k(t))$ is the grade of membership of $\upsilon_k(t)$ in $M^l_{\sigma(t)k}$.

It is assumed in this paper that

$$\xi_{\sigma(t)l}(v(t)) \geq 0,$$
$$\sum_{l=1}^{r_{\sigma(t)}} \xi_{\sigma(t)l}(v(t)) > 0, \tag{4}$$
$$l = 1, 2, \ldots, r_{\sigma(t)}, \ \forall t \geq 0.$$

Let

$$\mu_{\sigma(t)l}(v(t)) = \frac{\xi_{\sigma(t)l}(v(t))}{\sum_{l=1}^{r_{\sigma(t)}} \xi_{\sigma(t)l}(v(t))}, \quad l = 1, 2, \ldots, r_{\sigma(t)}. \tag{5}$$

Then

$$\mu_{\sigma(t)l}(v(t)) \geq 0,$$
$$\sum_{l=1}^{r_{\sigma(t)}} \mu_{\sigma(t)l}(v(t)) = 1, \tag{6}$$
$$l = 1, 2, \ldots, r_{\sigma(t)}, \ \forall t \geq 0.$$

For the convenience of notations, we denote $\mu_{\sigma(t)l} = \mu_{\sigma(t)l}(v(t))$, $l = 1, 2, \ldots, r_{\sigma(t)}$.

Then, the ith T-S fuzzy subsystem can be inferred as

$$E(\varepsilon)\dot{x}(t) = \sum_{l=1}^{r_i} \mu_{il}\left[A_{il}x(t) + B_{il}u(t) + E_{il}w(t)\right]$$
$$z(t) = \sum_{l=1}^{r_i} \mu_{il}C_{il}x(t). \tag{7}$$

Throughout the paper, it is assumed that the singular perturbation parameter ε is available for feedback. By using the concept of parallel distributed compensation (PDC), the state feedback fuzzy controller can be described by the following.

The lth rule is

Controller Rule l:

IF $v_1(t)$ is M_{i1}^l, $v_2(t)$ is $M_{i2}^l, \ldots, v_\phi(t)$ is $M_{i\phi}^l$

THEN (8)

$u(t) = K_{il}(\varepsilon)x(t)$

for $i = 1, 2, \ldots, M$, $l = 1, 2, \ldots, r_i$.

Because the controller rules are the same as the plant rules, the state feedback controller is given as follows:

$$u(t) = \sum_{l=1}^{r_i} \mu_{il}K_{il}(\varepsilon)x(t). \tag{9}$$

Remark 1. In many SPSs, ε is usually a known physical parameter. Based on the fact that ε is available for feedback control, some synthesis problems are considered in [19, 20, 22]. In [22], for a given ε-bound ε_0, under the dwell time switching law, the ε-dependent multiple Lyapunov function method was proposed to ensure exponential stability of the original switched system.

Substituting (9) into (7) yields the closed-loop system

$$E(\varepsilon)\dot{x}(t) = \sum_{l=1}^{r_i}\sum_{s=1}^{r_i} \mu_{il}\mu_{is}\left[\left(A_{il} + B_{il}K_{is}(\varepsilon)\right)x(t) + E_{il}w(t)\right]$$
$$z(t) = \sum_{l=1}^{r_i} \mu_{il}C_{il}x(t). \tag{10}$$

Upon introducing the indicator function

$$\theta(t) = \left[\theta_1(t), \ldots, \theta_M(t)\right], \tag{11}$$

where $\theta_i(t) = 1$ if the switching system is in mode i and $\theta_i(t) = 0$ if it is in a different mode, and the overall switched closed-loop system can be expressed as follows:

$$E(\varepsilon)\dot{x}(t) = \sum_{l=1}^{r_i}\sum_{s=1}^{r_i}\sum_{i=1}^{M} \mu_{il}\mu_{is}\theta_i(t) \cdot \left[\left(A_{il} + B_{il}K_{is}(\varepsilon)\right)x(t) + E_{il}w(t)\right]$$
$$z(t) = \sum_{l=1}^{r_i}\sum_{i=1}^{M} \mu_{il}\theta_i(t)C_{il}x(t). \tag{12}$$

We now recall standard notations and preliminaries, which will help formulate our main results.

Definition 2 (see [42]). For $u(t) = 0$, $w(t) = 0$ and the initial condition $x(t_0)$, the equilibrium $x = 0$ of system (7) is said to be asymptotically stable under certain switching signal $\sigma(t)$ if there exist constants $\alpha > 0, \delta > 0$ such that the solution of the system satisfies $\|x(t)\| < \alpha e^{-\delta t}\|x(t_0)\|$, $\forall t \geq t_0$.

Definition 3 (see [43]). For any switching signal $\sigma(t)$ and any $t_2 \geq t_1 \geq 0$, let $N_\sigma(t_1, t_2)$ denote the number of discontinuities $\sigma(t)$ in the interval (t_1, t_2). We say that $\sigma(t)$ has the average dwell time property if

$$N_\sigma(t_2, t_1) \leq N_0 + \frac{t_2 - t_1}{\tau_a}, \quad N_0 \geq 0, \ \tau_a > 0, \tag{13}$$

holds, where N_0 and τ_a are called the chatter bound and average dwell time, respectively. As commonly used in the literature, we choose $N_0 = 0$.

Definition 4 (see [30]). Given $\gamma > 0$, a system of the form (7) is said to be with an H_∞-norm less than or equal to γ if

$$\int_0^{T_f} z^T(t)z(t)\,dt \leq \gamma^2 \int_0^{T_f} w^T(t)w(t)\,dt \tag{14}$$

holds for $x(0) = 0$. Where T_f is the terminal time of control and $x(0)$ denotes the initial condition of system (7).

Lemma 5 (see [44]). *Given any constant η and any matrices N, Γ, Y of compatible dimensions, then we have*

$$2x^T N\Gamma Y y \leq \eta x^T NN^T x + \frac{1}{\eta} y^T Y^T Y y, \tag{15}$$

for all $x, y \in R^n$, where Γ is an uncertain matric satisfying $\Gamma^T\Gamma \le I$.

Lemma 6 (see [34]). *For a positive scalar ε_0 and the symmetric matrices S_1 and S_2 of compatible dimensions, if the inequalities*

$$\begin{aligned} S_1 &\ge 0, \\ S_1 + \varepsilon_0 S_2 &> 0 \end{aligned} \tag{16}$$

hold, then

$$S_1 + \varepsilon S_2 > 0, \quad \forall \varepsilon \in (0, \varepsilon_0]. \tag{17}$$

Lemma 7 (see [34]). *If there exist matrices Z_i $(i = 1, 2, 3)$ with $Z_i = Z_i^T$ $(i = 1, 2)$ satisfying*

$$\begin{aligned} Z_1 &> 0, \\ \begin{bmatrix} Z_1 & \varepsilon_0 Z_3^T \\ \varepsilon_0 Z_3 & \varepsilon_0 Z_2 \end{bmatrix} &> 0, \end{aligned} \tag{18}$$

then

$$E(\varepsilon) Z(\varepsilon) = Z^T(\varepsilon) E(\varepsilon) > 0, \quad \forall \varepsilon \in (0, \varepsilon_0], \tag{19}$$

where $Z(\varepsilon) = \left[\begin{smallmatrix} Z_1 & \varepsilon Z_3^T \\ Z_3 & Z_2 \end{smallmatrix}\right]$.

The problems under consideration are formulated as follows.

Problem 8. Given an H_∞ performance bound $\gamma > 0$ and an upper bound ε_0 for the singular perturbation parameter ε, under admissible switching signals with ADT property, determine a state feedback controller of form (9), such that, for all $\varepsilon \in (0, \varepsilon_0]$, the overall switched closed-loop system (12) is asymptotically stable and with an H_∞-norm less than or equal to γ.

Problem 9. Given an H_∞ performance bound $\gamma > 0$, determine a state feedback controller of the form (9), such that, under admissible switching signals with ADT property, the overall switched closed-loop system (12) is asymptotically stable and with an H_∞-norm less than or equal to γ for any sufficiently small ε.

Problem 10. Given an H_∞ performance bound $\gamma > 0$ and a controller, determine an ε-bound $\varepsilon_{\max}$, as large as possible, such that, for any $\varepsilon \in (0, \varepsilon_{\max}]$, under admissible switching signals with ADT property, the overall switched closed-loop system (12) is asymptotically stable and with an H_∞-norm less than or equal to γ.

Remark 11. The synthesis problems for T-S fuzzy SPSs have attracted much attention of many researchers. H_∞ control and ε-bound design for T-S fuzzy SPSs with pole placement constraints were considered in [34]. This paper will extend the stability analysis and control methods for normal systems to T-S fuzzy SPSSs. Problem 8 considers the stabilization controller design, ε-bound design, and H_∞ control. Problem 9 aims to design a controller without considering the ε-bound. Problem 10 is used to estimate the ε-bound of the switched system.

3. Controller Design

This section will present a controller design method to solve Problem 8.

Theorem 12. *Give an H_∞ performance bound $\gamma > 0$, an upper bound ε_0, and two constants, $\lambda > 0$ and $\mu \ge 1$, if there exist matrices F_{il} $(l = 1, 2, \ldots, r_i)$, Z_{i1}, Z_{i2}, and Z_{i3} of compatible dimensions with $Z_{ik} = Z_{ik}^T$ $(k = 1, 2)$, such that*

$$Z_{i1} > 0, \tag{20}$$

$$\begin{bmatrix} Z_{i1} & * \\ \varepsilon_0 Z_{i3} & \varepsilon_0 Z_{i2} \end{bmatrix} > 0, \tag{21}$$

$$\begin{bmatrix} He\{A_{il} Z_i(0) + B_{il} F_{il}\} + \lambda Z_i^T(0) E(0) & * & * \\ E_{il}^T & -I_r & * \\ C_{il} Z_i(0) & 0 & -\gamma^2 \end{bmatrix} < 0, \tag{22}$$

$$\begin{bmatrix} He\{A_{il} Z_i(\varepsilon_0) + B_{il} F_{il}\} + \lambda Z_i^T(\varepsilon_0) E(\varepsilon_0) & * & * \\ E_{il}^T & -I_r & * \\ C_{il} Z_i(\varepsilon_0) & 0 & -\gamma^2 \end{bmatrix} < 0, \tag{23}$$

$$\begin{bmatrix} \Upsilon_1 & * & * \\ E_{il}^T + E_{is}^T & -2I_r & * \\ C_{il} Z_i(0) + C_{is} Z_i(0) & 0 & -2\gamma^2 \end{bmatrix} < 0, \quad l < s, \tag{24}$$

$$\begin{bmatrix} \Upsilon_2 & * & * \\ E_{il}^T + E_{is}^T & -2I_r & * \\ C_{il} Z_i(\varepsilon_0) + C_{is} Z_i(\varepsilon_0) & 0 & -2\gamma^2 \end{bmatrix} < 0, \quad l < s, \tag{25}$$

$$Z_{j1} \le \mu Z_{i1}, \quad i \ne j, \tag{26}$$

$$\begin{bmatrix} Z_{j1} & * \\ \varepsilon_0 Z_{j3} & \varepsilon_0 Z_{j2} \end{bmatrix} \le \mu \begin{bmatrix} Z_{i1} & * \\ \varepsilon_0 Z_{i3} & \varepsilon_0 Z_{i2} \end{bmatrix}, \quad i \ne j, \tag{27}$$

where $l, s = 1, 2, \ldots, r_i$, $i, j = 1, 2, \ldots, M$, $\Upsilon_1 = He\{A_{il} Z_i(0) + B_{il} F_{is} + A_{is} Z_i(0) + B_{is} F_{il}\} + \lambda Z_i^T(0) E(0)$, $\Upsilon_2 = He\{A_{il} Z_i(\varepsilon_0) + B_{il} F_{is} + A_{is} Z_i(\varepsilon_0) + B_{is} F_{il}\} + \lambda Z_i^T(\varepsilon_0) E(\varepsilon_0)$, and $Z_i(\varepsilon) = \left[\begin{smallmatrix} Z_{i1} & \varepsilon Z_{i3}^T \\ Z_{i3} & Z_{i2} \end{smallmatrix}\right]$.

Then, for any $\varepsilon \in (0, \varepsilon_0]$, the overall switched closed-loop system (12) with $K_{il}(\varepsilon) = F_{il} Z_i^{-1}(\varepsilon)$ $(l = 1, 2, \ldots, r_i)$, $Z_i(\varepsilon) = U_{i1} + \varepsilon U_{i2}$ is asymptotically stable and with an H_∞-norm less than or equal to γ under any switching signal with ADT

$$\tau_a \ge \frac{\ln^\mu}{\lambda}. \tag{28}$$

Proof. Based on Lemma 6, LMIs (22) and (23) imply that

$$\begin{bmatrix} He\{A_{il} Z_i(\varepsilon) + B_{il} F_{il}\} + \lambda Z_i^T(\varepsilon) E(\varepsilon) & * & * \\ E_{il}^T & -I_r & * \\ C_{il} Z_i(\varepsilon) & 0 & -\gamma^2 \end{bmatrix} < 0, \quad \forall \varepsilon \in (0, \varepsilon_0]. \tag{29}$$

By the Schur complement, inequality (29) is equivalent to

$$He\left\{A_{il}Z_i(\varepsilon)+\mathrm{B}_{il}F_{il}\right\}+\lambda Z_i^T(\varepsilon)E(\varepsilon)+E_{il}E_{il}^T+\frac{1}{\gamma^2}Z_i^T(\varepsilon)C_{il}^TC_{il}Z_i(\varepsilon)<0,\quad \forall\varepsilon\in(0,\varepsilon_0]. \tag{30}$$

Pre- and postmultiplying (30) by $Z_i^{-T}(\varepsilon)$ and its transpose, respectively, we obtain

$$He\left\{P_i^T(\varepsilon)\left(A_{il}+B_{il}K_{il}(\varepsilon)\right)\right\}+\lambda E(\varepsilon)P_i(\varepsilon)+P_i^T(\varepsilon)E_{il}E_{il}^TP_i(\varepsilon)+\frac{1}{\gamma^2}C_{il}^T\times C_{il}<0,\quad \forall\varepsilon\in(0,\varepsilon_0], \tag{31}$$

where $K_{il}(\varepsilon)=F_{il}Z_i^{-1}(\varepsilon)$ and $P_i(\varepsilon)=Z_i^{-1}(\varepsilon)$.

Using Lemma 6 again, it follows from (24) and (25) that

$$\begin{bmatrix}\Upsilon_3 & * & *\\ E_{il}^T+E_{is}^T & -2I_r & *\\ C_{il}Z_i(\varepsilon)+C_{is}Z_i(\varepsilon) & 0 & -2\gamma^2\end{bmatrix}<0,\quad \forall\varepsilon\in(0,\varepsilon_0],\ l<s, \tag{32}$$

where $\Upsilon_3 = He\{A_{il}Z_i(\varepsilon)+B_{il}F_{is}+A_{is}Z_i(\varepsilon)+B_{is}F_{il}\}+\lambda Z_i^T(\varepsilon)E(\varepsilon)$.

By the Schur complement, inequality (32) can be replaced by the following inequality:

$$\Upsilon_3+\frac{1}{2}\left(E_{il}+E_{is}\right)\left(E_{il}^T+E_{is}^T\right)+\frac{1}{2\gamma^2}\left(C_{il}Z_i(\varepsilon)+C_{is}Z_i(\varepsilon)\right)^T\cdot\left(C_{il}Z_i(\varepsilon)+C_{is}\times Z_i(\varepsilon)\right)<0,\quad \forall\varepsilon\in(0,\varepsilon_0],\ l<s. \tag{33}$$

By using Lemma 5, we get from inequality (33) that

$$\Upsilon_3+He\left\{E_{il}E_{is}^T+\frac{1}{\gamma^2}Z_i^T(\varepsilon)C_{il}^TC_{is}Z_i(\varepsilon)\right\}<0,\quad \forall\varepsilon\in(0,\varepsilon_0],\ l<s. \tag{34}$$

Pre- and postmultiplying (34) by $Z_i^{-T}(\varepsilon)$ and its transpose, respectively, we have

$$He\left\{P_i^T(\varepsilon)\left(A_{il}+B_{il}K_{is}(\varepsilon)+A_{is}+B_{is}K_{il}(\varepsilon)\right)+P_i^T(\varepsilon)E_{il}E_{is}^TP_i(\varepsilon)+\frac{1}{\gamma^2}\times C_{il}^TC_{is}\right\}+\lambda E(\varepsilon)P_i(\varepsilon)<0,\quad \forall\varepsilon\in(0,\varepsilon_0],\ l<s. \tag{35}$$

By Lemma 7, LMI conditions (20) and (21) guarantee that the inequality

$$E(\varepsilon)Z_i(\varepsilon)=Z_i^T(\varepsilon)E(\varepsilon)>0,\quad \varepsilon\in(0,\varepsilon_0], \tag{36}$$

holds, which implies

$$E(\varepsilon)P_i(\varepsilon)=P_i^T(\varepsilon)E(\varepsilon)>0,\quad \varepsilon\in(0,\varepsilon_0]. \tag{37}$$

Define the piecewise Lyapunov function

$$V(t)=V_{\sigma(t)}(x(t))=x^T(t)E(\varepsilon)P_{\sigma(t)}(\varepsilon)x(t),\quad t\geq 0, \tag{38}$$

where $E(\varepsilon)P_{\sigma(t)}(\varepsilon)$ is switched among $E(\varepsilon)P_i(\varepsilon)$, $i=1,2,\ldots,M$, in accordance with the piecewise constant switching signal $\sigma(t)$.

Computing the derivative of $V_i(x(t))$ with respect to t along the trajectories of system (12), we have

$$\begin{aligned}\dot V_i(x(t))&=2x^T(t)E(\varepsilon)P_i(\varepsilon)\dot x(t)=2x^T(t)P_i^T(\varepsilon)\\&\cdot E(\varepsilon)\dot x(t)=\sum_{l=1}^{r_i}\sum_{i=1}^{M}\mu_{il}^2\theta_i(t)x^T(t)He\left\{P_i^T(\varepsilon)\right.\\&\cdot\left.\left(A_{il}+B_{il}K_{il}(\varepsilon)\right)\right\}x(t)+\sum_{l=1}^{r_i}\sum_{l<s}^{r_i}\sum_{i=1}^{M}\mu_{il}\mu_{is}\theta_i(t)x^T(t)\\&\cdot He\left\{P_i^T(\varepsilon)\left(A_{il}+B_{il}K_{is}(\varepsilon)+A_{is}+B_{is}K_{il}(\varepsilon)\right)\right\}\\&\cdot x(t)+\sum_{l=1}^{r_i}\sum_{i=1}^{M}\mu_{il}\theta_i(t)He\left\{x^T(t)P_i^T(\varepsilon)\times E_{il}w(t)\right\},\\&\qquad\varepsilon\in(0,\varepsilon_0].\end{aligned} \tag{39}$$

Using Lemma 5 again, we obtain

$$2x^T(t)P_i^T(\varepsilon)E_{il}w(t)\leq x^T(t)P_i^T(\varepsilon)E_{il}E_{il}^TP_i(\varepsilon)x(t)+w^T(t)w(t),\quad \varepsilon\in(0,\varepsilon_0]. \tag{40}$$

From equality (39) and inequality (40), it follows that

$$\begin{aligned}\dot V_i(x(t))\leq&\sum_{l=1}^{r_i}\sum_{i=1}^{M}\mu_{il}^2\theta_i(t)x^T(t)\left\{He\left\{P_i^T(\varepsilon)\right.\right.\\&\cdot\left.\left(A_{il}+B_{il}K_{il}(\varepsilon)\right)\right\}+P_i^T(\varepsilon)E_{il}E_{il}^T\times P_i(\varepsilon)\Big\}x(t)\\&+\sum_{l=1}^{r_i}\sum_{l<s}^{r_i}\sum_{i=1}^{M}\mu_{il}\mu_{is}\theta_i(t)x^T(t)\left\{He\left\{P_i^T(\varepsilon)\right.\right.\\&\cdot\left.\left(A_{il}+B_{il}\times K_{is}(\varepsilon)+A_{is}+B_{is}K_{il}(\varepsilon)\right)\right\}+P_i^T(\varepsilon)\\&\cdot\left.\left(E_{il}E_{is}^T+E_{is}E_{il}^T\right)P_i(\varepsilon)\right\}x(t)+w^T(t)w(t),\\&\qquad\varepsilon\in(0,\varepsilon_0].\end{aligned} \tag{41}$$

It follows from (31), (35), and (41) that

$$\begin{aligned}\dot{V}_i(x(t)) &\le -\lambda V_i(x(t)) - \sum_{l=1}^{r_i}\sum_{i=1}^{M}\mu_{il}^2\theta_i(t)\frac{1}{\gamma^2}x^T(t)\\ &\cdot C_{il}^T C_{il}x(t) - \sum_{l=1}^{r_i}\sum_{l<s}^{r_i}\sum_{i=1}^{M}\mu_{il}\mu_{is}\theta_i(t)\frac{1}{\gamma^2}x^T(t)\\ &\cdot\left(C_{il}^T C_{is} + C_{is}^T C_{il}\right)x(t) + w^T(t)w(t)\\ &= -\lambda V_i(x(t)) - \frac{1}{\gamma^2}z^T(t)z(t) + w^T(t)w(t),\\ &\qquad t \ge 0.\end{aligned} \tag{42}$$

Furthermore, by Lemma 6, LMIs (26) and (27) imply that

$$E(\varepsilon)Z_j(\varepsilon) \le \mu E(\varepsilon)Z_i(\varepsilon), \quad i \ne j,\ \forall\varepsilon \in (0,\varepsilon_0]. \tag{43}$$

Applying the Schur complement to (43) shows that

$$\begin{bmatrix} -Z_j^{-1}(\varepsilon)E^{-1}(\varepsilon) & * \\ I & -\mu E(\varepsilon)Z_i(\varepsilon)\end{bmatrix} \le 0, \quad i \ne j,\ \forall\varepsilon \in (0,\varepsilon_0]. \tag{44}$$

Pre- and postmultiplying (44) by $\left[\begin{smallmatrix} E(\varepsilon) & 0 \\ 0 & I\end{smallmatrix}\right]^T$ and its transpose, respectively, and taking into account the fact that $P_i(\varepsilon) = Z_i^{-1}(\varepsilon)$, inequality (44) is equivalent to

$$\begin{bmatrix} -E^T(\varepsilon)P_j(\varepsilon) & * \\ E(\varepsilon) & -\mu E(\varepsilon)P_i^{-1}(\varepsilon)\end{bmatrix} \le 0, \quad i \ne j,\ \forall\varepsilon \in (0,\varepsilon_0]. \tag{45}$$

By the Schur complement, it follows from (45) that

$$E(\varepsilon)P_i(\varepsilon) \le \mu E(\varepsilon)P_j(\varepsilon), \quad i \ne j,\ \forall\varepsilon \in (0,\varepsilon_0]. \tag{46}$$

Then, the following properties are obtained for (38):

(1) Each $V_i(x(t)) = x^T(t)E(\varepsilon)P_i(\varepsilon)x(t)$ is continuous and its derivative along the trajectories of the corresponding subsystem satisfies (42).

(2) There exist constant scalars $\kappa_1 > 0$, $\kappa_2 > 0$, such that

$$\kappa_1\|x(t)\|^2 \le V_i(x(t)) \le \kappa_2\|x(t)\|^2, \quad \forall x(t) \in \Omega\left(E(\varepsilon)P_i(\varepsilon)\right), \tag{47}$$

where $\kappa_1 = \inf_{i\in S}\lambda_m(E(\varepsilon)P_i(\varepsilon))$, $\kappa_2 = \sup_{i\in S}\lambda_M(E(\varepsilon)P_i(\varepsilon))$.

(3) There exists a constant scalar $\mu \ge 1$ such that (46) holds.

Thus, $V(t)$ is piecewise monotonically decreasing and its value at switching instants is nonincreasing.

Using the differential inequality (42), we obtain that

$$\begin{aligned}V(T_f) &\le V(t_{k+1})e^{-\lambda(T_f - t_{k+1})} + \int_{t_{k+1}}^{T_f} e^{-\lambda(T_f-\tau)}\Gamma(\tau)\,d\tau\\ &\le \mu V\left(t_{k+1}^{-1}\right)e^{-\lambda(T_f - t_{k+1})} + \int_{t_{k+1}}^{T_f} e^{-\lambda(T_f-\tau)}\Gamma(\tau)\,d\tau\\ &\le \mu\left[V(t_k)e^{-\lambda(t_{k+1}-t_k)} + \int_{t_k}^{t_{k+1}} e^{-\lambda(t_{k+1}-\tau)}\Gamma(\tau)\,d\tau\right]\\ &\cdot e^{-\lambda(T_f - t_{k+1})} + \int_{t_{k+1}}^{T_f} e^{-\lambda(T_f-\tau)}\Gamma(\tau)\,d\tau = \mu V(t_k)\\ &\cdot e^{-\lambda(T_f - t_k)} + \mu\int_{t_k}^{t_{k+1}} e^{-\lambda(T_f-\tau)}\Gamma(\tau)\,d\tau\\ &+ \int_{t_{k+1}}^{T_f} e^{-\lambda(T_f-\tau)}\Gamma(\tau)\,d\tau,\end{aligned} \tag{48}$$

where $\Gamma(\tau) = w^T(\tau)w(\tau) - (1/\gamma^2)z^T(\tau)z(\tau)$.

It follows from (48) that

$$\begin{aligned}V(T_f) &\le \mu^{k+1}e^{-\lambda T_f}V(0) + \mu^{k+1}\int_0^{t_1} e^{-\lambda(T_f-\tau)}\Gamma(\tau)\,d\tau\\ &+ \mu^k\int_{t_1}^{t_2} e^{-\lambda(T_f-\tau)}\times\Gamma(\tau)\,d\tau + \cdots\\ &+ \mu\int_{t_k}^{t_{k+1}} e^{-\lambda(T_f-\tau)}\Gamma(\tau)\,d\tau + \int_{t_{k+1}}^{T_f} e^{-\lambda(T_f-\tau)}\\ &\times\Gamma(\tau)\,d\tau\\ &= \mu^{N_\sigma(0,T_f)}e^{-\lambda T_f}V(0)\\ &+ \int_0^{T_f}\mu^{N_\sigma(\tau,T_f)}e^{-\lambda(T_f-\tau)}\Gamma(\tau)\,d\tau\\ &= e^{-\lambda T_f + N_\sigma(0,T_f)\ln^\mu}V(0)\\ &+ \int_0^{T_f} e^{-\lambda(T_f-\tau)+N_\sigma(\tau,T_f)\ln\mu}\Gamma(\tau)\,d\tau.\end{aligned} \tag{49}$$

The following proof consists of two parts. First, we will show that the overall switched closed-loop system (12) with $w(t) \equiv 0$ is asymptotically stable under any switching signal with ADT (28). Then, we will verify that system (12) is with an H_∞-norm less than or equal to γ.

Part 1. We consider the following average dwell time scheme: for any $T_f > 0$ and a positive scalar λ^* smaller than λ,

$$N_\sigma(0,T_f) \le \frac{T_f}{\tau_a^*}, \quad \tau_a^* = \frac{\ln^\mu}{\lambda^*}. \tag{50}$$

It follows from (50) that $N_\sigma(0,T_f)\ln^\mu \le \lambda^* T_f$. Then, from (49), we obtain

$$V(T_f) \le e^{-(\lambda-\lambda^*)T_f}V(0), \tag{51}$$

where $\lambda - \lambda^* > 0$, and one can see from [45] that

$$\left\|x\left(T_f\right)\right\|^2 \leq \max_{i,j\in[1,M]} \frac{\lambda_M\left(E\left(\varepsilon\right)P_i\left(\varepsilon\right)\right)}{\lambda_m\left(E\left(\varepsilon\right)P_j\left(\varepsilon\right)\right)} e^{-(\lambda-\lambda^*)T_f}\left\|x\left(0\right)\right\|^2, \tag{52}$$

which indicates that system (12) with $w(t) \equiv 0$ is asymptotically stable under any switching signal with ADT (28).

Part 2. Similar to Part 1, for a positive scalar λ^* smaller than λ, the inequality

$$N_\sigma\left(\tau, T_f\right)\ln\mu \leq \lambda^*\left(T_f - \tau\right) \tag{53}$$

holds.

Taking into account the fact that $x(0) = 0$ and $V(T_f) \geq 0$, it follows from (49) that

$$\int_0^{T_f} e^{-\lambda(T_f-\tau)+N_\sigma(\tau,T_f)\ln\mu}\Gamma\left(\tau\right)d\tau \geq 0. \tag{54}$$

It follows from (53) and (54) that

$$\int_0^{T_f} e^{-(\lambda-\lambda^*)(T_f-\tau)}\Gamma\left(\tau\right)d\tau \geq 0, \tag{55}$$

which implies that $\int_0^{T_f} z^T(t)z(t)dt \leq \gamma^2\int_0^{T_f} w^T(t)w(t)dt$. This completes the proof. □

Remark 13. $Z_i(\varepsilon) = \left[\begin{smallmatrix} Z_{i1} & \varepsilon Z_{i3} \\ Z_{i3} & Z_{i2}\end{smallmatrix}\right] = U_{i1} + \varepsilon U_{i2}$, $\varepsilon \in (0, \varepsilon_0]$, where $U_{i1} = \left[\begin{smallmatrix} Z_{i1} & 0 \\ Z_{i3} & Z_{i2}\end{smallmatrix}\right]$, $U_{i2} = \left[\begin{smallmatrix} 0 & Z_{i3} \\ 0 & 0\end{smallmatrix}\right]$. It follows from LMIs (20) and (21) that $Z_{i1} > 0$ and $Z_{i2} > 0$, which imply that the matrices $Z_i(0) = U_{i1}$ are nonsingular. So, the matrices $Z_i(\varepsilon)$ are nonsingular for all $\varepsilon \in (0, \varepsilon_0]$. This nonsingularity can ensure that $K_{il}(\varepsilon) = F_{il}Z_i^{-1}(\varepsilon)$ $(l = 1, 2, \ldots, r_i)$ always work well for all $\varepsilon \in (0, \varepsilon_0]$. For sufficiently small ε, the ε-dependent controller is reduced to an ε-independent one, since $\lim_{\varepsilon\to 0^+} K_{il} = F_{il}U_{i1}^{-1}$ $(l = 1, 2, \ldots, r_i)$.

Remark 14. The multiple Lyapunov functions method has been widely used in control design of switched systems [36–39]. By employing the average dwell time scheme, the problem of extended dissipative state estimation for a class of discrete-time Markov jump neural networks with unreliable links was addressed in [36]. In this paper, the ε-dependent piecewise Lyapunov function will be constructed to solve H_∞ control problem for T-S fuzzy SPSSs.

Remark 15. Theorem 12 is concerned with the situation that ε_0 is known according to prior information. Moreover, the bisectional search algorithm developed in [46] can be used to derive the ε-bound.

Remark 16. ε-bound, which is an essential index of SPSs, has attained much attention. ε-bound was considered in [40, 47]. Both results were derived by constructing a common Lyapunov function, which may lead to conservatism in some cases. In [41], the piecewise Lyapunov function was constructed and ε-bound estimation problem was solved for T-S fuzzy SSPSs without the external disturbance input.

By Theorem 12, under the assumption that the singular perturbation parameter ε is known, sufficient conditions for both stability and H_∞ performance of system (12) are derived. In the following theorem, for sufficiently small and unknown ε, the above sufficient conditions are generalized to design the ε-independent controller.

Theorem 17. *Given an H_∞ performance bound $\gamma > 0$, two constants, $\lambda > 0$ and $\mu \geq 1$, if there exist matrices F_{il}, Z_{i1}, Z_{i2}, and Z_{i3} of compatible dimensions with $Z_{ik} = Z_{ik}^T$ $(k = 1, 2)$, such that*

$$Z_{i1} > 0, \tag{56}$$

$$Z_{i2} > 0, \tag{57}$$

$$\begin{bmatrix} He\left\{A_{il}Z_i\left(0\right) + B_{il}F_{il}\right\} + \lambda Z_i^T\left(0\right)E\left(0\right) & * & * \\ E_{il}^T & -I_r & * \\ C_{il}Z_i\left(0\right) & 0 & -\gamma^2 \end{bmatrix} < 0, \tag{58}$$

$$\begin{bmatrix} \overline{\Upsilon}_1 & * & * \\ E_{il}^T + E_{is}^T & -2I_r & * \\ C_{il}Z_i\left(0\right) + C_{is}Z_i\left(0\right) & 0 & -2\gamma^2 \end{bmatrix} < 0, \quad l < s, \tag{59}$$

$$Z_{j1} \leq \mu Z_{i1}, \quad i \neq j, \tag{60}$$

$$Z_{j2} \leq \mu Z_{i2}, \quad i \neq j, \tag{61}$$

where $l, s = 1, 2, \ldots, r_i$, $i, j = 1, 2, \ldots, M$, $\overline{\Upsilon}_1 = He\{A_{il}Z_i(0) + B_{il}F_{is} + A_{is}Z_i(0) + B_{is}F_{il}\} + \lambda Z_i^T(0)E(0)$, $Z_i(0) = \left[\begin{smallmatrix} Z_{i1} & 0 \\ Z_{i3} & Z_{i2}\end{smallmatrix}\right]$, and $E(0) = \left[\begin{smallmatrix} 1 & * \\ 0 & 0\end{smallmatrix}\right]$.

Then there exists a positive scalar $\varepsilon_{\max}$ such that, for all $\varepsilon \in (0, \varepsilon_{\max}]$, the overall switched closed-loop system (12) with the controller gains of the form $K_{il} = F_{il}Z_i^{-1}(0)$ $(l = 1, 2, \ldots, r_i)$ is asymptotically stable and with an H_∞-norm less than or equal to γ under any switching signal with ADT

$$\tau_a \geq \frac{\ln^\mu}{\lambda}. \tag{62}$$

Proof. For sufficiently small ε, LMI conditions (20)–(27) in Theorem 12 can be reduced to LMI conditions (56)–(61) in Theorem 17. Thus, we omit the proof of Theorem 17 that can be carried out by referring to the standard techniques used in Theorem 12. □

ε-bound is an essential stability index of SPSs. Theorem 17 ensures the existence for ε-bound $\varepsilon_{\max}$. In the following theorem, we will propose a method to estimate the ε-bound of the closed-loop system with the obtained controllers in Theorem 17.

Theorem 18. *Give an H_∞ performance bound $\gamma > 0$, an upper bound $\varepsilon_{\max}$, controller gains K_{il}, and two constants, $\lambda > 0$ and $\mu \geq 1$, if there exist matrices Z_{i1}, Z_{i2}, and Z_{i3} of compatible dimensions with $Z_{ik} = Z_{ik}^T$ $(k = 1, 2)$, such that*

$$Z_{i1} > 0, \tag{63}$$

$$\begin{bmatrix} Z_{i1} & * \\ \varepsilon_{\max} Z_{i3} & \varepsilon_{\max} Z_{i2} \end{bmatrix} > 0, \tag{64}$$

$$\begin{bmatrix} He\left\{\left(A_{il} + B_{il}K_{il}\right) Z_i\left(0\right)\right\} + \lambda Z_i^T\left(0\right) E\left(0\right) & * & * \\ E_{il}^T & -I_r & * \\ C_{il} Z_i\left(0\right) & 0 & -\gamma^2 \end{bmatrix} < 0, \tag{65}$$

$$\begin{bmatrix} He\left\{\left(A_{il} + B_{il}K_{il}\right) Z_i\left(\varepsilon_{\max}\right)\right\} + \lambda Z_i^T\left(\varepsilon_{\max}\right) E\left(\varepsilon_{\max}\right) & * & * \\ E_{il}^T & -I_r & * \\ C_{il} Z_i\left(\varepsilon_{\max}\right) & 0 & -\gamma^2 \end{bmatrix} < 0, \tag{66}$$

$$\begin{bmatrix} \widetilde{\Upsilon}_1 & * & * \\ E_{il}^T + E_{is}^T & -2I_r & * \\ C_{il} Z_i\left(0\right) + C_{is} Z_i\left(0\right) & 0 & -2\gamma^2 \end{bmatrix} < 0, \quad l < s, \tag{67}$$

$$\begin{bmatrix} \widetilde{\Upsilon}_2 & * & * \\ E_{il}^T + E_{is}^T & -2I_r & * \\ C_{il} Z_i\left(\varepsilon_{\max}\right) + C_{is} Z_i\left(\varepsilon_{\max}\right) & 0 & -2\gamma^2 \end{bmatrix} < 0, \quad l < s, \tag{68}$$

$$Z_{j1} \le \mu Z_{i1}, \quad i \ne j, \tag{69}$$

$$\begin{bmatrix} Z_{j1} & * \\ \varepsilon_{\max} Z_{j3} & \varepsilon_{\max} Z_{j2} \end{bmatrix} \le \mu \begin{bmatrix} Z_{i1} & * \\ \varepsilon_{\max} Z_{i3} & \varepsilon_{\max} Z_{i2} \end{bmatrix}, \quad i \ne j, \tag{70}$$

where $l, s = 1, 2, \ldots, r_i$, $i, j = 1, 2, \ldots, M$, $\widetilde{\Upsilon}_1 = He\{(A_{il} + B_{il}K_{is} + A_{is} + B_{is}K_{il})Z_i(0)\} + \lambda Z_i^T(0)E(0)$, $\widetilde{\Upsilon}_2 = He\{(A_{il} + B_{il}K_{is} + A_{is} + B_{is}K_{il})Z_i(\varepsilon_{\max})\} + \lambda Z_i^T(\varepsilon_{\max})E(\varepsilon_{\max})$, *and* $Z_i(\varepsilon) = \begin{bmatrix} Z_{i1} & \varepsilon Z_{i3}^T \\ Z_{i3} & Z_{i2} \end{bmatrix}$.

Then, for all $\varepsilon \in (0, \varepsilon_{\max}]$, *the overall switched closed-loop system (12) is asymptotically stable and with an* H_∞*-norm less than or equal to* γ *under any switching signal with ADT*

$$\tau_a \ge \frac{\ln^\mu}{\lambda}. \tag{71}$$

4. Example

To illustrate the proposed results, we consider the well-known inverted pendulum system. The equations of motion for the pendulum are given by

$$\begin{aligned} \dot{x}_1\left(t\right) &= x_2\left(t\right) + 0.1w\left(t\right) \\ \dot{x}_2\left(t\right) &= \frac{g \sin\left(x_1\left(t\right)\right) - aml x_2^2\left(t\right) \sin\left(2x_1\left(t\right)\right)/2 - a\cos\left(x_1\left(t\right)\right) u\left(t\right)}{4l/3 - aml\cos^2\left(x_1\left(t\right)\right)} \\ &\quad + 0.1w\left(t\right) \\ z\left(t\right) &= 0.1x_1\left(t\right) + 0.1x_2\left(t\right), \end{aligned} \tag{72}$$

where $x_1(t) = \theta_p(t)$ denotes the angle of the pendulum from the vertical upward, $x_2(t) = \dot{\theta}_p(t)$, g is the gravity acceleration, $a = 1/(m + M)$, m and M are the masses of the pendulum and the cart, respectively, l is the length of the pendulum, u is a horizontal force applied to the cart, and $w(t)$ is the external disturbance variable, which is a piecewise function of time of the form

$$w\left(t\right) = \begin{cases} \sin\left(2\pi t\right) & 0 \le t < 5 \\ \sin\left(2\pi t\right) e^{-0.5t} & t \ge 5, \end{cases} \tag{73}$$

$z(t)$ is the controlled output. The parameters for the plant are as follows: $g = 9.8\ \mathrm{m/s^2}$, $m = 2\ \mathrm{Kg}$, $M = 8\ \mathrm{Kg}$, and $l = 0.5\ \mathrm{m}$.

The angle of the pendulum $[-30^\circ \quad 30^\circ]$ is divided into two areas R_1 and R_2, where R_1 is $|x_1| \le 15^\circ$; R_2 is $15^\circ < |x_1| \le 30^\circ$, which results in two fuzzy subsystems [39].

For the individual system, we choose the membership functions of the fuzzy sets as follows.

Mode 1

$$\begin{aligned} M_{11}\left(x_1\left(t\right)\right) &= 1 - \frac{\left|x_1\left(t\right)\right|}{15} \\ M_{12}\left(x_1\left(t\right)\right) &= \frac{\left|x_1\left(t\right)\right|}{15}. \end{aligned} \tag{74}$$

Mode 2

$$M_{21}\left(x_1(t)\right) = \frac{\left|x_1(t)\right|}{15} - 1$$
$$M_{22}\left(x_1(t)\right) = 2 - \frac{\left|x_1(t)\right|}{15}. \tag{75}$$

Then, the dynamics of Mode 1 can be exactly represented by the following T-S fuzzy model under $|x_1(t)| \le 15^\circ$:

Plant Rule 1:

IF $x_1(t)$ is $M_{11}\left(x_1(t)\right)$, THEN

$$\dot{x}(t) = A_{11}x(t) + B_{11}u(t) + E_{11}w(t)$$
$$z(t) = C_{11}x(t) \tag{76}$$

Plant Rule 2:

IF $x_1(t)$ is $M_{12}\left(x_1(t)\right)$, THEN

$$\dot{x}(t) = A_{12}x(t) + B_{12}u(t) + E_{12}w(t),$$
$$z(t) = C_{12}x(t),$$

where

$$A_{11} = \begin{bmatrix} 0 & 1 \\ 9.0673 & 0 \end{bmatrix},$$
$$B_{11} = \begin{bmatrix} 0 \\ -0.0688 \end{bmatrix},$$
$$E_{11} = \begin{bmatrix} 0.1 \\ 0.1 \end{bmatrix},$$
$$C_{11} = \begin{bmatrix} 0.1 & 0.1 \end{bmatrix},$$
$$A_{12} = \begin{bmatrix} 0 & 1 \\ 10.5717 & 0 \end{bmatrix}, \tag{77}$$
$$B_{12} = \begin{bmatrix} 0 \\ -0.0779 \end{bmatrix},$$
$$E_{12} = \begin{bmatrix} 0.1 \\ 0.1 \end{bmatrix},$$
$$C_{12} = \begin{bmatrix} 0.1 & 0.1 \end{bmatrix}.$$

The dynamics of Mode 2 can be exactly represented by the following T-S fuzzy model under $15^\circ < |x_1| \le 30^\circ$:

Plant Rule 1:

IF $x_1(t)$ is $M_{21}\left(x_1(t)\right)$, THEN

$$\dot{x}(t) = A_{21}x(t) + B_{21}u(t) + E_{21}w(t)$$
$$z(t) = C_{21}x(t)$$

Plant Rule 2:

IF $x_1(t)$ is $M_{22}\left(x_1(t)\right)$, THEN

$$\dot{x}(t) = A_{22}x(t) + B_{22}u(t) + E_{22}w(t),$$
$$z(t) = C_{22}x(t), \tag{78}$$

where

$$A_{21} = \begin{bmatrix} 0 & 1 \\ 10.5717 & 0 \end{bmatrix},$$
$$B_{21} = \begin{bmatrix} 0 \\ -0.0779 \end{bmatrix},$$
$$E_{21} = \begin{bmatrix} 0.1 \\ 0.1 \end{bmatrix},$$
$$C_{21} = \begin{bmatrix} 0.1 & 0.1 \end{bmatrix},$$
$$A_{22} = \begin{bmatrix} 0 & 1 \\ 11.1243 & 0 \end{bmatrix}, \tag{79}$$
$$B_{22} = \begin{bmatrix} 0 \\ -0.0811 \end{bmatrix},$$
$$E_{22} = \begin{bmatrix} 0.1 \\ 0.1 \end{bmatrix},$$
$$C_{22} = \begin{bmatrix} 0.1 & 0.1 \end{bmatrix}.$$

Choosing $\varepsilon = 0.1$, the above switched system can be modeled by a SPSS (1) with the following.

Mode 1

$$E(\varepsilon) = \begin{bmatrix} 1 & * \\ 0 & \varepsilon \end{bmatrix},$$
$$\overline{A}_{11} = \begin{bmatrix} 0 & 1 \\ 0.90673 & 0 \end{bmatrix},$$
$$\overline{B}_{11} = \begin{bmatrix} 0 \\ -0.00688 \end{bmatrix},$$
$$\overline{E}_{11} = \begin{bmatrix} 0.1 \\ 0.01 \end{bmatrix}, \tag{80}$$
$$E(\varepsilon) = \begin{bmatrix} 1 & * \\ 0 & \varepsilon \end{bmatrix},$$
$$\overline{A}_{12} = \begin{bmatrix} 0 & 1 \\ 1.05717 & 0 \end{bmatrix},$$
$$\overline{B}_{12} = \begin{bmatrix} 0 \\ -0.00779 \end{bmatrix},$$
$$\overline{E}_{12} = \begin{bmatrix} 0.1 \\ 0.01 \end{bmatrix}.$$

Mode 2

$$E(\varepsilon) = \begin{bmatrix} 1 & * \\ 0 & \varepsilon \end{bmatrix},$$
$$\overline{A}_{21} = \begin{bmatrix} 0 & 1 \\ 1.05717 & 0 \end{bmatrix},$$
$$\overline{B}_{21} = \begin{bmatrix} 0 \\ -0.00779 \end{bmatrix},$$
$$\overline{E}_{21} = \begin{bmatrix} 0.1 \\ 0.01 \end{bmatrix},$$
$$E(\varepsilon) = \begin{bmatrix} 1 & * \\ 0 & \varepsilon \end{bmatrix},$$
$$\overline{A}_{22} = \begin{bmatrix} 0 & 1 \\ 1.11243 & 0 \end{bmatrix},$$
$$\overline{B}_{22} = \begin{bmatrix} 0 \\ -0.00811 \end{bmatrix},$$
$$\overline{E}_{22} = \begin{bmatrix} 0.1 \\ 0.01 \end{bmatrix}. \quad (81)$$

The fuzzy controller is described as follows.

Mode 1

Plant Rule 1:

IF $x_1(t)$ is $M_{11}(x_1(t))$, THEN

$u(t) = K_{11}(\varepsilon)x(t)$

Plant Rule 2:

IF $x_1(t)$ is $M_{12}(x_1(t))$, THEN

$u(t) = K_{12}(\varepsilon)x(t)$. (82)

Mode 2

Plant Rule 1:

IF $x_2(t)$ is $M_{21}(x_1(t))$, THEN

$u(t) = K_{21}(\varepsilon)x(t)$

Plant Rule 2:

IF $x_2(t)$ is $M_{22}(x_1(t))$, THEN

$u(t) = K_{22}(\varepsilon)x(t)$. (83)

Taking $\varepsilon = 0.1$, $\lambda = 10$, and $\mu = 20$ and solving the LMIs in Theorem 12, we obtain the stabilization controller gains:

$$K_{11} = \begin{bmatrix} 7.3418 * 10^3 & 5.7720 * 10^2 \end{bmatrix},$$
$$K_{12} = \begin{bmatrix} 6.6701 * 10^3 & 5.2617 * 10^2 \end{bmatrix},$$
$$K_{21} = \begin{bmatrix} 6.4503 * 10^3 & 4.8956 * 10^2 \end{bmatrix},$$
$$K_{22} = \begin{bmatrix} 6.2518 * 10^3 & 4.7497 * 10^2 \end{bmatrix}. \quad (84)$$

Taking $\lambda = 10$ and $\mu = 20$ and solving the LMIs in Theorem 17, we obtain the stabilization controller gains:

$$\overline{K}_{11} = \begin{bmatrix} 1.0908 * 10^4 & 8.6334 * 10^2 \end{bmatrix},$$
$$\overline{K}_{12} = \begin{bmatrix} 1.0237 * 10^4 & 8.1009 * 10^2 \end{bmatrix},$$
$$\overline{K}_{21} = \begin{bmatrix} 9.8518 * 10^3 & 7.7925 * 10^2 \end{bmatrix},$$
$$\overline{K}_{22} = \begin{bmatrix} 9.6513 * 10^3 & 7.6329 * 10^2 \end{bmatrix}. \quad (85)$$

Under the controller obtained by Theorem 17, the ε-bound of the closed-loop system is $\varepsilon_{\max} = 0.5493$ by using Theorem 18 and the bisectional search algorithm developed in [46].

To illustrate the proposed method, we first consider the simulation of system (10) without the controller and then apply the designed controller to system (10).

Choosing $\varepsilon = 0.1$, $x_1(0) = 0^\circ$, $x_2(0) = 0^\circ$, $\lambda = 10$, $= 20$, $\gamma = 1$, and any switching signal with ADT (71), the simulation result without the controller is shown in Figure 1. It can be seen from Figure 1 that system (10) is not stable. Applying the fuzzy controller obtained by Theorem 12 to the original system, the sate trajectories of the overall switched closed-loop system are shown in Figure 2 and the ratio of the output energy to the disturbance input energy, that is, $\int_0^{T_f} z^T(s)z(s)ds / \int_0^{T_f} w^T(s)w(s)ds$, is depicted in Figure 3. It is easy to find that after 5 seconds the ratio of the output energy to the disturbance input energy is fixed at a constant

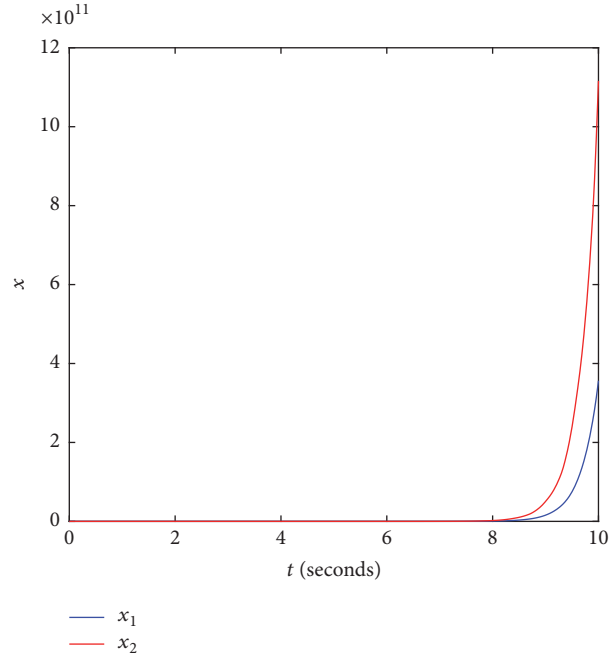

Figure 1: State trajectories without the controller.

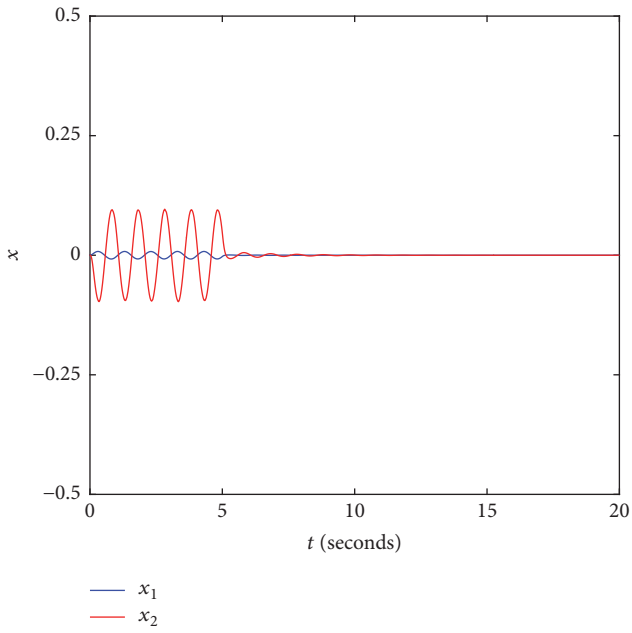

Figure 2: State trajectories.

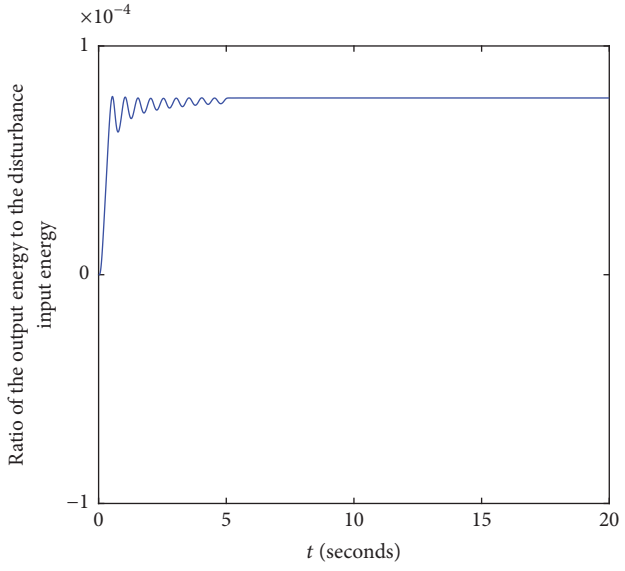

Figure 3: The ratio of the output energy to the disturbance input energy.

value, which is about $7.7265 * 10^{-5}$. So $\gamma = \sqrt{7.7265 * 10^{-5}} = 8.79 * 10^{-3}$, which is less than the prescribed value 1.

5. Conclusion

In this paper, we are concerned with the design of fuzzy controller with guaranteed H_∞ performance for T-S fuzzy SPSSs. An LMI-based method of designing an ε-dependent controller has been proposed. Through this method, the obtained controller can work well for any $\varepsilon \in (0, \varepsilon_0]$. This controller guarantees that, for a given upper bound ε_0 for ε and a prespecified H_∞ performance bound $\gamma > 0$, under admissible switching signals, the switched system is asymptotically stable and with an H_∞-norm less than or equal to γ. Then, for sufficiently small ε, the ε-independent feedback controller has been developed. Furthermore, under this controller, the ε-bound estimation problem of the switched system has been solved. The involved example has shown the feasibility and effectiveness of the obtained results.

Conflicts of Interest

The authors declare that they have no conflicts of interest.

Acknowledgments

This work was supported by the National Natural Science Foundation of China (61374043, 61603392, 61603393, and 61503384), Nature Science Foundation of Jiangsu Province (BK20160275, BK2010275, and BK20150199), the Open Project Foundation of State Key Laboratory of Synthetical Automation for Process Industries under Grant PAL-N201706, Postdoctoral Science Foundation of China (2015M581885), and Ordinary University Graduate Student Scientific Research Innovation Projects of Jiangsu Province (KYLX16–0533).

References

[1] G. Peponides, P. Kokotovic, and J. Chow, "Singular perturbations and time scales in nonlinear models of power systems," *IEEE Transactions on Circuits and Systems*, vol. 29, no. 11, pp. 758–767, 1982.

[2] W. W. Chen, M. Niepel, and P. K. Sorger, "Classic and contemporary approaches to modeling biochemical reactions," *Genes & Development*, vol. 24, no. 17, pp. 1861–1875, 2010.

[3] P. Kokotović, H. K. Khalil, and J. O'reilly, *Singular Perturbation Methods in Control: Analysis and Design*, Siam, 1999.

[4] S. Bellew and E. O'Riordan, "A parameter robust numerical method for a system of two singularly perturbed convection-diffusion equations," *Applied Numerical Mathematics*, vol. 51, no. 2-3, pp. 171–186, 2004.

[5] P. V. Kokotovic, R. E. Omalley, and P. Sannuti, "Singular perturbations and order reduction in control theory-an overview," *Automatica*, vol. 12, no. 2, pp. 123–132, 1976.

[6] A. Saberi and H. Khalil, "Quadratic-type Lyapunov functions for singularly perturbed systems," *Institute of Electrical and Electronics Engineers Transactions on Automatic Control*, vol. 29, no. 6, pp. 542–550, 1984.

[7] E. Fridman, "Effects of small delays on stability of singularly perturbed systems," *Automatica*, vol. 38, no. 5, pp. 897–902, 2002.

[8] F. Sun, L. Zhou, Q. Zhang, and Y. Shen, "Stability bound analysis and synthesis for singularly perturbed systems with time-varying delay," *Mathematical Problems in Engineering*, vol. 2013, Article ID 517258, 8 pages, 2013.

[9] L. Saydy, "New stability/performance results for singularly perturbed systems," *Automatica*, vol. 32, no. 6, pp. 807–818, 1996.

[10] H. D. Tuan and S. Hosoe, "Multivariable circle criteria for multiparameter singularly perturbed systems," *Institute of Electrical*

and Electronics Engineers Transactions on Automatic Control, vol. 45, no. 4, pp. 720–725, 2000.

[11] H. Liu, F. Sun, and Y. Hu, "H∞ control for fuzzy singularly perturbed systems," *Fuzzy Sets and Systems*, vol. 155, no. 2, pp. 272–291, 2005.

[12] L. Cao and H. M. Schwartz, "Complementary results on the stability bounds of singularly perturbed systems," *Institute of Electrical and Electronics Engineers Transactions on Automatic Control*, vol. 49, no. 11, pp. 2017–2021, 2004.

[13] I. Malloci, Z. Lin, and G. Yan, "Stability of interconnected impulsive switched systems subject to state dimension variation," *Nonlinear Analysis: Hybrid Systems*, vol. 6, no. 4, pp. 960–971, 2012.

[14] I. Malloci, J. Daafouz, C. Iung, R. Bonidal, and P. Szczepanski, "Switched system modeling and robust steering control of the tail end phase in a hot strip mill," *Nonlinear Analysis: Hybrid Systems*, vol. 3, no. 3, pp. 239–250, 2009.

[15] I. Malloci, J. Daafouz, C. Iung, R. Bonidal, and P. Szczepanski, "Robust steering control of hot strip mill," *IEEE Transactions on Control Systems Technology*, vol. 18, no. 4, pp. 908–917, 2010.

[16] F. El Hachemi, M. Sigalotti, and J. Daafouz, "Stability analysis of singularly perturbed switched linear systems," *Institute of Electrical and Electronics Engineers Transactions on Automatic Control*, vol. 57, no. 8, pp. 2116–2121, 2012.

[17] I. Malloci, J. Daafouz, and C. Iung, "Stabilization of continuous-time singularly perturbed switched systems," in *Proceedings of the Joint 48th IEEE Conference on Decision and Control Held Jointly with the 28th Chinese Control Conference (CDC/CCC '09)*, pp. 6371–6376, Shanghai, China, December 2009.

[18] I. Malloci, J. Daafouz, and C. Tung, "Stability and stabilization of two time scale switched systems in discrete time," *Institute of Electrical and Electronics Engineers Transactions on Automatic Control*, vol. 55, no. 6, pp. 1434–1438, 2010.

[19] M. Alwan, X. Liu, and B. Ingalls, "Exponential stability of singularly perturbed switched systems with time delay," *Nonlinear Analysis: Hybrid Systems*, vol. 2, no. 3, pp. 913–921, 2008.

[20] M. S. Alwan and X. Liu, "Stability of singularly perturbed switched systems with time delay and impulsive effects," *Nonlinear Analysis: Theory, Methods & Applications*, vol. 71, no. 9, pp. 4297–4308, 2009.

[21] G. S. Deaecto, J. Daafouz, and J. C. Geromel, "H2 and H∞ performance optimization of singularly perturbed switched systems," *SIAM Journal on Control and Optimization*, vol. 50, no. 3, pp. 1597–1615, 2012.

[22] J. Lian and X. Wang, "Exponential stabilization of singularly perturbed switched systems subject to actuator saturation," *Information Sciences*, vol. 320, pp. 235–243, 2015.

[23] H. O. Wang, K. Tanaka, and M. F. Griffin, "An approach to fuzzy control of nonlinear systems: stability and design issues," *IEEE Transactions on Fuzzy Systems*, vol. 4, no. 1, pp. 14–23, 1996.

[24] G. Feng, "A survey on analysis and design of model-based fuzzy control systems," *IEEE Transactions on Fuzzy Systems*, vol. 14, no. 5, pp. 676–697, 2006.

[25] X. Liu and Q. Zhang, "New approaches to H∞ controller designs based on fuzzy observers for T-S fuzzy systems via LMI," *Automatica*, vol. 39, no. 9, pp. 1571–1582, 2003.

[26] H. Shen, J. H. Park, and Z.-G. Wu, "Finite-time reliable L2-L∞/H∞ control for Takagi-Sugeno fuzzy systems with actuator faults," *IET Control Theory & Applications*, vol. 8, no. 9, pp. 688–696, 2014.

[27] H. Shen, L. Su, and J. H. Park, "Reliable mixed H∞/passive control for T-S fuzzy delayed systems based on a semi-Markov jump model approach," *Fuzzy Sets and Systems*, vol. 314, pp. 79–98, 2017.

[28] H. Liu, F. Sun, and Z. Sun, "Stability analysis and synthesis of fuzzy singularly perturbed systems," *IEEE Transactions on Fuzzy Systems*, vol. 13, no. 2, pp. 273–284, 2005.

[29] W. Assawinchaichote, S. K. Nguang, and P. Shi, "H∞ output feedback control design for uncertain fuzzy singularly perturbed systems: an LMI approach," *Automatica*, vol. 40, no. 12, pp. 2147–2152, 2004.

[30] W. Assawinchaichote and S. K. Nguang, "H∞ fuzzy control design for nonlinear singularly perturbed systems with pole placement constraints: an LMI approach," *IEEE Transactions on Systems, Man, and Cybernetics, Part B: Cybernetics*, vol. 34, no. 1, pp. 579–588, 2004.

[31] W. Assawinchaichote and S. K. Nguang, "Fuzzy H∞ output feedback control design for singularly perturbed systems with pole placement constraints: An LMI approach," *IEEE Transactions on Fuzzy Systems*, vol. 14, no. 3, pp. 361–371, 2006.

[32] T.-H. S. Li and K.-J. Lin, "Composite fuzzy control of nonlinear singularly perturbed systems," *IEEE Transactions on Fuzzy Systems*, vol. 15, no. 2, pp. 176–187, 2007.

[33] G.-H. Yang and J. Dong, "Control synthesis of singularly perturbed fuzzy systems," *IEEE Transactions on Fuzzy Systems*, vol. 16, no. 3, pp. 615–629, 2008.

[34] C. Yang and Q. Zhang, "Multiobjective control for T-S fuzzy singularly perturbed systems," *IEEE Transactions on Fuzzy Systems*, vol. 17, no. 1, pp. 104–115, 2009.

[35] K. Tanaka, M. Iwasaki, and H. O. Wang, "Stable switching fuzzy control and its application to a hovercraft type vehicle," in *Proceedings of the FUZZ-IEEE 2000: 9th IEEE International Conference on Fuzzy Systems*, vol. 2, pp. 804–809, May 2000.

[36] H. Shen, Y. Zhu, L. Zhang, and J. H. Park, "Extended dissipative state estimation for Markov jump neural networks with unreliable links," *IEEE Transactions on Neural Networks and Learning Systems*, vol. 28, no. 2, pp. 346–358, 2017.

[37] C. Qin, Z. Xiang, and H. R. Karimi, "Robust stability and H∞ stabilization of switched systems with time-varying delays using delta operator approach," *Mathematical Problems in Engineering*, vol. 2013, Article ID 230576, 11 pages, 2013.

[38] W.-J. Wang, Y.-J. Chen, and C.-H. Sun, "Relaxed stabilization criteria for discrete-time T–S fuzzy control systems based on a switching fuzzy model and piecewise Lyapunov function," *IEEE Transactions on Systems, Man, and Cybernetics, Part B: Cybernetics*, vol. 37, no. 3, pp. 551–559, 2007.

[39] Y. Liu and J. Zhao, "Nonfragile control for a class of uncertain switching fuzzy time-delay systems," *Control Theory and Technology*, vol. 8, no. 2, pp. 229–232, 2010.

[40] L. Zhou, Q. Wang, X. Ma, and C. Yang, "Fuzzy controllers for nonaffine-in-control singularly perturbed switched systems," *Mathematical Problems in Engineering*, vol. 2015, Article ID 896413, 11 pages, 2015.

[41] X. Ma, Q. Wang, J. Cheng, Y. Guo, C. Yang, and L. Zhou, "Controller design for T-S fuzzy singularly perturbed switched systems," in *Proceedings of the IEEE International Conference on Fuzzy Systems (FUZZ-IEEE '16)*, pp. 1159–1166, 2016.

[42] D. Liberzon, *Switching in Cystems and Control*, Birkhäuser, Boston, Mass, USA, 2003.

[43] J. P. Hespanha and A. S. Morse, "Stability of switched systems with average dwell-time," in *Proceedings of the 38th IEEE*

Conference on Decision and Control (CDC '99), pp. 2655–2660, Phoenix, Ariz, USA, December 1999.

[44] I. R. Petersen, "A stabilization algorithm for a class of uncertain linear systems," *Systems & Control Letters*, vol. 8, no. 4, pp. 351–357, 1987.

[45] X. Li and Z. Chen, "Stability properties for Hopfield neural networks with delays and impulsive perturbations," *Nonlinear Analysis: Real World Applications*, vol. 10, no. 5, pp. 3253–3265, 2009.

[46] C. Yang, L. Ma, X. Ma, and X. Wang, "Stability analysis of singularly perturbed control systems with actuator saturation," *Journal of The Franklin Institute*, vol. 353, no. 6, pp. 1284–1296, 2016.

[47] X. Ma, Q. Wang, L. Zhou, and C. Yang, "Controller design and analysis for singularly perturbed switched systems with actuator saturation," *International Journal of Robust and Nonlinear Control*, vol. 26, no. 15, pp. 3404–3420, 2016.

Hindawi
Mathematical Problems in Engineering
Volume 2017, Article ID 8937356, 13 pages
https://doi.org/10.1155/2017/8937356

Research Article

Data-Driven Incipient Sensor Fault Estimation with Application in Inverter of High-Speed Railway

Hongtian Chen, Bin Jiang, and Ningyun Lu

College of Automation Engineering, Nanjing University of Aeronautics and Astronautics, Nanjing 210016, China

Correspondence should be addressed to Bin Jiang; binjiang@nuaa.edu.cn

Received 10 May 2017; Accepted 3 August 2017; Published 10 September 2017

Academic Editor: Wanquan Liu

Incipient faults in high-speed railway have been rarely considered before developing into faults or failures. In this paper, a new data-driven incipient fault estimate (FE) methodology is proposed under multivariate statistics frame, which incorporates with Kullback-Leibler divergence (KLD) in information domain and neural network approximation in machine learning. By defining one sensitive fault indicator (SFI), the incipient fault amplitude can be precisely estimated. According to the experimental platform of China Railway High-speed 2 (CRH2), the proposed incipient FE algorithm is examined, and the more sensitivity and accuracy to tiny abnormality are demonstrated. Followed by the incipient FE results, several factors on FE performance are further analyzed.

1. Introduction

Due to its high efficiency and loading capacity, high-speed railway has been rapidly developed in the past two decades [1–3]. As one of the most important equipment of high-speed railway, inverter is the actuator of motors, and its sensor information is used to construct the control law of motors [4]. Typically, sensors equipped in inverter are vulnerable to faults as they are direct interactions with the working environment [3, 5]. This may lead to abnormal operation of motors and effectiveness loss of the traction force and even cause an emergency stop. Thus, the real-time sensor fault detection and diagnosis (FDD) and fault estimation (FE) are urgently needed in high-speed railway to improve its reliability.

There exists abundant researches for inverter sensor FDD over the past several decades [2, 4, 6–9]. All of them can be mainly classified into two general categories, including model-based methods and knowledge-based methods. For the model-based FDD methods, they are mainly to build the mathematical model of electrical traction systems via outputs or work mechanisms of being monitored system. Usually, a residual is to generate the fault indicating by available input and output information from sensors of inverter [4, 6, 9, 10]. In addition, the knowledge-based methods [2, 8] mainly depend on prior knowledge of inverter whose characteristics are to be summarized to distinguish or diagnose the faults.

Besides that, the data-driven FDD methods coming from chemical industry use the information of sampling data to directly analyze some features, such as data correlation, spectrum, and mean value. These kinds of latent information are crucial factors to identify and diagnose the sensor faults without considering the mathematical model of system. Recently, some modified data-driven methods were proposed to improve the process monitoring performance. For example, key-performance-indicator-related PLS was developed to acquire more meaningful fault information [11]; and fault-relevant PCA was designed to select variable optimally [12]. In addition, some detailed reviews on data-driven methods can be found in [13–15]. But these methods are rarely found to be FDD in electrical domains.

The accurate inverter mathematical model of high-speed railway is needed for model-based incipient fault estimation method. However, due to the complex operation environments, the model of inverter is time-varying and effected by unknown noise and cannot be represented by some accurate functions. In addition, the expertise cannot be completely acquired and is often invalid when coming to incipient faults. Therefore, the data-driven method is considered to estimate incipient faults in inverter of high-speed railway.

In this paper, the main contributions of the proposed method are summarized as follows:

(1) Considering non-Gaussian characteristics of traction system, the rotary principal component subspace (RPCS) and rotary residual subspace (RRS) are firstly used and introduced for data-driven FE problems.

(2) Aiming at incipient FE, a sensitive fault indicator (SFI) is defined without any improper assumptions on measuring signals.

(3) The analytic relation between incipient fault amplitude and SFI is analyzed and is then estimated by the neural network.

The rest of this paper is organized as follows. In Section 2, a brief introduction on inverter of China Railway High-speed 2 (CRH2), PCA, and Kullback-Leibler divergence (KLD) scheme is given. In Section 3, a rotary data space including RPCS and RRS is presented, in which SFI is defined by a information distance named KLD; then the relation between incipient fault amplitude and SFI is analyzed and obtained by theoretical derivations and function approximation. The whole FE strategy is presented in Section 4. Section 5 presents FE results and discussions about the performance of the proposed method. Finally, the conclusion drawn from the research along with discussions is given in Section 6.

2. Related Work

2.1. A Three-Phase Three-Level VSI of CRH2. CRH2 traction system is a complex electrical system consisting of several electrical types of equipment, such as traction transformers, traction rectifiers, traction inverters, and traction motors. Traction inverter is reviewed as a major part which supply variable velocity variable frequency voltage. A three-phase three-level voltage source inverter (VSI) of CRH2 is mainly component of a filter circuit, overvoltage suppression unit, Insulated-Gate Bipolar Transistor (IGBT), and so on. As shown in Figure 1, every IGBT switch is composed of transistor unit (TU) and diode unit (DU), and there are altogether twelve switches in the inverter.

The incipient faults in CRH2 had not been considered sufficiently. Numerous studies [5, 16, 17] have mentioned that the incipient fault should be characterized with the following features:

(i) Qualitative aspect: the degree of deteriorated system performance is such insignificant that it is not enough to trigger any set alarms.

(ii) Quantitative aspect: the gain percent of deviation, fault signal comparing with the actual value under normal condition, is quite small, for example, ranking from 1% to 10%.

(iii) Necessity aspect: if the incipient fault cannot be detected successfully and no action is taken, it must develop to fault or even failure as time goes on.

Based on the main circuit protection list of CRH2, there are altogether 41 types of faults [1]. Though some 3%–15% abnormalities can be detected, many missing alarm and false alarm cases still exist actually. For example, the over current fault encoded Fault 28 will not trigger any fault alarm.

A physical model of common train systems via first principals contains 84 differential equations together [18]. When coming to the more complex CRH2, it is impossible to set up accurate system model. Besides that, charging and discharging of many energy storage devices in high frequency make signals change frequently. This leads, predominantly, to the fact that all signals in inverter obey non-Gaussian distribution. In the following two subsections, preliminaries of SFI are presented.

2.2. Basic Form of PCA Process Monitoring. PCA is a popular multivariate statistical method which is proposed for dimensionality reduction of a mass correlated data [19]. The lower dimensional subspace obtained by projecting contains most of the original data features [20]. This data-driven method and its many variants [13, 21, 22] have been successfully applied in fault detection and diagnosis [14, 15].

The offline training data X_{off} contains N sampling measurements from m sensors and can be completely denoted as $X_{\text{off}} = [x_1, \ldots, x_N]$, where x_i is i-th sampling. It is usually normalized to zero mean and unit variance before PCA modeling and its normalized former can be written as $\overline{X}_{\text{off}}$. Then, the sample covariance matrix can be denoted as

$$S_{\text{off}} = \frac{1}{N-1} \overline{X}_{\text{off}}^T \overline{X}_{\text{off}}. \tag{1}$$

Doing SVD on the covariance matrix S_{off} as

$$S_{\text{off}} = P \Lambda P^T, \tag{2}$$

where $\Lambda = \text{diag}(\lambda_1, \lambda_2, \ldots, \lambda_m)$, all eigenvalues rank in descending order. As given in [20], the loading matrix P and the diagonal eigenvalue matrix Λ are usually divided into the following formers according to l:

$$P = \begin{bmatrix} P_p & P_r \end{bmatrix}, \qquad \Lambda = \begin{bmatrix} \Lambda_p & 0 \\ 0 & \Lambda_r \end{bmatrix}, \tag{3}$$

where $P_p \in R^{m \times l}$, $P_r \in R^{m \times (m-l)}$, $\Lambda_p \in R^{l \times l}$, $\Lambda_r \in R^{(m-l) \times (m-l)}$, and l is the number of principal components. In this application, l can be obtained by cumulative percent variance. Then the principal and residual parts of X_{off} can be calculated by $\widehat{X} = X_{\text{off}} P_p P_p^T$ and $\widetilde{X} = X - \widehat{X}$, respectively.

2.3. Kullback-Leibler Divergence. The KLD is a most fundamental quantity in information domain [23]. It has been reviewed as a power tool in many applications [24, 25]. The original definition can be found in [26] with the following former:

$$I(f_1 \parallel f_2) = \int f_1(x) \log \frac{f_1(x)}{f_2(x)} dx, \tag{4}$$

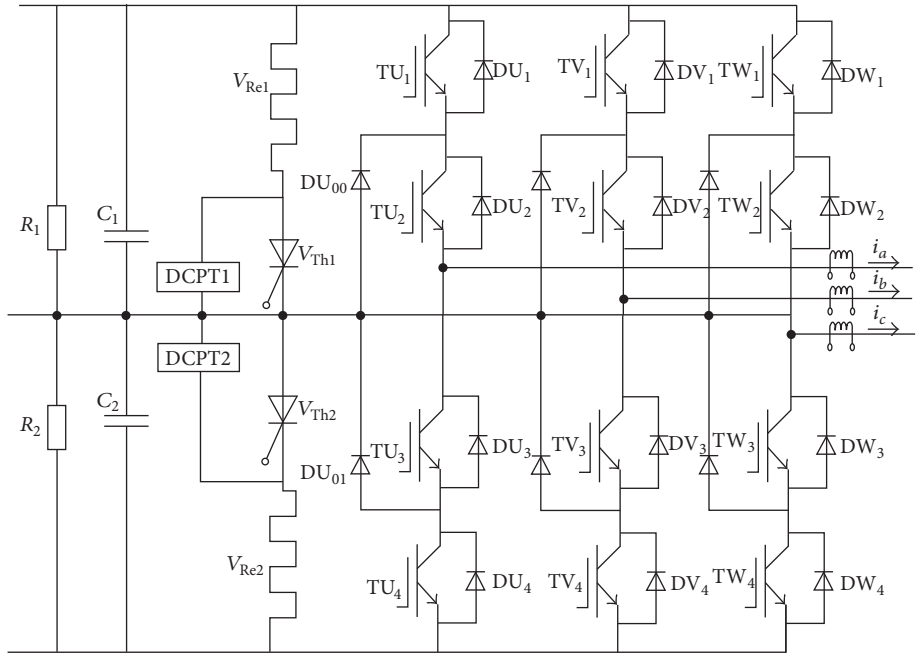

Figure 1: Schematic diagram of CRH2 inverter.

where log(·) has base e, $f_1(x)$ and $f_2(x)$ are the continuous probability density functions (PDFs), and $I(f_1 \parallel f_2)$ is the defined KLD of $f_2(x)$ with respect to $f_1(x)$. As pointed in [23], KLD have the characteristic with Pythagorean inequality, so a symmetric quantity is usually defined to be

$$K(f_1, f_2) = I(f_1 \parallel f_2) + I(f_2 \parallel f_1). \tag{5}$$

Given two normal PDFs such that

$$f_1(x) = \frac{1}{\sqrt{2\pi}\delta_1} \exp\left\{-\frac{(x-\mu_1)^2}{2\delta_1^2}\right\},$$
$$f_2(x) = \frac{2}{\sqrt{2\pi}\delta_2} \exp\left\{-\frac{(x-\mu_2)^2}{2\delta_2^2}\right\} \tag{6}$$

then the KLD between two above normal distributions in case of positive variances in (5) can be equal to

$$K(f_1, f_2) = \frac{1}{2}\left[\frac{\delta_1^2}{\delta_2^2} + \frac{\delta_2^2}{\delta_1^2} + (\mu_1 - \mu_2)^2\left(\frac{1}{\delta_1^2} + \frac{1}{\delta_2^2}\right) - 2\right]. \tag{7}$$

3. Incipient Fault Estimation Method

3.1. Data Preprocessing. As explained in Section 2.1, CRH2 is a non-Gaussian system which prevents from adapting existed PCA-based FDD methods. Therefore, preprocessing the system data combined with its properties should be considered to cater for the Gaussian distribution of the measurements from three current sensors in Figure 1. Followed by this problem, some preprocessing steps based on the characteristic of selected signals should be implemented before incipient FE.

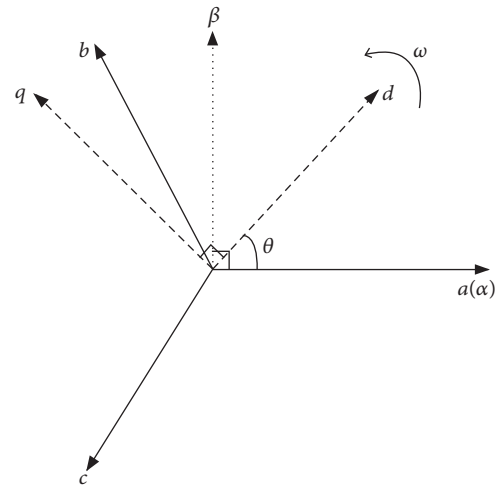

Figure 2: Two data space transformations to deal with non-Gaussian data set.

Let $X_{abc,\text{off}} = [i_a \;\; i_b \;\; i_c] \in R^{N\times m}$ be the offline normal current signals of the CRH2; it is straightforward to know that $m = 3$. Figure 2 gives the relationship among three date spaces, as a-b-c coordinate, α-β coordinate, and d-q coordinate. In Figure 1, the currents, i_a, i_b, and i_c, are revolving axes with the same constant length in original a-b-c coordinate if there is no fault.

In stationary coordinates, the phase currents can be transformed from a-b-c frame to α-β frame by Clarke

transformation, and the mathematical formulation is given in

$$\begin{bmatrix} i_\alpha \\ i_\beta \end{bmatrix} = \frac{2}{3}\begin{bmatrix} \cos\Theta & \cos\left(\Theta - \frac{2}{3}\pi\right) & \cos\left(\Theta + \frac{2}{3}\pi\right) \\ \sin\Theta & \sin\left(\Theta - \frac{2}{3}\pi\right) & \sin\left(\Theta + \frac{2}{3}\pi\right) \end{bmatrix} X_{abc,\text{off}}^T = C_{3S/2S} X_{abc,\text{off}}^T, \quad (8)$$

where $C_{3S/2S}$ is the Clarke transformation matrix and Θ is the angle between the coordinate α and the coordinate a. In order to reduce complexity, Θ is used to be chosen as 0, which is depicted in Figure 2.

d-q coordinate in Figure 2 is a rotary frame, and its rotary angular velocity ω is synchronous angular velocity. And the transformation angle can be calculated by $\theta = \omega t$. Then the currents i_d and i_q can be derived from i_α and i_β in stationary α-β frame, and the Park transformation matrix $C_{2S/2R}$ is given as follows:

$$C_{2S/2R} = \begin{bmatrix} \cos\theta & \sin\theta \\ -\sin\theta & \cos\theta \end{bmatrix}. \quad (9)$$

Furthermore, the transformation matrix from a-b-c coordinate to d-q coordinate can be obtained by combination of Clarke and Park transformation matric, and its form can be given as

$$C_{3S/2R} = C_{2S/2R} C_{3S/2S} = \frac{2}{3}\begin{bmatrix} \cos\theta & \cos\left(\theta - \frac{2}{3}\pi\right) & \cos\left(\theta + \frac{2}{3}\pi\right) \\ -\sin\theta & -\sin\left(\theta - \frac{2}{3}\pi\right) & -\sin\left(\theta + \frac{2}{3}\pi\right) \end{bmatrix}. \quad (10)$$

With $X_{dq,\text{off}} \in R^{N\times 2} = \begin{bmatrix} i_d & i_q \end{bmatrix}^T$, it can be obtained by

$$X_{dq,\text{off}} = X_{abc,\text{off}} C_{3S/2R}^T. \quad (11)$$

By the nonlinear projections in (11), $X_{dq,\text{off}}$ can be expressed as

$$X_{dq,\text{off}} = \widehat{X}_{dq,\text{off}} + \widetilde{X}_{dq,\text{off}} = X_{dq,\text{off}} P_{\text{pc}} P_{\text{pc}}^T + X_{dq,\text{off}} P_{\text{res}} P_{\text{res}}^T = X_{abc,\text{off}} C_{3S/2R}^T P_{\text{pc}} P_{\text{pc}}^T + X_{abc,\text{off}} C_{3S/2R}^T P_{\text{res}} P_{\text{res}}^T, \quad (12)$$

where $\widehat{X}_{dq,\text{off}}$ and $\widetilde{X}_{dq,\text{off}}$ are the principal and residual subspace belonging, respectively, to $X_{dq,\text{off}}$, and P_{pc} and P_{res} are principal and residual vectors of $X_{dq,\text{off}}$. Since $C_{3S/2R}$ is closely related to the rotary angular velocity ω of d-q coordinate, both of the two subspaces must be rotary. Then, the three-phase sine currents can be projected on RPCS and RRS, which are, respectively, spanned by P_{pc} and P_{res}.

Remark 1. The data processing in (12) transforms the original data set $X_{abc,\text{off}}$ into a new rotary data set $X_{dq,\text{off}}$ which obeys Gaussian distribution approximately. It make an important connection between Λ in (2) and δ^2 in (7). Rewriting $T = (t_1, \ldots, t_m)$ and combining (1) with (2), it is easy to know that $\delta_i^2 = \text{var}(t_i) = \lambda_i$, where $i = 1, \ldots, m$. Considering $f(k)$ as the referenced model obtained by offline data and calculating $\widetilde{f}(k)$ from the online data, then KLD can be used as a SFI to estimate amplitude of incipient fault online.

3.2. SFI. After the above nonlinear projections, the measurement signals obey Gaussian distribution. Let the reference PDF of score be that $f_k = \mathcal{N}(\mu_k, \delta_k^2)$, $k \in [1, m]$. After data normalization for $X_{dq,\text{off}}$, every column of $\overline{X}_{dq,\text{off}}$ will have zero mean and unit variance. Then, μ_k is zero and every variance parameter δ_k of principal score t_k can be obtained by Λ_p in (3). For online sampling, the online PDF $\widetilde{f}(k) = \mathcal{N}(\widetilde{\mu}_k, \widetilde{\delta}_k^2)$ can be estimated via scores in RPCS and RRS.

If the incipient fault can be estimated accurately, one SFI with high sensitivity to fault should be chosen. In order to emphasize the unpredictable small changes caused by incipient faults, the SFI using KLD can be defined as

$$\text{SFI}_k = K\left(f_k, \widetilde{f}_k\right) = \frac{1}{2}\,\text{sgn}\left(\mu_k - \widetilde{\mu}_k\right) \cdot \left[\frac{\delta_k^2}{\widetilde{\delta}_k^2} + \frac{\widetilde{\delta}_k^2}{\delta_k^2} + \left(\mu_k - \widetilde{\mu}_k\right)^2\left(\frac{1}{\delta_k^2} + \frac{1}{\widetilde{\delta}_k^2}\right) - 2\right], \quad (13)$$

where $\text{sgn}(x)$ is the sign of x.

For the SFI in (13), it contains two terms of parameters, as μ_k and δ_k^2 obtained from offline data and $\widetilde{\mu}_k$ and $\widetilde{\delta}_k^2$ calculated in real-time.

Remark 2. If the slight abnormality can be estimated accurately, SFI in (13) should conform with four conditions: (i) sufficient sensitivity to faults; (ii) appropriate robustness to noises; (iii) precise relation between fault amplitude and SFI; (iv) the relation from fault amplitude to SFI which is a double mapping function.

For condition (i), the proposed SFI is more sensitive than Mahalanobis distance and Euclidean; similar theoretical demonstration can be found in [27]. For condition (ii), the satisfied robustness to noises is analyzed in Section 5.3. Condition (iii) is easy to achieve because many curve fitting techniques can be used. In this application, neural network is adopted; this relation and approving experimental results are presented in Sections 3.3 and 5.2, respectively. And the mapping relation in condition (iv) is established, because sgn function ensures that fault and SFI share the same sign, and the positive correlation between fault amplitude and SFI can be known from Sections 3.3 and 3.4.

Remark 3. The developed SFI in (13) has three advantages over other related works. Firstly, it is more effective in detecting the change in mean deviation, while the methods in [16, 17] are not capable because they used the assumption that

$(\mu_k - \widetilde{\mu}_k)$ is 0. Secondly, it can determine the sign of the faulty parameter, which is useful in the subsequent fault isolation. Thirdly, it is more robust to noises and disturbances than the methods in [16], because a moving window strategy is used in (13).

3.3. Covariance Matrix Analysis. For simplicity, $X_{dq,\text{off}}$ is replaced by $X_{\text{off}} = [x_d \ \ x_q]$ in the following analysis. In this study, let i-th measurement variable of fault-free portion be x_i. In the presence of an incipient fault f_i, the sample value x_f can be described as follows [13]:

$$x_f = x_i + f_i. \tag{14}$$

In order to simplify analysis, (14) can be further rewritten as

$$x_f = (1 + \zeta_i)\, x_i, \tag{15}$$

where $\zeta_i = f_i./x_i$ is the amplitude variation rate on x_i. Assume that there are N observations; then (15) within multivariate statistical former can be expressed as the following expression:

$$X_f = X_{\text{off}} + \Xi \circ X_{\text{off}}, \tag{16}$$

where $\Xi = [\zeta_1, \ldots, \zeta_i, \ldots, \zeta_m] \in R^{N\times m}$ is fault magnitude rate (FMR) matrix and $\circ$ denotes Hadamard product.

Assume that d-th sensor is affected by incipient fault after the sampling step b, and the change of fault amplitude a depends on sampling step j; then $\Xi = [0 \cdots \zeta_d \cdots 0]$, and the FMR vector $\zeta_d = [0 \cdots a_{bd} \cdots a_{Nd}]^T$. For simplicity, the single FMR value a_{jd} is abbreviated as $a(j)$ where $j = 1, \ldots, N$. Here, $a(j) = 0$ when $j \in [1, b-1]$; and $\exists a(j) \neq 0$ if $j \geq b$. For incipient fault, the fault magnitude satisfy $a(j)x_{ji} = \delta_i$ in a size of small moving window n; then one can know that $a(b) = \cdots = a(n) = a$. After data normalization using the means and variances obtained by offline data set, X_f in (16) can be rewritten as

$$\overline{X}_f = \overline{X}_{\text{off}} + \Xi \circ \widehat{X}_{\text{off}}, \tag{17}$$

where $\widehat{X}_{\text{off}} = [x_1/\delta_1, x_2/\delta_2, \ldots, x_m/\delta_m] \in \mathscr{R}^{N\times m}$. Substituting $\overline{X}_{\text{off}}$ by $\overline{X}_f$ in (2), the online covariance matrix is

$$\begin{aligned} S_f &= \frac{1}{N-1}\overline{X_f}^T\overline{X_f} = S_{\text{off}} + \frac{1}{N-1}\left[\overline{X}_n^T\left(\Xi \circ \widehat{X}_n\right)\right. \\ &\quad \left. + \left(\Xi \circ \widehat{X}_n\right)^T \overline{X}_n + \left(\Xi \circ \widehat{X}_n\right)^T \Xi \circ \widehat{X}_n\right] = S_{\text{off}} \\ &\quad + \frac{a}{N-1}\left(\Psi_1 + \Psi_2 + \Psi_3\right) = S_{\text{off}} + \Delta S, \end{aligned} \tag{18}$$

where $\Psi_1 = \overline{X}_{\text{off}}^T(\Xi \circ \widehat{X}_{\text{off}})/a$, $\Psi_2 = (\Xi \circ \widehat{X}_{\text{off}})^T\overline{X}_{\text{off}}/a$, $\Psi_3 = (\Xi \circ \widehat{X}_{\text{off}})^T\Xi \circ \widehat{X}_{\text{off}}/a$, and $\Delta S = (a/(N-1))(\Psi_1 + \Psi_2 + \Psi_3)$.

Based on the computation rule of Hadamard product, we can see that

$$\Psi_1 = \begin{bmatrix} 0 & \cdots & \beta_1 & \cdots & 0 \\ \vdots & \vdots & \vdots & \vdots & \vdots \\ 0 & \cdots & \beta_d & \cdots & 0 \\ \vdots & \vdots & \vdots & \vdots & \vdots \\ 0 & \cdots & \beta_m & \cdots & 0 \end{bmatrix},$$

$$\Psi_2 = \begin{bmatrix} 0 & \cdots & 0 & \cdots & 0 \\ \vdots & \vdots & \vdots & \vdots & \vdots \\ \beta_1 & \cdots & \beta_d & \cdots & \beta_m \\ \vdots & \vdots & \vdots & \vdots & \vdots \\ 0 & \cdots & 0 & \cdots & 0 \end{bmatrix}, \tag{19}$$

$$\Psi_3 = \begin{bmatrix} 0 & \cdots & 0 & \cdots & 0 \\ \vdots & \vdots & \vdots & \vdots & \vdots \\ 0 & \cdots & \varphi & \cdots & 0 \\ \vdots & \vdots & \vdots & \vdots & \vdots \\ 0 & \cdots & 0 & \cdots & 0 \end{bmatrix},$$

where $\beta_i = \overline{x}_i^T\tau_d$, $\tau_d = [0, \ldots, x_{bd}/\delta_d, \ldots, x_{Nd}/\delta_d]^T$, and $\varphi = \sum_{j=1}^{N}[a(j)\tau_{jd}]^2$.

Asymptotically, $\Delta S \to 0$ as $a \to 0$. Comparing the covariance matrices S_f to S_{off}, the statistical parameters ΔS will be changed slightly by the amplitude of incipient fault a. Because the spanned vectors in RPCS and RRS share the same directions, variations in the eigenvalues will be tinily affected by a from the expression of S_f. Based on (18), there is

$$S_f = S_n + \Delta S = P\left(\Lambda_n + \Delta\Lambda\right)P^T = P\Lambda_f P^T. \tag{20}$$

That is to say that $\Delta\Lambda \approx 0$ when the measurements are affected by tiny abnormal value. Then Taylor development for Λ_f can be used in the neighborhood of $a = 0$ with the following form:

$$\begin{aligned} \Lambda_f &= \Lambda_n + \frac{\partial\Lambda_f}{\partial a}a + \frac{1}{2}\frac{\partial^2\Lambda_f}{\partial a^2}a^2 + \cdots + \frac{1}{o!}\frac{\partial^o\Lambda_f}{\partial a^o}a^o \\ &\quad + R_o(a). \end{aligned} \tag{21}$$

From (20), $\Lambda_f = P^T S_f P$. Substituting (21) into (20), it has

$$\begin{aligned} \Delta\Lambda &= \Lambda_f - \Lambda_n \\ &= a \times P^T\frac{\partial S_f}{\partial a}P + \frac{a^2}{2!} \times P^T\frac{\partial^2 S_f}{\partial a^2}P + \cdots + \frac{a^o}{o!} \\ &\quad \times P^T\frac{\partial^o S_f}{\partial a^o}P + P^T R_o(a)\, P, \end{aligned} \tag{22}$$

where

$$\frac{\partial S_f}{\partial a} = \frac{1}{N-1}\left(\Psi_1 + \Psi_2\right) + \frac{2a}{N-1}\Psi_3,$$
$$\frac{\partial^2 S_f}{\partial a^2} = \frac{2}{N-1}\Psi_3; \tag{23}$$

then $\partial^3 S_f/\partial a^3 = \cdots = \partial^o S_f/\partial a^o = R_o(a) = 0$. It is interesting to find that all higher-order partial derivatives of S_f are equal to 0 if their order is more than 2. Thus, $\Delta\Lambda$ can be described as

$$\Delta\Lambda = \frac{a}{N-1}P^T\left(\Psi_1 + \Psi_2\right)P + \frac{3a^2}{N-1}P^T\Psi_3 P. \tag{24}$$

Remark 4. From (24), $\Delta\Lambda$ is only affected by fault amplitude. As $\Lambda = \mathrm{Var}(X_{\mathrm{off}}P)$ and $\Delta\Lambda = \mathrm{Var}(X_f P)$, the KLD between offline and online PDFs can be directly calculated by Λ and $\Delta\Lambda$ instead of obtaining PDFs by kernel density estimation, the merit of which is a remarkable computational cost reduction.

3.4. Incipient FE Analysis. Recall (13) and combine assumptions f_k and $\widetilde{f}_k$ which are the PDFs of t_k and $\widetilde{t}_k$; then the k-th SFI can be written as

$$\mathrm{SFI}_k = \frac{\mathrm{sign}\left(\mu_k - \widetilde{\mu}_k\right)}{2}\left[\frac{\lambda_k}{\widetilde{\lambda}_k} + \frac{\widetilde{\lambda}_k}{\lambda_k} + \left(\mu_k - \widetilde{\mu}_k\right)^2\left(\frac{1}{\lambda_k} + \frac{1}{\widetilde{\lambda}_k}\right) - 2\right] = \mathrm{sign}\left(\eta_3\right) \cdot \frac{\left(a\eta_1 + a^2\eta_2\right)^2 + \eta_3^2\left[2\lambda_k + a\eta_1 + a^2\eta_2\right]}{2\left(\lambda_k + a\eta_1 + a^2\eta_2\right)}, \tag{25}$$

where

$$\eta_1 = \frac{1}{N-1}P^T\left(\Psi_1 + \Psi_2\right)P,$$
$$\eta_2 = \frac{3}{N-1}P^T\Psi_3 P, \tag{26}$$
$$\eta_3 = \mu_k - \widetilde{\mu}_k.$$

In (25), η_1, η_2, and η_3 can be obtained according to online data. The variations of SFI caused by incipient fault only depend on fault magnitude from the above expressions. In fact, there exists four candidate items for analytical expression of $\widehat{a}$ which allow one to derive relation among fault amplitude and KLD. However, two main reasons make this solution improper results: (i) this may lead to a undetermined result from four analytical expressions of $\widehat{a}$; (ii) some approximate conditions are used in the above expressions, which must introduce estimation bias on fault amplitude even if the system noise is considered.

By considering the relation in (25), the correlation between SFI and fault amplitude can be hence given as

$$\widehat{a} = f\left(\mathrm{SFI}_k\right) \propto \mathrm{SFI}_k. \tag{27}$$

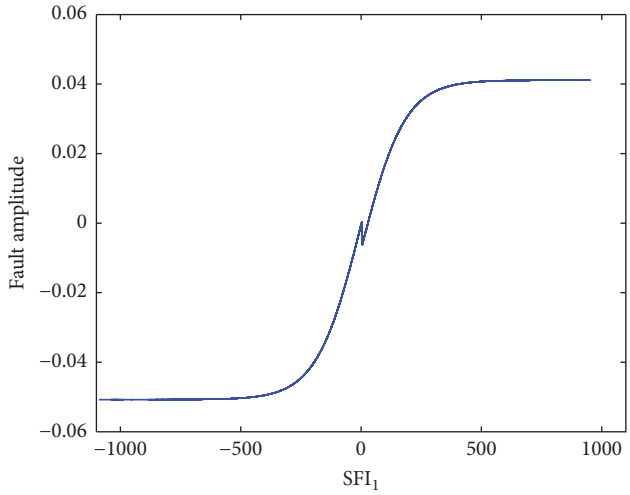

Figure 3: The relation between $\widehat{a}$ and SFI_1.

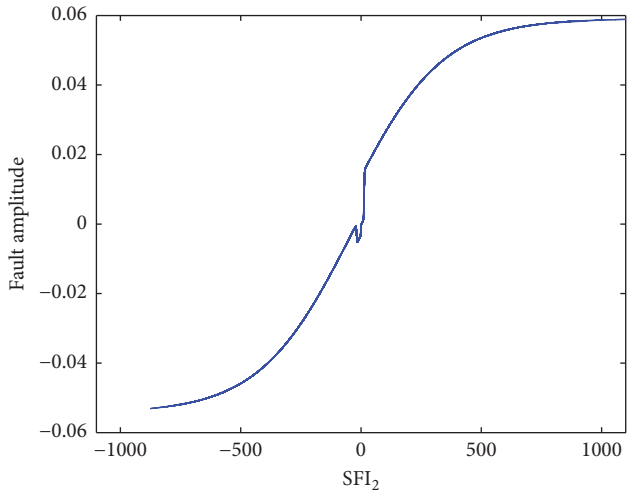

Figure 4: The relation between $\widehat{a}$ and SFI_2.

In (27), the correlation f must be nonlinear and monotonic increasing. Then, an alternative solution based on neural network is used to determine the nonlinear relationship f. By backpropagation neural network, the correlations for application in Section 5 are shown in Figures 3 and 4. Both curves reflect the correlations which are described in (27). The curves in both Figures 3 and 4 providing an indicator proportional to abnormality allow for the possibility of FE.

4. On-Line Fault Estimation Strategy

The flow diagram of fault estimation strategy is given in Figure 5, which contains data preprocessing, SFI, and fault estimation. The data processing is one of the key steps in Figure 5, which can make the original data set obey Gaussian distribution in the rotary space. And the rotary speed depends on the rotary angular velocity ω of traction motor in CRH2. In addition, data normalization is needed, which gives the same weighting for i_d and i_q and simplifies the

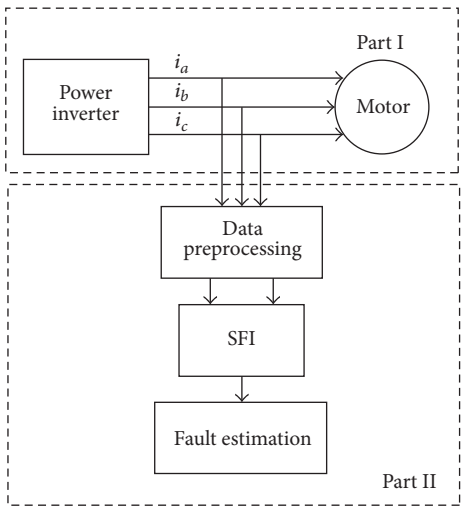

Figure 5: Flow diagram of incipient FE based on the proposed approach.

online fault diagnosis algorithms. The data normalization steps are summarized in Algorithm 5, and projecting original data into a rotary space is embedded in Algorithms 6 and 7. In addition, the complete fault estimation strategy shown in Figure 5 can be implemented by Algorithms 6 and 7.

Algorithm 5. Consider the following.

Step 1. Define $X = [x_k(1), \ldots, x_k(m)] \in R^{N\times m}$, where $k = 1, \ldots, N$ and $i = 1, \ldots, m$; then calculate the mean value and variance of every column as

$$\begin{aligned} \overline{x}(i) &= \frac{1}{N}\sum_{k=1}^{N} x_k(i), \\ \sigma^2(i) &= \frac{1}{N-1}\sum_{k=1}^{N}\left(x_k(i) - \overline{x}(i)\right)^2. \end{aligned} \tag{28}$$

Step 2. Based on $\overline{x}(i)$ and σ, the normalization data $x_k(i)$ can be defined by the following equation:

$$x(i) = \left[\frac{x_1(i) - \overline{x}(i)}{\sigma(i)} \cdots \frac{x_N(i) - \overline{x}(i)}{\sigma(i)}\right]^T. \tag{29}$$

4.1. Offline Modeling Steps

Algorithm 6. Consider the following.

Step 1. Collect normal operating data $X_{abc,\text{off}} \in R^{N\times 3}$ from three current sensors in CRH2 under steady state.

Step 2. Project X_{abc} into a rotary data space $X_{dq,\text{off}} \in R^{N\times 2}$ by (11).

Step 3. Normalize $X_{dq,\text{off}}$ by Algorithm 5.

Step 4. Do an SVD as follows:

$$\frac{1}{N-1}\overline{X}_{dq,\text{off}}^T\overline{X}_{dq,\text{off}} = P\Lambda_n P^T, \tag{30}$$

where $\Lambda_n = \text{diag}(\lambda_1, \lambda_2)$ and $\lambda_1 > \lambda_2$.

Step 5. Calculate the score matrix in RPCS by

$$T = (t_1, t_2) = \overline{X}_{dq,\text{off}}P, \tag{31}$$

where $t_i = [t_{1,i} \cdots t_{j,i} \cdots t_{N,i}]^T$, $i = 1, 2$.

Step 6. Obtain the mean value and variance of score vector by

$$\begin{aligned} \mu_i &= \frac{1}{N}\sum_{j=1}^{N} t_{j,i}, \\ \delta_i^2 &= \lambda_i. \end{aligned} \tag{32}$$

Step 7. Determine the nonlinear double mapping relations between a and SFI_1, SFI_2.

4.2. Online FE Steps

Algorithm 7. Consider the following.

Step 1. Load a new current data x_{new} from the running CRH2.

Step 2. Project x_{new} into RPCS and normalize the data $x_{dq,\text{new}}$ as $\overline{x}_{dq,\text{new}}$ using Algorithm 5.

Step 3. Obtain online score vector T_{new} by

$$T_{dq,\text{new}} = (\widetilde{t}_1, \widetilde{t}_2) = \overline{X}_{dq,\text{new}}P, \tag{33}$$

where $\widetilde{t}_i = [t_{1,i} \cdots t_{j,i} \cdots t_{n,i}]^T$ and n is the size of moving window.

Step 4. Calculate the mean value and variance of the online score vector by

$$\begin{aligned} \widetilde{\mu}_i &= \frac{1}{n}\sum_{j=1}^{n}\widetilde{t}_{j,i}, \\ \widetilde{\delta}_i^2 &= \text{var}\left(\widetilde{t}_{j,i}\right). \end{aligned} \tag{34}$$

Step 5. Compute SFI by (13).

Step 6. Estimate the fault amplitude according to the obtained relations in Step 7 of Algorithm 6. And then go back to Step 1.

Remark 8. The reasons for adopting moving window approach in Step 3 of Algorithm 6 are the following: (i) the single sampling value has no mean and variance; (ii) the moving window approach can weaken the influences caused by noises.

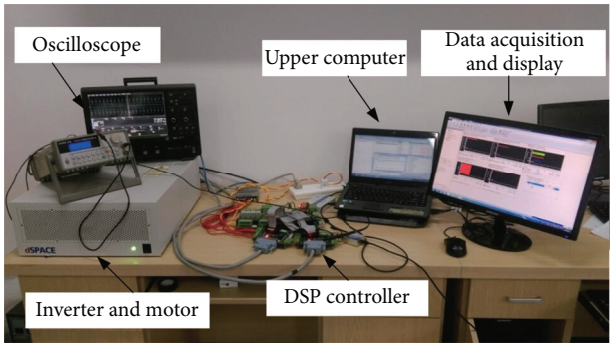

Figure 6: Experimental setup with fault injection.

5. Results and Illustrations

In order to test the performance of the proposed method, some experiments of CRH2 explored by Central South University [28] are conducted in this section, as shown in Figure 6. The experimental setup with fault injection operations of CRH2 consists of DSP controller, upper computer, dSPACE, data acquisition, and display devices. Its main parameters in electric multiple unit (EMU) are given in Table 1. In this part, we concentrate on incipient sensor FE to illustrate the effectiveness of the proposed methodology.

5.1. Incipient Fault Injections. When the reference running speed 200 Km/h is given, the tendency of six curves will be invariable after 1 s. It indicates that the traction system is running in the steady state. Therefore, the historical data are generated after 1 s to establish the offline data model. In this paper, we consider three continuous output currents as the selected signals.

For simplification without generality, a-phase current is chosen as the corrupted signal. And two types of incipient current sensor faults are considered.

Case 1 (incipient bias fault f_1). After 0.5 s, $f_1 = 0.5$ A is injected into i_a.

Case 2 (incipient ramp fault f_2). After 0.5 s, $f_2 = 2(t - 0.5)$ A is injected into i_a.

5.2. Incipient Fault Estimation Results

(1) Results for f_1. For the normal and the corrupted current signals with f_1, both data sets under SNR = 30 db are provided in rotary space, as shown in Figure 7. The added sensor noise allows the SNR of 30 db which is a reasonable noise level for electric system. And the equivalent value of actual fault is presented in Figure 8. As the current sensors are infected by the zero-mean Gaussian noises, there exists extreme tiny value in the case of normal condition which can be filtered out by using the proposed method. After 0.5 s, the constant bias fault will be invariably fluctuating by the preprocessing, as shown in Figure 8. In rotary data space, this waving abnormality is sine wave whose period and amplitude is

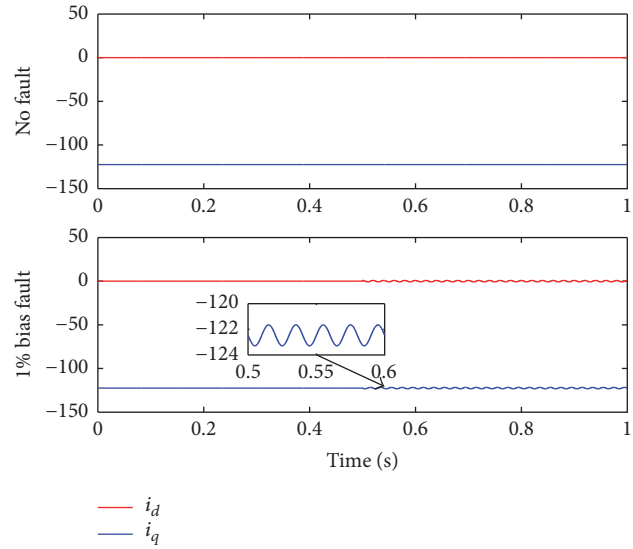

Figure 7: The influence on rotary date space caused by f_1.

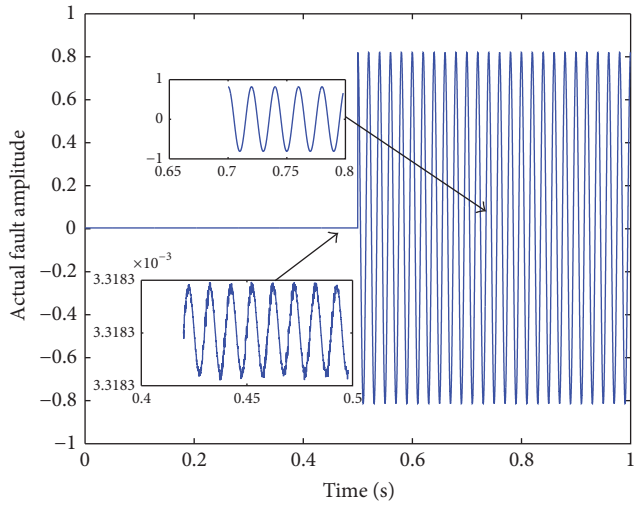

Figure 8: Fault amplitude of f_1 in rotary date space under SNR = 30 db.

dependent on synchronous angular velocity ω and abnormal value, respectively.

Based on the online strategy in Section 4, two latent components are selected to describe the data model in rotary space. This is caused by two approximate equalities of eigenvalues in (30). In Figures 9 and 10, two SFIs display the sensitivity to tiny distortion. Both figures clearly show this effectiveness for small bias. This performance is actually perfect for practical application under 30 db noise level.

In Figures 11 and 12, the red line is actual incipient fault value on i_a, and the blue line marked by + is the estimation value $\hat{a}$ by using the proposed method. On the basis of the enlarge figure in Figure 11, the estimation amplitude is close to actual fault value, which can show the correctness of the proposed incipient fault estimation method. However, there exists small acceptable delay for estimation results. The

Table 1: The system parameter for EMU in CRH2.

Variables	Variable name	Setting value (units)
U_d	Intermediate DC voltage	2600 (V)
ϕ	Set magnetic flux linkage	1.858 (Wb)
T_s	Inverter switching time	$1e-4$ (s)
t_s	Sampling time	$1e-5$ (s)
T	Rectifier switching time	$8e-4$ (s)
L_m	Mutual inductance	$3.285e-2$ (H)
L_r	Rotor self-inductance	$3.414e-2$ (H)
L_{rl}	Leakage inductance in rotor side	$1.294e-3$ (H)
L_s	Inductance in stator side	$3.427e-2$ (H)
L_{sl}	Leakage inductance in stator side	$1.417e-3$ (H)
n_p	Pole pairs	2 (1)
K_{IM}	Integral value in the first phase controller	0 (1)
K_{PM}	Proportion value in the first phase controller	30 (1)
K_{IT}	Integral value in the second phase controller	0 (V)
K_{PT}	Proportion value in the second phase controller	50 (V)
R_r	Rotor resistance	0.146 (Ω)
R_s	Stator resistance	0.114 (Ω)
L_N	Leakage inductance in secondary side of transformer	0.002 (H)
C_1, C_2	Supported capacitance	16 (mF)

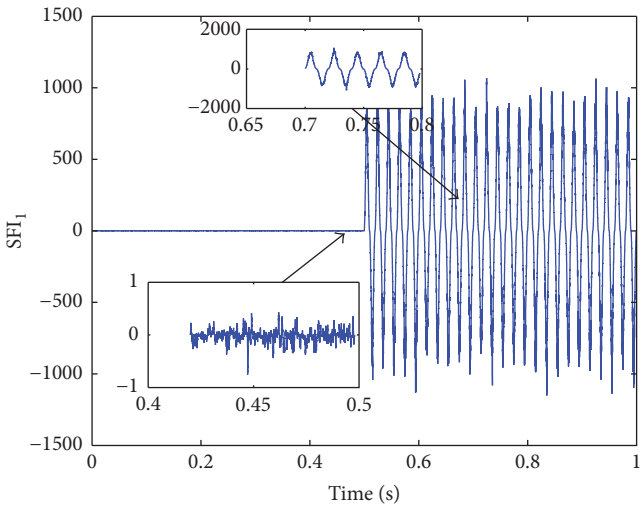

Figure 9: SFI_1 for f_1 in the case of SNR = 30 db.

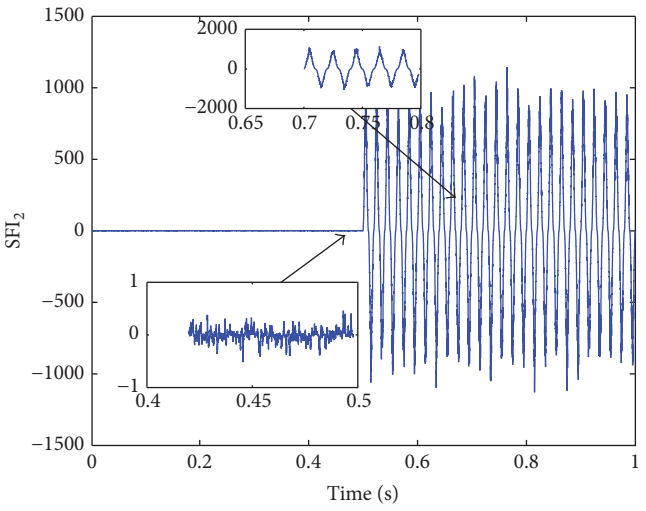

Figure 10: SFI_2 for f_1 in the case of SNR = 30 db.

reason for this phenomenon will be discussed in the following subpart. Similarly, the result depended on SFI_2 in Figure 12 also showing its satisfied estimation performance.

(2) Results for f_2. For a ramp incipient fault, its wave and the corresponding corrupted signals i_a are shown in Figure 13. In this case, the tiny amplitude a is steadily climbing from 0 to 1% when the time ranged from 0.5 s to 1 s. Therefore, this must lead to the higher difficulty for FE than constant bias distortion. By using the nonlinear projection onto the rotary space, its characteristic of gradually changing is invariable, which is depicted in Figure 14.

For this type of slight abnormality, Figures 15 and 16 present SFI_1 and SFI_2. From two indicators, both SFI_1 and SFI_2 can emphasize the tiny fault successfully. It is interesting to see that two curves are fluctuated with fault amplitude.

After successfully detecting drifting fault, Figures 17 and 18 display the actual and estimated incipient fault amplitude under SNR = 30 db. In Figures 17 and 18, the estimated amplitude is close to actual fault value according to the red

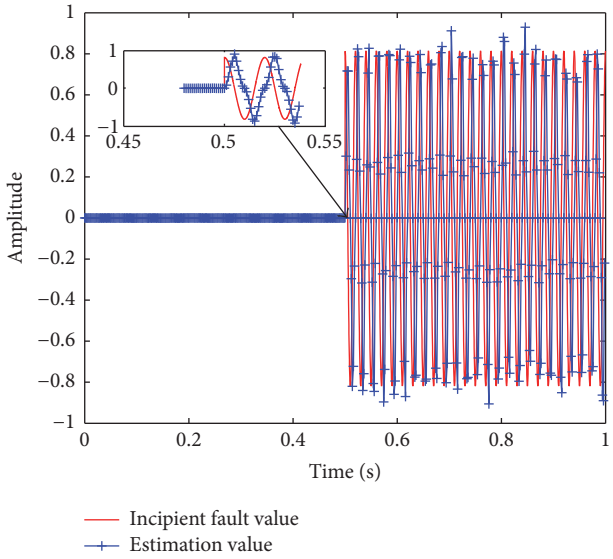

Figure 11: FE result for f_1 via SFI_1.

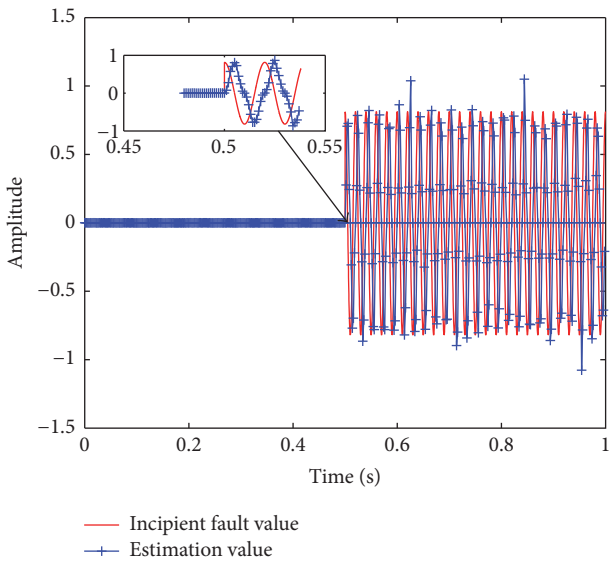

Figure 12: FE result for f_1 via SFI_2.

line and marked blue line. Even coming to the very tiny fault amplitude, the accuracy of results is still acceptable.

5.3. Discussions. Based on (11), if there exists an incipient fault f_{abc} in current sensors, the derived forms in rotary space can be described as

$$f_{d,a} = \frac{2}{3}\cos\theta f_{abc,a},$$
$$f_{q,a} = -\frac{2}{3}\sin\theta f_{abc,a}, \tag{35}$$

where $f_{abc,i}$ is the incipient fault in i-th sensor, $i = a, b, c$, and $f_{dq,j}$ is its equivalent form in j coordinate, $j = d, q$. Therefore, both bias and drifting fault will be transformed to periodic signals which are described in Figures 7 and 14.

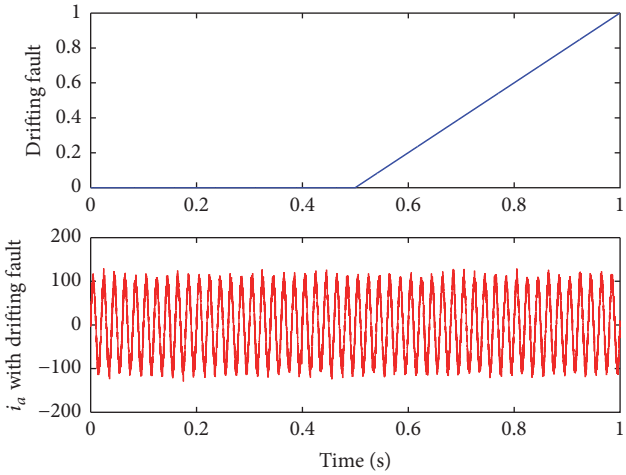

Figure 13: i_a sensor with f_2.

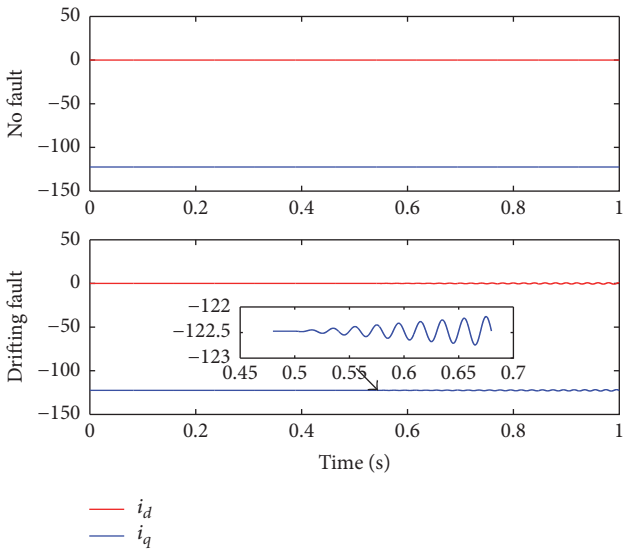

Figure 14: The influence on the rotary space cased by f_2.

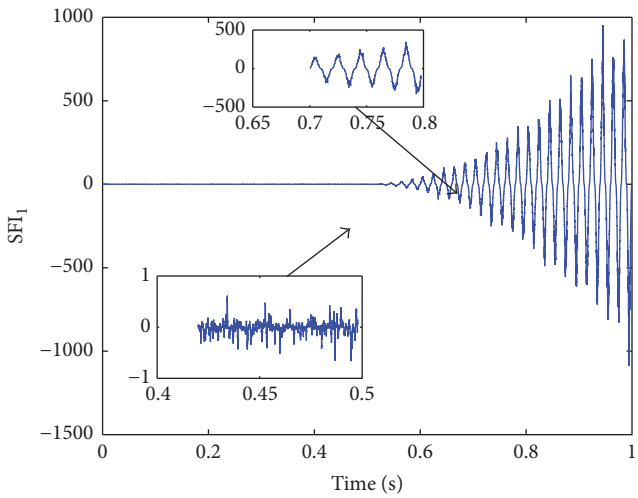

Figure 15: SFI_1 for f_2 in the case of SNR = 30 db.

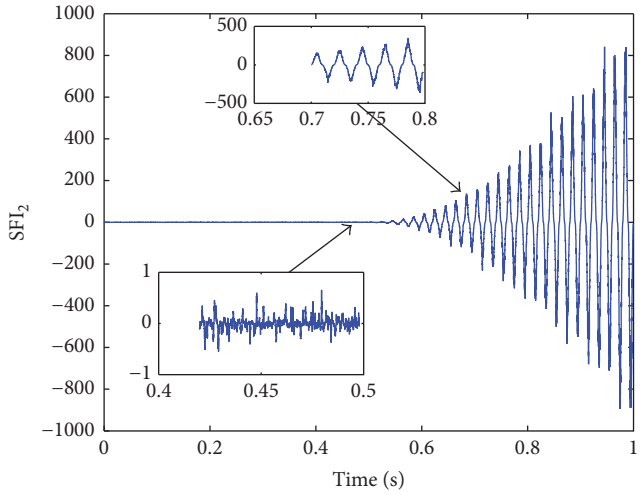

Figure 16: SFI_2 for f_2 in the case of SNR = 30 db.

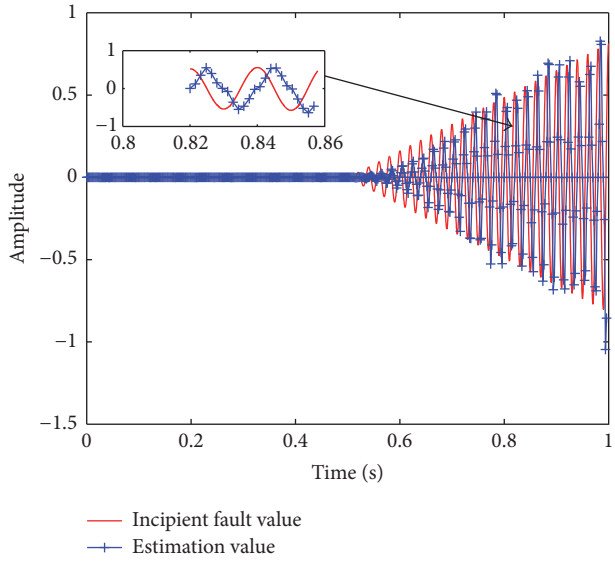

Figure 17: FE result for f_2 via SFI_1.

In this paper, the number of scores within the moving window is chosen, 20. Following the results in two examples, a window size of $n = 20$ is sufficient for perfect FE performance. However, it has a little flaw which is the short delay. On the online stage, the estimated mean $\tilde{\mu}$ and variance $\tilde{\delta}$ of score vector in (34) are calculated by using multiple current measurements. This will lead to two results.

(i) Improving the robustness: by using the moving window approach in online computation part, the sensor noise effect can be notably reduced. Theoretically, the effect caused by noise will be completely filtered out if the window size trends toward infinity.

(ii) Producing the time or step delay: because of periodicity of fault value after nonlinear projection, the amplitude will fluctuate between its bottom and peak in the rotary space. Combining with multiple score values, the evaluation function at step k will be impacted by $t_{k-n+1}, \ldots, t_{k-1}$ which are in the window. In fact, the length of delay is dependent on the moving window size. If n is chosen as 1, the SFI can be only determined by the current score value. In this case, the delay can be eliminated.

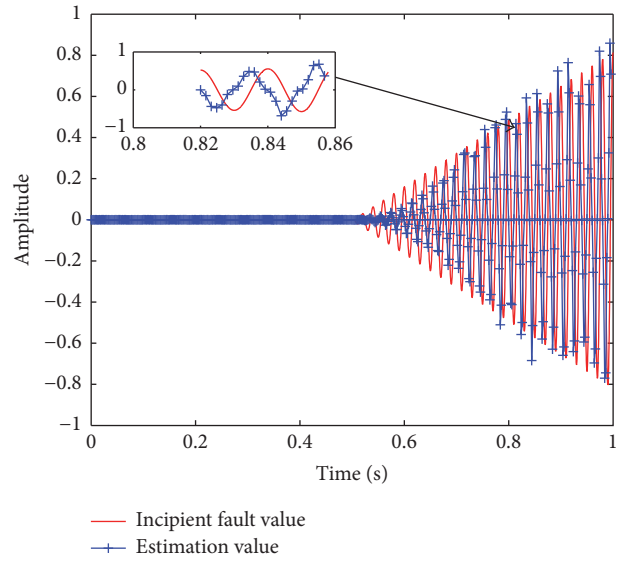

Figure 18: FE result for f_2 via SFI_2.

Therefore, the tradeoff between robustness and the estimation delay should be considered in choosing the window size n. From the asymptotic behavior of SFI, increasing the number of score value does not affect the robustness when $n > 30$. In fact, this effect can be approximately achieved if $n \geq 20$. This characteristic was illustrated and shown in incipient fault detection [27]. Moreover, the waves of SFI and estimation values are similar to actual fault value. As the longer window size is chosen, the similarity among them will be reduced, and fault estimation delay will become bigger. In addition, for the degradation in sensor precision, the large window size is problematic.

The sampling time of the experimental platform in Table 1 gives the step time. Then, the constant delay time is 0.4 ms which can be obtained by the size of moving window. From the enlarge pictures in four fault estimation figures, the short delay is acceptable for industrial application. Among them, Figures 11 and 12 perform better amplitude estimation because of the bigger fault amplitude.

Beyond the moving size, Fault-to-Noise-Ratio (FNR) is introduced to explain the effectiveness of the proposed method from the results in Figures 17 and 18. It is well known that FNR is defined as $FNR = 10\log(\delta_F^2/\delta_N^2)$, where δ_F^2 and δ_N^2 are fault power and noise level, respectively, although the weaker results than Figures 11, 12, 17, and 18 show more useful information by varying FNR. For the drifting fault in Figure 13, the peak of FNR level in every period ranges from minus infinity to 10 db after 0.5 s. From the FE results, it can be seen that the proposed SFI in this paper is sensitive enough to emphasize such tiny abnormality under high noise levels.

6. Conclusion

In this paper, the real-time incipient sensor FE in CRH2 is investigated. An effective SFI based on KLD and PCA is developed and analyzed. In order to cater for the latent requirement of PCA, a rotary space is firstly introduced into data-driven FDD and FE domain. The proposed FE methodology can not only emphasize the tiny abnormality but also be insensitive to sampling noises. Through testing incipient faults in experimental setup of CRH2, the feasibility and efficiency of the developed method are validated. The effect of some factors on FE results have further been explored. Moreover, the proposed method can be extended to other electrical systems based on the nonlinear projections and SFI from both theoretical and practical points.

Conflicts of Interest

The authors declare no conflicts of interest.

Acknowledgments

This work is partially supported by the National Natural Science Foundation of China (Grants nos. 61490703 and 61573180) and Funding of Jiangsu Innovation Program for Graduate Education (Grant no. KYLX16_0378).

References

[1] S. Zhang, *Fundamental Application Theory and Engineering Technology for Railway High-Speed Trains*, Science Press, Beijing, China, 2007.

[2] Y. Wu, B. Jiang, N. Lu, and Y. Zhou, "Bayesian network based fault prognosis via bond graph modeling of high-speed railway traction device," *Mathematical Problems in Engineering*, vol. 2015, Article ID 321872, 11 pages, 2015.

[3] Z. Mao, Y. Zhan, G. Tao, B. Jiang, and X. Yan, "Sensor fault detection for rail vehicle suspension systems with disturbances and stochastic noises," *IEEE Transactions on Vehicular Technology*, vol. 66, no. 6, pp. 4691–4705, 2017.

[4] S. Diao, Z. Makni, J.-F. Bisson, D. Diallo, and C. Marchand, "Current sensor fault diagnosis in the stationary frame for PMSM drive in automotive systems," in *Proceedings of the 9th International Conference on Ecological Vehicles and Renewable Energies (EVER '14)*, pp. 1–7, March 2014.

[5] L. Ren, Z. Y. Xu, and X. Q. Yan, "Single-sensor incipient fault detection," *IEEE Sensors Journal*, vol. 11, no. 9, pp. 2102–2107, 2011.

[6] S. Yang, D. Xiang, A. Bryant, P. Mawby, L. Ran, and P. Tavner, "Condition monitoring for device reliability in power electronic converters: A review," *IEEE Transactions on Power Electronics*, vol. 25, no. 11, pp. 2734–2752, 2010.

[7] K. Zhang, B. Jiang, X.-G. Yan, and Z. Mao, "Sliding mode observer based incipient sensor fault detection with application to high-speed railway traction device," *ISA Transactions*, vol. 63, pp. 49–59, 2016.

[8] G.-A. Capolino, J. A. Antonino-Daviu, and M. Riera-Guasp, "Modern diagnostics techniques for electrical machines, power electronics, and drives," *IEEE Transactions on Industrial Electronics*, vol. 62, no. 3, pp. 1738–1745, 2015.

[9] G. H. B. Foo, X. Zhang, and D. M. Vilathgamuwa, "A sensor fault detection and isolation method in interior permanent-magnet synchronous motor drives based on an extended kalman filter," *IEEE Transactions on Industrial Electronics*, vol. 60, no. 8, pp. 3485–3495, 2013.

[10] X.-G. Yan and C. Edwards, "Nonlinear robust fault reconstruction and estimation using a sliding mode observer," *Automatica*, vol. 43, no. 9, pp. 1605–1614, 2007.

[11] S. Yin, X. Zhu, and O. Kaynak, "Improved PLS focused on key performance indictor related fault diagnosis," *IEEE Transactions on Industrial Electronics*, vol. 62, no. 3, pp. 1651–1658, 2015.

[12] Q. Jiang, X. Yan, and B. Huang, "Performance-driven distributed PCA process monitoring based on fault-relevant variable selection and bayesian inference," *IEEE Transactions on Industrial Electronics*, vol. 63, no. 1, pp. 377–386, 2016.

[13] S. J. Qin, "Survey on data-driven industrial process monitoring and diagnosis," *Annual Reviews in Control*, vol. 36, no. 2, pp. 220–234, 2012.

[14] S. Yin, H. Gao, and O. Kaynak, "Data-driven control and process monitoring for industrial applications-Part I," *IEEE Transactions on Industrial Electronics*, vol. 61, no. 11, pp. 6356–6359, 2014.

[15] S. Yin, H. Gao, and O. Kaynak, "Data driven control and process monitoring for industrial applications—part II," *IEEE Transactions on Industrial Electronics*, vol. 62, no. 1, pp. 583–586, 2015.

[16] J. Harmouche, C. Delpha, and D. Diallo, "Incipient fault detection and diagnosis based on Kullback-Leibler divergence using principal component analysis: Part II," *Signal Processing*, vol. 109, pp. 334–344, 2015.

[17] J. Harmouche, C. Delpha, and D. Diallo, "Incipient fault amplitude estimation using KL divergence with a probabilistic approach," *Signal Processing*, vol. 120, pp. 1–7, 2016.

[18] R. M. Goodall and W. Kortüm, "Mechatronic developments for railway vehicles of the future," *Control Engineering Practice*, vol. 10, no. 8, pp. 887–898, 2002.

[19] S. Yin, S. Ding, X. Xie, and H. Luo, "A review on basic data-driven approaches for industrial process monitoring," *IEEE Transactions on Industrial Electronics*, vol. 61, no. 11, pp. 6418–6428, 2014.

[20] S. X. Ding, *Data-driven Design of Fault Diagnosis and Fault-tolerant Control Systems*, Advances in Industrial Control, Springer, London, UK, 2014.

[21] S. X. Ding, Y. Yang, Y. Zhang, and L. Li, "Data-driven realizations of kernel and image representations and their application to fault detection and control system design," *Automatica*, vol. 50, no. 10, pp. 2615–2623, 2014.

[22] N. Lu, F. Gao, and F. Wang, "Sub-PCA modeling and on-line monitoring strategy for batch processes," *AIChE Journal*, vol. 50, no. 1, pp. 255–259, 2004.

[23] T. van Erven and P. Harremës, "Rényi divergence and Kullback-Leibler divergence," *IEEE Transactions on Information Theory*, vol. 60, no. 7, pp. 3797–3820, 2014.

[24] X. Nguyen, M. J. Wainwright, and M. . Jordan, "Estimating divergence functionals and the likelihood ratio by convex risk minimization," *IEEE Transactions on Information Theory*, vol. 56, no. 11, pp. 5847–5861, 2010.

[25] A.-K. Seghouane, "A Kullback-Leibler divergence approach to blind image restoration," *IEEE Transactions on Image Processing*, vol. 20, no. 7, pp. 2078–2083, 2011.

[26] S. Kullback and R. A. Leibler, "On information and sufficiency," *Annals of Mathematical Statistics*, vol. 22, pp. 79–86, 1951.

[27] J. Zeng, U. Kruger, J. Geluk, X. Wang, and L. Xie, "Detecting abnormal situations using the Kullback-Leibler divergence," *Automatica*, vol. 50, no. 11, pp. 2777–2786, 2014.

[28] C. Yang, C. Yang, T. Peng, X. Yang, and W. Gui, "A fault-injection strategy for traction drive control systems," *IEEE Transactions on Industrial Electronics*, vol. 64, no. 7, pp. 5719–5727, 2017.

Hindawi
Mathematical Problems in Engineering
Volume 2017, Article ID 6402012, 14 pages
https://doi.org/10.1155/2017/6402012

Research Article

Robust Course Keeping Control of a Fully Submerged Hydrofoil Vessel with Actuator Dynamics: A Singular Perturbation Approach

Sheng Liu, Changkui Xu, and Lanyong Zhang

College of Automation, Harbin Engineering University, Harbin 150001, China

Correspondence should be addressed to Changkui Xu; xuchangkui@hrbeu.edu.cn

Received 27 May 2017; Accepted 26 July 2017; Published 5 September 2017

Academic Editor: Shoudong Huang

This paper presents a two-time scale control structure for the course keeping of an advanced marine surface vehicle, namely, the fully submerged hydrofoil vessel. The mathematical model of course keeping control for the fully submerged hydrofoil vessel is firstly analyzed. The dynamics of the hydrofoil servo system is considered during control design. A two-time scale model is established so that the controllers of the fast and slow subsystems can be designed separately. A robust integral of the sign of the error (RISE) feedback control is proposed for the slow varying system and a disturbance observer based state feedback control is established for the fast varying system, which guarantees the disturbance rejection performance for the two-time scale systems. Asymptotic stability is achieved for the overall closed-loop system based on Lyapunov stability theory. Simulation results show the effectiveness and robustness of the proposed methodology.

1. Introduction

With the development of science and technology, maritime transport has entered a high-speed era. As an advanced marine surface vehicle, the fully submerged hydrofoil vessel (FSHV) can cruise at a high speed under rough sea wave. The lift force of the hydrofoils generated by the high-speed fluid can elevate the ship hull from the water, which highly reduces the wave resistance and friction to the ship [1–3]. However, it also leads to instability of the open loop system of the FSHV. Therefore, an autopilot is necessary for this type of hydrofoil vessels. Currently, the commercial control system equipped on board is based on optimal control theory which has a weak disturbance rejection property [3–5]. For the sake of the high cruising speed, the nonlinear hydrodynamic damping of the FSHV cannot be neglected [6], so that the widely used model of marine surface vessels can be no longer applicable for the existence of strong coupling between yaw and roll dynamics. Moreover, the model uncertainties and stochastic disturbance caused by wind, waves and currents also make it difficult for precise steering of this species of marine vehicle.

In fact, the path of marine vessels is usually straight line or straight lines formed by waypoints, on which condition there is little coupling between the heave/pitch dynamics and the yaw/roll dynamics. Some literatures have been investigated about the riding control [3, 4]. This paper mainly focuses on the steering control of the FSHV.

As for the nonlinear steering control for marine vessels, a series of control methodologies have been explored, such as advanced sliding mode control [7–9], robust control [10, 11], and adaptive control [12–14]. But these passive disturbance attenuation control methods may suffer from actuator chattering, system conservation, derivative explosion, and rigorous proof for stability. In some literatures, intelligent approximations, such as fuzzy logic [15] and neural network [16], are introduced as feedforward components for estimation and disturbance compensation. But the convergence rate of weight function and the problem of extremum solving still remain to be settled. Disturbance rejection control is widely applied in rigid-body dynamics and servo systems [17–19]. Disturbance observer based control (DOBC) approaches can estimate the generalized disturbances and improve the robustness of the systems in an active way. Control applications in many different fields have validated the effectiveness of the DOBC, such as manipulator tracking control [20], power system control [17, 18], and missile guidance and

control [19, 21]. Due to the simple structure of the DOB, it is often used in real-time control applications for high precision. To enhance the disturbance rejection performance, a composite hierarchical antidisturbance control (CHADC) is proposed in [22–25]. In this method, the disturbance observer is built in the inner-loop to estimate the generalized disturbance, and an outer-loop robust controller is also developed to compensate for the residual error of the DOB [22]. However, time scale separation and cascade analysis for multi-time scale subsystem are not included.

In the existing literatures about motion control of marine vehicles with actuator dynamics, the actuator system is always regarded as a first-order inertial element [26]. However, most actuator systems are servo systems driven by electric motors or electronic-hydraulic mediums. The first-order inertial model cannot present the main features of these servo systems since there are high-order dynamic elements and model uncertainties in the servo systems, and most servo systems do not have static stability. Therefore, the controller for the inner-loop needs to be designed additionally. Current approaches for control design together with actuator dynamics are based on backstepping and cascade system theory, which consider the rigid-body dynamics and the actuator dynamics as an integrated system [26], so that the control input can be calculated directly. However, these methodologies take little emphasis on the interconnection between actuator dynamics and attitude stabilization, as well as the closed-loop stability analysis for the overall system with different time scales. The main reasons for this problem are listed as follows.

(1) In most cases, adding the servo system for the actuator mechanism into the control objective will lead to the increase of the relative degree of the overall system, which will cause the so-called "explosion of complexity," such that backstepping based control strategies are no longer conventional.

(2) The frequency response of the actuator servo system is different from that of the attitude tracking system. Therefore, it is not advisable to make the system control design using classical state feedback control methodologies just in a simply single scheme.

(3) External disturbance and model uncertainties exist in both of the systems mentioned above, where their physical characteristics are different according to the time scales of the attitude tracking subsystem and the actuator subsystem. In order to guarantee the control precision and disturbance rejection performance, time scale separation is required to justify the implementation of the controller design for each subsystem.

When the actuator dynamics is considered in the control design for the course keeping control of the FSHV, multi-time scale phenomenon tends to be particularly sensitive for the interconnection analysis of the overall system. Singular perturbation approach is such a method to analyze and separate different time scale motions in control problems [27–30]. In this approach, by introducing a small time scale parameter ε, the overall system is decomposed into two different time scale subsystems, namely, the quasi-steady-state (slow) subsystem and the boundary-layer (fast) subsystem. For the course keeping control of the FSHV, the attitude stabilization for rigid-body dynamics is obviously the slow dynamic subsystem while the actuator servo system is the fast dynamic subsystem since natural frequency of the servo system is definitely much higher than the rigid-body dynamics and the response time of the servo system to a steady state is much less than the rigid-body dynamics of the FSHV for the different inertias of these subsystems. Accordingly, to analyze the characteristic of the multi-time scales and design a control strategy without the drawbacks of the aforementioned high-order controllers, a singular perturbation based hierarchical control structure is required for the compound system.

The basis of singular perturbation theory can be referred to [27]. And this methodology has been applied in nonlinear systems such as control practices in aerospace and UAV systems [27–30] for many years. However, to the best of our knowledge, although singular perturbation method has been reported for motion control of conventional marine vessels [31, 32], applications on multi-degree-of-freedom stabilization of marine vessels with actuator dynamics can rarely be seen in the open literatures. Moreover, in the literatures above, the proposed controllers for the fast and slow subsystems are basic state feedback methods and feedback linearization based approaches, which are designed based on the nominal models of the objective systems without the consideration of the lumped disturbances. Therefore, the disturbance rejection performance cannot be guaranteed. For the complex motion control of marine vehicles, the disturbances caused by winds, waves, and currents severely affect the control performance and precision, so the robustness of the closed-loop system must be particularly evaluated in control design.

In this paper, a hierarchical robust control structure is proposed for the course keeping of the FSHV with actuator dynamics against composite disturbances. The main contributions are listed as follows.

(1) Different from the CHADC methodology, singular perturbation theory is used for the time scale separation of the lateral dynamics of the FSHV and the actuator servo system to explore the interconnection of the slow dynamics and the fast dynamics.

(2) A robust integral of the sign of the error (RISE) feedback control is presented for the stabilization of the slow-time scale subsystem and a DOB based feedback control is utilized for the fast-time scale subsystem. All control signals are continuous which are practical for engineering implementation.

(3) Disturbance attenuation performance is guaranteed in both quasi-steady-state subsystem and boundary-layer subsystem. Interconnection of the subsystems is analyzed and uniformly asymptotic stability is achieved at the equilibrium point.

The rest of the paper is organized as follows. In Section 2, the mathematical models of the lateral dynamics of a FSHV

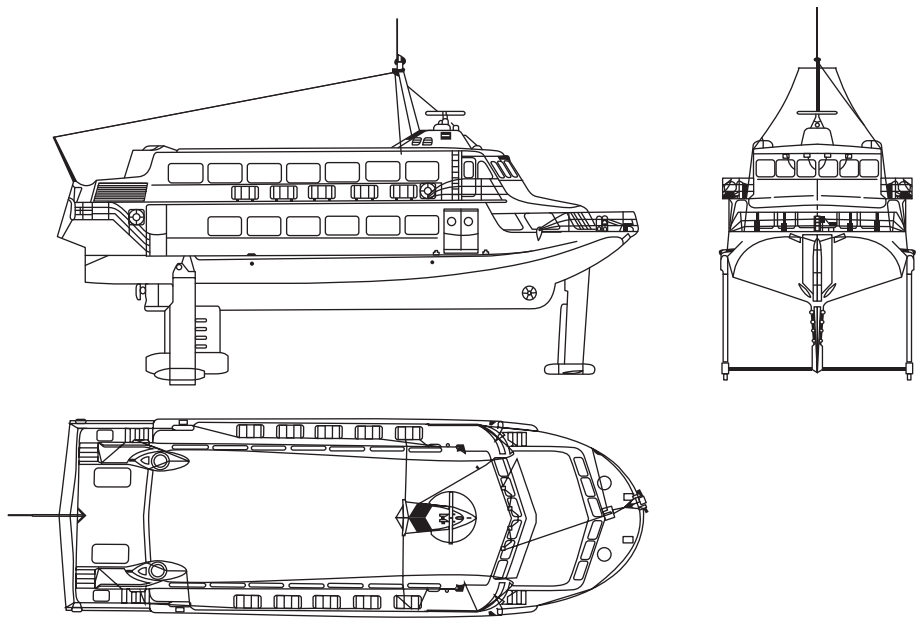

Figure 1: Fully submerged hydrofoil vessel.

and its hydrofoil servo system are developed. In Section 3, a hierarchical robust disturbance rejection control strategy is proposed based on singular perturbation theory. Stability of the hierarchical system is analyzed via Lyapunov stability theory. Simulation is carried out in Section 4 to validate the effectiveness of the proposed control method, followed by conclusions in Section 5.

2. Problem Formulation

A typical configuration of a fully submerged hydrofoil vessel is shown in Figure 1. The T-shaped bow foil is equipped with two controlled flaps, acting together. The aft foil has a pair of central flaps and two pairs of ailerons. Struts of the aft foil are equipped with rudders, which is used for roll and yaw dynamics together with the ailerons. And the bow foil and the central part of the aft foil are for longitudinal motion control.

Assuming that the surge speed is controlled by an individual propulsion system, the maneuvering model of a typical marine vehicle is shown as follows:

$$\begin{aligned} \dot{\eta} &= J(\eta)\nu, \\ M\dot{\nu} + C(u_0,\nu)\nu + D(u_0,\nu)\nu + G(\eta) &= Bu + \tau_d, \end{aligned} \tag{1}$$

where $\eta \in [\phi, \psi]^T$ is a vector of position and orientation with coordinates in the earth-fixed frame and $\nu \in [p, r]^T$ is a vector of linear and angular velocities with coordinates in the body-fixed frame.

$$J = \begin{bmatrix} 1 & 0 \\ 0 & \cos\phi \end{bmatrix} \tag{2}$$

is the Jacobian transformation matrix related to the above frames. $M \in R^{2\times 2}$ denotes the inertia including added mass.

$$M = \begin{bmatrix} I_x - K_{\dot{p}} & mx_g - K_{\dot{r}} \\ mx_g - N_{\dot{p}} & I_z - N_{\dot{r}} \end{bmatrix}. \tag{3}$$

$C(u_0, \nu)$ is the Coriolis and centripetal matrix with the following form:

$$C(u_0,\nu) = \begin{bmatrix} 0 & 0 \\ 0 & mx_g u_0 \end{bmatrix}. \tag{4}$$

$D(u_0, \nu)$ is the coupling interactions caused by the nonlinear hydrodynamic damping, which is expressed as

$$D(u_0,\nu) = \begin{bmatrix} -K_p & -K_r - K_{r\phi\phi}\phi^2 \\ -N_p & -N_r - N_{rr\phi} r\phi \end{bmatrix}, \tag{5}$$

where K_p, $K_{r\phi\phi}$, and K_r, and N_p, N_r, and $N_{rr\phi}$ are the hydrodynamic coefficients. On the low-speed mode, however, the high-order terms and coupling interactions among the forces from each DOF are not considered; that is, $D(u_0, \nu)$ is often regarded as a linear term, even canceled in many literatures.

$G(\eta)$ represents the gravity term which is described as $G(\eta) = [W\overline{GM_T}, 0]^T$, where $W = mg$ is the weight and $\overline{GM_T}$ is the transverse metacenter height.

$$B = \begin{bmatrix} K_{\delta_R} & K_{\delta_A} \\ N_{\delta_R} & N_{\delta_A} \end{bmatrix} \tag{6}$$

is the control moment coefficient matrix subjected to the control surface, and $\delta = [\delta_R \ \ \delta_A]^T$ is the control input, where δ_R and δ_A represent the rudder angle and aileron angle of the hydrofoil system.

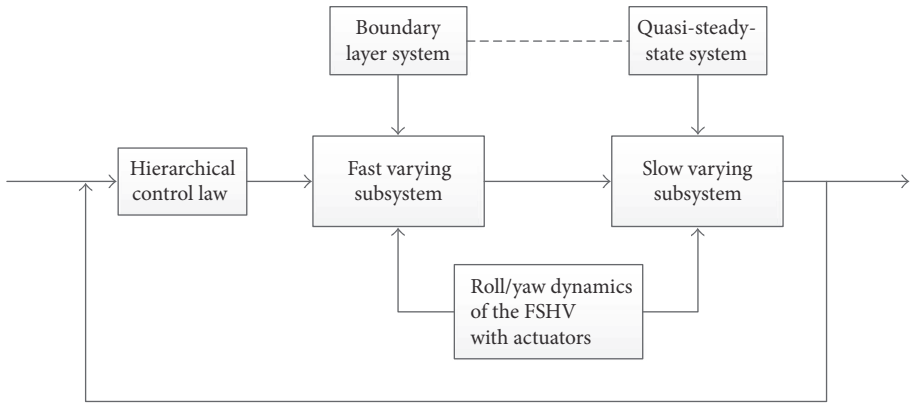

Figure 2: Control structure for the course keeping of FSHV.

By substituting (16) into (17), we rewrite the dynamics of the FSHV as follows:

$$M^*\ddot{\eta} + C^*(u_0, v, \eta)\dot{\eta} + D^*(u_0, v, \eta)\dot{\eta} + G^*(\eta) = J^{-T}(\eta)(B\delta + \tau_d), \tag{7}$$

where $M^* = J^{-T}MJ^{-1}$, $C^* = J^{-T}[C - MJ^{-1}\dot{J}]J^{-1}$, $D^* = J^{-T}DJ^{-1}$, and $G^* = J^{-T}G$.

Define $[x_1, x_2]^T \triangleq [\eta, \dot{\eta}]^T$; then (18) can be rewritten into the following form:

$$\dot{x}_1 = x_2, \quad \dot{x}_2 = \overline{F}(x_1, x_2) + \overline{B}(x_1, x_2)\delta + \overline{\tau}_d, \tag{8}$$

where $\overline{F}(x_1, x_2) = -M^{*-1}[C^*x_2 + D^*x_2 + G^*(x_1)]$, $\overline{B}(x_1, x_2) = M^{*-1}J^{-T}B$, and $\overline{\tau}_d = M^{*-1}J^{-T}\tau_d$.

If the parameter uncertainties are considered in the modeling and control of the FSHV, the following notation is introduced:

$$\overline{F}(x_1, x_2) = \overline{F}_0(x_1, x_2) + \overline{F}_\Delta(x_1, x_2), \tag{9}$$

where subscript 0 denotes the nominal part of the corresponding matrix and the subscript Δ represents the perturbed part of the system dynamics. The yaw/roll dynamics of the FSHV with model uncertainties can be rewritten as follows:

$$\dot{x}_1 = x_2, \quad \dot{x}_2 = \overline{F}_0(x_1, x_2) + \overline{B}(x_1, x_2)\delta + f_1(t), \tag{10}$$

where $f_1(t) = \overline{F}_\Delta(x_1, x_2) + \overline{\tau}_d$.

As to the actuator system, AC motor based electric servo solution and hydraulic servo scheme are often used for the implementation of the hydrofoil servo system [5, 6]. Without loss of generality, a typical second-order system is established for the mathematical model of the hydrofoil transmission system as follows:

$$\ddot{\delta} = -a_2\dot{\delta} + b_2u_c + d_2(t). \tag{11}$$

Define $z_1 \triangleq \delta \in R^2$ and $z_2 \triangleq \dot{\delta} \in R^2$. Considering the model uncertainties of the actuator dynamics, (11) can be rewritten as the following form:

$$\dot{z}_1 = z_2, \quad \dot{z}_2 = -a_2z_2 + b_2u_c + f_2(t), \tag{12}$$

where $a_2 = \mathrm{diag}[a_{21}, a_{22}]$ represents the speed factor of the servo system; $b_2 = \mathrm{diag}[b_{21}, b_{22}]$ is the gain of the power amplifier for the servo system. $u_c = [u_{c1}, u_{c2}]^T$ is the flap command of the hydrofoil transmission system, and $f_2(t) = d_2(t) - \Delta a_2 z_2$ is the composite disturbance caused by model uncertainties and external wave disturbance, and Δa_2 is the perturbation item of a_2.

The control objective is to stabilize the maneuvering dynamics of the FSHV for the task of course keeping based on time scale separation and singular perturbation control theory. The control scheme of the overall system is summarized in Figure 2. For the subsequent control design, the following assumptions are brought in for convenience.

Assumption 1. The nonlinear functions $M(\cdot)$, $C(\cdot)$, $D(\cdot)$, and $G(\cdot)$ are continuously differentiable and locally Lipschitz.

Assumption 2. The generalized disturbances $f_1(t)$, $f_2(t)$ are bounded, and $f_2(t)$ varies slowly.

3. Time Scale Separation and Control Design

3.1. Multi-Time Scale Analysis of the FSHV. In this section, the multi-time scale decomposition of the full model (10) is analyzed. Generally, in marine vehicle control problems, no singular perturbation parameter appears explicitly in the dynamical model of the marine vessels. As for the fully submerged hydrofoil vessels, the mathematical model is more complex than that of the ordinary marine vessels, making it more difficult for the modeling of the singular perturbation system. In such cases, a singular perturbation parameter may be artificially inserted to define a rapid response of a certain dynamics. In other cases, this parameter may be inserted to suppress the variables in the equations that are expected to have relatively slight effects on the original system model.

The slow-fast time scale character is often associated with a small parameter multiplying some of the state variables of the state equations describing a physical system. However, usually that parameter may not be identifiable at all and only by physical insight and experiences does one know the details of fast and slow dynamics for the system.

Experience implies that the yaw and roll dynamics are slow relative to the dynamics of the servo system for flap mechanism among the state variables of the proposed mathematical model of the FSHV, which is the motivation to establish a singular perturbation control scheme as follows:

$$\begin{aligned} \dot{x}_1 &= x_2, \\ \dot{x}_2 &= \overline{F}_0(x_1, x_2) + \overline{B}(x_1, x_2) z_1 + f_1(t), \\ \varepsilon \dot{z}_1 &= \theta z_2, \\ \varepsilon \dot{z}_2 &= -\overline{a}_2 z_2 + \overline{b}_2 u_c + \overline{f}_2(t), \end{aligned} \tag{13}$$

where $\theta = \varepsilon$, $\overline{a}_2 = \varepsilon a_2$, $\overline{b}_2 = \varepsilon b_2$, $\overline{f}_2(t) = \varepsilon f_2(t)$, and $0 < \varepsilon \ll 1$ is the artificial parameter for singularly perturbed system analysis. Hence, the overall system can be divided into a slow varying subsystem $\sum_S(\dot{x} = f(t, x, z, \varepsilon))$ and a fast varying subsystem $\sum_F(\varepsilon \dot{z} = g(t, x, z, \varepsilon))$ as follows:

$$\sum_S \begin{cases} \dot{x}_1 = x_2 \\ \dot{x}_2 = \overline{F}_0(x_1, x_2) + \overline{B}(x_1, x_2) z_1 + f_1(t), \end{cases} \tag{14}$$

$$\sum_F \begin{cases} \varepsilon \dot{z}_1 = \theta z_2 \\ \varepsilon \dot{z}_2 = -\overline{a}_2 z_2 + \overline{b}_2 u_c + \overline{f}_2(t). \end{cases} \tag{15}$$

According to the two-time scale structure of the FSHV system with actuator dynamics, a hierarchical control strategy can be deployed for the maneuvering control of the FSHV. Before the following control design, a brief introduction of the singular perturbation control theory is given for convenience.

Singular perturbations cause a multi-time scale behavior of dynamical systems characterized by the presence of slow and fast transients in the system's response to external stimuli. Loosely speaking, the slow response is appropriated by the reduced model, while the discrepancy between the response of the reduced model and the full model is the fast transient. To see this point, let us consider the following generalized state equations:

$$\begin{aligned} \dot{x} &= f(t, x, z, \varepsilon), \\ x(t_0) &= x_0(\varepsilon), \end{aligned} \tag{16}$$

$$\begin{aligned} \varepsilon \dot{z} &= g(t, x, z, \varepsilon), \\ z(t_0) &= z_0(\varepsilon). \end{aligned} \tag{17}$$

Let $\varepsilon = 0$; we can get

$$0 = g(t, \overline{x}, \overline{z}, 0), \tag{18}$$

where the bar is used to indicate that the variables belong to a system with $\varepsilon = 0$. Then it yields the quasi-steady-state equilibrium of the fast dynamics in (17); namely,

$$\overline{z} = h(t, \overline{x}). \tag{19}$$

Substituting (19) into (16), we can get

$$\dot{\overline{x}} = f(t, \overline{x}, h(\overline{x}), 0), \tag{20}$$

which is called quasi-steady-state subsystem.

Stretching the time to $\tau = t/\varepsilon$, the fast subsystem becomes

$$\frac{dz}{d\tau} = g(x, z(\tau)), \quad \tau = \frac{t}{\varepsilon}, \tag{21}$$

which is called boundary-layer subsystem. It describes the fast dynamics in a stretched time scale, where x can be regarded as a constant parameter.

Since the system is separated into the quasi-steady-state subsystem and the boundary-layer subsystem, the control strategy can be designed individually for each subsystem; namely, the hierarchical control law is integrated by two parts as follows:

$$u_c = u_s + u_f, \tag{22}$$

where u_s is designed for the slow varying subsystem and u_f is for the fast varying subsystem.

3.2. Control Design for the FSHV. In this section, the composite control law is designed individually for the slow subsystem and fast subsystem. Inspired by [28], the fast control law is designed first to stabilize the fast varying system. The feasibility of this proposed procedure will be analyzed afterwards.

Because of the disturbance property of the actuator servo system, a disturbance observer based state feedback controller is designed for the fast subsystem as

$$u_f = \overline{b}_2^{-1}\left(c_1 z_1 + c_2 z_2 - \widehat{\overline{f}}_2\right), \tag{23}$$

where c_1, c_2 are two control gain matrices with appropriate dimensions to be determined; $\widehat{\overline{f}}_2$ is the estimate of $\overline{f}_2$. And the disturbance observer is presented as follows:

$$\begin{aligned} \widehat{\overline{f}}_2 &= \xi + l z_2, \\ \dot{\xi} &= -l\xi - l\left(l z_2 + \overline{a}_2 z_2 + \overline{b}_2 u_f\right), \end{aligned} \tag{24}$$

where $\xi \in R^2$ is the internal state of the observer, and l is the gain matrix of the observer with appropriate dimension to be determined.

Define $\widetilde{f}_2$ as the disturbance estimate error. Differentiate $\widetilde{f}_2$ with respect to time. Based on the assumptions above, it yields that

$$\begin{aligned} \dot{\widetilde{f}}_2 &= \dot{\widehat{\overline{f}}}_2 - \dot{\overline{f}}_2 = \dot{\xi} + l\dot{z}_2 \\ &= -l\left(z_2 + \overline{a}_2 z_2 + \overline{b}_2 u_f\right) + l\overline{a}_2 z_2 + l\overline{b}_2 u_f + l\overline{f}_2 \\ &= -l\widehat{\overline{f}}_2 + l\overline{f}_2 = -l\dot{\widetilde{f}}_2, \end{aligned} \tag{25}$$

which implies that the disturbance estimate error can converge to zero asymptotically if the gain matrix is Hurwitz.

Remark 3. Sometimes the external disturbance is fast varying; namely, the derivative of the disturbance is not zero. In this condition, the error dynamics of disturbance estimation still can be ultimately uniformly bounded [20, 21, 25]. The bound of the estimate error can be arbitrarily small by approximately selecting the gain function.

Despite the fast control law (23) being established first, the fast varying subsystem together with the above control law remains to be a standard singular perturbation system, and in fact the fast controller u_f is inactive for the quasi-steady-state subsystem $z = h(t, x, u_s)$ [27]. Analysis for this point is derived as follows.

Rewriting subsystem $\sum_F$ in a block form by substituting (23) into (15) results in

$$\varepsilon \begin{bmatrix} \dot{z}_1 \\ \dot{z}_2 \end{bmatrix} = \begin{bmatrix} 0 & \theta \\ c_1 & c_2 - \overline{a}_2 \end{bmatrix} \begin{bmatrix} z_1 \\ z_2 \end{bmatrix} + \begin{bmatrix} 0 \\ \overline{b}_2 \end{bmatrix} u_s. \tag{26}$$

Let $\varepsilon = 0$; then we can get $z = h(t, x) = [c_1^{-1} u_s, 0]^T$ as

$$h(t, x) = -\overline{A}^{-1} \overline{B} u_s, \tag{27}$$

where

$$\overline{A} = \begin{bmatrix} 0 & \theta \\ c_1 & c_2 - \overline{a}_2 \end{bmatrix}, \quad \overline{B} = \begin{bmatrix} 0 \\ \overline{b}_2 \end{bmatrix}. \tag{28}$$

Hence, the equation $g(t, x, z, c_1 z_1 + c_2 z_2 - \overline{b}_2^{-1} \widehat{\overline{f}}_2 + u_s) = 0$ has a unique root, which satisfies the requirements for a singularly perturbed system. It is more convenient to work in the (x, y) coordinate where

$$y = z - h(t, x), \tag{29}$$

because this change of variables shifts the equilibrium of the boundary-layer model to the origin. In the new coordinate, the singularly perturbed system is given by

$$\begin{aligned} \dot{x} &= f(x, y + h(t, x)), \\ \varepsilon \dot{y} &= g(x, y + h(t, x)) - \varepsilon \frac{\partial h}{\partial x} f(x, y + h(t, x)). \end{aligned} \tag{30}$$

The reduced system $\dot{x} = f(x, y + h(t, x))$ has equilibrium point at $x = 0$ and the boundary-layer system

$$\frac{dy}{d\tau} = g(x, y + h(t, x)) = \overline{A}(y + h(t, x)) + \overline{B} u_s. \tag{31}$$

By substituting (27) into (31), it yields

$$\frac{dy}{d\tau} = \overline{A} y. \tag{32}$$

Define the following Lyapunov function candidate:

$$W = \frac{1}{2} y^T P y, \tag{33}$$

where P is positively defined symmetric matrices with appropriate dimension to be determined. Then it yields

$$\frac{\partial W}{\partial y} g(x, y + h(t, x)) = \frac{1}{2} y^T \left(A^T P + P A \right) y. \tag{34}$$

If there exists positively defined symmetric matrices Q satisfied with $A^T P + P A = -Q$, then we can get

$$\frac{\partial W}{\partial y} g(x, y + h(t, x)) = -\frac{1}{2} y^T Q y \le -\lambda_{\min}(Q) \|y\|^2, \tag{35}$$

where $\lambda_{\min}(Q)$ is the minimum eigenvalue of Q.

Hence the closed-loop boundary-layer system has an asymptotically stable equilibrium point.

Then consider control design of the slow varying subsystem. Assume $\varepsilon = 0$. Then the reduced system $\dot{x} = f(t, x, h(t, x), 0)$ is given by

$$\begin{aligned} \dot{x}_1 &= x_2, \\ \dot{x}_2 &= \overline{F}_0(x_1, x_2) + \overline{B}(x_1, x_2) c_1^{-1} u_s + f_1(t). \end{aligned} \tag{36}$$

To stabilize the slow varying system, an adaptive RISE feedback control strategy is proposed.

Define a stabilizing error $e_1 \in R^2$ as

$$e_1 \triangleq x_d - x_1, \tag{37}$$

where $x_d = [\phi_d, \psi_d]^T$.

Two auxiliary tracking errors $e_2, r \in R^2$ are defined as

$$e_2 \triangleq \dot{e}_1 + \alpha_1 e_1, \tag{38}$$

$$r \triangleq \dot{e}_2 + \alpha_2 e_2. \tag{39}$$

Substituting (37) and (38) into (39), then it yields

$$r = \ddot{x}_d - \overline{F}_0(x_1, x_2) - \overline{B}(x_1, x_2) c_1^{-1} u_s - f(t) + \alpha_1 \dot{e}_1 + \alpha_2 e_2. \tag{40}$$

Define an auxiliary function $S \in R^2$ as

$$S \triangleq \overline{F}_0(x_d, t) - \overline{F}_0(x_1, x_2) + \alpha_1 \dot{e}_1 + \alpha_2 e_2. \tag{41}$$

Then (40) can be rewritten as

$$r = \ddot{x}_d + S - \overline{F}_0(x_d, t) - f(t) - \overline{B}(x_1, x_2) c_1^{-1} u_s. \tag{42}$$

A RISE based controller can be designed as

$$\begin{aligned} u_s &= c_1 \overline{B}^{-1}(x_1, x_2) \left[(k_1 + 1) e_2 - (k_1 + 1) e_2(0) + u_{\text{int}} \right] \\ \dot{u}_{\text{int}} &= (k_1 + 1) \alpha_2 e_2 + \beta \operatorname{sgn}(e_2), \end{aligned} \tag{43}$$

where $\beta \in R^+$ is a constant control gain and $k_1 \in R^+$ is a time-varying control gain. An adaptive law is applied as follows for the time-varying gain design:

$$\dot{k}_1 = \alpha_3 e_2^T r. \tag{44}$$

By substituting (46) into (42), the time derivative of r can be expressed as

$$\begin{aligned} \dot{r} = {} & \ddot{x}_d + \dot{S} - \dot{\overline{F}}_0 (x_d, t) - \dot{f}(t) - (k_1 + 1) r - \dot{k}_1 e_2 \\ & - \beta \operatorname{sgn}(e_2). \end{aligned} \tag{45}$$

Define auxiliary variables as follows:

$$\widetilde{N} = \dot{S} + e_2. \tag{46}$$

$$N_d = \ddot{x}_d - \dot{\overline{F}}_0 (x_d, t) - \dot{f}(t), \tag{47}$$

Then it yields

$$\dot{r} = \widetilde{N} + N_d - e_2 - (k_1 + 1) r - \dot{k}_1 e_2 - \beta \operatorname{sgn}(e_2). \tag{48}$$

Using (40) and (41) together with the mean value theorem, we can obtain

$$\left\| \widetilde{N} \right\| \leq \rho(\|z\|) \|z\|, \tag{49}$$

where $z \in R^{3\times 2}$ is defined as

$$z \triangleq \left[e_1^T, e_2^T, r^T \right]^T, \tag{50}$$

and $\rho(\cdot)$ is a positively defined, globally invertible, nondecreasing function.

Assuming that the generalized disturbances and the guidance command input are sufficiently smooth, the following inequalities can be obtained:

$$\begin{aligned} \|N_d\| &\leq \zeta_1, \\ \left\| \dot{N}_d \right\| &\leq \zeta_2, \end{aligned} \tag{51}$$

where $\zeta_1, \zeta_2 \in R^+$ are known constants.

Define $Y(z, P) \in R^{3\times 2+1}$ as

$$Y \triangleq \left[z^T, \sqrt{P} \right]^T, \tag{52}$$

where $P(e_2, t) \in R$ is defined as the Filippov solution to the following differential equation:

$$\begin{aligned} \dot{P} &= -r^T (N_d - \beta \operatorname{sgn}(e_2)), \\ P(e_2(t_0), t_0) &= \beta \sum_{i=1}^{n} |e_{2i}(t_0)| - e_2(t_0)^T N_d(t_0), \end{aligned} \tag{53}$$

where the subscript $i = 1, \ldots, n$ denotes the ith element of the vector. Accordingly, P is expressed as

$$P(t) = \beta \sum_{i=1}^{n} |e_{2i}(0)| - e_2(0)^T N_d(0) - \int_0^t L(\sigma) d\sigma, \tag{54}$$

where the auxiliary function $L(t) \in R$ is defined as

$$L(t) \triangleq r^T (N_d - \beta \operatorname{sgn}(e_2)). \tag{55}$$

If the control gain β satisfies

$$\beta > \zeta_1 + \frac{1}{\alpha_2} \zeta_2, \tag{56}$$

the following inequality can be obtained:

$$\int_0^t L(\sigma) d\sigma L(t) \leq \beta \sum_{i=1}^{n} |e_{2i}(0)| - e_2(0)^T N_d(0), \tag{57}$$

which can conclude that $P(t) \geq 0$.

Theorem 4. *Given the slow varying dynamics of a FSHV presented in (36), if the following conditions are satisfied:*

$$\begin{aligned} \alpha_1 &> \frac{1}{2}, \\ \alpha_2 &> \frac{1}{2}, \\ \beta &> \zeta_1 + \frac{1}{\alpha_2} \zeta_2, \end{aligned} \tag{58}$$

the controller designed in (43) and (44) guarantees that all the signals of the error dynamics of the slow varying subsystem are bounded under closed-loop operation and the stabilizing error converges in the sense that

$$\left\| e_1(t) \right\| \longrightarrow 0 \quad \text{as } t \longrightarrow \infty. \tag{59}$$

Proof. Define the following Lyapunov function as

$$V = \frac{1}{2} e_1^T e_1 + \frac{1}{2} e_2^T e_2 + \frac{1}{2} r^T r + P, \tag{60}$$

which satisfies the following inequalities:

$$U_1(Y) \leq V(Y, t) \leq U_2(Y), \tag{61}$$

where $U_1(Y), U_2(Y) \in R$ are positively defined functions defined as

$$\begin{aligned} U_1(y) &\triangleq m_1 \|Y\|^2, \\ U_2(y) &\triangleq m_2 \|Y\|^2. \end{aligned} \tag{62}$$

Differentiate V with respect to time; then it yields

$$\dot{V} = e_1^T \dot{e}_1 + e_2^T \dot{e}_2 + r^T \dot{r} + \dot{P}. \tag{63}$$

According to (37)–(48), $\dot{V}$ can be further expanded as

$$\begin{aligned} \dot{V} = {} & r^T \widetilde{N} - (k_1 + 1) \|r\|^2 - \dot{k}_1 r^T e_2 - \alpha_1 \|e_1\|^2 \\ & - \alpha_2 \|e_2\|^2 + e_1^T e_2. \end{aligned} \tag{64}$$

Substituting the adaptive law in (47) into (64) together with (49), we can obtain

$$\dot{V} \le \rho(\|z\|)\|r\|\|z\| - (k_1+1)\|r\|^2 - \alpha_3\left\|r^T e_2\right\|^2 - \alpha_1\|e_1\|^2 - \alpha_2\|e_2\|^2 + e_1^T e_2. \tag{65}$$

Since $2e_1^T e_2 \le \|e_1\|^2 + \|e_2\|^2$, (65) becomes

$$\begin{aligned}\dot{V} &\le \rho(\|z\|)\|r\|\|z\| - (k_1+1)\|r\|^2 - \alpha_3\|r\|^2\|e_2\|^2 - \left(\alpha_1 - \frac{1}{2}\right)\|e_1\|^2 - \left(\alpha_2 - \frac{1}{2}\right)\|e_2\|^2 \\ &= -\|r\|^2 - \left(\alpha_1 - \frac{1}{2}\right)\|e_1\|^2 - \left(\alpha_2 - \frac{1}{2}\right)\|e_2\|^2 - \alpha_3\|r\|^2\|e_2\|^2 + \frac{4k_1\left(-k_1\|r\|^2 + \rho(\|z\|)\|r\|\|z\|\right)}{4k_1} \\ &= -\|r\|^2 - \left(\alpha_1 - \frac{1}{2}\right)\|e_1\|^2 - \left(\alpha_2 - \frac{1}{2}\right)\|e_2\|^2 - \alpha_3\|r\|^2\|e_2\|^2 + \frac{-4k_1^2\|r\|^2 + 2\cdot 2k_1\|r\|\rho(\|z\|)\|z\|}{4k_1}, \\ \dot{V} &\le -\|r\|^2 - \left(\alpha_1 - \frac{1}{2}\right)\|e_1\|^2 - \left(\alpha_2 - \frac{1}{2}\right)\|e_2\|^2 - \alpha_3\|r\|^2\|e_2\|^2 + \frac{-4k_1^2\|r\|^2 + 4k_1^2\|r\|^2 + \rho^2(\|z\|)\|z\|^2}{4k_1} \\ &\le -\|r\|^2 - \left(\alpha_1 - \frac{1}{2}\right)\|e_1\|^2 - \left(\alpha_2 - \frac{1}{2}\right)\|e_2\|^2 + \frac{\rho^2(\|z\|)\|z\|^2}{4k_1} \le -\lambda\|z\|^2 + \frac{\rho^2(\|z\|)\|z\|^2}{4k_1},\end{aligned} \tag{66, 67}$$

where $\lambda = \min\{\alpha_1 - 1/2, \alpha_2 - 1/2, 1\}$, and the bounding function $\rho(\|z\|)$ is a positive, globally invertible, nondecreasing function. Therefore, α_1 and α_2 must be selected based on the sufficient conditions in Theorem 4.

The expression in (67) can be further upper bounded by a continuous, positive semidefinite function

$$\dot{V} \le -c\|z\|^2 = U(Y), \tag{68}$$

where $c \in R$ is a positive constant.

According to the inequalities in (61) and (67), we can prove that $V(Y, t) \in L_\infty$. Thus $e_1, e_2, r \in L_\infty$. The closed-loop error system can be utilized to guarantee that the remaining signals are bounded and the definition of $U(y)$ and $z(t)$ can conclude that $U(Y)$ is uniformly continuous. According to Theorem 8.4 of [24], $c\|z\|^2 \to 0$ as $t \to \infty$. Then based on the definition of $z(t)$, it can be concluded that $\|e_1(t)\| \to 0$ as $t \to \infty$. Hence the asymptotical stability is achieved for the equilibrium point of the slow varying subsystem. □

Theorem 5. *Consider the multi-time scale mathematical model for course keeping of a FSHV with actuator dynamics in (14), (15). With a hierarchical control strategy designed in (22), (23), (24), and (43), there exists $\varepsilon^* > 0$ so that, for all $\varepsilon < \varepsilon^*$, the overall system can achieve asymptotic stability at the equilibrium point.*

Proof. In order to analyze the closed-loop stability of the overall system, we need to explore the interconnection between the slow varying subsystem and the fast varying subsystem.

Define a composite Lyapunov function candidate as follows:

$$\nu(x, y) = (1-d)V(x) + dW(x, y), \quad 0 < d < 1, \tag{69}$$

where the constant d is to be chosen. Calculating the derivative of ν along the trajectories of the full system (14), (15), we can obtain

$$\begin{aligned}\dot{\nu} &= (1-d)\frac{\partial V}{\partial x}f(x, y + h(x)) + \frac{d}{\varepsilon}\frac{\partial W}{\partial y}g(x, y + h(x)) - d\frac{\partial W}{\partial y}\frac{\partial h}{\partial x}f(x, y + h(x)) + d\frac{\partial W}{\partial x}f(x, y + h(x)) \\ &= (1-d)\frac{\partial V}{\partial x}f(x, y + h(x)) + \frac{d}{\varepsilon}\frac{\partial W}{\partial y}g(x, y + h(x)) + (1-d)\frac{\partial V}{\partial x}[f(x, y + h(x)) - f(x, h(x))] \\ &\quad + d\left[\frac{\partial W}{\partial x} - \frac{\partial W}{\partial y}\frac{\partial h}{\partial x}\right]f(x, y + h(x)).\end{aligned} \tag{70}$$

According to the former analysis,

$$\begin{aligned}&\frac{\partial V}{\partial x}f(x, y + h(x)) \le -c\|z\|^2, \quad \text{namely } \omega_1 = c,\ \psi_1(x) = \|z\|. \\ &\frac{\partial W}{\partial y}g(x, y + h(x)) \le -\lambda_{\min}(Q)\|y\|^2, \quad \text{namely } \omega_2 = -\lambda_{\min}(Q),\ \psi_2(y) = \|y\|.\end{aligned} \tag{71}$$

Then the restrictions of the last two terms are derived as follows:

$$\begin{aligned}
&\frac{\partial V}{\partial x}\left[f\left(x, y+h\left(x\right)\right)-f\left(x, h\left(x\right)\right)\right] \\
&\quad = x_1\dot{x}_1 + x_2\dot{x}_2 - x_1\dot{x}_1 \\
&\qquad + x_2\left(\overline{F}_0\left(x_1, x_2\right) + \overline{B}\left(x_1, x_2\right)c_1^{-1}u_s\right) \\
&\quad = x_2\overline{B}\left(z_1 - c_1^{-1}u_s\right) \le \beta_1\|z\|\|y\| \\
&\left[\frac{\partial W}{\partial x} - \frac{\partial W}{\partial y}\frac{\partial h}{\partial x}\right] f\left(x, y+h\left(x\right)\right) \\
&\quad = -c_1^{-1}\frac{\partial u_s}{\partial x_1}y_1x_2 \\
&\qquad - c_1^{-1}\frac{\partial u_s}{\partial x_2}y_1\left(\overline{F}_0\left(x_1, x_2\right) + \overline{B}\left(x_1, x_2\right)c_1^{-1}u_s\right) \\
&\quad \le -2c_1^{-1}\sqrt{\frac{\partial u_s}{\partial x_1}y_1x_2\frac{\partial u_s}{\partial x_2}y_1\dot{x}_2} \\
&\quad \le \beta_2\|y\|\|z\| + \gamma\|y\|^2.
\end{aligned} \tag{72}$$

(73)

Therefore, according to Theorem 11.3 in [24], it yields

$$\dot{v} \le \psi^T\left(x, y\right)\Lambda\psi\left(x, y\right), \tag{74}$$

where $\psi(x, y) = [\psi_1(x), \psi_2(y)]^T$, and

$$\Lambda = \begin{bmatrix} \left(1-d\right)\omega_1 & -\frac{1}{2}\left(1-d\right)\beta_1 - \frac{1}{2}d\beta_2 \\ -\frac{1}{2}\left(1-d\right)\beta_1 - \frac{1}{2}d\beta_2 & d\left(\left(\frac{\omega_2}{\varepsilon}\right) - \gamma\right) \end{bmatrix}. \tag{75}$$

The right-hand side of the last inequality is a quadratic form in $\psi(x, y)$. The quadratic form is negative definite when

$$d\left(1-d\right)\omega_1\left(\frac{\omega_2}{\varepsilon} - \gamma\right) > \frac{1}{4}\left[\left(1-d\right)\beta_1 + d\beta_2\right]^2 \tag{76}$$

which is equivalent to

$$\varepsilon < \frac{\omega_1\omega_2}{\omega_1\gamma + \left(1/4d\left(1-d\right)\right)\left[\left(1-d\right)\beta_1 + d\beta_2\right]^2} \triangleq \varepsilon_d. \tag{77}$$

It can be seen that the maximum value of ε_d occurs at $d^* = \beta_1/(\beta_1 + \beta_2)$, which is given by

$$\varepsilon^* = \frac{\omega_1\omega_2}{\left(\omega_1\gamma + \beta_1\beta_2\right)}. \tag{78}$$

Then the origin of (14) and (15) is asymptotically stable for all $\varepsilon < \varepsilon^*$. □

4. Simulation

In this section, a mathematical model of a fully submerged hydrofoil vessel is applied to validate the performance of the proposed control laws (22), (23), (24), and (43) through simulations [1, 2, 5]. The parameters of the model are given in Table 1.

Table 1: Model parameters of the FSHV.

Parameter	Value	SI-unit
u_0	23.15	m/s
m	$2.62 * 10^5$	kg
I_x	$2.59 * 10^5$	kgm^2
I_z	$1.47 * 10^7$	kgm^2
$\overline{GM_T}$	0.025	m
K_p	$-13.0354 * 10^5$	kgm^2/s
K_r	$-2.4864 * 10^5$	kgm^2/s
$K_{r\phi\phi}$	$12.5615 * 10^5$	kgm^2/s
N_p	$-0.2182 * 10^7$	kgm^2/s
N_r	$-1.3818 * 10^7$	kgm^2/s
$N_{rr\phi}$	$0.9261 * 10^7$	kgm^2/s
a_{21}	−15.27	kgm^2/s
a_{22}	−38.27	kgm^2/s
b_{21}	22.18	kgm^2/s
b_{22}	32.45	kgm^2/s

In the simulation, the irregular wave disturbance is simulated based on trip theory and equivalent energy division method, with the significant wave height $H_{1/3} = 1.5$ m. To validate the disturbance attenuation performance, a standard state feedback singular perturbation approach [28, 30] is established for comparison.

The command course angle is set to be −30° and 60°, respectively, to verify the proposed control design. The control parameters are selected as follows:

$$\begin{aligned}
c_1 &= \text{diag}\ [6.75, 5.41], \\
c_2 &= \text{diag}\ [7.56, 4.89], \\
d &= 0.9147, \\
l &= \text{diag}\ [1352, 835], \\
\alpha_3 &= 15.45, \\
\alpha_1 &= 40, \\
\alpha_2 &= 28, \\
\beta &= 12.81, \\
\beta_1 &= 1, \\
\beta_2 &= 1, \\
\varepsilon &= 0.0214.
\end{aligned} \tag{79}$$

Figures 3–6 show the roll/yaw angles and angle velocities of the FSHV with command course of −30 degrees and 60 degrees. It can be seen that during the changes of course angle, the coupling roll movement will appear, and the composite control law could stabilize this dynamics quickly and there is no reciprocating roll movement as ordinary vessel does.

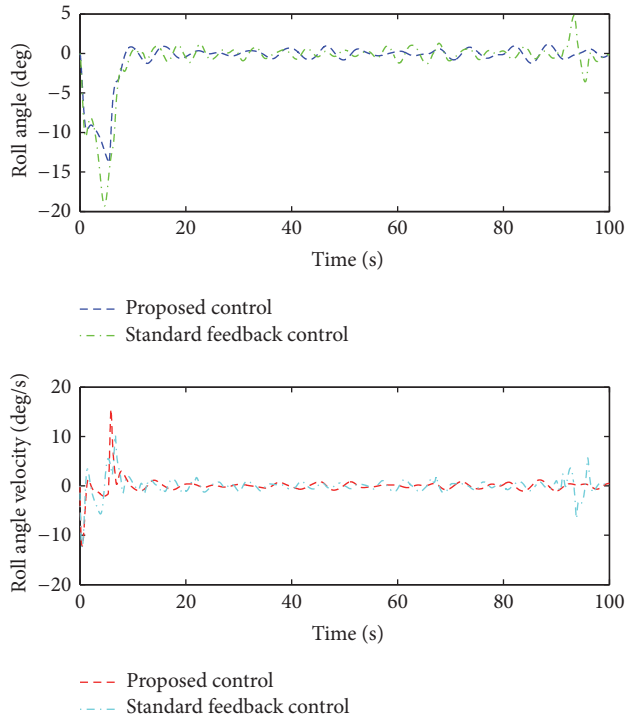

Figure 3: Roll dynamics of the FSHV with command course angle of −30°.

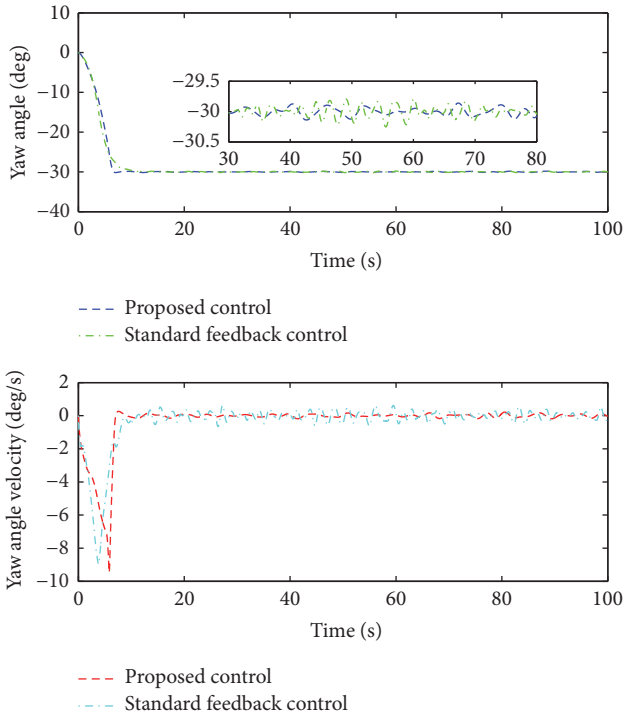

Figure 4: Yaw dynamics of the FSHV with command course angle of −30°.

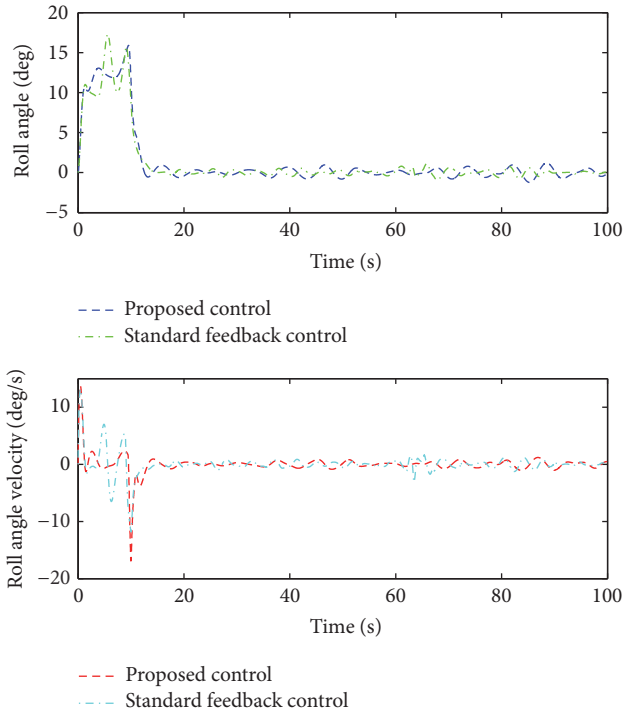

Figure 5: Roll dynamics of the FSHV with command course angle of 60°.

According to Figures 4 and 6, with the stochastic wave disturbances, the proposed methodology acquires a faster convergence than the standard singular perturbation control. During the transient process, the roll motion using standard singular perturbation control is much larger than that of the proposed control, and the severely reciprocating motion is more obvious, which has a negative effect on the sea-keeping capacity of the FSHV.

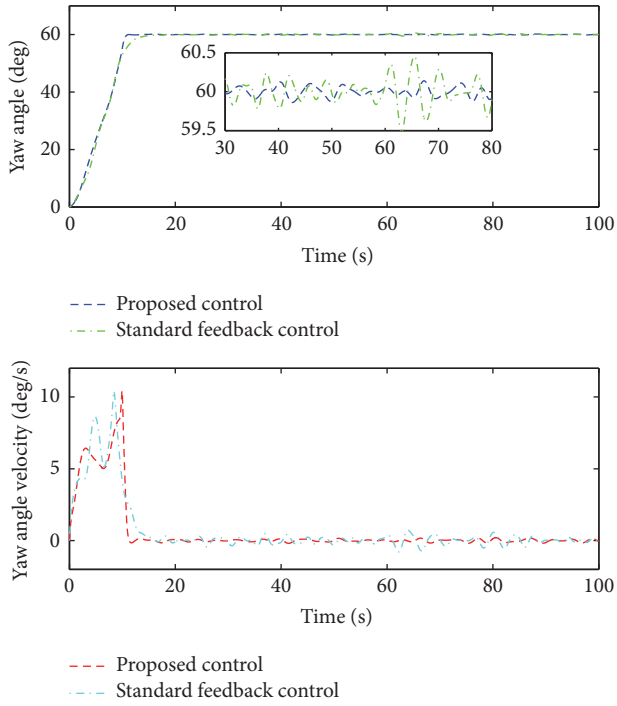

FIGURE 6: Yaw dynamics of the FSHV with command course angle of 60°.

At the steady state of the lateral dynamics, the proposed control acquires higher precision and better disturbance attenuation performance since the model uncertainties and external disturbances are considered in both slow dynamics and fast dynamics of the FSHV. The composite control law guarantees the robustness against the lumped disturbances while the control design of the standard singular perturbation approach does not take the disturbance effects into account.

From Figures 7–10, the slow-time scale and fast-time scale response of each subsystem can be seen to verify the different system characteristic of the servo system and the lateral dynamics of the FSHV. The position of the heading of arrows point out the time of convergence. When course command is generated, the servo system has a fast response to step into the steady state first. Due to the large inertia, the trajectory of the lateral dynamics of the FSHV moves relatively slower than the hydrofoil servo system.

Figures 11 and 12 show the composite control input u_c for the system. We can see that the proposed control input is continuous, and the amplitude is lower than the standard singular perturbation approach. According to the fast dynamics in Figures 7–10 and the composite control input in Figures 11 and 12, it implies that, based on the proposed method, the robust stabilization can be guaranteed with less energy consumption. And the conservation is less than standard singular perturbation approach with no disturbance rejection performance.

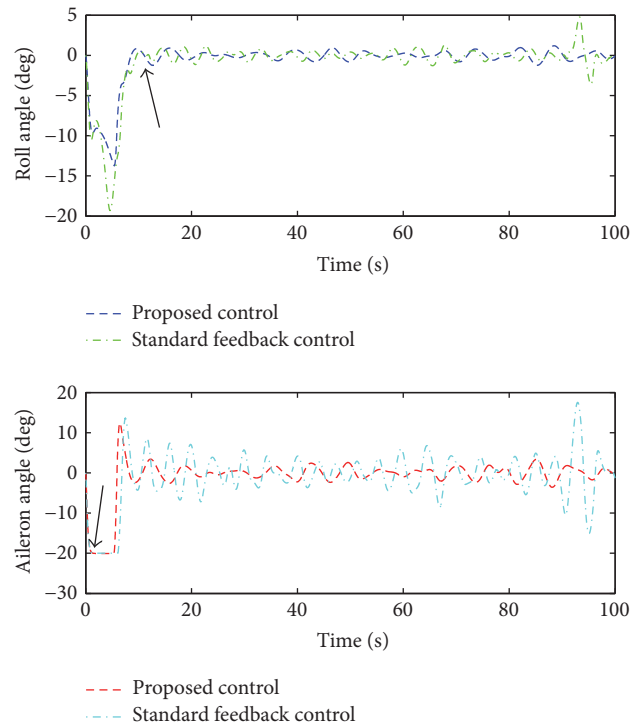

FIGURE 7: Roll response of different time scale with command course angle of −30°.

5. Conclusion

In this paper, a two-time scale robust control structure is proposed for the course keeping control of the FSHV with actuator dynamics. We first analyze the lateral model of the FSHV as well as the hydrofoil servo system. Then a two-time scale separated model is established for the hierarchical control design. A RISE feedback control is designed for the slow

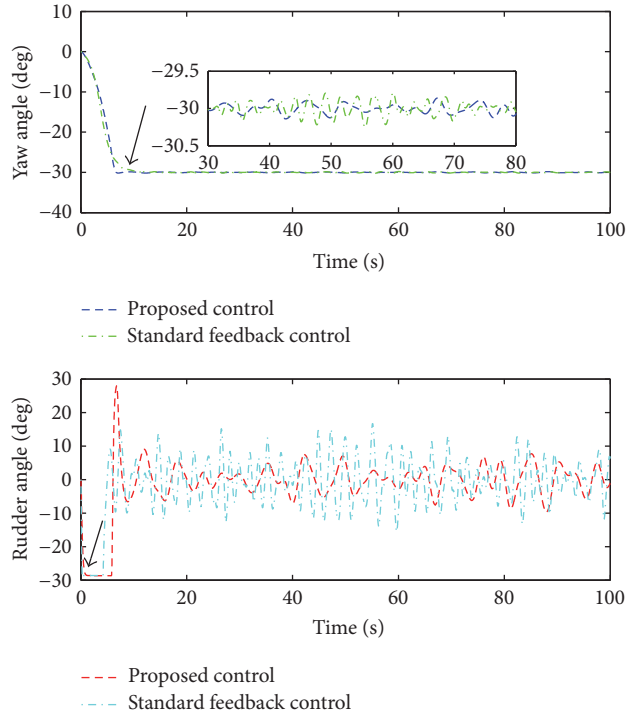

Figure 8: Yaw response of different time scale with command course angle of −30°.

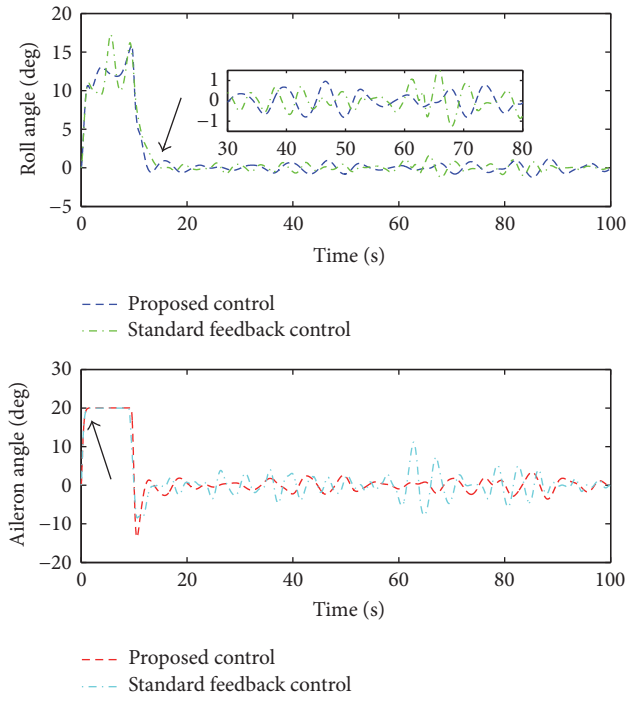

Figure 9: Roll response of different time scale with command course angle of 60°.

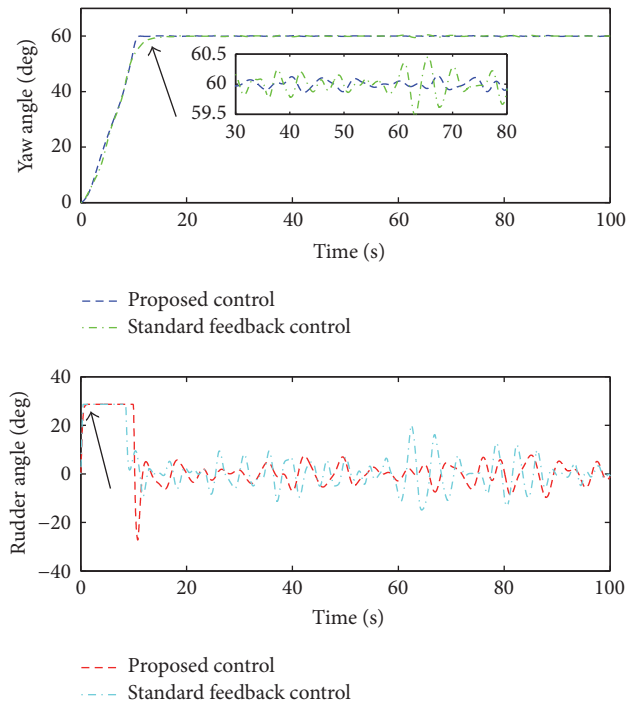

Figure 10: Yaw response of different time scale with command course angle of 60°.

varying subsystem and a DOB based state feedback control is used for the fast varying subsystem to achieve disturbance attenuation performance. Uniformly asymptotic convergence is achieved for the overall system. Simulation results indicate the effectiveness of the time separation method, which shows the advantages for control design of complicated interconnection systems with different time scale. In future work, a hardware-in-loop simulation testbed will be implemented so that further experiments can be assigned to verify the effectiveness of the proposed methodology. New structures of

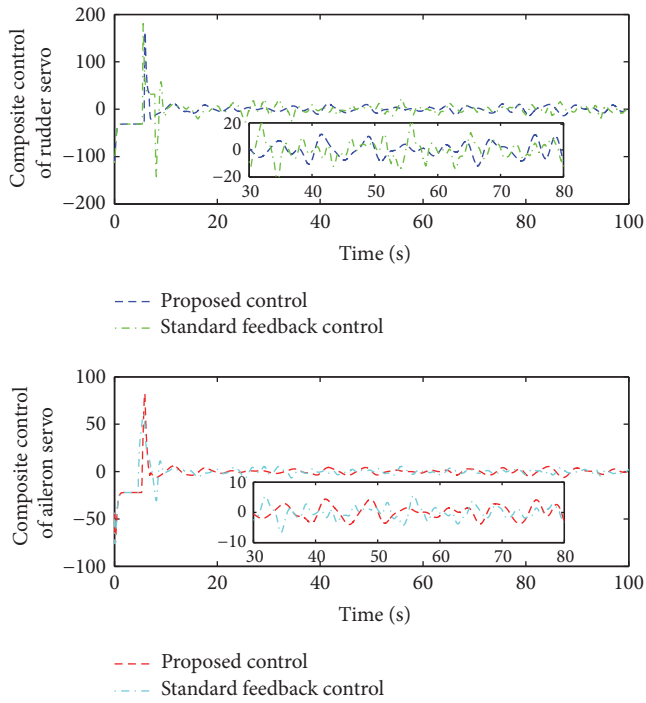

Figure 11: Composite control input of the FSHV with command course angle of −30°.

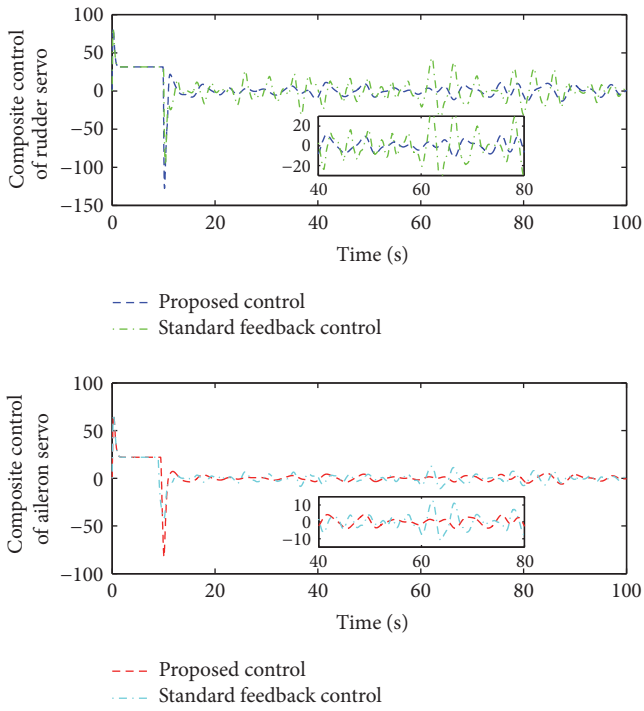

Figure 12: Composite control input of the FSHV with command course angle of 60°.

DOB will be discussed to relax the restrictions of the lumped disturbances. And adaptive estimator is to be considered to handle unknown hydrodynamics combined with the RISE feedback.

Conflicts of Interest

The authors declare that there are no conflicts of interest regarding the publication of this paper.

Acknowledgments

This work is supported by the National Natural Science Foundation of China under Grant 51579047.

References

[1] Y. Saito and T. Ikebuchi, "Fully submerged hydrofoil vessel," 1990, 7th Marine Dynamics Symposium on Prediction of Seakeeping Qualities of High-Speed Vessel, pp. 107-141.

[2] H. Imamura, Y. Saito, and M. Asao, "Automatic control system for jetfoil," *Kawasaki Technical Review*, pp.107: 1-9, 1990.

[3] S.-H. Kim and H. Yamato, "An experimental study of the longitudinal motion control of a fully submerged hydrofoil model in following seas," *Ocean Engineering*, vol. 31, no. 5-6, pp. 523–537, 2004.

[4] S.-H. Kim and H. Yamato, "On the design of a longitudinal motion control system of a fully-submerged hydrofoil craft based on the optimal preview servo system," *Ocean Engineering*, vol. 31, no. 13, pp. 1637–1653, 2004.

[5] S. Liu, C. Xu, and Y. Wang, "Disturbance rejection control for the course keeping of the fully-submerged hydrofoil craft," in *Proceedings of the 35th Chinese Control Conference, CCC 2016*, pp. 747–751, IEEE, Chengdu, China, July 2016.

[6] T. I. Fossen, *Handbook of Marine Craft Hydrodynamics and Motion Control*, John Wiley & Sons, New York, NY, USA, 2011.

[7] A. Rosales and I. Boiko, "Disturbance attenuation for systems with second-order sliding modes via linear compensators," *IET Control Theory & Applications*, vol. 9, no. 4, pp. 526–537, 2015.

[8] J. D. Sánchez-Torres, A. Navarrete-Guzman, G. Rubio-Astorga, and A. G. Loukianov, "High order integral nested sliding mode control," in *Proceedings of the 13th International Workshop on Variable Structure Systems, VSS 2014*, pp. 1–5, IEEE, Nantes, France, July 2014.

[9] Y. Feng, F. Han, and X. Yu, "Chattering free full-order sliding-mode control," *Automatica*, vol. 50, no. 4, pp. 1310–1314, 2014.

[10] S.-W. Ji, V. P. Bui, B. Balachandran, and Y.-B. Kim, "Robust control allocation design for marine vessel," *Ocean Engineering*, vol. 63, pp. 105–111, 2013.

[11] K. D. Do and J. Pan, "State- and output-feedback robust path-following controllers for underactuated ships using Serret-Frenet frame," *Ocean Engineering*, vol. 31, no. 5-6, pp. 587–613, 2004.

[12] N. E. Kahveci and P. A. Ioannou, "Adaptive steering control for uncertain ship dynamics and stability analysis," *Automatica*, vol. 49, no. 3, pp. 685–697, 2013.

[13] P. M. Patre, W. MacKunis, M. Johnson, and W. E. Dixon, "Composite adaptive control for Euler-Lagrange systems with additive disturbances," *Automatica*, vol. 46, no. 1, pp. 140–147, 2010.

[14] B. Xian, D. M. Dawson, M. S. de Queiroz, and J. Chen, "A continuous asymptotic tracking control strategy for uncertain nonlinear systems," *Institute of Electrical and Electronics Engineers. Transactions on Automatic Control*, vol. 49, no. 7, pp. 1206–1211, 2004.

[15] W. Ji, A. Wang, and J. Qiu, "Decentralized Fixed-Order Piecewise Affine Dynamic Output Feedback Controller Design for Discrete-Time Nonlinear Large-Scale Systems," *IEEE Access*, vol. 5, pp. 1977–1989, 2017.

[16] L. J. Zhang, H. M. Jia, and X. Qi, "NNFFC-adaptive output feedback trajectory tracking control for a surface ship at high speed," *Ocean Engineering*, vol. 38, no. 13, pp. 1430–1438, 2011.

[17] J. Wang, S. Li, J. Yang, B. Wu, and Q. Li, "Extended state observer-based sliding mode control for PWM-based DC-DC buck power converter systems with mismatched disturbances," *IET Control Theory and Applications*, vol. 9, no. 4, pp. 579–586, 2015.

[18] C. Wang, X. Li, L. Guo, and Y. W. Li, "A nonlinear-disturbance-observer-based DC-Bus voltage control for a hybrid AC/DC microgrid," *IEEE Transactions on Power Electronics*, vol. 29, no. 11, pp. 6162–6177, 2014.

[19] H. Sun, S. Li, J. Yang, and L. Guo, "Non-linear disturbance observer-based back-stepping control for airbreathing hypersonic vehicles with mismatched disturbances," *IET Control Theory and Applications*, vol. 8, no. 17, pp. 1852–1865, 2014.

[20] A. Mohammadi, M. Tavakoli, H. J. Marquez, and F. Hashemzadeh, "Nonlinear disturbance observer design for robotic manipulators," *Control Engineering Practice*, vol. 21, no. 3, pp. 253–267, 2013.

[21] W.-H. Chen, "Nonlinear disturbance observer-enhanced dynamic inversion control of missiles," *Journal of Guidance, Control, and Dynamics*, vol. 26, no. 1, pp. 161–166, 2003.

[22] L. Guo and S. Cao, "Anti-disturbance control theory for systems with multiple disturbances: a survey," *ISA Transactions*, vol. 53, no. 4, pp. 846–849, 2014.

[23] D. Ginoya, P. D. Shendge, and S. B. Phadke, "Sliding mode control for mismatched uncertain systems using an extended disturbance observer," *IEEE Transactions on Industrial Electronics*, vol. 61, no. 4, pp. 1983–1992, 2014.

[24] X. Lei, Y. Zou, and F. Dong, "A composite control method based on the adaptive RBFNN feedback control and the ESO for two-axis inertially stabilized platforms," *ISA Transactions*, vol. 59, pp. 424–433, 2015.

[25] S. Li, J. Yang, W. H. Chen, and X. Chen, *Disturbance Observer-Based Control: Methods and Applications*, CRC Press, 2014.

[26] T. Li, B. Yu, and B. Hong, "A novel adaptive fuzzy design for path following for underactuated ships with actuator dynamics," in *Proceedings of the 2009 4th IEEE Conference on Industrial Electronics and Applications, ICIEA 2009*, pp. 2796–2800, chn, May 2009.

[27] H. K. Khalil, *Nonlinear Systems Third Edition*, Prentice-Hall, Inc, Upper Saddle River, NJ, 2002.

[28] S. Esteban, F. Gordillo, and J. Aracil, "Three-time scale singular perturbation control and stability analysis for an autonomous helicopter on a platform," *International Journal of Robust and Nonlinear Control*, vol. 23, no. 12, pp. 1360–1392, 2013.

[29] S. Esteban, F. Gavilan, and J. A. Acosta, "Singular perturbation control of the lateral-directional flight dynamics of an UAV," *IFAC-PapersOnLine*, vol. 28, no. 9, pp. 120–125, 2015.

[30] G. Flores and R. Lozano, "Lyapunov-based controller using singular perturbation theory: An application on a mini-UAV," in *Proceedings of the 2013 1st American Control Conference, ACC 2013*, pp. 1596–1601, Washington, DC, USA, June 2013.

[31] R.-Y. Ren, Z.-J. Zou, and X.-G. Wang, "A two-time scale control law based on singular perturbations used in rudder roll stabilization of ships," *Ocean Engineering*, vol. 88, pp. 488–498, 2014.

[32] B. Yi, L. Qiao, and W. Zhang, "Two-time scale path following of underactuated marine surface vessels: Design and stability analysis using singular perturbation methods," *Ocean Engineering*, vol. 124, pp. 287–297, 2016.

Hindawi
Mathematical Problems in Engineering
Volume 2017, Article ID 2608140, 9 pages
https://doi.org/10.1155/2017/2608140

Research Article

Robust H_∞ Fault Detection for Networked Markov Jump Systems with Random Time-Delay

Yanfeng Wang, Zuxin Li, Peiliang Wang, and Zhe Zhou

School of Engineering, Huzhou University, Huzhou, Zhejiang 313000, China

Correspondence should be addressed to Yanfeng Wang; neu2009wyf@163.com

Received 5 April 2017; Revised 21 June 2017; Accepted 5 July 2017; Published 30 August 2017

Academic Editor: Xinggang Yan

This paper investigates the problem of robust H_∞ fault detection for networked Markov jump systems with random time-delay which is introduced by the network. The random time-delay is modeled as a Markov process, and the networked Markov jump systems are modeled as control systems containing two Markov chains. The delay-dependent fault detection filter is constructed. Furthermore, the sufficient and necessary conditions which make the closed-loop system stochastically stable and achieve prescribed H_∞ performance are derived. The method of calculating controller, fault detection filter gain matrices, and the minimal H_∞ attenuation level is also obtained. Finally, one numerical example is used to illustrate the effectiveness of the proposed method.

1. Introduction

Feedback control systems wherein the control loop is closed through a real-time network are called networked control systems (NCSs) [1, 2]. The information is exchanged among control system components (sensor, controller, actuator, etc.). Due to the advantages such as simple installation, reduced wiring, increased system agility, and high reliability, NCSs have been widely used in broad areas, for example, unmanned aerial vehicles, mobile sensor networks, environment monitoring, and automated highway systems [3–5]. However, the introduction of communication networks also brings communication constraints to the control systems, for example, network-induced time-delays and packet dropouts [6–8]. Fault detection (FD) is very important for practical control systems, especially in safe-critical systems [9–11]. The theory of FD for NCSs is different from that of the traditional control systems due to the limitations induced by the network, such as time-delays and data packet dropouts which should be taken into consideration.

In recent years, many results of FD for NCSs have been reported. In [12], the problem of FD for a kind of nonlinear NCS with time-delays and data packet dropouts was investigated, and the sufficient conditions for the existence of FD filter were presented in terms of linear matrix inequalities (LMIs) using Lyapunov function in the continuous domain. In [13], by considering random time-delays, the NCSs were modeled as discrete-time, finite-dimensional Markov jump linear systems (MJLSs). The FD problem was formulated as a robust H_∞ FD filter design problem, and the sufficient condition to solve this problem was given in terms of LMIs. In [14], with the presence of stochastic packet dropouts in the network, the problem of FD filter design for NCSs was investigated. A design method for FD filter which made the residual generation system stable in the mean-square sense was proposed by the MJLSs theory. In [15], the problem of robust FD filter design and optimization was investigated for NCSs with random delays. The NCSs were modeled as Markov jump systems by assuming that the random delays obeyed the Markov characteristics. Based on the model, an observer-based residual generator was constructed and the corresponding FD problem was formulated as a filtering problem. A sufficient condition for the existence of the desired FD filter was derived in terms of LMIs. In [16], by employing the multirate sampling method and the augmented state matrix method, the NCSs with long random delays were modeled as MJLSs. Then based on the model, a filter was designed for detecting faults. In [17], two independent Markov chains were introduced to describe the transmission characterization of the data packet dropouts in

both channels from sensors to controller and from controller to actuator, and a nonlinear Markov jump system model was established. By employing a mode-dependent FD filter as residual generator, the FD filter design problem of nonlinear NCSs was formulated as a nonlinear H_∞ filtering problem. In [18], by use of the augmented matrix approach, the FD error dynamic systems were transformed to the MJLSs. With the established model and using the bounded real lemma (BRL) for MJLSs, a H_∞ observer-based FD filter was established in terms of LMIs to guarantee that the error between the residual and the weighted faults was made as small as possible. In [19], the problem of FD was investigated for NCSs with signal quantization and random packet dropouts. A residual generator was constructed, and the corresponding FD problem was converted into a H_∞ filtering problem. In [20], the time-delays from sensor to controller and the time-delays from sensor to actuator are both considered which were described by two independent Markov chains. H_∞ FD problem for NCSs with time-delays on condition that the transition probabilities were partly unknown was investigated.

Markov jump systems are appropriate to model the systems whose structures are subject to the random changes which are widely used in the field of communications systems, power systems, and so on; thus, they have attracted much attention [21–24]. It is significant and necessary to investigate the FD problems for NCSs with the Markov jump controlled plants. However, the controlled plants in most of the existing literature were assumed to be the time-invariant systems (see [12–20]). To the best of the authors' knowledge, up to now, very limited efforts have been devoted to investigating the FD problem for NCSs with the Markov jump controlled plant, which motivates our investigation.

Compared to the previous relevant works, the main contribution of this paper is that, for the Markov jump NCSs, the sufficient and necessary conditions for the stochastically stability of the closed-loop system are derived, and the method of calculating the minimal H_∞ attenuation $\gamma_{\min}$ is obtained by constructing proper Lyapunov function candidate.

The rest of this paper is organized as follows. The FD filter is constructed and the closed-loop system model is obtained in Section 2. The sufficient and necessary conditions which make the closed-loop system stochastically stable and achieve prescribed H_∞ performance are derived in Section 3. Section 4 presents the simulation results to show the effectiveness of the proposed method. The conclusions are provided in Section 5.

2. Problem Formulation

Without loss of generality, we assume that the time-delay τ_k only exists between sensor and controller, and τ_k is modeled as a homogeneous Markov chin which takes value in the set $M \triangleq \{0, \ldots, \tau\}$, and the transition probability matrix is $\Lambda = [\lambda_{ij}]$. That is, τ_k jumps from mode i to j with probability λ_{ij}, which is defined by $\lambda_{ij} = \Pr(\tau_{k+1} = j \mid \tau_k = i)$, where $\lambda_{ij} \geq 0$ and $\sum_{j=0}^{\tau} \lambda_{ij} = 1$, for all $i, j \in M$.

In this paper, the following Markov jump controlled plant is considered:

$$\begin{aligned} x_{k+1} &= A_{\theta_k} x_k + B_{u\theta_k} u_k + B_{d\theta_k} d_k + B_{f\theta_k} f_k, \\ y_k &= C_{\theta_k} x_k, \end{aligned} \tag{1}$$

where $x_k \in R^n$ is the state vector, $u_k \in R^m$ is the input vector, $y_k \in R^r$ is the measured output vector, $d_k \in R^d$ is the external disturbance noise belonging to $l_2 \in [0, \infty)$, and $f_k \in R^f$ is the fault to be detected. A_{θ_k}, $B_{u\theta_k}$, $B_{d\theta_k}$, $B_{f\theta_k}$, and C_{θ_k} are all known real constant matrices with appropriate dimensions. $\{\theta_k, k \geq 0\}$ is a discrete-time homogeneous Markov chain, which takes values in a finite set $G \triangleq \{1, \ldots, N\}$ with a transition probability matrix $\Pi = [\pi_{pq}]$; namely, for $\theta_k = p$, $\theta_{k+1} = q$, one has $\pi_{ij} = \Pr(\theta_{k+1} = q \mid \theta_k = p)$, where $\pi_{pq} \geq 0$ and $\sum_{q=1}^{N} \pi_{pq} = 1$, for all $p, q \in G$.

It is noticed that the information of θ_k is not available for the controller at the time instant k duo to the time-delay τ_k; however, the information of τ_k is known to the controller. Consequently, the controller gain can be designed depending on τ_k; that is,

$$u_k = K_{\tau_k} x_{k-\tau_k}. \tag{2}$$

Construct a full-order FD filter at the side of controller as follows:

$$\begin{aligned} \widehat{x}_{k+1} &= A_{\theta_k} \widehat{x}_k + B_{u\theta_k} K_{\tau_k} x_{k-\tau_k} + L_{\tau_k} \left(y_{k-\tau_k} - \widehat{y}_{k-\tau_k} \right), \\ \widehat{y}_k &= C_{\theta_k} \widehat{x}_k, \\ r_k &= V \left(y_{k-\tau_k} - \widehat{y}_{k-\tau_k} \right), \end{aligned} \tag{3}$$

where $\widehat{x}_k \in R^n$ is the filter state vector, $r_k \in R^g$ is the residual vector which is sensitive to the fault, L_{τ_k} is the filter gain matrix to be determined, and V is the gain matrix of the residual r_k.

Define the state estimation error and residual error as follows:

$$\begin{aligned} e_k &= x_k - \widehat{x}_k, \\ r_{ek} &= r_k - f_k. \end{aligned} \tag{4}$$

The closed-loop systems can be obtained as

$$\begin{aligned} \xi_{k+1} &= \widetilde{A}_{\theta_k} \xi_k + \left(\widetilde{B}_{u\theta_k} K_{\tau_k} I_1 - I_2 L_{\tau_k} \widetilde{C}_{\theta_k} \right) \xi_{k-\tau_k} + B_{\omega\theta_k} \omega_k, \\ r_{ek} &= V \widetilde{C}_{\theta_k} \xi_{k-\tau_k} - I_3 \omega_k, \\ \xi_k &= \eta_k, \quad k \in \{-\tau, \ldots, 0\}, \end{aligned} \tag{5}$$

where

$$\widetilde{A}_{\theta_k} = \begin{bmatrix} A_{\theta_k} & 0 \\ 0 & A_{\theta_k} \end{bmatrix},$$

$$\widetilde{B}_{u\theta_k} = \begin{bmatrix} B_{u\theta_k} \\ 0 \end{bmatrix},$$

$$\widetilde{C}_{\theta_k} = \begin{bmatrix} 0 & C_{\theta_k} \end{bmatrix},$$

$$\widetilde{B}_{\omega\theta_k} = \begin{bmatrix} B_{d\theta_k} & B_{f\theta_k} \\ B_{d\theta_k} & B_{f\theta_k} \end{bmatrix},$$
$$I_1 = \begin{bmatrix} I & 0 \end{bmatrix},$$
$$I_2 = \begin{bmatrix} 0 \\ I \end{bmatrix},$$
$$I_3 = \begin{bmatrix} 0 & I \end{bmatrix},$$
$$\xi_k^T = \begin{bmatrix} x_k^T & e_k^T \end{bmatrix},$$
$$\omega_k^T = \begin{bmatrix} d_k^T & f_k^T \end{bmatrix}. \tag{6}$$

Definition 1 (see [25]). System (5) is stochastically stable if for $\omega_k = 0$ and every initial mode $\tau_0 \in M$, $\theta_0 \in G$, there exists a finite matrix $W > 0$ such that

$$E\left\{\sum_{k=0}^{\infty} \|\xi_k\|^2 \mid \xi_0, \tau_0, \theta_0\right\} < \xi_0^T W \xi_0. \tag{7}$$

In this paper, our objective is to design controller (2) and the FD filter (3), such that one has the following:

(a) The closed-loop system (5) is stochastically stable for $\omega_k = 0$.

(b) Under the zero-initial conditions, the residual error r_{ek} satisfies the following H_∞ noise attenuation performance:

$$E\left\{\sum_{k=0}^{\infty} r_{ek}^T r_{ek}\right\} < \gamma^2 E\left\{\sum_{k=0}^{\infty} \omega_k^T \omega_k\right\}, \tag{8}$$

where $\gamma > 0$ is the attenuation level.

For the purpose of FD, an evaluation function and a threshold should be provided, and in this paper the evaluation function J_k and a threshold J_{th} are selected as

$$J_k = E\left\{\sum_{\rho=l_0}^{l_0+k} \sqrt{r_\rho^T r_\rho}\right\},$$
$$J_{\text{th}} = \sup_{\omega_k \in L_2, f_k = 0} E\left\{\sum_{\rho=l_0}^{l_0+L_0} \sqrt{r_\rho^T r_\rho}\right\}, \tag{9}$$

where l_0 is the initial evaluation time instant and L_0 is the evaluation step length. The occurrence of fault can be detected by comparing J_k and J_{th} with the following rule:

$$J_k \le J_{\text{th}} \Longrightarrow \text{normal},$$
$$J_k > J_{\text{th}} \Longrightarrow \text{fault}. \tag{10}$$

Remark 2. It should be pointed out that if time-delay also exists between controller and actuator which is written as ν_k, the control input of the controlled plant (1) should be $K_{\tau_k} x_{k-\tau_k-\nu_k}$ which is different from the control input of the FD filter which is $K_{\tau_k} x_{k-\tau_k}$.

Remark 3. If there is no time-delay in system (5), the FD filter (3) can still detect the fault effectively.

Remark 4. In almost all the existing literatures related to the FD for NCSs, the standard infinite impulse response (IIR) filter (3) is commonly used. However, the researches about FD for NCSs using finite impulse response (FIR) filter including deadbeat dissipative FIR filtering, hybrid particle FIR filtering, and composite particle FIR filtering have not been reported, which is a completely new research area.

3. Main Results

In this section, the sufficient and necessary conditions which make system (5) stochastically stable will be derived. Further, we will present the calculation method of the controller gain matrix K_{τ_k}, the FD filter gain matrix L_{τ_k}, and the minimal H_∞ attenuation $\gamma_{\min}$ in terms of matrix inequalities. To proceed, we will need the following lemma.

Lemma 5 (see [26]). *For any positive-definite matrix R, scalars δ, δ_0 satisfying $\delta \ge \delta_0 \ge 1$, and vector function υ_l, one always has $(\sum_{l=\delta_0}^{\delta} \upsilon_l)^T R \sum_{l=\delta_0}^{\delta} \upsilon_l \le (\delta - \delta_0 + 1) \sum_{l=\delta_0}^{\delta} \upsilon_l^T R \upsilon_l$.*

Theorem 6. *When $\omega_k = 0$, the closed-loop system (5) is stochastically stable if and only if there exist positive-definite matrices $P_{i,p} > 0$, $P_{j,q} > 0$, $Q_1 > 0$, $Q_2 > 0$, $Z_1 > 0$ and matrices K_i, L_i such that the inequality*

$$\Omega \triangleq \begin{bmatrix} \Omega_{11} & * & * \\ \Omega_{21} & \Omega_{22} & * \\ 0 & Z_1 & -Q_1 - Z_1 \end{bmatrix} < 0, \tag{11}$$

where

$$\begin{aligned}
\Omega_{11} &= \widetilde{A}_p^T \overline{P}_{j,q} \widetilde{A}_p + \tau^2 \widetilde{A}_p^T Z_1 \widetilde{A}_p + Q_1 + (\tau + 1) Q_2 - Z_1 \\
&\quad - P_{i,p}, \\
\Omega_{21} &= \left(\widetilde{B}_{up} K_i I_1 - I_2 L_i \widetilde{C}_p\right)^T \overline{P}_{j,q} \widetilde{A}_p \\
&\quad + \tau^2 \left(\widetilde{B}_{up} K_i I_1 - I_2 L_i \widetilde{C}_p\right)^T Z_1 \widetilde{A}_p + Z_1, \\
\Omega_{22} &= \left(\widetilde{B}_{up} K_i I_1 - I_2 L_i \widetilde{C}_p\right)^T \overline{P}_{j,q} \left(\widetilde{B}_{up} K_i I_1 - I_2 L_i \widetilde{C}_p\right) \\
&\quad + \tau^2 \left(\widetilde{B}_{up} K_i I_1 - I_2 L_i \widetilde{C}_p\right)^T Z_1 \left(\widetilde{B}_{up} K_i I_1 - I_2 L_i \widetilde{C}_p\right) \\
&\quad - Q_2 - 2 Z_1, \\
\overline{P}_{j,q} &= \sum_{j=0}^{\tau} \sum_{q=1}^{N} \lambda_{ij} \pi_{pq} P_{j,q},
\end{aligned} \tag{12}$$

holds for all $i, j \in M$ and $p, q \in G$.

Proof.

Sufficiency. Choose the Lyapunov function candidate as

$$V(\xi_k, \tau_k, \theta_k) \triangleq \xi_k^T \Psi_{\tau_k,\theta_k} \xi_k = \sum_{\mu=1}^{4} V_\mu(\xi_k, \tau_k, \theta_k), \quad (13)$$

where

$$\begin{aligned} V_1(\xi_k, \tau_k, \theta_k) &= \xi_k^T P_{\tau_k,\theta_k} \xi_k, \\ V_2(\xi_k, \tau_k, \theta_k) &= \sum_{m=k-\tau}^{k-1} \xi_m^T Q_1 \xi_m, \\ V_3(\xi_k, \tau_k, \theta_k) &= \sum_{m=k-\tau_k}^{k-1} \xi_m^T Q_2 \xi_m + \sum_{n=-\tau+1}^{0} \sum_{m=k+n}^{k-1} \xi_m^T Q_2 \xi_m, \\ V_4(\xi_k, \tau_k, \theta_k) &= \sum_{n=-\tau+1}^{0} \sum_{m=k+n}^{k-1} \tau \varphi_m^T Z_1 \varphi_m, \\ \varphi_m &= \xi_{m+1} - \xi_m. \end{aligned} \quad (14)$$

Apparently, we have $\Psi_{\tau_k,\theta_k} > 0$.

Along the solution of system (5), we have

$$\begin{aligned} E\{\Delta V_1\} &= E\left\{\xi_{k+1}^T P_{\tau_{k+1},\theta_{k+1}} \xi_{k+1} \mid \tau_k = i,\ \theta_k = p\right\} \\ &\quad - \xi_k^T P_{\tau_k,\theta_k} \xi_k \\ &= \left(\widetilde{A}_p \xi_k + \left(\widetilde{B}_{up} K_i I_1 - I_2 L_i \widetilde{C}_p\right) \xi_{k-\tau_k}\right)^T \\ &\quad \cdot \sum_{j=0}^{\tau} \sum_{q=1}^{N} \lambda_{ij} \pi_{pq} P_{j,q} \\ &\quad \cdot \left(\widetilde{A}_p \xi_k + \left(\widetilde{B}_{up} K_i I_1 - I_2 L_i \widetilde{C}_p\right) \xi_{k-\tau_k}\right) - \xi_k^T P_{i,p} \xi_k, \\ E\{\Delta V_2\} &= \xi_k^T Q_1 \xi_k - \xi_{k-\tau}^T Q_1 \xi_{k-\tau}, \\ E\{\Delta V_3\} &= \xi_k^T Q_2 \xi_k - \xi_{k-i}^T Q_2 \xi_{k-i} + \sum_{l=k+1-\tau_{k+1}}^{k-1} \xi_l^T Q_2 \xi_l \\ &\quad - \sum_{l=k+1-\tau_k}^{k-1} \xi_l^T Q_2 \xi_l + \tau \xi_k^T Q_2 \xi_k - \sum_{l=k+1-\tau}^{k} \xi_l^T Q_2 \xi_l. \end{aligned} \quad (15)$$

Note that

$$\begin{aligned} \sum_{l=k+1-\tau_{k+1}}^{k-1} \xi_l^T Q_2 \xi_l &= \sum_{l=k+1-\tau_k}^{k-1} \xi_l^T Q_2 \xi_l + \sum_{l=k+1-\tau_{k+1}}^{k-\tau_k} \xi_l^T Q_2 \xi_l \\ &\le \sum_{l=k+1-\tau_k}^{k-1} \xi_l^T Q_2 \xi_l + \sum_{l=k+1-\tau}^{k} \xi_l^T Q_2 \xi_l. \end{aligned} \quad (16)$$

Hence, we can obtain

$$\begin{aligned} E\{\Delta V_3\} &\le \xi_k^T Q_2 \xi_k - \xi_{k-i}^T Q_2 \xi_{k-i} + \tau \xi_k^T Q_2 \xi_k, \\ E\{\Delta V_4\} &= \tau^2 \varphi_k^T Z_1 \varphi_k - \sum_{l=k-\tau}^{k-1} \tau \varphi_l^T Z_1 \varphi_l \\ &= \tau^2 \varphi_k^T Z_1 \varphi_k - \sum_{l=k-i}^{k-1} \tau \varphi_l^T Z_1 \varphi_l - \sum_{l=k-\tau}^{k-i-1} \tau \varphi_l^T Z_1 \varphi_l \\ &\le \tau^2 \varphi_k^T Z_1 \varphi_k - \sum_{l=k-i}^{k-1} i \varphi_l^T Z_1 \varphi_l \\ &\quad - \sum_{l=k-\tau}^{k-i-1} (\tau - i) \varphi_l^T Z_1 \varphi_l. \end{aligned} \quad (17)$$

By Lemma 5, one can obtain

$$\begin{aligned} &- \sum_{l=k-i}^{k-1} i \varphi_l^T Z_1 \varphi_l - \sum_{l=k-\tau}^{k-i-1} (\tau - i) \varphi_l^T Z_1 \varphi_l \\ &\le - \left[\xi_k - \xi_{k-i}\right]^T Z_1 \left[\xi_k - \xi_{k-i}\right] \\ &\quad - \left[\xi_{k-i} - \xi_{k-\tau}\right]^T Z_1 \left[\xi_{k-i} - \xi_{k-\tau}\right]. \end{aligned} \quad (18)$$

From (15)–(18), we have

$$\begin{aligned} E\{\Delta V(\xi_k, \tau_k, \theta_k) \mid \tau_k = i,\ \theta_k = p\} &\le \zeta_k^T \Omega \zeta_k \\ &\le -\lambda_{\min}(-\Omega) \zeta_k^T \zeta_k \\ &= -\lambda_{\min}(-\Omega) \left(\xi_k^T \xi_k + \xi_{k-i}^T \xi_{k-i} + \xi_{k-\tau}^T \xi_{k-\tau}\right) \\ &\le -\alpha \left\|\xi_k\right\|^2, \end{aligned} \quad (19)$$

where

$$\begin{aligned} \zeta_k^T &= \left[\xi_k^T \ \ \xi_{k-i}^T \ \ \xi_{k-\tau}^T\right], \\ \alpha &= \inf\{-\lambda_{\min}(-\Omega)\} > 0. \end{aligned} \quad (20)$$

From (19), we can see that for any $T \ge 1$

$$\begin{aligned} E\left\{\sum_{k=0}^{\infty} \left\|\xi_k\right\|^2\right\} &\le \frac{1}{\alpha} E\{V(\xi_0, \tau_0, \theta_0)\} \\ &\quad - \frac{1}{\alpha} E\{V(\xi_{T+1}, \tau_{T+1}, \theta_{T+1})\} \\ &\le \frac{1}{\alpha} E\{V(\xi_0, \tau_0, \theta_0)\} = \xi_0^T \Psi_{\tau_0,\theta_0} \xi_0. \end{aligned} \quad (21)$$

That is, the closed-loop system (5) is stochastically stable according to Definition 1.

Necessity. Assume that the closed-loop system (5) is stochastically stable. Thus, we have

$$E\left\{\sum_{k=0}^{\infty} \left\|\xi_k\right\|^2 \mid \xi_0, \tau_0\right\} < \xi_0^T W \xi_0. \quad (22)$$

Let

$$\xi_k^T \widehat{\Psi}_{\tau_k,\theta_k} \xi_k = E\left\{\sum_{t=k}^{T} \xi_t^T H_{\tau_t,\theta_t} \xi_t\right\}, \tag{23}$$

where $H_{\tau_t,\theta_t} > 0$.

Assume $\xi_k \neq 0$, from (23), it can be easily inferred that $\widehat{\Psi}_{\tau_k,\theta_k}$ is bounded, and the following limit exists:

$$\begin{aligned} \xi_k^T \Psi_{\tau_k,\theta_k} \xi_k &\triangleq \lim_{T\to\infty} \xi_k^T \widehat{\Psi}_{\tau_k,\theta_k} \xi_k \\ &= \lim_{T\to\infty} E\left\{\sum_{t=k}^{T} \xi_t^T H_{\tau_t,\theta_t} \xi_t\right\}. \end{aligned} \tag{24}$$

Since (24) holds for any ξ_k, we have $\Psi_{\tau_k,\theta_k} = \lim_{T\to\infty} \widehat{\Psi}_{\tau_k,\theta_k}$. Since $H_{\tau_t,\theta_t} > 0$, it can be seen that $\Psi_{\tau_k,\theta_k} > 0$ from (24).

Let us consider

$$\begin{aligned} &E\left\{\xi_k^T \widehat{\Psi}_{\tau_k,\theta_k} \xi_k - \xi_{k+1}^T \widehat{\Psi}_{\tau_{k+1},\theta_{k+1}} \xi_{k+1} \mid \tau_k = i,\ \theta_k = p\right\} \\ &\quad = \xi_k^T H_{\tau_k,\theta_k} \xi_k > 0. \end{aligned} \tag{25}$$

Letting $T \to \infty$, we have

$$\begin{aligned} &E\left\{\xi_k^T \Psi_{\tau_k,\theta_k} \xi_k - \xi_{k+1}^T \Psi_{\tau_{k+1},\theta_{k+1}} \xi_{k+1} \mid \tau_k = i,\ \theta_k = p\right\} \\ &\quad = -E\left\{\Delta V\left(\xi_k, \tau_k, \theta_k\right) \mid \tau_k = i,\ \theta_k = p\right\} \geq -\zeta_k^T \Omega \zeta_k \\ &\quad > 0, \end{aligned} \tag{26}$$

which completes the proof. □

Corollary 7. *When $\omega_k \neq 0$, consider the closed-loop system (5) and let $\gamma > 0$ be a given real scalar. If there exist $P_{i,p} > 0$, $P_{j,q} > 0$, $F_{j,q} > 0$, $Q_1 > 0$, $Q_2 > 0$, $Y_1 > 0$, $Z_1 > 0$ and matrices K_i, L_i such that*

$$\begin{bmatrix} \Xi_{11} & * & * \\ \Xi_{21} & \Xi_{22} & * \\ \Xi_{31} & 0 & \Xi_{33} \end{bmatrix} < 0, \tag{27}$$

$$\begin{aligned} P_{j,q}^{-1} F_{j,q} &= I, \\ Z_1^{-1} Y_1 &= I, \end{aligned} \tag{28}$$

where

$$\Xi_{11} = \begin{bmatrix} Q_1 + (\tau+1)Q_2 - Z_1 - P_{i,p} & * & * \\ Z_1 & -Q_2 - 2Z_1 & * \\ 0 & 0 & -\gamma^2 I \end{bmatrix},$$

$$\Xi_{21} = \begin{bmatrix} 0 & Z_1 & 0 \\ \widetilde{A}_p - I & \widetilde{B}_{up} K_i I_1 - I_2 L_i \widetilde{C}_p & \widetilde{B}_{\omega p} \end{bmatrix},$$

$$\Xi_{22} = \begin{bmatrix} Q_1 - Z_1 & * \\ 0 & -Y_1 \end{bmatrix},$$

$$\Xi_{31} = \begin{bmatrix} \sqrt{\lambda_{i0}\pi_{p1}}\widetilde{A}_p & \sqrt{\lambda_{i0}\pi_{p1}}\left(\widetilde{B}_{up} K_i I_1 - I_2 L_i \widetilde{C}_p\right) & \sqrt{\lambda_{i0}\pi_{p1}}\widetilde{B}_{\omega p} \\ \vdots & \vdots & \vdots \\ \sqrt{\lambda_{i\tau}\pi_{pN}}\widetilde{A}_p & \sqrt{\lambda_{i\tau}\pi_{pN}}\left(\widetilde{B}_{up} K_i I_1 - I_2 L_i \widetilde{C}_p\right) & \sqrt{\lambda_{i\tau}\pi_{pN}}\widetilde{B}_{\omega p} \end{bmatrix},$$

$$\Xi_{33} = \operatorname{diag}\left\{-F_{0,1}, \ldots, -F_{\tau,N}\right\}, \tag{29}$$

holds for all $i, j \in M$, $p, q \in G$, system (5) is stochastically stable with H_∞ performance index γ.

Proof. From (19), we can obtain

$$\begin{aligned} &E\left\{\Delta V\left(\xi_k, \tau_k, \theta_k\right) \mid \tau_k = i,\ \theta_k = p\right\} + E\left\{r_{ek}^T r_{ek}\right\} \\ &\quad - \gamma^2 E\left\{\omega_k^T \omega_k\right\} \leq \varsigma_k^T \overline{\Omega} \varsigma_k, \end{aligned} \tag{30}$$

where

$$\overline{\Omega} = \begin{bmatrix} \Omega_{11} & * & * & * \\ \Omega_{21} & \overline{\Omega}_{22} & * & * \\ \Omega_{31} & \Omega_{32} & \Omega_{33} & * \\ 0 & Z_1 & 0 & -Q_1 - Z_1 \end{bmatrix},$$

$$\begin{aligned} \overline{\Omega}_{22} &= \left(\widetilde{B}_{up} K_i I_1 - I_2 L_i \widetilde{C}_p\right)^T \overline{P}_{j,q} \left(\widetilde{B}_{up} K_i I_1 - I_2 L_i \widetilde{C}_p\right) \\ &\quad + \tau^2 \left(\widetilde{B}_{up} K_i I_1 - I_2 L_i \widetilde{C}_p\right)^T Z_1 \left(\widetilde{B}_{up} K_i I_1 - I_2 L_i \widetilde{C}_p\right) \\ &\quad - Q_2 - 2Z_1 + \left(V\widetilde{C}_p\right)^T V \widetilde{C}_p, \end{aligned} \tag{31}$$

$$\Omega_{31} = \widetilde{B}_p^T \overline{P}_{j,q} \widetilde{A}_p,$$

$$\Omega_{32} = \widetilde{B}_p^T \overline{P}_{j,q} \left(\widetilde{B}_{up} K_i I_1 - I_2 L_i \widetilde{C}_p\right) - I_3^T V \widetilde{C}_p,$$

$$\Omega_{33} = \widetilde{B}_p^T \overline{P}_{j,q} \widetilde{B}_p + I_3^T I_3 - \gamma^2 I,$$

$$\varsigma_k^T = \left[\xi_k^T \ \ \xi_{k-i}^T \ \ \omega_k^T \ \ \xi_{k-\tau}^T\right].$$

If $\overline{\Omega} < 0$, from (30) and under zero-initial condition, we have $E\{\sum_{k=0}^{\infty} r_{ek}^T r_{ek}\} < \gamma^2 E\{\sum_{k=0}^{\infty} \omega_k^T \omega_k\}$.

By Schur compliment, $\overline{\Omega} < 0$ is equivalent to

$$\begin{bmatrix} \Xi_{11} & * & * \\ \Xi_{21} & \overline{\Xi}_{22} & * \\ \Xi_{31} & 0 & \overline{\Xi}_{33} \end{bmatrix} < 0, \tag{32}$$

where

$$\begin{aligned} \overline{\Xi}_{22} &= \begin{bmatrix} Q_1 - Z_1 & * \\ 0 & -Z_1^{-1} \end{bmatrix}, \\ \overline{\Xi}_{33} &= \operatorname{diag}\left\{-P_{0,1}^{-1}, \ldots, -P_{\tau,N}^{-1}\right\}. \end{aligned} \tag{33}$$

Letting $P_{j,q}^{-1} = F_{j,q}$, $j \in M$, $q \in G$, $Z_1^{-1} = Y_1$, (27) and (28) can be obtained, which completes the proof. □

In Corollary 7, the conditions are a set of LMIs with some inversion constraints. Though they are nonconvex which cannot be solved by using the existing convex optimization tool, we can use the cone complementarity linearization (CCL) algorithm [27] to transform this problem into the nonlinear minimization problem as follows:

$$\begin{aligned} \min \quad & \operatorname{tr}\left(\sum_{j=0}^{\tau}\sum_{q=1}^{N} P_{j,q}F_{j,q} + Z_1Y_1\right) \\ \text{s.t.} \quad & (27), (35), \end{aligned} \tag{34}$$

$$\begin{bmatrix} P_{j,q} & I \\ I & F_{j,q} \end{bmatrix} > 0, \quad j \in M,\ q \in G, \tag{35}$$

$$\begin{bmatrix} Z_1 & I \\ I & Y_1 \end{bmatrix} > 0.$$

Furthermore, the iterative algorithm which can be used to calculate the controller gain K_i, FD gain matrix L_i, and the minimal H_∞ attenuation $\gamma_{\min}$ is given bellow.

Algorithm 8.

Step 1. Let $\gamma = \gamma_0$ and set the maximum iterations number as $n_{\max}$.

Step 2. Find a feasible solution satisfying (27), (35) and set it as $(P_{j,s}^0, F_{j,s}^0, Z_1^0, Y_1^0, K_i^0, L_i^0)$. Let $k = 0$.

Step 3. Solve the following LMI optimization problem for variables $(P_{j,q}, F_{j,q}, Z_1, Y_1, K_i, L_i)$:

$$\begin{aligned} \min \quad & \operatorname{tr}\left(\sum_{j=0}^{\tau}\sum_{q=1}^{N}\left(P_{j,q}^k F_{j,q} + P_{j,q}F_{j,q}^k\right) + Z_1^k Y_1 + Z_1 Y_1^k\right), \\ \text{subject to} \quad & (27), (35); \end{aligned} \tag{36}$$

set $(P_{j,s}^k = P_{j,s}, F_{j,s}^k = F_{j,s}, Z_1^k = Z_1, Y_1^k = Y_1, K_i^k = K_i, L_i^k = L_i)$.

Step 4. If (27) and (28) are satisfied, let $\gamma = \gamma - \delta$, $\delta > 0$ and return to Step 3. If the number of iterations exceeds $n_{\max}$, the iteration is terminated.

Step 5. Check γ: if $\gamma = \gamma_0$, the optimization problem has no solutions within the maximum iterations number $n_{\max}$. Otherwise, $\gamma_{\min} = \gamma + \delta$.

Remark 9. In this paper, we assume that the transition probabilities of τ_k and θ_k are completely known. When transition probabilities of τ_k and θ_k are partly unknown, we can separate the unknown ones from the known ones; see [28].

4. Numerical Example

In this section, we present an example to demonstrate the effectiveness of the proposed method. Consider the controlled plant with the following parameter:

$$\begin{aligned} A_1 &= \begin{bmatrix} 1 & 0 \\ 0.25 & 0.15 \end{bmatrix}, \\ B_{u1} &= \begin{bmatrix} 0.3 \\ 0.5 \end{bmatrix}, \\ B_{d1} &= \begin{bmatrix} 0.2 \\ 0.1 \end{bmatrix}, \\ B_{f1} &= \begin{bmatrix} 0.23 \\ 0.81 \end{bmatrix}, \\ C_1 &= \begin{bmatrix} 0.1 & 0.3 \end{bmatrix}, \\ A_2 &= \begin{bmatrix} 0.65 & 0.05 \\ 0.1 & 0.3 \end{bmatrix}, \\ B_{u2} &= \begin{bmatrix} 0.2 \\ 0.6 \end{bmatrix}, \\ B_{d2} &= \begin{bmatrix} 0.1 \\ 0.3 \end{bmatrix}, \\ B_{f2} &= \begin{bmatrix} 0.37 \\ 0.32 \end{bmatrix}, \\ C_2 &= \begin{bmatrix} 0.2 & 0.3 \end{bmatrix}, \end{aligned} \tag{37}$$

the system mode $\theta_k \in \{1, 2\}$, and the transition probability matrix of θ_k is $\Omega = \left[\begin{smallmatrix} 0.2 & 0.8 \\ 0.9 & 0.1 \end{smallmatrix}\right]$. The random time-delay $\tau_k \in \{0, 1\}$ and the transition probability matrix is $\Lambda = \left[\begin{smallmatrix} 0.7 & 0.3 \\ 0.6 & 0.4 \end{smallmatrix}\right]$. Given $V = 0.1$, by Corollary 7, we can obtain the delay-dependent controller gain matrix K_i, filter gain matrix L_i, and $\gamma_{\min}$ as follows:

$$\begin{aligned} K_0 &= \begin{bmatrix} -0.0004 & 0.003 \end{bmatrix}, \\ L_0 &= \begin{bmatrix} 0.0481 \\ -0.1333 \end{bmatrix}, \\ K_1 &= \begin{bmatrix} 0.0036 & -0.0020 \end{bmatrix}, \\ L_1 &= \begin{bmatrix} -0.0342 \\ -0.0906 \end{bmatrix}, \\ \gamma_{\min} &= 1.6125. \end{aligned} \tag{38}$$

The initial value $x_{-1} = \begin{bmatrix} 0 & 0 \end{bmatrix}^T$, $x_0 = \begin{bmatrix} -1.1 & 1 \end{bmatrix}^T$, $\widehat{x}_{-1} = \begin{bmatrix} 0 & 0 \end{bmatrix}^T$, $\widehat{x}_0 = \begin{bmatrix} 1 & -1.1 \end{bmatrix}^T$, $\tau_{-1} = \tau_0 = 0$, $\theta_{-1} = \theta_0 = 0$. Assume that the external disturbance d_k is uniformly distributed random signal on $\begin{bmatrix} -0.15 & 0.15 \end{bmatrix}$; when there is no

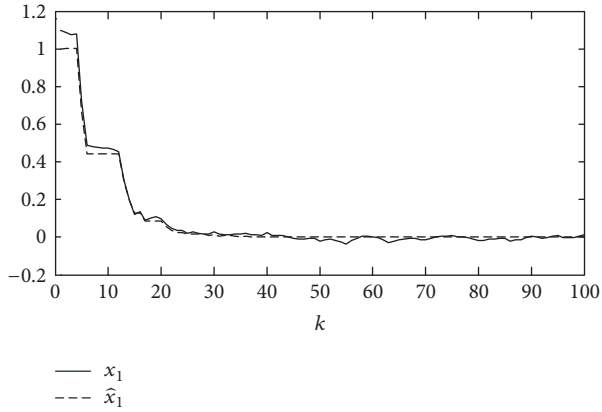

Figure 1: The state x_1 and its estimated value $\hat{x}_1$.

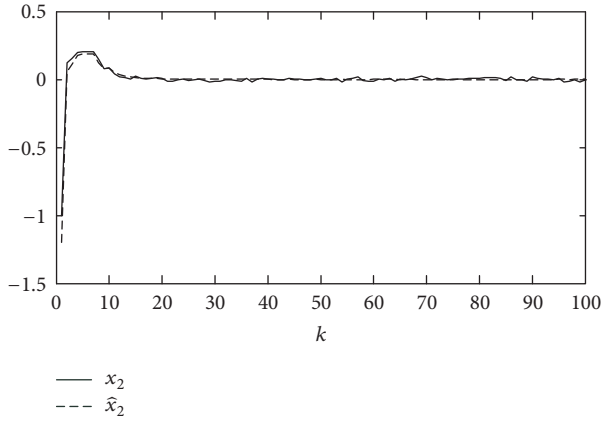

Figure 2: The state x_2 and its estimated value $\hat{x}_2$.

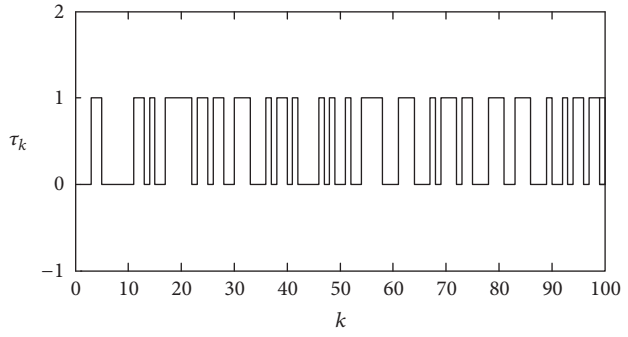

Figure 3: The time-delay τ_k.

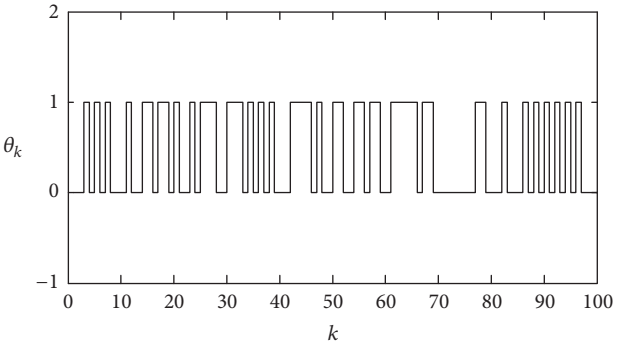

Figure 4: The system mode θ_k.

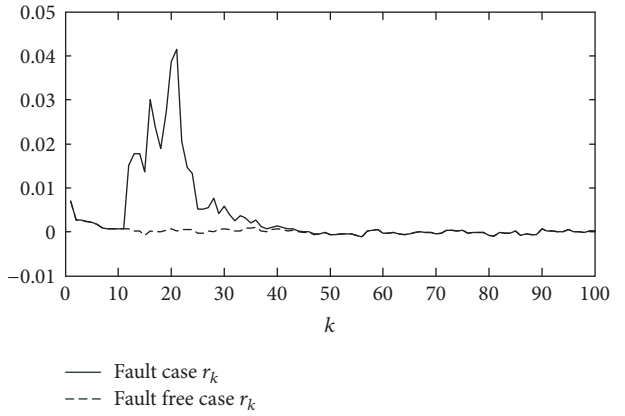

Figure 5: The residual signal r_k.

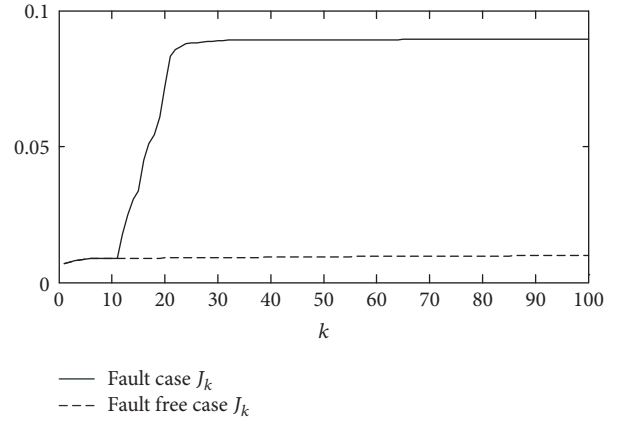

Figure 6: The residual evaluation function J_k and the threshold J_{th}.

fault, the trajectories of the closed-loop system's states and the corresponding estimated value are shown in Figures 1 and 2.

We can see that the filter can track the states of the system closely. Assume the fault signal is

$$f_k = \begin{cases} 0.5, & k = 10, \ldots, 20 \\ 0, & \text{others.} \end{cases} \tag{39}$$

The residual evaluation function is adopted as $J_k = E\{\sum_{\rho=0}^{k} \sqrt{r_\rho^T r_\rho}\}$, and the FD threshold can be obtained as $J_k = \sup_{\omega_k \in L_2, f_k=0} E\{\sum_{\rho=0}^{k} \sqrt{r_\rho^T r_\rho}\} = 0.0122$. Figures 3 and 4 show one simulation run of the time-delay and the system mode under the transition probability matrices Π and Λ, respectively.

Figures 5 and 6 show the residual signal r_k and the residual evaluation function J_k, respectively, from which we can see that when fault occurs, r_k and J_k change obviously. Moreover, it is noticed that $J_{11} = 0.0114 < J_{\text{th}} < J_{12} = 0.0170$. This means that the fault has been detected at the third time period after it occurs.

5. Conclusion

With the presence of random time-delay introduced by the network, the problem of robust H_∞ FD for networked Markov jump systems is investigated in this paper. By constructing delay-dependent FD filter, the closed-loop systems are established. The sufficient and necessary conditions which make the closed-loop system stochastically stable and achieve prescribed H_∞ performance are derived. The method of calculating controller, FD filter gain matrices, and the minimal H_∞ attenuation level is also obtained. The numerical example shows that the proposed FD filter is both sensitive to the fault and also robust to the exogenous disturbance.

Conflicts of Interest

The authors declare that there are no conflicts of interest regarding the publication of this paper.

Acknowledgments

The research is supported by the National Natural Science Foundation of China (Grant nos. 61503136, 61573137, 61573136, and 61503213).

References

[1] H. Lin, H. Su, Z. Shu, Z. G. Wu, and Y. Xu, "Optimal estimation in UDP-like networked control systems with intermittent inputs: stability analysis and suboptimal filter design," *IEEE Transactions on Automatic Control*, vol. 61, no. 7, pp. 1794–1809, 2016.

[2] X. G. Yan and S. K. Spurgeon, "Delay-independent decentralised output feedback control for large-scale systems with nonlinear interconnections," *International Journal of Control*, vol. 87, no. 3, pp. 473–482, 2014.

[3] S. Dong, H. Su, P. Shi, R. Lu, and Z. G. Wu, "Filtering for discrete-time switched fuzzy systems with quantization," *IEEE Transactions on Fuzzy Systems*, vol. PP, no. 99, 2016.

[4] W. A. Zhang and L. Yu, "Modelling and control of networked control systems with both network-induced delay and packet-dropout," *Automatica. A Journal of IFAC, the International Federation of Automatic Control*, vol. 44, no. 12, pp. 3206–3210, 2008.

[5] Y. Zhang and H. Fang, "Stabilization of nonlinear networked systems with sensor random packet dropout and time-varying delay," *Applied Mathematical Modelling. Simulation and Computation for Engineering and Environmental Systems*, vol. 35, no. 5, pp. 2253–2264, 2011.

[6] S. Dong, Z.-G. Wu, P. Shi, H. Su, and R. Lu, "Reliable control of fuzzy systems with and switched actuator failures," *IEEE Transactions on Systems, Man, and Cybernetics: Systems*, vol. 47, no. 8, pp. 2198–2208.

[7] H. Gao, X. Meng, and T. Chen, "Stabilization of networked control systems with a new delay characterization," *IEEE Transactions on Automatic Control*, vol. 53, no. 9, pp. 2142–2148, 2008.

[8] E. Tian, D. Yue, and X. Zhao, "Quantised control design for networked control systems," *IET Control Theory and Applications*, vol. 1, no. 6, pp. 1693–1699, 2007.

[9] M. Zhong, S. X. Ding, J. Lam, and H. Wang, "An LMI approach to design robust fault detection filter for uncertain LTI systems," *Automatica*, vol. 39, no. 3, pp. 543–550, 2003.

[10] M. Abid, W. Chen, S. X. Ding, and A. Q. Khan, "Optimal residual evaluation for nonlinear systems using post-filter and threshold," *International Journal of Control*, vol. 84, no. 3, pp. 526–539, 2011.

[11] N. Meskin and K. Khorasani, "Actuator fault detection and isolation for a network of unmanned vehicles," *IEEE Transactions on Automatic Control*, vol. 54, no. 4, pp. 835–840, 2009.

[12] W. Ding, Z. Mao, B. Jiang, and W. Chen, "Fault detection for a class of nonlinear networked control systems with Markov transfer delays and stochastic packet drops," *Circuits, Systems, and Signal Processing*, vol. 34, no. 4, pp. 1211–1231, 2015.

[13] H. Huang, D. X. Zhang, D. F. Zhang, and Z. Q. Wang, "H_∞ fault detection for networked control systems with random Markov delays," *Information and Control*, vol. 39, no. 1, pp. 6–12, 2009.

[14] H. Huang, D. X. Xie, X. D. Han et al., "Fault detection for networked control system with random packet dropout," *Control Theory & Applications*, vol. 28, no. 1, pp. 79–86, 2011.

[15] W. Jiang, C. Dong, E. Niu, and Q. Wang, "Observer-based robust fault detection filter design and optimization for networked control systems," *Mathematical Problems in Engineering*, vol. 2015, Article ID 231749, pp. 1–11, 2015.

[16] Z. Mao, B. Jiang, and P. Shi, "H_∞ fault detection filter design for networked control systems modelled by discrete Markovian jump systems," *IET Control Theory & Applications*, vol. 1, no. 5, pp. 1336–1343, 2007.

[17] Y. Zhang, H. Fang, and Z. Liu, "Fault detection for nonlinear networked control systems with Markov data transmission pattern," *Circuits, Systems, and Signal Processing*, vol. 31, no. 4, pp. 1343–1358, 2012.

[18] C. Peng, D. Yue, E. Tian, and Z. Gu, "Observer-based fault detection for networked control systems with network quality of services," *Applied Mathematical Modelling. Simulation and Computation for Engineering and Environmental Systems*, vol. 34, no. 6, pp. 1653–1661, 2010.

[19] F. Li, P. Shi, X. Wang, and R. Agarwal, "Fault detection for networked control systems with quantization and Markovian packet dropouts," *Signal Processing*, vol. 111, pp. 106–112, 2015.

[20] Y. F. Wang, P. L. Wang, and Z. D. Cai, "Robust H_∞ fault detection for networked control systems with partly unknown time-delay transition probabilities," *Control Theory & Applications*, vol. 34, no. 2, pp. 273–279, 2017.

[21] Z. Wu, S. Dong, P. Shi, H. Su, T. Huang, and R. Lu, "Fuzzy-model-based nonfragile guaranteed cost control of nonlinear Markov jump systems," *IEEE Transactions on Systems, Man, and Cybernetics: Systems*, vol. 47, no. 8, pp. 2388–2397, 2017.

[22] Q. Zhou, D. Yao, J. Wang, and C. Wu, "Robust control of uncertain semi-Markovian jump systems using sliding mode control method," *Applied Mathematics and Computation*, vol. 286, pp. 72–87, 2016.

[23] G. Wang, Q. Zhang, and X. Yan, *Analysis and Design of Singular Markovian Jump Systems*, Springer, New York, NY, USA, 2015.

[24] Z. Wu, P. Shi, Z. Shu, H. Su, and R. Lu, "Passivity-based asynchronous control for Markov jump systems," *IEEE Transactions on Automatic Control*, vol. 62, no. 4, pp. 2020–2025, 2017.

[25] L. Zhang, Y. Shi, T. Chen, and B. Huang, "A new method for stabilization of networked control systems with random delays," *IEEE Transactions on Automatic Control*, vol. 50, no. 8, pp. 1177–1181, 2005.

[26] X. F. Jiang, Q. L. Han, and X. H. Yu, "Stability criteria for linear discrete-time systems with interval-like time-varying delay," in *Proceedings of the American Control Conference*, pp. 2817–2822, Portland, Ore, USA, June 2005.

[27] L. El Ghaoui, F. Oustry, and M. AitRami, "A cone complementarity linearization algorithm for static output-feedback and related problems," *IEEE Transactions on Automatic Control*, vol. 42, no. 8, pp. 1171–1176, 1997.

[28] Y. Wang, P. Wang, Z. Li, and H. Chen, "Observer-based controller design for a class of nonlinear networked control systems with random time-delays modeled by Markov chains," *Journal of Control Science and Engineering*, vol. 2017, Article ID 1523825, pp. 1–13, 2017.

Hindawi
Mathematical Problems in Engineering
Volume 2017, Article ID 4324370, 14 pages
https://doi.org/10.1155/2017/4324370

Research Article

Robust Fault Detection and Estimation in Nonlinear Systems with Unknown Constant Time-Delays

Wenxu Yan,[1] Dezhi Xu,[1] and Qikun Shen[2]

[1]*School of Internet of Things Engineering, Jiangnan University, Wuxi 214122, China*
[2]*College of Information Engineering, Yangzhou University, Yangzhou 225009, China*

Correspondence should be addressed to Dezhi Xu; xudezhi@jiangnan.edu.cn

Received 23 March 2017; Accepted 29 May 2017; Published 7 August 2017

Academic Editor: Xinggang Yan

This paper studies the problem of fault detection and estimation in nonlinear time-delayed systems with unknown inputs, where the time-delays are supposed to be constant but unknown. A new fault detection filter, which can estimate online the time-delays, is first introduced. Then, a reference residual model is proposed to formulate the robust fault detection filter design problem as an H_∞ model-matching problem. Furthermore, by a novel robust adaptive fault estimation algorithm, the classical assumption that the time derivative of the output error should be known is removed. In addition, applying a robust H_∞ optimization control technique, sufficient conditions for the existence of the fault detection filter (FDF) are derived in terms of linear matrix inequality (LMI). Finally, simulation results are presented to illustrate the effectiveness of the proposed algorithm.

1. Introduction

Modern industrial control systems become more and more complex, with an increasing number of interconnected physical components, such as actuators and sensors [1]. In the system life, faults inevitably occur in these elements, which leads to the drop of systems performances, or even worse to system damage, with dramatic consequences on the environment. Consequently, in parallel with the development of high-performance technological systems, industrials express a growing demand for reliability, maintainability, and survivability [2]. Fault Tolerant Control (FTC) is an effective way of maintaining system performances under faulty conditions. FTC can be achieved either by a passive way or using an active method. Passive FTC uses feedback control laws that are robust with respect to an a priori fixed set of possible system faults [3, 4]. On the other hand, active FTC uses a Fault Detection and Isolation (FDI) module that provides online fault information. Active FTC may consist of a fault accommodation scheme [5, 6], which is in fact an adaptive control with respect to the fault information, or may be a control system reconfiguration scheme, which consists of a switching control with a supervision layer that selects the most suitable control law for the identified faulty situation [7–10]. One difficulty is that FDI module and active FTC algorithm have to be designed jointly because of their mutual interactions.

In distributed or large-scale processes, the dynamic contains time-delays which may cause instability and degrade the system performances [11]. These time-delays may generally be considered as constant ones for given operating conditions. However these constant values are generally not known. The existence of such time-delays renders the control design problem much more difficult [12]. Increasing attention has recently been devoted to stability control and fault diagnosis of linear/nonlinear time-delayed systems, see, for example, [4–6, 11–16]. In [14], an observer-based fuzzy control scheme with adaptation to the time-delay was proposed. In [15], fault detection and identification for uncertain linear time-delay systems were investigated. In [16], by using H_∞ control theory, a robust fault detection scheme was proposed for a class of discrete time-delay systems with parameter uncertainty. However, the sensitivity of the residual signals to the faults was not studied. In [17], the fault detection filter design problem for linear time-delay systems was studied by introducing an idealized reference residual model. Based

on [16, 17], the robust fault detection filter (RFDF) design problem was studied in [18] for nonlinear time-delay systems with unknown inputs. In [19], H_∞ fault detection filter design for linear discrete time systems with multiple time-delays was discussed. The fault detection filter design problem was investigated in [20] for LTI (Linear Time-Invariant) system with time-delays. In [21, 22], the fault estimation problem for linear systems with state time-delays was studied, and an adaptive fault detection observer was designed. Many observers that are proposed in the literature, as in [16–23], use explicitly the time-delay value that is supposed to be accessible. However, in practical applications, this time-delay is generally not available, which makes these techniques not applicable. Another drawback of many diagnosis techniques that are proposed in the literature is that they need the derivative of the output signal for the fault estimation algorithm. These derivatives are generally not directly measured and are difficult to compute in a noisy environment.

In this paper, we investigate the problem of fault detection and estimation of nonlinear time-delayed systems. Five main contributions are worth emphasis.

(1) Compared with some results (see [16–22], for instance), by online estimating the real value of state time-delay, the assumption that the time-delay must be a priori known is removed.

(2) An adaptive fault estimation algorithm is proposed where the classical assumption that the time derivative of the output errors has to be known (see [22], for instance) and is removed. Moreover, our scheme is robust to bounded disturbances.

(3) Differing from numerous FDI schemes in the literature, the bounds of the time derivatives of the faults have not been known in our proposed adaptive fault estimation algorithm.

(4) In this paper, in contrast with [18], not only the fault detection filter design problem is discussed, but also an adaptive fault estimation algorithm is proposed.

(5) Sufficient conditions for the existence of the adaptive fault observer are expressed using the Lyapunov stability theory.

The paper is organized as follows. The problem formulation is presented in Section 2. In Section 3, the main technical results of this paper are given, which include the choice of the reference residual model, the design of a robust fault detection observer/filter, and the fault estimation algorithm. Simulations are presented in Section 4. Finally, Section 5 draws the conclusion.

2. Problem Formulation

Consider the following class of nonlinear time-delay systems [18]:

$$\begin{aligned}\dot{x}(t) &= Ax(t) + A_d x(t-h) + Bu(t) \\ &\quad + Gg(x(t), x(t-h)) + B_f f(t) + B_d d(t), \\ y(t) &= Cx(t) + Du(t) + D_f f(t) + D_d d(t), \\ x(t) &= 0, \quad t \in \left[-\bar{h}, 0\right],\end{aligned} \tag{1}$$

where $x(t) \in R^n$ is the unknown state vector, $u(t) \in R^p$ is the control input vector, $y(t) \in R^q$ is the measured output, $d(t) \in R^m$ that belongs to $L_2^m[0, +\infty]$ is an exogenous disturbance input vector that regroups all the model uncertainties, $f(t) \in R^l$ is the fault vector to be detected, $h \geq 0$ is an unknown but constant time-delay that satisfies $h \leq \bar{h}$, where $\bar{h}$ is a known constant, $g(\cdot,\cdot) : R^n \times R^n \to R^{n_g}$ is a known nonlinear function, and $A, A_d, B, B_f, B_d, C, D, D_f, D_d, G$ are all known matrices with appropriate dimensions.

Throughout this paper, the following assumptions are made.

Assumption 1. The pair (C, A) is detectable.

Assumption 2 (Lipschitz condition). It is supposed that $g(0,0) = 0$ and $\|g(x_1, x_2) - g(y_1, y_2)\| \leq \|\rho_1(x_1 - y_1)\| + \|\rho_2(x_2 - y_2)\|$, $\forall x_1, x_2, y_1, y_2 \in R^n$, where $\rho_1 > 0 \in R$, $\rho_2 > 0 \in R$, are known constant.

To detect the fault, the following so-called fault detection filter (FDF) is proposed:

$$\begin{aligned}\dot{\hat{x}}(t) &= A\hat{x}(t) + A_d\hat{x}\left(t - \hat{h}\right) + Bu(t) \\ &\quad + Gg\left(\hat{x}(t), \hat{x}\left(t - \hat{h}\right)\right) + H\left[y(t) - \hat{y}(t)\right], \\ \hat{y}(t) &= C\hat{x}(t) + Du(t), \\ r(t) &= V\left[y(t) - \hat{y}(t)\right],\end{aligned} \tag{2}$$

where $\hat{x}(t) \in R^n$ and $\hat{y}(t) \in R^q$ denote the state and the output of the filter, respectively; $\hat{h}$ is the estimation of the unknown constant time-delay h; $r(t)$ is the so-called residual signal. The observer gain matrix H and the residual weighting matrix V will be defined later.

For the above observer design, the following assumption is made.

Assumption 3. There exists a known constant $M > 0 \in R$ such that $\|x(t) - \hat{x}(t)\| \leq M$.

Remark 4. Assumption 3 is not restrictive. In fact, this is a common assumption in the literature concerning filter/observer design. In practical application, it may be difficult to know accurately the upper bound of the observer error. Therefore, M can be chosen large in practical applications. It must be pointed out that M is only needed for stability analysis of the closed-loop system. Choosing a large M does not degrade the performance of the closed-loop system.

Define

$$e = x(t) - \hat{x}(t). \tag{3}$$

The error dynamics can be computed as

$$\begin{aligned}\dot{e}(t) &= (A-HC)e(t) + A_d\hat{x}\left(t-\hat{h}\right) - A_d x(t-h) \\ &\quad + \left(B_f - HD_f\right)f(t) + \left(B_d - HD_d\right)d(t) + G\Psi \\ &= (A-HC)e(t) + A_d\hat{x}\left(t-\hat{h}\right) - A_d\hat{x}(t-h) \\ &\quad + A_d\hat{x}(t-h) - A_d x(t-h) \\ &\quad + \left(B_f - HD_f\right)f(t) + \left(B_d - HD_d\right)d(t) + G\Psi \\ &= (A-HC)e(t) + A_d e(t-h) + A_d\hat{x}\left(t-\hat{h}\right) \\ &\quad - A_d\hat{x}(t-h) + \left(B_f - HD_f\right)f(t) \\ &\quad + \left(B_d - HD_d\right)d(t) + G\Psi,\end{aligned} \tag{4}$$

where $\Psi = g(x(t), x(t-h)) - g(\hat{x}(t), \hat{x}(t-\hat{h}))$.

From Newton-Leibniz formula, we have

$$\hat{x}\left(t-\hat{h}\right) - \hat{x}(t-h) = \int_{-h}^{-\hat{h}} \dot{\hat{x}}(t+s)\,ds. \tag{5}$$

Thus, error dynamics (4) can further be described as

$$\begin{aligned}\dot{e}(t) &= (A-HC)e(t) + A_d e(t-h) \\ &\quad + A_d\int_{-h}^{-\hat{h}} \dot{\hat{x}}(t+s)\,ds + \left(B_f - HD_f\right)f(t) \\ &\quad + \left(B_d - HD_d\right)d(t) + G\Psi, \\ r(t) &= VCe(t) + VD_f f(t) + VD_d d(t).\end{aligned} \tag{6}$$

From (6), it is seen that the dynamics of the residual signal depends not only on fault $f(t)$ and uncertainty $d(t)$, but also on the nonlinear part Ψ. Motivated by the method presented in [18], we propose using a reference residual model that describes the desired behavior of the residual vector $r(t)$, to formulate the RFDF design problem as an H_∞ model-matching problem. In other words, the objectives are finding an idealized reference residual and minimizing the distance between the generated residual and the idealized reference residual. In the idealized case, the observed state $\hat{x}(t)$ and the time-delayed state $\hat{x}(t-\hat{h})$ should be equal, respectively, to $x(t)$ and $x(t-h)$; thus we have $x(t) - \hat{x}(t) = 0$ and $x(t-h) - \hat{x}(t-\hat{h}) = 0$. Consequently, $\Psi = g(x(t), x(t-h)) - g(\hat{x}(t), \hat{x}(t-\hat{h})) = 0$. Therefore, according to (6), and assuming $\Psi = 0$, the corresponding reference residual error model is given by

$$\begin{aligned}\dot{e}_f(t) &= \left(A - \overline{H}C\right)e_f(t) + A_d e_f(t-h) \\ &\quad + \left(B_f - \overline{H}D_f\right)f(t) + \left(B_d - \overline{H}D_d\right)d(t), \\ r_f(t) &= \overline{V}Ce_f(t) + \overline{V}D_f f(t) + \overline{V}D_d d(t), \\ e_f(t) &= 0 \quad (t \le 0),\end{aligned} \tag{7}$$

where $e_f(t) \in R^n$ is the reference model error state vector, $r_f(t)$ is the reference model residual signal, and $\overline{H}$ and $\overline{V}$ are the parameters of the reference residual model to be designed.

Thus the overall system can be described by

$$\begin{aligned}\dot{\eta}(t) &= \overline{A}\eta(t) + \overline{A}_d\eta(t-h) + \overline{\overline{A}}_d\int_{-h}^{-\hat{h}} \dot{\hat{x}}(t+s)\,ds \\ &\quad + \overline{B}w(t) + \overline{G}\Psi, \\ r_e(t) &= r(t) - r_f(t) = \overline{C}\eta(t) + \overline{D}w(t),\end{aligned} \tag{8}$$

where

$$\begin{aligned}\eta(t) &= \begin{bmatrix} e(t) \\ e_f(t)\end{bmatrix}, \\ w(t) &= \begin{bmatrix} f \\ d\end{bmatrix}, \\ \overline{A} &= \begin{bmatrix} A-HC & 0 \\ 0 & A-\overline{H}C\end{bmatrix}, \\ \overline{A}_d &= \begin{bmatrix} A_d & 0 \\ 0 & A_d\end{bmatrix}, \\ \overline{\overline{A}}_d &= \begin{bmatrix} A_d \\ 0\end{bmatrix}, \\ \overline{G} &= \begin{bmatrix} G \\ 0\end{bmatrix}, \\ \overline{B} &= \begin{bmatrix} B_f - HD_f & B_d - HD_d \\ B_f - \overline{H}D_f & B_d - \overline{H}D_d\end{bmatrix}, \\ \overline{C} &= \begin{bmatrix} VC & -\overline{V}C\end{bmatrix}, \\ \overline{D} &= \begin{bmatrix} VD_f - \overline{V}D_f & VD_d - \overline{V}D_d\end{bmatrix}.\end{aligned} \tag{9}$$

From (8), the design of the robust fault detection filter, which is the main objective of this work, may be formulated as an H_∞ model-matching design problem. Applying a robust H_∞ optimization control technique, for all exogenous disturbance inputs and nonlinear parts, the generated residual $r(t)$ will be designed as closely as possible to the reference model residual $r_f(t)$, independently of the unknown time-delay h. Thus, the problem of designing an observer-based RFDF can be described as designing the observer gain matrix H and the residual weighting matrix V such that

(i) systems (8) are robustly asymptotically stable;

(ii) under zero initial condition, for given constant $\gamma > 0$ and any nonzero $w(t) \in L_2[0, \infty)$, systems (8) satisfy the following inequality:

$$\|r_e(t)\|_2 < \gamma \|w(t)\|_2. \tag{10}$$

After designing the RFDF, the remaining important task is to decide, from the generated residual, if an alarm has to be

generated. One of the widely adopted approaches is to choose a so-called threshold $J_{\text{th}} > 0$ and, based on this, use the following logical relationship for fault detection:

$$\begin{aligned} &\|r(t)\|_{2,\tau} > J_{\text{th}} \Longrightarrow \text{a fault has occured} \Longrightarrow \text{alarm} \\ &\|r(t)\|_{2,\tau} < J_{\text{th}} \Longrightarrow \text{no fault has occured,} \end{aligned} \tag{11}$$

where $\|r(t)\|_{2,\tau} = [\int_{t_1}^{t_2} r(t)^T r(t)dt]^{1/2}$, $\tau = t_1 - t_2$, $t \in [t_1, t_2]$.

The threshold $J_{\text{th}} > 0$ can be chosen as $J_{\text{th}} = \overline{f} + \overline{d}$, where $\overline{f} > 0 \in R$ and $\overline{d} > 0 \in R$ denote, respectively, the upper bound of the norm of fault f and exogenous disturbance d, that is, $\|f\|_2 \le \overline{f}$, $\|d\|_2 \le \overline{d}$.

Remark 5. There are many results on fault detection observer/filter design for time-delayed systems in the literature. In general, the observer, as the one in [16, 18], is designed in the following form:

$$\begin{aligned} \dot{\widehat{x}}(t) &= A\widehat{x}(t) + A_d\widehat{x}(t-h) + Bu(t) \\ &\quad + Gg(\widehat{x}(t), \widehat{x}(t-h)) \\ &\quad + Gg(\widehat{x}(t), \widehat{x}(t-h)) + H[y(t) - \widehat{y}(t)], \\ \widehat{y}(t) &= C\widehat{x}(t) + Du(t), \\ r(t) &= V[y(t) - \widehat{y}(t)]. \end{aligned} \tag{12}$$

However, just as said in [14], the shortcoming of the above-mentioned observer is that the constant state time-delay h must be exactly known. If the time-delay h is unknown, the above observer will not work in practical applications.

3. Main Results and Proof

As mentioned in [24, 25], the design of a RFDF for the nonlinear time-delay system (1) can be formulated as an H_∞ model-matching problem. In this section, we first design the reference residual model and then express the RFDF design problem under an LMI formulation.

3.1. Choice of the Reference Residual Model. As pointed out in [18], the selection of a suitable reference residual model is one of the key steps to design an RFDF for nonlinear time-delay systems. If the reference residual model is not selected suitably, miss alarms or false alarms may occur. In order to select a suitable reference residual model, we consider the following performance index J_f:

$$J_f = \left\|T_{r_f d}(s)\right\|_\infty - \left\|T_{r_f f}(s)\right\|_\infty, \tag{13}$$

where $T_{r_f d}(s)$ and $T_{r_f f}(s)$ are the transfer functions from f and d to the reference model residual r_f.

Notice that if $J_f \to \min\{J_f\}$, then one has

$$\begin{aligned} \left\|T_{r_f d}(s)\right\|_\infty &\longrightarrow \max\left\{T_{r_f d}(s)\right\}, \\ \left\|T_{r_f f}(s)\right\|_\infty &\longrightarrow \min\left\{T_{r_f f}(s)\right\}. \end{aligned} \tag{14}$$

Therefore, according to the performance index J_f (13), the reference residual model can be designed, which takes into account not only the robustness of the reference model residual against disturbance but also the sensitivity to faults.

For the sake of simplicity, we assume that $l = m$.

Consider the following transfer function:

$$T = MT_{r_f\vartheta}N = M\left[T_{r_f f}T_{r_f d}\right]N, \tag{15}$$

where the matrices $M \in R^{q\times q}, N \in R^{2l\times l}$ select the appropriate input/output channels or channels combinations and T satisfies the following equalities:

$$T\begin{cases} \dot{e}_f(t) = \left(A - \overline{H}C\right)e_f(t) + A_d e_f(t-h) + B_1\vartheta(t), \\ r_f(t) = M\overline{V}Ce_f(t) + MD_1N\vartheta(t), \end{cases} \tag{16}$$

where $B_1 = \left[B_f - \overline{H}D_f \quad B_d - \overline{H}D_d\right]$, $D_1 = [D_f \quad D_d]$, and $\vartheta(t) = [d - f]$.

Choosing $M = I_{q\times q}$, $N = [-I_{l\times l} \quad I_{l\times l}]^T$, and giving $\alpha > 0$, it follows that

$$\begin{aligned} &\|T\|_\infty = \left\|T_{r_f d} - T_{r_f f}\right\|_\infty > \left\|T_{r_f d}\right\|_\infty - \left\|T_{r_f f}\right\|_\infty, \\ &\|T\|_\infty < \alpha \Longrightarrow \left\|T_{r_f d}\right\|_\infty - \left\|T_{r_f f}\right\|_\infty < \alpha. \end{aligned} \tag{17}$$

Then the reference residual model can be designed by solving the following optimization problem:

$$\begin{aligned} &\min \quad \alpha \\ &\text{s.t.} \quad (13), (17) \text{ hold.} \end{aligned} \tag{18}$$

The following theorem provides a sufficient condition to ensure that, for a given $\alpha > 0$, the reference RFDF satisfies (16).

Theorem 6. *Given $\alpha > 0$ and the reference residual model (7), if there exist symmetric matrices $P = P^T > 0$, $Q = Q^T > 0$, $Z > 0$, and Y such that*

$$\Xi = \begin{bmatrix} A^TP + PA - C^TY^T - YC + C^TZC + Q & P\left(B_d - B_f\right) + Y\left(B_f - B_d\right) + C^TZ\left(D_d - D_f\right) & PA_d \\ * & \left(D_d - D_f\right)^T Z\left(D_d - D_f\right) - \alpha^2 I & 0 \\ * & * & -Q \end{bmatrix} < 0 \tag{19}$$

holds and applying the time-delay adaptive law

$$\dot{\widehat{h}} = -\frac{1}{\eta}M\left(\|PA_d\| + \left\|P\overline{G}\rho_2\right\|\right)\alpha(t), \quad \widehat{h}(0) > \overline{h} \tag{20}$$

then system (7), subject to Assumptions 1–3, is stable and satisfies $\|T_{r_f d}\|_\infty - \|T_{r_f f}\|_\infty < \alpha$, where $\alpha(t) = \|\dot{\widehat{x}}(t)\|$, $\eta > 0$, $\widehat{h}(t) \ge \overline{h}$, $\overline{H} = P^{-1}Y$, and $\overline{V} = Z^{1/2}$.

Proof. Consider the following Lyapunov-Krasovskii function:

$$\begin{aligned} V_1(t) &= e_f^T(t) P e_f(t) + \int_{t-h}^{t} e_f^T(\tau) Q e_f(\tau)\, d\tau \\ &\quad + 2M \left\| PA_d \right\| \int_{-\widehat{h}}^{-h} d\theta \int_{\theta}^{0} \alpha(t+s)\, ds \\ &\quad + \frac{\eta}{2} \left(\widehat{h} - h\right)^2. \end{aligned} \tag{21}$$

Differentiating V_1 with respect to time t, one has

$$\begin{aligned} \dot{V}_1 &\le e_f^T(t) \left(P\left(A - \overline{H}C\right) + \left(A - \overline{H}C\right)^T P \right) e_f(t) \\ &\quad + e_f^T(t) P A_d A_d^T P e_f(t) + e_f^T(t-h) Q e_f(t-h) \\ &\quad + 2 e_f^T(t) P A_d \int_{-h}^{-\widehat{h}} \dot{\hat{x}}(t+s)\, ds + e_f^T(t) Q e_f(t) \\ &\quad - e_f^T(t-h) Q e_f(t-h) + \eta \left(\widehat{h} - h\right) \dot{\widehat{h}} \\ &\quad - 2M \left(\left\| PA_d \right\| + \left\| P\overline{G}\rho_2 \right\| \right) \left[\left(\widehat{h} - h\right) \alpha(t) \right. \\ &\quad \left. - \int_{-\widehat{h}}^{-h} \alpha(t+\theta)\, d\theta + \dot{\widehat{h}} \int_{-\widehat{h}}^{0} \alpha(t+s)\, ds \right]. \end{aligned} \tag{22}$$

Since $\dot{\widehat{h}} = -(1/\eta) M \| PA_d \| \alpha(t) \le 0$, one has $\dot{\widehat{h}} \int_{-\widehat{h}}^{0} \alpha(t+s) ds \le 0$. Under idealized condition, using the FDF (2), the observer error is asymptotically converging to zero; that is, $x(t) - \widehat{x}(t) \to 0$, $x(t-h) - \widehat{x}(t-\widehat{h}) \to 0$.

Then, one has

$$\begin{aligned} \dot{V}_1 &\le e_f^T(t) \\ &\quad \cdot \left(P\left(A - \overline{H}C\right) + \left(A - \overline{H}C\right)^T P + P A_d A_d^T P + Q \right) \\ &\quad \cdot e_f(t). \end{aligned} \tag{23}$$

Define the following performance index J_1:

$$\begin{aligned} J_1 &= \int_0^\infty r_f^T(t) r_f(t)\, dt - \alpha^2 \int_0^\infty \vartheta^T(t) \vartheta(t)\, dt \\ &= \int_0^\infty \left[r_f^T(t) r_f(t) - \alpha^2 \vartheta^T(t) \vartheta(t) + \dot{V}_1(t) \right] dt \\ &\quad - V_1(t)\big|_t + V_1(t)\big|_{t=0}. \end{aligned} \tag{24}$$

Then, we have

$$J_1 < \int_0^\infty \left[r_f^T(t) r_f(t) - \alpha^2 \vartheta^T(t) \vartheta(t) + \dot{V}_1(t) \right] dt. \tag{25}$$

Let $Y = P\overline{H}$, $Z = \overline{V}^T \overline{V}$, $M = I_{q\times q}$, and $N = \left[-I_{l\times l} \;\; I_{l\times l}\right]^T$; then

$$\begin{aligned} r_f^T r_f &= \left(M\overline{V}Ce_f + MD_1 N\vartheta \right)^T \left(M\overline{V}Ce_f + MD_1 N\vartheta \right) \\ &= \left(\overline{V}Ce_f + D_1 \left[-\vartheta \;\; \vartheta\right]^T \right)^T \left(\overline{V}Ce_f + D_1 \left[-\vartheta \;\; \vartheta\right]^T \right) \\ &= \left(e_f^T C^T \overline{V}^T + \left[-\vartheta \;\; \vartheta\right] D_1^T \right) \left(\overline{V}Ce_f + D_1 \left[-\vartheta \;\; \vartheta\right]^T \right) \\ &= e_f^T C^T \overline{V}^T \overline{V} C e_f - e_f^T C^T \overline{V}^T D_f \vartheta^T + e_f^T C^T \overline{V}^T D_d \vartheta^T \\ &\quad - \vartheta D_f^T \overline{V} C e_f + \vartheta D_f^T D_f \vartheta^T - \vartheta D_f^T D_d \vartheta^T \\ &\quad + \vartheta D_d^T \overline{V} C e_f - \vartheta D_d^T D_f \vartheta^T + \vartheta D_d^T D_d \vartheta^T. \end{aligned} \tag{26}$$

Therefore,

$$J_1 < \int_0^\infty \Delta dt, \tag{27}$$

where

$$\begin{aligned} \Delta &= e_f^T C^T \overline{V}^T \overline{V} C e_f - e_f^T C^T \overline{V}^T D_f \vartheta^T + e_f^T C^T \overline{V}^T D_d \vartheta^T \\ &\quad - \vartheta D_f^T \overline{V} C e_f + \vartheta D_f^T D_f \vartheta^T - \vartheta D_f^T D_d \vartheta^T \\ &\quad + \vartheta D_d^T \overline{V} C e_f - \vartheta D_d^T D_f \vartheta^T + \vartheta D_d^T D_d \vartheta^T + e_f^T(t) \\ &\quad \cdot \left(P\left(A - \overline{H}C\right) + \left(A - \overline{H}C\right)^T P + P A_d A_d^T P + Q \right) \\ &\quad \cdot e_f(t) + -\alpha^2 \vartheta^T(t) \vartheta(t) \end{aligned} \tag{28}$$

which may be rewritten as

$$J_1 < \int_0^\infty \begin{bmatrix} r_f(t) \\ \vartheta(t) \end{bmatrix}^T \Xi \begin{bmatrix} r_f(t) \\ \vartheta(t) \end{bmatrix} dt. \tag{29}$$

Since $\Xi < 0$, we have $J_1 < 0$ and $\| T_{r_f d}(s) - T_{r_f f}(s) \|_\infty < \alpha$. And since $\| T_{r_f d} \|_\infty - \| T_{r_f f} \|_\infty \le \| T_{r_f d} - T_{r_f f} \|_\infty$, we get $\| T_{r_f d} \|_\infty - \| T_{r_f f} \|_\infty < \alpha$.

If $P(A - \overline{H}C) + (A - \overline{H}C)^T P + PA_d A_d^T P + Q < 0$ holds, that is,

$$\begin{bmatrix} A^T P + PA - YC - C^T Y^T + Q & PA_d \\ A_d^T P & -Q \end{bmatrix} < 0 \tag{30}$$

then, $\dot{V}_1 < 0$ under the condition $\vartheta = 0$. If (19) holds, then (30) holds. Thus, system (7) is asymptotically stable.

The proof is completed. □

3.2. Design of Robust Fault Detection Filter. In this section, we propose a theorem that gives a sufficient condition to guarantee that the RFDF system is stable and has a prescribed H_∞ performance, independently of the time-delay. Before presenting the theorem, the following lemmas are introduced.

Lemma 7. *Given constant matrices $\chi_1 = \chi_1^T$, $\chi_2 = \chi_2^T > 0$, and χ_3, then $\chi_1 + \chi_3^T \chi_2^{-1} \chi_3 < 0$, if and only if*

$$\begin{bmatrix} \chi_1 & \chi_3^T \\ \chi_3 & -\chi_2 \end{bmatrix} < 0$$
$$\text{or equivalently} \begin{bmatrix} -\chi_2 & \chi_3 \\ \chi_3^T & -\chi_1 \end{bmatrix} < 0. \tag{31}$$

Lemma 8. *Let A and B be real matrices of appropriate dimensions. For any scalar $\varepsilon > 0$ and vectors $x, y \in R^n$, the following inequality holds:*

$$2x^T ABy \le \varepsilon^{-1} x^T AA^T x + \varepsilon y^T B^T By. \tag{32}$$

Recall the nonlinear time-delay system (8).

Theorem 9. *For a given positive constant $\gamma > 0$, if there exist a scalar $\varepsilon > 0$ ($2\varepsilon\rho_2^T\rho_2 < Q_1$) and matrices $P_1 = P_1^T > 0$, $P_2 = P_2^T > 0$, $Q_1 = Q_1^T > 0$, $Q_2 = Q_2^T > 0$, Y, and V such that the following LMI:*

$$\begin{bmatrix} \Omega_1 & 0 & P_1A_d & 0 & P_1B_f - YD_f & P_1B_d - YD_d & C^TV^T & P_1G \\ * & \Omega_2 & 0 & P_2A_d & P_2\left(B_f - \overline{H}D_f\right) & P_2\left(B_d - \overline{H}D_d\right) & -C^T\overline{V}^T & 0 \\ * & * & 2\varepsilon\rho_2^T\rho_2 - Q_1 & 0 & 0 & 0 & 0 & 0 \\ * & * & * & Q_2 & 0 & 0 & 0 & 0 \\ * & * & * & * & -\gamma^2 I & 0 & D_f^T\left(V^T - \overline{V}^T\right) & 0 \\ * & * & * & * & * & -\gamma^2 I & D_d^T\left(V^T - \overline{V}^T\right) & 0 \\ * & * & * & * & * & * & -I & 0 \\ * & * & * & * & * & * & * & -\varepsilon I \end{bmatrix} < 0 \tag{33}$$

holds and applying the time-delay adaptive law

$$\dot{\hat{h}} = -\frac{1}{\eta} M \left(\left\| P\overline{\overline{A}}_d \right\| + \left\| P\overline{G}\rho_2 \right\| \right) \alpha(t), \quad \hat{h}(0) > h \tag{34}$$

then system (8), subject to Assumptions 1–3, is stable and satisfies $\|z\|_2 < \gamma\|w\|_2$, where $\hat{h}(t) \ge \overline{h}$, $\Omega_1 = P_1A + A^TP_1 - YC - C^TY^T + 2\varepsilon\rho_1^T\rho_1 + Q_1$, $\Omega_2 = P_2A + A^TP_2 - P_2\overline{H}C - C^T\overline{H}^TP_2 + Q_2$, $\eta > 0$, $\overline{H} = P^{-1}Y$, $\alpha(t) = \|\dot{\hat{x}}(t)\|$, and $Q - I > 0$; I denotes the identity matrix with appropriate dimensions.

Proof. Define the following Lyapunov-Krasovskii function:

$$V_2 = V_1' + V_2' + V_3' + V_4' \tag{35}$$

with

$$\begin{aligned} V_1' &= \eta^T(t) P \eta(t), \\ V_2' &= \int_{t-h}^{t} \eta^T(s) Q \eta(s)\, ds, \\ V_3' &= \frac{\sigma}{2}\left(\hat{h} - h\right)^2, \\ V_4' &= 2M \left(\left\| P\overline{\overline{A}}_d \right\| + \left\| P\overline{G}\rho_2 \right\| \right) \int_{-\hat{h}}^{-h} d\theta \int_{\theta}^{0} \alpha(t+s)\, ds, \end{aligned} \tag{36}$$

where $P = \left[\begin{smallmatrix} P_1 & 0 \\ 0 & P_2 \end{smallmatrix}\right]$, $Q = \left[\begin{smallmatrix} Q_1 & 0 \\ 0 & Q_2 \end{smallmatrix}\right]$.

Differentiating V with respect to time t, one has

$$\begin{aligned} \dot{V}_1'(t) &= 2\eta^T(t) P \left[\overline{A}\eta(t) + \overline{A}_d\eta(t-h) + \overline{G}\Psi + \overline{G}\Delta \right. \\ &\quad \left. + \overline{B}w(t) \right] + 2\eta^T(t) P\overline{\overline{A}}_d \int_{-\hat{h}}^{-h} \dot{\hat{x}}(t+s)\, ds, \\ \dot{V}_2'(t) &= \eta^T(t) Q \eta(t) - \eta^T(t-h) Q \eta(t-h), \\ \dot{V}_3'(t) &= \sigma\left(\hat{h} - h\right)\dot{\hat{h}}, \\ \dot{V}_4'(t) &= 2M \left(\left\| P\overline{\overline{A}}_d \right\| + \left\| P\overline{G}\rho_2 \right\| \right) \\ &\quad \cdot \left\{ \int_{-\hat{h}}^{-h} \left[\alpha(t) - \alpha(t+\theta) \right] d\theta + \dot{\hat{h}} \int_{-\hat{h}}^{0} \alpha(t+s)\, ds \right\} \\ &= 2M \left(\left\| P\overline{\overline{A}}_d \right\| + \left\| P\overline{G}\rho_2 \right\| \right) \left[\int_{-\hat{h}}^{-h} \alpha(t)\, d\theta \right. \\ &\quad \left. - \int_{-h}^{-\hat{h}} \alpha(t+\theta)\, d\theta + \dot{\hat{h}} \int_{-\hat{h}}^{0} \alpha(t+s)\, ds \right] \\ &= -2M \left(\left\| P\overline{\overline{A}}_d \right\| + \left\| P\overline{G}\rho_2 \right\| \right) \\ &\quad \cdot \left[\left(\hat{h} - h\right) \alpha(t) \int_{-\hat{h}}^{-h} \alpha(t+\theta)\, d\theta \right. \\ &\quad \left. + \dot{\hat{h}} \int_{-\hat{h}}^{0} \alpha(t+s)\, ds \right]. \end{aligned} \tag{37}$$

From Assumption 2, it yields

$$\begin{aligned}\|\Psi\| &\le \left\|\rho_1\left(x(t)-\widehat{x}(t)\right)\right\| \\ &\quad+\left\|\rho_2\left(x(t-h)-\widehat{x}\left(t-\widehat{h}\right)\right)\right\| \\ &\le \left\|\rho_1 e(t)\right\|+\left\|\rho_2\left(\widehat{x}(t-h)-\widehat{x}\left(t-\widehat{h}\right)\right)\right\| \\ &= \left\|\rho_1 e(t)\right\|+\left\|\rho_2\int_{-\widehat{h}}^{-h}\dot{\widehat{x}}(t+s)\,ds\right\|.\end{aligned} \tag{38}$$

From Lemma 8, one has

$$\begin{aligned}2\eta^T(t)P\overline{G}\Psi &\le 2\left\|\eta^T(t)\right\|\cdot\left\|P\overline{G}\right\|\cdot\|\Psi\| \\ &\le 2\|\eta(t)\|\cdot\left\|P\overline{G}\right\| \\ &\quad\cdot\left(\left\|\rho_1 e(t)\right\|+\left\|\rho_2\int_{-\widehat{h}}^{-h}\dot{\widehat{x}}(t+s)\,ds\right\|\right) \\ &\le 2\|\eta(t)\|\cdot\left\|P\overline{G}\right\| \\ &\quad\cdot\left(\left\|\rho_1 e(t)\right\|+\|\rho_2\|\int_{-\widehat{h}}^{-h}\left\|\dot{\widehat{x}}(t+s)\right\|ds\right) \\ &\le 2\|\eta(t)\|\cdot\left\|P\overline{G}\right\| \\ &\quad\cdot\left(\left\|\rho_1 e(t)\right\|+\|\rho_2\|\int_{-\widehat{h}}^{-h}\alpha(t+s)\,ds\right) \\ &\le \varepsilon^{-1}\eta^T(t)P\overline{G}\,\overline{G}^T P\eta(t)+2\varepsilon e^T(t)\rho_1^T\rho_1 e(t) \\ &\quad+2\|\eta(t)\|\cdot\left\|P\overline{G}\rho_2\right\|\int_{-\widehat{h}}^{-h}\alpha(t+s)\,ds.\end{aligned} \tag{39}$$

Then

$$\begin{aligned}\dot{V}_2 &\le \varepsilon^{-1}\eta^T(t)P\overline{G}\,\overline{G}^T P\eta(t)+2\varepsilon e^T(t)\rho_1^T\rho_1 e(t) \\ &\quad+2\|\eta(t)\|\cdot\left\|P\overline{G}\right\|\cdot\|\rho_2\|\int_{-\widehat{h}}^{-h}\alpha(t+s)\,ds+\eta^T(t) \\ &\quad\cdot Q\eta(t)-\eta^T(t-h)Q\eta(t-h)+\sigma\left(\widehat{h}-h\right)\dot{\widehat{h}} \\ &\quad-2M\left\|P\overline{\overline{A}}_d\right\|\left[\left(\widehat{h}-h\right)\alpha(t)-\int_{-\widehat{h}}^{-h}\alpha(t+\theta)\,d\theta\right. \\ &\quad\left.+\dot{\widehat{h}}\int_{-\widehat{h}}^{0}\alpha(t+s)\,ds\right].\end{aligned} \tag{40}$$

Since $\dot{\widehat{h}}=-(1/\eta)M(\|P\overline{\overline{A}}_d\|+\|P\overline{G}\rho_2\|)\alpha(t)$, we have $\dot{\widehat{h}}\int_{-\widehat{h}}^{0}\alpha(t+s)ds\le 0$. Because $\|x(t)-\widehat{x}(t)\|=\|e(t)\|\le M$, and the above fault detection observer error is equal to zero under ideal condition, it holds that $\|\eta(t)\|\le M$. □

From Lemma 8, one has

$$\begin{aligned}\dot{V}_2 &\le 2\eta^T(t)P\left[\overline{A}\eta(t)+\overline{A}_d\eta(t-h)+\overline{B}w(t)\right] \\ &\quad+\varepsilon^{-1}\eta^T(t)P\overline{G}\,\overline{G}^T P\eta(t)+2\varepsilon e^T(t)\rho_1^T\rho_1 e(t) \\ &\quad+\eta^T(t)Q\eta(t)-\eta^T(t-h)Q\eta(t-h).\end{aligned} \tag{41}$$

And $e(t)=\begin{bmatrix}I & 0\end{bmatrix}\begin{bmatrix}e(t)\\ e_f(t)\end{bmatrix}=\begin{bmatrix}I & 0\end{bmatrix}\eta(t)$, $e(t-h)=\begin{bmatrix}I & 0\end{bmatrix}\begin{bmatrix}e(t-h)\\ e_f(t-h)\end{bmatrix}=\begin{bmatrix}I & 0\end{bmatrix}\eta(t-h)$. Thus, (41) can be rewritten as

$$\begin{aligned}\dot{V}_2 &\le 2\eta^T(t)P\left[\overline{A}\eta(t)+\overline{A}_d\eta(t-h)+\overline{B}w(t)\right] \\ &\quad+\varepsilon^{-1}\eta^T(t)P\overline{G}\,\overline{G}^T P\eta(t) \\ &\quad+2\varepsilon\eta^T(t)\begin{bmatrix}I\\0\end{bmatrix}\rho_1^T\rho_1\begin{bmatrix}I\\0\end{bmatrix}^T\eta(t)+\eta^T(t)Q\eta(t) \\ &\quad-\eta^T(t-h)Q\eta(t-h) \\ &= \eta^T(t)P\left[\overline{A}\eta(t)+\overline{A}_d\eta(t-h)+\overline{B}w(t)\right] \\ &\quad+\left[\overline{A}\eta(t)+\overline{A}_d\eta(t-h)+\overline{B}w(t)\right]^T P\eta(t) \\ &\quad+\varepsilon^{-1}\eta^T(t)P\overline{G}\,\overline{G}^T P\eta(t) \\ &\quad+2\varepsilon\eta^T(t)\begin{bmatrix}\rho_1^T\rho_1 & 0\\ 0 & 0\end{bmatrix}\eta(t)+\eta^T(t)Q\eta(t) \\ &\quad-\eta^T(t-h)Q\eta(t-h).\end{aligned} \tag{42}$$

Consider the following performance index:

$$\begin{aligned}J_2 &= \int_0^\infty r_e^T(t)r_e(t)\,dt-\gamma^2\int_0^\infty w^T(t)w(t)\,dt \\ &= \int_0^\infty\left[r_e^T(t)r_e(t)-\gamma^2 w^T(t)w(t)+\dot{V}_2(t)\right]dt \\ &\quad-V_2(t)\big|_t+V_2(t)\big|_{t=0} \\ &\le \int_0^\infty\left[r_e^T(t)r_e(t)-\gamma^2 w^T(t)w(t)+\dot{V}_2(t)\right]dt \\ &\le \int_0^\infty\begin{bmatrix}\eta(t)\\ \eta(t-h)\\ w(t)\end{bmatrix}^T\Omega\begin{bmatrix}\eta(t)\\ \eta(t-h)\\ w(t)\end{bmatrix}dt,\end{aligned} \tag{43}$$

where

$$\Omega = \begin{bmatrix} \overline{A}^T P + P\overline{A} + \begin{bmatrix} 2\varepsilon\rho_1^T\rho_1 & 0 \\ 0 & 0 \end{bmatrix} + Q & P\overline{A}_d & P\overline{B} & \overline{C}^T & P\overline{G} \\ \overline{A}_d^T P & \begin{bmatrix} 2\varepsilon\rho_2^T\rho_2 & 0 \\ 0 & 0 \end{bmatrix} & 0 & 0 & 0 \\ \overline{B}^T P & 0 & -\gamma^2 I & D^T & 0 \\ C & 0 & D & -I & 0 \\ \overline{G}^T P & 0 & 0 & 0 & -\varepsilon I \end{bmatrix}. \tag{44}$$

From (35), one has $\Omega < 0$. Hence $J_2 < 0$ and $\|z\|_2 < \gamma\|w\|_2$.

If $w(t) = 0$, from the above analysis, one has

$$J_2 \le \int_0^\infty \begin{bmatrix} \eta(t) \\ \eta(t-h) \\ w(t) \end{bmatrix}^T \Omega' \begin{bmatrix} \eta(t) \\ \eta(t-h) \\ w(t) \end{bmatrix} dt, \tag{45}$$

where $\Omega' = \begin{bmatrix} \overline{A}^T P + P\overline{A} + \varepsilon^{-1} P\overline{G}\overline{G}^T P + 2\varepsilon\rho_1^T\rho_1 + \overline{C}^T\overline{C} + Q & P\overline{A}_d & 0 \\ \overline{A}_d^T P & -Q & 0 \\ 0 & 0 & -\gamma^2 I \end{bmatrix}$.

Obviously, $\Omega < 0 \Rightarrow \Omega' < 0$. Furthermore, transferring Ω', one has

$$\begin{bmatrix} \overline{A}^T P + P\overline{A} + 2\varepsilon\rho_1^T\rho_1 + \overline{C}^T\overline{C} + Q & P\overline{A}_d & P\overline{G} \\ \overline{A}_d^T P & -Q & 0 \\ \overline{G}^T P & 0 & -\varepsilon I \end{bmatrix} < 0 \tag{46}$$

which implies that if $w(t) = 0$, then $\dot{V}_2 < 0$. If (35) holds, then (46) holds. Hence, system (8) is stable.

The proof is completed.

The last step of fault detection is to evaluate the residual. This is a decision making process that always comes down to a threshold logic of a decision function. From Assumption 2 ($d \in L_2$), we can further have $\|d(t)\|_2 = S$, where $S > 0$ is a constant. By using Theorem 9, we obtain $\gamma_d = \sup_{d\in L_2}\|r\|_2/\|d\|_2$. In the fault-free case, the generated residual $r(t)$ is only affected by the disturbance input $d(t)$. Therefore, the threshold J_{th} can be determined by

$$J_{\text{th}} = \gamma_d \|d(t)\|_2 = \gamma_d S. \tag{47}$$

The fault detection decision logic can be designed as

$$\begin{aligned} &\|r(t)\|_{2,\tau} > J_{\text{th}} \Longrightarrow \text{a fault has occured} \Longrightarrow \text{alarm} \\ &\|r(t)\|_{2,\tau} < J_{\text{th}} \Longrightarrow \text{no fault has occured.} \end{aligned} \tag{48}$$

Remark 10. In [18], Ψ was described as $\Psi = g(x(t), x(t-h)) - g(\hat{x}(t), \hat{x}(t-h))$. From Assumption 2 in [18], one has

$$\begin{aligned} \|\Psi\| &\le \|\rho_1(x(t) - \hat{x}(t))\| \\ &\quad + \|\rho_2(x(t-h) - \hat{x}(t-h))\| \\ &\le \|\rho_1 e(t)\| + \|\rho_2 e(t-h)\|, \\ \|\Psi\|^2 &\le 2\|\rho_1 e(t)\|^2 + 2\|\rho_2 e(t-h)\|^2. \end{aligned} \tag{49}$$

However, if time-delay h is an unknown constant, $\|\Psi\|$ and $\|\Psi\|^2$ are not available and can not be used in the design procedure. In this paper, an improved observer is proposed, in which h is replaced by the estimation value $\hat{h}$. Then, Ψ is presented in the following form:

$$\Psi = g(x(t), x(t-h)) - g\left(\hat{x}(t), \hat{x}\left(t-\hat{h}\right)\right). \tag{50}$$

Furthermore, by using Newton-Leibniz Formula, one has

$$\begin{aligned} \|\Psi\| &\le \|\rho_1(x(t) - \hat{x}(t))\| \\ &\quad + \left\|\rho_2\left(x(t-h) - \hat{x}\left(t-\hat{h}\right)\right)\right\| \\ &\le \|\rho_1 e(t)\| + \left\|\rho_2 \int_{-\hat{h}}^{-h} \dot{\hat{x}}(t+s)\, ds\right\|. \end{aligned} \tag{51}$$

3.3. Fault Estimation. After detecting the fault, fault isolation and estimation are considered. Similar to [21], by a bank of so-called fault isolation observers, fault pattern and location can be obtained. In this paper, it is assumed that faults have been isolated and fault isolation is not studied further. In the following, we will investigate the fault estimation problem.

In order to estimate the fault, a following observer is constructed:

$$\begin{aligned} \dot{\hat{x}}(t) &= A\hat{x}(t) + A_d\hat{x}\left(t-\hat{h}\right) + Bu(t) \\ &\quad + Gg\left(\hat{x}(t), \hat{x}\left(t-\hat{h}\right)\right) + B_f\hat{f}(t) \\ &\quad + H\left[y(t) - \hat{y}(t)\right], \\ \hat{y}(t) &= C\hat{x}(t) + Du(t) + D_f\hat{f}(t), \\ r(t) &= V\left[y(t) - \hat{y}(t)\right], \end{aligned} \tag{52}$$

where $\hat{x}(t) \in R^n$ is the observer state vector, $\hat{y}(t) \in R^q$ is the observer output vector, $\hat{h}$ and $\hat{f}$ are the estimation values of h and f, respectively, and $r(t)$ is the so-called generated residual signal. The observer gain matrix H and the residual weighting matrix V will be defined later.

Let

$$\begin{aligned} e &= x(t) - \hat{x}(t), \\ \tilde{f} &= f(t) - \hat{f}(t). \end{aligned} \tag{53}$$

Then, the error dynamics can be described as

$$\begin{aligned} \dot{e}(t) &= (A - HC)e(t) + A_d\hat{x}\left(t - \hat{h}\right) - A_d x(t-h) \\ &\quad + \left(B_f - HD_f\right)\tilde{f}(t) + \left(B_d - HD_d\right)d(t) \\ &\quad + G\Psi \\ &= (A - HC)e(t) + A_d\hat{x}\left(t - \hat{h}\right) - A_d\hat{x}(t-h) \\ &\quad + A_d\hat{x}(t-h) - A_d x(t-h) \\ &\quad + \left(B_f - HD_f\right)\tilde{f}(t) + \left(B_d - HD_d\right)d(t) \\ &\quad + G\Psi \\ &= (A - HC)e(t) + A_d e(t-h) + A_d\hat{x}\left(t - \hat{h}\right) \\ &\quad - A_d\hat{x}(t-h) + \left(B_f - HD_f\right)\tilde{f}(t) \\ &\quad + \left(B_d - HD_d\right)d(t) + G\Psi, \end{aligned} \tag{54}$$

where $\Psi = g(x(t), x(t-h)) - g(\hat{x}(t), \hat{x}(t-\hat{h}))$.

By using Newton-Leibniz Formula, one has

$$\hat{x}\left(t - \hat{h}\right) - \hat{x}(t-h) = \int_{-h}^{-\hat{h}} \dot{\hat{x}}(t+s)\,ds. \tag{55}$$

Equation (54) can be rewritten as

$$\begin{aligned} \dot{e}(t) &= (A - HC)e(t) + A_d e(t-h) \\ &\quad + A_d\int_{-h}^{-\hat{h}} \dot{\hat{x}}(t+s)\,ds + \left(B_f - HD_f\right)\tilde{f}(t) \\ &\quad + \left(B_d - HD_d\right)d(t) + G\Psi, \\ r(t) &= VCe(t) + VD_f\tilde{f}(t) + VD_d d(t). \end{aligned} \tag{56}$$

To realize the above-mentioned fault diagnosis objective, the following Theorem 11 is proposed.

Theorem 11. *Consider system (1) subject to Assumptions 1–3. For a given positive constant $\alpha > 0$, if there exist a scalar $\varepsilon > 0$ and matrices $P_1 = P_1^T > 0$, $P_2 = P_2^T > 0$, $Q_1 = Q_1^T > 0$, $Q_2 = Q_2^T > 0$, Y, and V such that*

$$\Xi = \begin{bmatrix} \Omega_1 & 0 & P_1A_d & 0 & P_1B_f - YD_f & P_1B_d - YD_d & C^TV^T & P_1G \\ * & \Omega_2 & 0 & P_2A_d & P_2\left(B_f - \overline{H}D_f\right) & P_2\left(B_d - \overline{H}D_d\right) & -C^T\overline{V}^T & 0 \\ * & * & 2\varepsilon\rho_2^T\rho_2 - Q_1 & 0 & 0 & 0 & 0 & 0 \\ * & * & * & Q_2 & 0 & 0 & 0 & 0 \\ * & * & * & * & -\gamma^2 I & 0 & D_f^T\left(V^T - \overline{V}^T\right) & 0 \\ * & * & * & * & * & -\gamma^2 I & D_d^T\left(V^T - \overline{V}^T\right) & 0 \\ * & * & * & * & * & * & -I & 0 \\ * & * & * & * & * & * & * & -\varepsilon I \end{bmatrix} < 0, \tag{57}$$

$$FC = \left(B_f - HD_f\right)^T P \tag{58}$$

then, using the following adaptive laws:

$$\begin{aligned} \dot{\hat{h}} &= -\frac{1}{\eta}M\left(\|PA_d\| + \|PG\rho_2\|\right)\alpha(t), \quad \hat{h}(0) > \overline{h}, \\ \dot{\hat{f}}(t) &= -\eta_f^{-1}\Gamma F e_y(t), \quad \dot{\hat{f}}(0) = 0, \end{aligned} \tag{59}$$

the closed-loop system (56) is stable with $\|e\|_2 < \alpha\|d\|_2$, where $\alpha(t) = \|\dot{\hat{x}}(t)\|$, $\eta_f > 0$, and $\Gamma = \Gamma^T > 0$ are adaptive rates, and η is selected such that $\hat{h}(0) \geq \overline{h}$, $Q - I > 0$, and I denotes the identity matrix with appropriate dimensions.

Proof. Define the following Lyapunov-Krasovskii function:

$$\begin{aligned} V_3(t) &= e^T(t)Pe(t) + \int_{t-h}^{t} e^T(\tau)Qe(\tau)\,d\tau \\ &\quad + 2M\left(\|PA_d\| + \|PG\rho_2\|\right)\int_{-\hat{h}}^{-h} d\theta\int_{\theta}^{0}\alpha(t+s)\,ds \\ &\quad + \frac{\eta}{2}\left(\hat{h} - h\right)^2 + \eta_f\left(\hat{f} - f\right)^T\Gamma^{-1}\left(\hat{f} - f\right), \end{aligned} \tag{60}$$

where $P = \left[\begin{smallmatrix} P_1 & 0 \\ 0 & P_2 \end{smallmatrix}\right]$, $Q = \left[\begin{smallmatrix} Q_1 & 0 \\ 0 & Q_2 \end{smallmatrix}\right]$.

Differentiating V_3 with respect to time t, one has

$$\begin{aligned}\dot{V}_3 \le{}& e^T(t)\left(P(A-HC)+(A-HC)^T P\right)e(t)\\ &+ e^T(t)PA_dA_d^TPe(t)+e^T(t-h)e(t-h)+2e^T(t)\\ &\cdot P\left(A_d\int_{-h}^{-\hat{h}}\dot{\hat{x}}(t+s)\,ds+G\Psi\right)+2e^T(t)P\left(B_f\right.\\ &\left.-HD_f\right)\tilde{f}+2e^T(t)P\left(B_d-HD_d\right)d(t)+e^T(t)\\ &\cdot Qe(t)-e^T(t-h)Qe(t-h)+\eta\left(\hat{h}-h\right)\dot{\hat{h}}\\ &-2M\left(\|PA_d\|+\|PG\rho_2\|\right)\left[\left(\hat{h}-h\right)\alpha(t)\right.\\ &\left.-\int_{-\hat{h}}^{-h}\alpha(t+\theta)\,d\theta+\dot{\hat{h}}\int_{-\hat{h}}^{0}\alpha(t+s)\,ds\right]\\ &+2\eta_f\tilde{f}^T\Gamma^{-1}\dot{\tilde{f}}.\end{aligned}\tag{61}$$

From Assumption 2 and $\|\Psi\| \le \|\rho_1 e(t)\| + \|\rho_2 \int_{-\hat{h}}^{-h}\dot{\hat{x}}(t+s)ds\|$, it yields

$$\begin{aligned}2e^T(t)PG\Psi \le{}& \varepsilon^{-1}e^T(t)PGG^TPe(t)\\ &+2\varepsilon e^T(t)\rho_1^T\rho_1 e(t)+2\|e(t)\|\\ &\cdot\|PG\rho_2\|\int_{-\hat{h}}^{-h}\alpha(t+s)\,ds.\end{aligned}\tag{62}$$

Because $\dot{\hat{h}} = -(1/\eta)M(\|PA_d\| + \|PG\rho_2\|)\alpha(t) \le 0$, we have $\dot{\hat{h}}\int_{-\hat{h}}^{0}\alpha(t+s)ds \le 0$. Notice that $Q - I > 0$; then

$$\begin{aligned}\dot{V}_3 \le{}& e^T(t)\left(P(A-HC)+(A-HC)^TP+PA_dA_d^TP\right.\\ &\left.+Q+\varepsilon^{-1}PGG^TP+2\varepsilon\rho_1^T\rho_1\right)e(t)+2e^T(t)P\left(B_f\right.\\ &\left.-HD_f\right)\tilde{f}+2e^T(t)P\left(B_d-HD_d\right)d(t)\\ &+2\eta_f\tilde{f}^T\Gamma^{-1}\dot{\tilde{f}}\le e^T(t)\left(P(A-HC)\right.\\ &+(A-HC)^TP+PA_dA_d^TP+Q+\varepsilon^{-1}PGG^TP\\ &\left.+2\varepsilon\rho_1^T\rho_1\right)e(t)-2\tilde{f}^TFD_f\tilde{f}(t)-2\tilde{f}^TFD_dd(t)\\ &+2e^T(t)P\left(B_d-HD_d\right)d(t).\end{aligned}\tag{63}$$

Now, define the following performance index:

$$\begin{aligned}J_3 &= \int_0^\infty e^T(t)e(t)\,dt-\alpha^2\int_0^\infty d^T(t)d(t)\,dt\\ &= \int_0^\infty\left[e^T(t)e(t)-\alpha^2d^T(t)d(t)+\dot{V}_3(t)\right]dt\\ &\quad -V_1(t)\big|_t+V_3(t)\big|_{t=0}\end{aligned}\tag{64}$$

Since under zero initial condition and $\hat{h}(0) > h$ and $V_1(t)|_{t=0} = 0$, $V_1(t) \ge 0$ for all t. Thus,

$$\begin{aligned}J_3 <{}& \int_0^\infty\left[e^T(t)\left(P(A-HC)+(A-HC)^TP\right.\right.\\ &+PA_dA_d^TP+Q+\varepsilon^{-1}PGG^TP+2\varepsilon\rho_1^T\rho_1+I\left.\right)e(t)\\ &-2\tilde{f}^TFD_f\tilde{f}(t)-2\tilde{f}^TFD_dd(t)+2e^T(t)P\left(B_d\right.\\ &\left.\left.-HD_d\right)d(t)-\alpha^2d^T(t)d(t)\right]dt\end{aligned}\tag{65}$$

which can be rewritten as

$$J_3 < \int_0^\infty\begin{bmatrix}e(t)\\ \tilde{f}(t)\\ d(t)\end{bmatrix}^T\Xi_1\begin{bmatrix}e(t)\\ \tilde{f}(t)\\ d(t)\end{bmatrix}dt,\tag{66}$$

where

$$\Xi_1 = \begin{bmatrix}P(A-HC)+(A-HC)^TP+PA_dA_d^TP+Q+\varepsilon^{-1}PGG^TP+2\varepsilon\rho_1^T\rho_1+I & 0 & \left(B_d-HD_d\right)^TP\\ 0 & -FD_f & -D_d^TF\\ P\left(B_d-HD_d\right) & -D_dF & -\alpha^2I\end{bmatrix}\tag{67}$$

From (57), one has $\Xi_1 < 0$. Therefore, $J_3 < 0$ with $\|e\|_2 < \alpha\|d\|_2$. If

$$\Xi_1' = \begin{bmatrix}P(A-HC)+(A-HC)^TP+PA_dA_d^TP+Q+\varepsilon^{-1}PGG^TP+2\varepsilon\rho_1^T\rho_1+I & 0 & 0\\ 0 & -FD_f & 0\\ 0 & 0 & -\alpha^2I\end{bmatrix} < 0.\tag{68}$$

holds, then, $\dot{V}_3 < 0$ under the condition $d(t) = 0$. Obviously, if (57) holds, then (68) holds. Therefore, system (56) is asymptotically stable.

The proof is completed. □

Remark 12. Because of the existence of unknown disturbances, from the fault detection mechanism (54), the adaptive laws can be redesigned as

$$\dot{\hat{f}} = P\left\{-\eta_f^{-1}\Gamma F e_y(t) D\left[e_y(t), J(t)\right]\right\}, \tag{69}$$

where the dead-zone operator $D[\cdot]$ is defined by

$$D\left[e_y(t), r(t)\right] = \begin{cases} 0, & \|J(t)\| \le J_{\text{th}} \\ e_y(t), & \|J(t)\| > J_{\text{th}}, \end{cases} \tag{70}$$

where $J_{\text{th}} = \gamma_d \|d(t)\|_2 = \gamma_d S$.

Remark 13. If there exist two known constants $f_{\min}, f_{\max}$ such that $f_{\min} \le |f(t)| \le f_{\max}$, then the fault $f(t)$ can be modeled in the following form:

$$f(t) = \frac{1}{2}\left(f_{\max} - f_{\min}\right)(1 - \tanh\theta) + f_{\min}, \tag{71}$$

where θ is an unknown constant. Thus, estimating the fault $f(t)$ consists in estimating θ; that is to say

$$\dot{\hat{f}}(t) = \frac{1}{2}\left(f_{\max} - f_{\min}\right)\left(1 - \tanh\dot{\hat{\theta}}\right) + f_{\min} \tag{72}$$

which prevents the phenomenon of parameter drift in the presence of bounded disturbances and ensures $f_{\min} \le |\hat{f}(t)| \le f_{\max}$.

4. Simulation Results

Consider the following time-delayed nonlinear system:

$$\begin{aligned} \dot{x}(t) &= Ax(t) + A_d x(t-d) + Bu(t) \\ &\quad + Gg(x(t), x(t-h)) + B_f f(t) + B_d d(t), \\ y(t) &= Cx(t) + Du(t) + Gg(x(t), x(t-h)) \\ &\quad + D_f f(t) + D_d d(t), \\ x(t) &= 0, \quad t \in [-h, 0], \end{aligned} \tag{73}$$

where

$$\begin{aligned} A &= \begin{bmatrix} -1.2 & 0.1 \\ -0.1 & -1.0 \end{bmatrix}, \\ A_d &= \begin{bmatrix} -0.6 & 0.7 \\ -1.0 & -0.8 \end{bmatrix}, \\ B &= \begin{bmatrix} 0 \\ 0.2 \end{bmatrix}, \\ C &= \begin{bmatrix} 1 & 0 \\ 0 & 1 \end{bmatrix}, \\ D &= 0, \\ G &= \begin{bmatrix} 0.1 & 0.3 \\ 0.2 & 0.5 \end{bmatrix}, \\ B_f &= \begin{bmatrix} 0.7 & 0 \\ -0.5 & 0 \end{bmatrix}, \\ B_d &= \begin{bmatrix} 0 & 1.0 \\ 0 & 0.2 \end{bmatrix}, \\ D_f &= \begin{bmatrix} 0 & -0.4 \\ 0 & 0.8 \end{bmatrix}, \\ D_d &= \begin{bmatrix} 1.5 & 0 \\ 0.2 & 0 \end{bmatrix}, \\ g(x(t), x(t-h)) &= \sin 0.2x(t) + \sin 0.1x(t-h), \\ h &= 0.5\,\text{s}, \\ d &= 0.1\sin t. \end{aligned} \tag{74}$$

From Theorem 6, by solving LMI (19), one has

$$\begin{aligned} P &= \begin{bmatrix} 0.6248 & 0.0610 \\ 0.0610 & 0.4262 \end{bmatrix}, \\ Q &= \begin{bmatrix} 1.1752 & -0.1434 \\ -0.1434 & 1.4028 \end{bmatrix}, \\ Z &= \begin{bmatrix} 0.8685 & 0.0672 \\ 0.0672 & 1.8887 \end{bmatrix}, \\ Y &= \begin{bmatrix} 0.8536 & -0.5914 \\ 0.2573 & 1.9270 \end{bmatrix}, \\ \alpha_{\min} &= 0.6391. \end{aligned} \tag{75}$$

Furthermore, we obtain the observer gain matrix $\overline{H}$ and the residual weighting matrix $\overline{V}$,

$$\overline{H} = \begin{bmatrix} 1.3259 & -1.4076 \\ 0.4140 & 4.7225 \end{bmatrix},$$
$$\overline{V} = \begin{bmatrix} 0.9315 & 0.0291 \\ 0.0291 & 1.3740 \end{bmatrix}. \quad (76)$$

In this study, $\varepsilon, \rho_1, \rho_2$ are selected as [16, 18]

$$\varepsilon = 0.1,$$
$$\rho_1 = \begin{bmatrix} 0.2 & 0.1 \\ 0.3 & 0.2 \end{bmatrix}, \quad (77)$$
$$\rho_2 = \begin{bmatrix} 0.1 & 0.2 \\ 0.3 & 0.1 \end{bmatrix}.$$

By using Theorem 11, we obtain the solutions of LMI (35) with P_1, P_2, Q_1, Q_2, V, Y and minimal $\gamma_{\min}$, respectively, as follows:

$$P_1 = \begin{bmatrix} 24.0724 & -12.6296 \\ -12.6296 & 10.7939 \end{bmatrix},$$
$$Q_1 = \begin{bmatrix} 44.0436 & 2.0634 \\ 2.0634 & 71.8486 \end{bmatrix},$$
$$P_2 = \begin{bmatrix} 29.9378 & 8.3931 \\ 8.3931 & 16.0890 \end{bmatrix},$$
$$Q_2 = \begin{bmatrix} 64.3589 & 17.5958 \\ 17.5958 & 67.3153 \end{bmatrix}, \quad (78)$$
$$V = \begin{bmatrix} 0.4468 & -0.0364 \\ -0.0364 & 0.0128 \end{bmatrix},$$
$$Y = \begin{bmatrix} 35.0527 & 28.7520 \\ 28.7520 & 78.3480 \end{bmatrix},$$
$$\gamma_{\min} = 0.6402.$$

Then, one has the observer gain matrix H:

$$H = \begin{bmatrix} 4.2442 & 12.9558 \\ 5.3140 & 22.4176 \end{bmatrix}. \quad (79)$$

In this paper, to illustrate the effectiveness of the proposed algorithm, two fault cases are considered: abrupt fault case and incipient fault case.

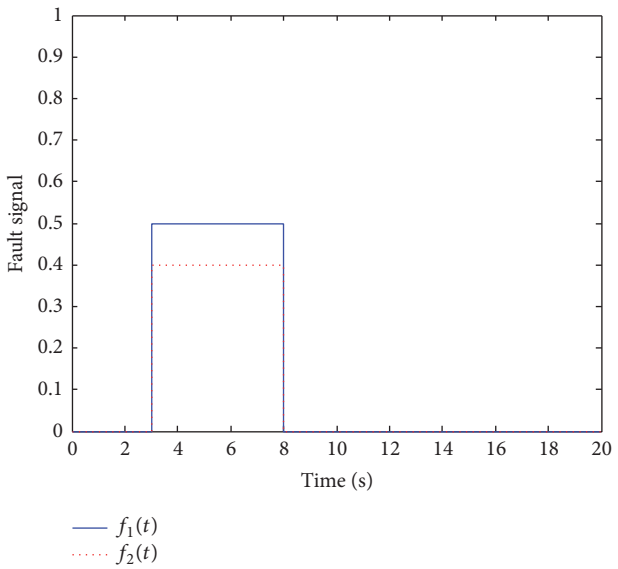

Figure 1: Fault signal $f(t)$.

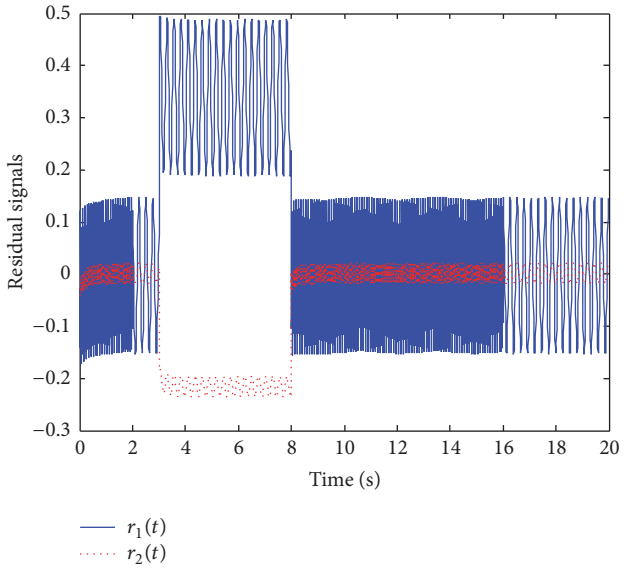

Figure 2: Generated residual $r(t)$.

4.1. Abrupt Fault Case. In this case, fault $f(t) = [f_1(t), f_2(t)]^T$ is defined in following form:

$$f_1(t) = \begin{cases} 0, & 0 \le t \le 3 \\ 0.5, & 3 < t \le 8 \\ 0, & t > 8, \end{cases}$$
$$f_2(t) = \begin{cases} 0, & 0 \le t \le 3 \\ 0.4, & 3 < t \le 8 \\ 0, & t > 8. \end{cases} \quad (80)$$

The fault signal $f(t)$ and the generated residual signals $r(t)$ (including $r_1(t)$ and $r_2(t)$) are shown in Figures 1 and 2, respectively. Figure 3 shows the evolution of residual

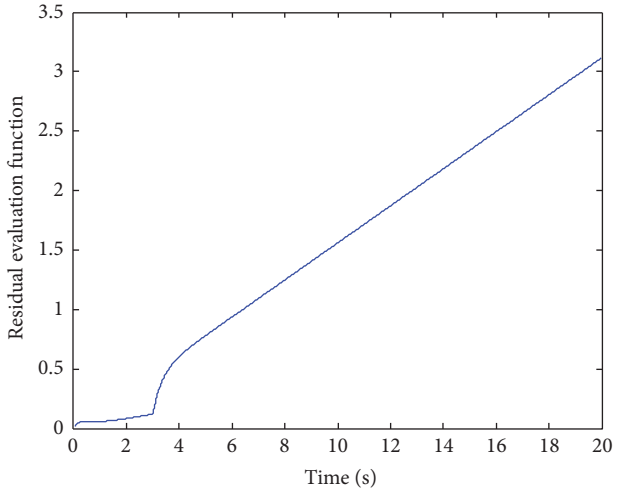

Figure 3: Evolution of the residual evaluation function $\|r(t)\|$.

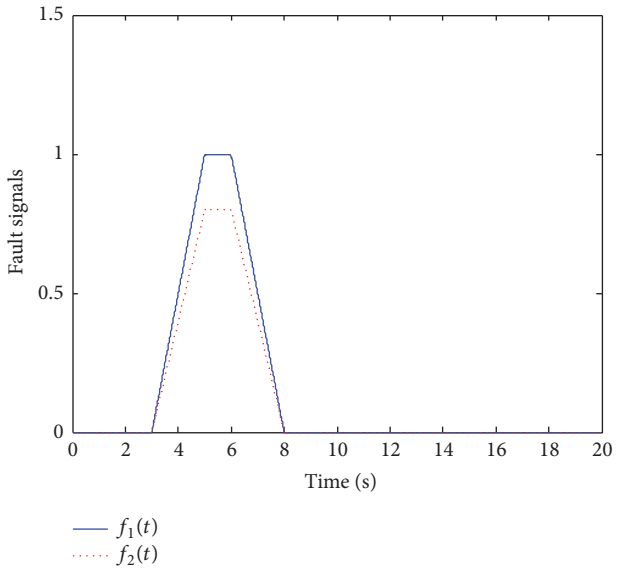

Figure 4: Fault signal $f(t)$.

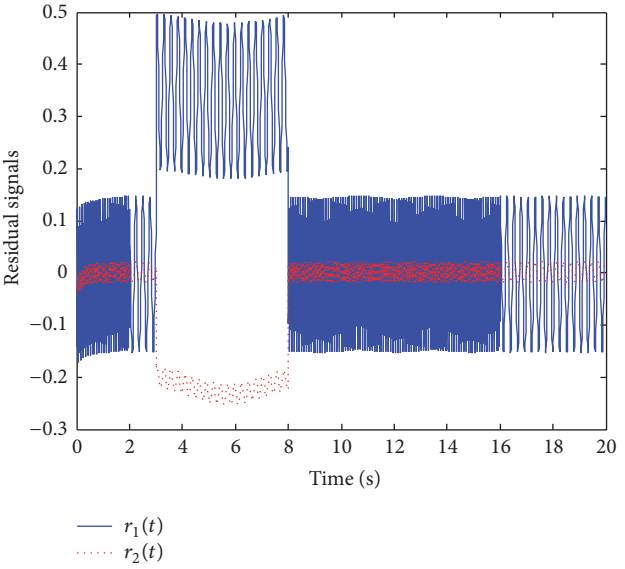

Figure 5: Generated residual $r(t)$.

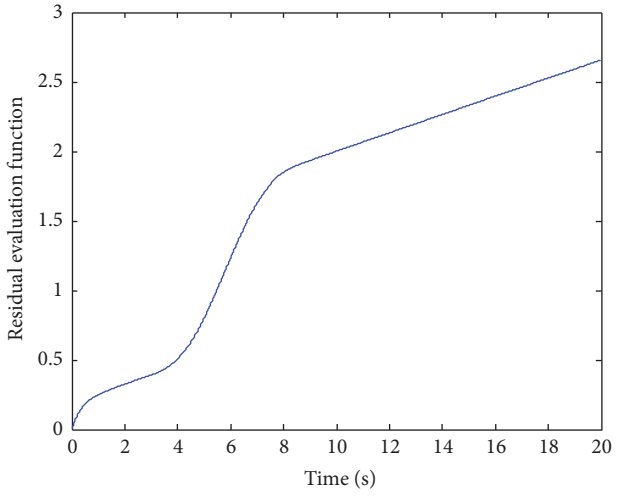

Figure 6: Evolution of the residual evaluation function $\|r(t)\|$.

evaluation function $\|r(t)\|$, from which the fault can be detected.

4.2. Incipient Fault Case. As pointed out in [18], in many real physical systems, the fault evolves slowly. In this case, the fault $f(t)$ is assumed to be an incipient fault, which is shown in Figure 4. The generated residual signals $r(t)$ (including $r_1(t)$ and $r_2(t)$) and the evolution of residual evaluation function are illustrated in Figures 5 and 6, respectively.

5. Conclusions

In this paper, the problem of fault detection and estimation of nonlinear time-delayed systems with constant but unknown state time-delay is studied. A new fault detection filter with adaptation to the time-delay is proposed. Then, a reference residual model is introduced to formulate the robust fault detection filter design problem as an H_∞ model-matching problem. A novel robust adaptive fault estimation algorithm is proposed where the time derivative of the output errors has not been computed. In addition, applying a robust H_∞ optimization control technique, sufficient conditions for the existence of the fault detection filter are derived in terms of LMI. In future, we will consider the fault diagnosis and fault tolerant control of actuators and sensors when both the input and the state are time-delay.

Conflicts of Interest

The authors declare that they have no conflicts of interest.

Acknowledgments

This work is supported by National Natural Science Foundation of China (61503156, 61403161, and 61473250) and the Fundamental Research Funds for the Central Universities (JUSRP11562, NJ20150011) and National Key Research and Development Program (2016YFD0400301).

References

[1] J. Liu, W. Luo, X. Yang, and L. Wu, "Robust Model-Based Fault Diagnosis for PEM Fuel Cell Air-Feed System," *IEEE Transactions on Industrial Electronics*, vol. 63, no. 5, pp. 3261–3270, 2016.

[2] J. Liu, C. Wu, Z. Wang, and L. Wu, "Reliable Filter Design for Sensor Networks in the Type-2 Fuzzy Framework," *IEEE Transactions on Industrial Informatics*, vol. PP, no. 99, 1 page, 2017.

[3] Q. Zhao and J. Jiang, "Reliable state feedback control systems designs against actuator failures," *Automatica*, vol. 34, no. 10, pp. 1267–1272, 1998.

[4] X. Tang, G. Tao, and S. M. Joshi, "Adaptive output feedback actuator failure compensation for a class of non-linear systems," *International Journal of Adaptive Control and Signal Processing*, vol. 19, no. 6, pp. 419–444, 2005.

[5] X.-G. Yan and C. Edwards, "Nonlinear robust fault reconstruction and estimation using a sliding mode observer," *Automatica. A Journal of IFAC, the International Federation of Automatic Control*, vol. 43, no. 9, pp. 1605–1614, 2007.

[6] B. Jiang, M. Staroswiecki, and V. Cocquempot, "Fault accommodation for nonlinear dynamic systems," *Institute of Electrical and Electronics Engineers. Transactions on Automatic Control*, vol. 51, no. 9, pp. 1578–1583, 2006.

[7] H. Yang, B. Jiang, and V. Cocquempot, *Fault tolerant control design for hybrid systems*, vol. 397 of *Lecture Notes in Control and Information Sciences (LNCIS)*, Springer Verlag, 2010.

[8] H. Yang, B. Jiang, V. Cocquempot, and L. Lu, "Supervisory fault tolerant control with integrated fault detection and isolation: a switched system approach," *International Journal of Applied Mathematics and Computer Science*, vol. 22, no. 1, pp. 87–97, 2012.

[9] M. Blanke, M. Kinnaert, J. Lunze, and M. Staroswiecki, *Diagnosis and fault-tolerant control*, Springer, Heidelberg, Third edition, 2016.

[10] T. Steffen, *Control Reconfiguration Of Dynamical Systems: Linear Approaches And Structural Tests Lecture Notes in Control and Information Sciences (LNCIS)*, vol. 320 of *Lecture Notes in Control and Information Sciences*, Springer, Berlin, Germany, 2005.

[11] J.-P. Richard, "Time-delay systems: an overview of some recent advances and open problems," *Automatica. A Journal of IFAC, the International Federation of Automatic Control*, vol. 39, no. 10, pp. 1667–1694, 2003.

[12] X.-G. Yan, S. K. Spurgeon, and C. Edwards, "Decentralised stabilisation for nonlinear time delay interconnected systems using static output feedback," *Automatica. A Journal of IFAC, the International Federation of Automatic Control*, vol. 49, no. 2, pp. 633–641, 2013.

[13] B. Jiang, J. L. Wang, and Y. C. Soh, "An adaptive technique for robust diagnosis of faults with independent effects on system outputs," *International Journal of Control*, vol. 75, no. 11, pp. 792–802, 2002.

[14] X. Jiang, W. Xu, and Q.-L. Han, "Observer-based fuzzy control design with adaptation to delay parameter for time-delay systems," *Fuzzy Sets and Systems. An International Journal in Information Science and Engineering*, vol. 152, no. 3, pp. 637–649, 2005.

[15] C. Jiang and D. H. Zhou, "Fault detection and identification for uncertain linear time-delay systems," *Computers and Chemical Engineering*, vol. 30, no. 2, pp. 228–242, 2005.

[16] J. Kim and M. K. P, "Fault detection for time-delay system by using robust control theory," in *Proceedings of the ISIE*, pp. 869–873, 2001.

[17] S. X. Ding, Z. Maiying, T. Bingyong, and P. Zhang, "An LMI approach to the design of fault detection filter for time-delay LTI systems with unknown input," in *Proceedings of the 2001 American Control Conference*, pp. 2137–2142, usa, June 2001.

[18] L. Bai, Z. Tian, and S. Shi, "Robust fault detection for a class of nonlinear time-delay systems," *Journal of the Franklin Institute. Engineering and Applied Mathematics*, vol. 344, no. 6, pp. 873–888, 2007.

[19] B. Jiang, M. Staroswiecki, and V. Cocquempot, "H∞ fault detection filter design for linear discrete-time systems with multiple time-delays," *International Journal of Systems Science*, vol. 34, no. 5, pp. 365–373, 2003.

[20] M. Zhong, S. X. Ding, J. Lam, and C. Zhang, "Fault Detection Filter Design for LTI System with Time Delays," in *Proceedings of the 42nd IEEE Conference on Decision and Control*, pp. 1467–1472, 2003.

[21] B. Jiang, M. Staroswiecki, and V. Cocquempot, "Fault identification for a class of time-delay systems," in *Proceedings of the American Control Conference*, pp. 2239–2244, Anchorage, Alaska, USA, 2002.

[22] K. Zhang and B. Jiang, "Analysis and design of adaptive fault estimation for time-varying delay systems," in *Proceedings of the 27th Chinese Control Conference, CCC*, pp. 38–42, chn, July 2008.

[23] S. Vazquez, . Jianxing Liu, . Huijun Gao, and L. G. Franquelo, "Extended State Observer-Based Sliding-Mode Control for Three-Phase Power Converters," in *Proceedings of the IEEE Transactions on Industrial Electronics*, vol. 64, pp. 22–31, Yokohama, 2016.

[24] P. D. Roberts, *Robust Model-based Fault Diagnosis for Dynamic Systems*, vol. 11, Kluwer Academic Publishers, Boston, Mass, USA, 2001.

[25] M. Zhong, S. X. Ding, J. Lam, and H. Wang, "An LMI approach to design robust fault detection filter for uncertain LTI systems," *Automatica. A Journal of IFAC, the International Federation of Automatic Control*, vol. 39, no. 3, pp. 543–550, 2003.

Hindawi
Mathematical Problems in Engineering
Volume 2017, Article ID 6803530, 9 pages
https://doi.org/10.1155/2017/6803530

Research Article

Optimization of Multiresonant Wireless Power Transfer Network Based on Generalized Coupled Matrix

Qiang Zhao and Anna Wang

College of Information Science and Engineering, Northeastern University, Shenyang, Liaoning 110819, China

Correspondence should be addressed to Qiang Zhao; lnshzq@126.com

Received 21 April 2017; Accepted 21 May 2017; Published 21 June 2017

Academic Editor: Wanquan Liu

Magnetic coupling resonant wireless power transfer network (MCRWPTN) system can realize wireless power transfer for some electrical equipment real-time and high efficiency in a certain spatial scale, which resolves the contradiction between power transfer efficiency and the power transfer distance of the wireless power transfer. A fully coupled resonant energy transfer model for multirelay coils and ports is established. A dynamic adaptive impedance matching control based on fully coupling matrix and particle swarm optimization algorithm based on annealing is developed for the MCRWPTN. Furthermore, as an example, the network which has twenty nodes is analyzed, and the best transmission coefficient which has the highest power transfer efficiency is found using the optimization algorithm, and the coupling constraints are considered simultaneously. Finally, the effectiveness of the proposed method is proved by the simulation results.

1. Introduction

Since wireless power transfer was firstly proposed by Nikola Tesla 100 years ago [1], much attempts have been devoted to this field. But these attempts did not get much breakthrough for several decades. Until 2006, a MIT research team found that efficient mid-range wireless power transfer could be achieved by utilizing near field magnetic coupling between two identical resonators [2, 3]. This progress excited renewed interest in this subject.

The magnetic coupling resonant wireless power transmission network (MCRWPTN) is to achieve wireless energy transmission through the resonant coils. In order to improve the transmission efficiency and power and adapt to the needs of the system, the MCRWPT has a variety of advanced multiresonator transmission structures, including relay resonator structure, multitransmit coil, or transmit coil array structure, multireceive coil, or multiple load structure. With the increase of the complexity of the multiresonator structure, a series of new design problems have been introduced in the MCRWPT system, which is a hot research direction in the field of MCRWPT technology.

From the mutual inductance formula, the transmission distance can be increased by increasing the size of the coil, but it is not feasible to apply the method to the limit of the coil geometry. Reducing the load of the transmitter and receiver can also increase the transmission distance of [4], but the actual application of the load cannot be arbitrarily changed; this method also has a lot of limitations. The increase of relay resonator is an effective way to improve the transmission distance.

The concept of relay coil was put forward in [5] based on the induction of electromagnetically induced transparency in quantum interference. By using the coupled mode theory, the energy transfer efficiency of the system was greatly improved by adding a coil with the same resonant frequency between the transmitting coil and the receiving coil. Further study in [6–10] showed that the higher transmission efficiency and power level can be achieved at a larger distance by increasing the relay resonator.

The effect of the addition of 1 relay coil on the transmission efficiency of the MCRWPT system with four coils was studied in [7], and the coaxial relay coil placed on the system to enhance the transmission efficiency was greater, but the vertical display had wider practical application prospects. The [8] proposed MCRWPT array resonator based on N resonator through the relay placed level could achieve N times the diameter of the resonator of wireless power

transmission (WPT) distance, when using the 10-array resonator, the efficiency of energy transmission was still close to 85%. An efficient WPT system with a relay coil was designed in [10]. Based on the analysis and simulation of the circuit model, the appropriate operating frequency was selected to achieve a transmission power of 6.6 kW at a distance of 200 mm and transmission efficiency was 95.57%.

In the practical application of radio energy transmission, such as charging for mobile electronic devices, there was a large demand for the supply of multiple devices simultaneously. With the development of WPT system, more and more attention had been paid to the research of multireceiving coil and multiple load structure.

The basic transmission characteristics such as transmission efficiency and power of multireceiving coil in [11–13] were studied by using circuit model or coupled mode theory. The research on the multireceiver coil structure in WPT was carried out in [11], which verified the feasibility of transmitting the power to a plurality of receiving coils. In a single transmitting coil to the two receiving coils power supply research in [12], the results show that although the transmission efficiency of each single coil is relatively not high, it overall can achieve higher transmission efficiency of the system. Based on the coupled mode theory, [13] was used to study the transmission of multiple load coils. With the same conclusion as in [12], with the two receiving coils, the overall transmission efficiency of multiple receive coils is higher than that of a single receiver coil, but as the number of receivers increases, the overall efficiency of the system tends to saturate and the efficiency of each individual receive coil becomes very low. In [14], the cross-coupling of multireceiving coils was considered, and the optimal design of multiload reception was realized by impedance matching of the transmitter. The paper [15] presented a novel analysis method using band-pass filter model, which made the circuit model with multireceiving coil system more simple and easier to analyze, but its use conditions were relatively harsh.

In [16], the concept of time-sharing transmission in communication system was used to study the multiload charging in MCRWPT system. It was found that time-sharing wireless transmission can achieve efficient and uniform power transmission. The literature [17] was further extended to N resonant coils. The simulation results showed that when there were N resonant coils in the system and the frequency splitting occurred, there would be N efficiency peak points. When there were odd resonant coils, the system transmission efficiency could reach the peak at the original resonant frequency of the coil, and when the number of resonant coils was even, the transmission efficiency was shifted at the original resonant frequency.

The impedance matching method on the load side can simultaneously realize the compensation of the frequency splitting phenomenon and the control of the power distribution. Considering the limitation of the frequency tracking method, the impedance matching is the main control strategy in the multicoil system. The impedance matching strategy for power allocation was studied in [15, 18, 19]. In the actual system, the coupling cannot be ignored when the number of receiving coils is very close [15, 18], considering the cross-coupling between multiple receiving coils. The impedance matching and power division method utilizing impedance inverters only at receiver sides was proposed. The mathematical equations in the proposed method were then generalized for arbitrary number of receivers and arbitrary number of repeaters. The coupling of the driving coil and the multiple receiving coils was studied in [19], and it was pointed out that the coupling will change the optimal impedance matching condition given the design method of matching impedance at this time.

Using the scattering parameters as the objective function of the fully coupling matrix extraction and combining the particle swarm optimization algorithm with simulated annealing technique to optimize impedance matching are the goal of this work. The control strategy must overcome some difficulties such as the highly nonlinear and coupled dynamics more over the dynamic, complex, and unstructured environments which may cause unpredictable disturbances to the impedance matching. So dealing with some states in each step will improve matching speed and accuracy. Using the coupling analysis and extraction condition of fully coupling matrix to design an optimal impedance matching strategy for MCRWPTN, it has been shown that the resulting optimization has excellent performance, as demonstrated by simulations.

The paper is outlined as follows. The model of multirelay MCRWPTN is established, and the coupling relation between multiple coils is analyzed in Section 2. The generalized coupling matrix of the system is extracted and an optimal design method is given in Sections 3 and 4. Simulations using FEKO and MATLAB and experiments are performed to validate the new method in Section 5. Finally, Section 6 presents some conclusions.

2. Problem Formulation

Wireless power transfer network (WPTN) is an energy-centric network, which includes an exciting coil, a transmitting coil, a relay coil, a receiving coil, and a pickup coil. The generalized coupling model of the single energy transmission link composed of n relay energy nodes in the WPTN network is shown in Figure 1.

An internal resonance network is composed of a transmitting, a relay, and a receiving coil, and the resonant frequency and the structure of the transmitting coil, the relay coil, and the receiving coil are the same. The exciting coil and the pickup coil are connected to the power and load ports, respectively, and form an external resonant network with the internal resonant network. The magnetic coupling of the internal resonant network forms a contactless energy transmission link, and multiple transmission links constitute the entire WPTN.

In Figure 1, C_p, L_p, and R_p $(p = S, L)$ are power and load port parameters; C_i, L_i, and R_i are the parameters of each coupling node. M_{ip} is the mutual inductance between the port and the node; $M_{i,i+1}$ is the mutual inductance between adjacent nodes.

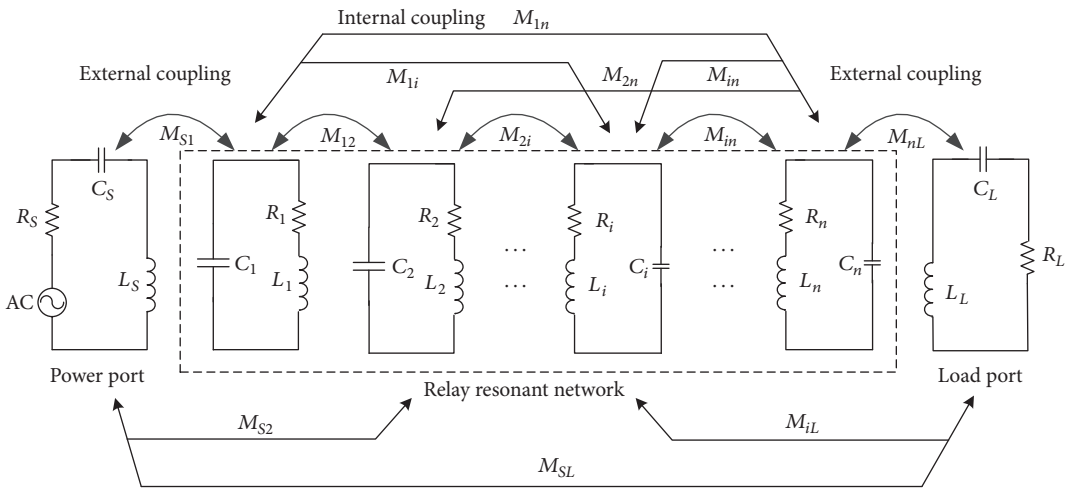

Figure 1: Schematic of a wireless power transfer route.

The Z parameter equation of the two-port system can be expressed as

$$[Z] * [I] = j\left(m_n - \lambda r - jp\right) * [I] = [V], \tag{1}$$

$$\begin{bmatrix} Z_{SS} & Z_{S1} & \cdots & Z_{Sn} & Z_{SL} \\ Z_{S1} & Z_{11} & \cdots & Z_{1n} & Z_{1L} \\ \vdots & \vdots & \ddots & \vdots & \vdots \\ Z_{Sn} & jZ_{1n} & \cdots & Z_{nn} & Z_{nL} \\ Z_{SL} & Z_{1L} & \cdots & Z_{nL} & Z_{LL} \end{bmatrix} \begin{bmatrix} I_S \\ I_1 \\ \vdots \\ I_n \\ I_L \end{bmatrix} = \begin{bmatrix} V_s \\ 0 \\ \vdots \\ 0 \\ 0 \end{bmatrix}, \tag{2}$$

where $[Z]$ is the system equivalent impedance matrix and $[m]$ is a fully coupling matrix. For systems with i ($i = 1, \ldots, n$) resonant networks and p ports, the order of the equivalent impedance matrix $[Z]$ is $n+2$. λ is the normalized frequency factor; r is the unit matrix. p is the port matrix, except for $p_{11} = Z_{SS}$ and $p_{n+2,n+2} = Z_{LL}$ and other elements are zero.

The impedance matrix of the system is shown in (3). Matrix $[Z]$ is derived from the loop equation formulation of the source and load, external and inner-resonator couplings, and resonator impedances.

$$[Z] = \begin{bmatrix} R_S + j\omega L_S - j\frac{1}{\omega C_S} & j\omega_0 M_{S1} & j\omega_0 M_{S2} & \cdots & j\omega_0 M_{S,n-1} & j\omega_0 M_{Sn} & j\omega_0 M_{SL} \\ j\omega_0 M_{S1} & R_1 + j\omega L_1 - j\frac{1}{\omega C_1} & j\omega_0 M_{12} & \cdots & j\omega_0 M_{1,n-1} & j\omega_0 M_{1n} & j\omega_0 M_{1L} \\ j\omega_0 M_{S2} & j\omega_0 M_{12} & R_2 + j\omega L_2 - j\frac{1}{\omega C_2} & \cdots & j\omega_0 M_{2,n-1} & j\omega_0 M_{2n} & j\omega_0 M_{2L} \\ \vdots & \vdots & \vdots & \ddots & \vdots & \vdots & \vdots \\ j\omega_0 M_{S,n-1} & j\omega_0 M_{1,n-1} & j\omega_0 M_{2,n-1} & \cdots & R_{n-1,n-1} + j\omega L_{n-1,n-1} - j\frac{1}{\omega C_{n-1,n-1}} & j\omega_0 M_{n-1,n} & j\omega_0 M_{n-1,L} \\ j\omega_0 M_{Sn} & j\omega_0 M_{1n} & j\omega_0 M_{2n} & \cdots & j\omega_0 M_{n-1,n} & R_n + j\omega L_n - j\frac{1}{\omega C_n} & j\omega_0 M_{nL} \\ j\omega_0 M_{SL} & j\omega_0 M_{1L} & j\omega_0 M_{2L} & \cdots & j\omega_0 M_{n-1,L} & j\omega_0 M_{nL} & R_L + j\omega L_L - j\frac{1}{\omega C_L} \end{bmatrix}. \tag{3}$$

Without loss of generality, we can assume that all nodes are fixed and stationary randomly distributed within the network, and each node has a unique number. All nodes have the same structure and circuit topology, and the coupling

between nonadjacent nodes is negligible. Each node has the same function and status equivalence as the source node, relay node, and destination node.

The impedance matrix $[Z]$ is normalized as shown in

$$\left[\widetilde{Z}\right] = \begin{array}{c} \\ \times\left(\sqrt{R_S}\right)^{-1} \\ \times\left(\sqrt{\omega_0 L_1}\right)^{-1} \\ \times\left(\sqrt{\omega_0 L_2}\right)^{-1} \\ \vdots \\ \vdots \\ \times\left(\sqrt{\omega_0 L_n}\right)^{-1} \\ \times\left(\sqrt{R_L}\right)^{-1} \end{array} \begin{array}{c} \begin{array}{ccccccc} \times\left(\sqrt{R_S}\right)^{-1} & \times\left(\sqrt{\omega_0 L_1}\right)^{-1} & \times\left(\sqrt{\omega_0 L_2}\right)^{-1} & \cdots & \cdots & \times\left(\sqrt{\omega_0 L_n}\right)^{-1} & \times\left(\sqrt{R_L}\right)^{-1} \end{array} \\ \begin{bmatrix} Z_{SS} & Z_{S1} & 0 & \cdots & 0 & 0 & 0 \\ Z_{S1} & Z_{11} & Z_{12} & \cdots & 0 & 0 & 0 \\ 0 & Z_{12} & Z_{22} & \cdots & 0 & 0 & 0 \\ \vdots & \vdots & \vdots & \ddots & \vdots & \vdots & \vdots \\ 0 & 0 & 0 & \cdots & Z_{n-1,n-1} & Z_{n-1,n} & 0 \\ 0 & 0 & 0 & \cdots & Z_{n-1,n} & Z_{nn} & Z_{nL} \\ 0 & 0 & 0 & \cdots & 0 & Z_{nL} & Z_{LL} \end{bmatrix} \end{array}, \tag{4}$$

where $1/\sqrt{R_p}$ is an impedance scaling factor ($p = S, L$), $1/\sqrt{\omega_0 L_i}$ ($i = 1, \ldots, n$) is a resonator scaling factor, and $\omega_0 = 1/\sqrt{L_i C_i}$.

Generalize matrix $[Z]$ such that the resultant matrix can be normalized in terms of couplings and port impedances only. The resultant matrix is the normalized impedance matrix $[\widetilde{Z}]$, as shown in

$$\left[\widetilde{Z}\right] = \begin{bmatrix} 1 + j\dfrac{X_S}{R_S} & j\dfrac{\omega M_{S1}}{\sqrt{\omega_0 R_S L_1}} & 0 & \cdots & 0 & 0 & 0 \\ j\dfrac{\omega M_{S1}}{\sqrt{\omega_0 R_S L_1}} & \dfrac{1}{Q_1} + j\lambda & j\dfrac{M_{12}}{\sqrt{L_1 L_2}} & \cdots & 0 & 0 & 0 \\ 0 & j\dfrac{M_{12}}{\sqrt{L_1 L_2}} & \dfrac{1}{Q_2} + j\lambda & \cdots & 0 & 0 & 0 \\ \vdots & \vdots & \vdots & \ddots & \vdots & \vdots & \vdots \\ 0 & 0 & 0 & \cdots & \dfrac{1}{Q_{n-1}} + j\lambda & j\dfrac{M_{n-1,n}}{\sqrt{L_{n-1} L_n}} & 0 \\ 0 & 0 & 0 & \cdots & j\dfrac{M_{n-1,n}}{\sqrt{L_{n-1} L_n}} & \dfrac{1}{Q_n} + j\lambda & j\dfrac{\omega M_{nL}}{\sqrt{\omega_0 L_n R_L}} \\ 0 & 0 & 0 & \cdots & 0 & j\dfrac{\omega M_{nL}}{\sqrt{\omega_0 L_n R_L}} & 1 + j\dfrac{X_L}{R_L} \end{bmatrix}. \tag{5}$$

Normalized variables are used in representing the impedance matrix as follows. $Q_i = \omega_0 L_i / R_i$ is the unloaded Q factor of resonator i, $\lambda = (\omega/\omega_0 - \omega_0/\omega)$ is the normalized frequency factor, which reflects the relationship between the resonant network and the frequency in the frequency response of MCRWPT. The coupling coefficient of the internal resonator is defined as $k_{i,i+1} = M_{i,i+1}/\sqrt{L_i L_{i+1}}$, and the external coupling between resonator i and port p for $i = 1, n$ and $p = S, L$ is defined as $E_{S1} = \omega M_{S1}/\sqrt{\omega_0 R_S L_1}$ and $E_{nL} = \omega M_{nL}/\sqrt{\omega_0 L_n R_L}$. The normalized reactance of port p for $p = S, L$ is $x_S = X_S/R_S$ and $x_L = X_L/R_L$.

This normalized impedance matrix will be referred to as $[\widetilde{Z}]$. Substituting in these variables allows us to make the decomposition of the matrix seen below:

$$\begin{aligned}\left[\widetilde{Z}\right] = j &\begin{bmatrix} x_S & E_{s1} & 0 & \cdots & 0 & 0 & 0 \\ E_{s1} & -\dfrac{j}{Q_1} & k_{12} & \cdots & 0 & 0 & 0 \\ 0 & k_{12} & -\dfrac{j}{Q_2} & \cdots & 0 & 0 & 0 \\ \vdots & \vdots & \vdots & \ddots & \vdots & \vdots & \vdots \\ 0 & 0 & 0 & \cdots & -\dfrac{j}{Q_{n-1}} & k_{n-1,n} & 0 \\ 0 & 0 & 0 & \cdots & k_{n-1,n} & -\dfrac{j}{Q_n} & E_{nL} \\ 0 & 0 & 0 & \cdots & 0 & E_{nL} & x_L \end{bmatrix} \\ &+ \begin{bmatrix} 1 & 0 & 0 & \cdots & 0 & 0 & 0 \\ 0 & 0 & 0 & \cdots & 0 & 0 & 0 \\ 0 & 0 & 0 & \cdots & 0 & 0 & 0 \\ \vdots & \vdots & \vdots & \ddots & \vdots & \vdots & \vdots \\ 0 & 0 & 0 & \cdots & 0 & 0 & 0 \\ 0 & 0 & 0 & \cdots & 0 & 0 & 0 \\ 0 & 0 & 0 & \cdots & 0 & 0 & 1 \end{bmatrix} \\ &+ j\lambda \begin{bmatrix} 0 & 0 & 0 & \cdots & 0 & 0 & 0 \\ 0 & 1 & 0 & \cdots & 0 & 0 & 0 \\ 0 & 0 & 1 & \cdots & 0 & 0 & 0 \\ \vdots & \vdots & \vdots & \ddots & \vdots & \vdots & \vdots \\ 0 & 0 & 0 & \cdots & 1 & 0 & 0 \\ 0 & 0 & 0 & \cdots & 0 & 1 & 0 \\ 0 & 0 & 0 & \cdots & 0 & 0 & 0 \end{bmatrix}. \end{aligned} \tag{6}$$

Using algebraic manipulation, $[\widetilde{Z}]$ is separated into constitutive components into the form given by

$$\left[\widetilde{Z}\right] = j\,[m] + j\lambda\,[r] + [p]\,. \tag{7}$$

For the purposes of WPT optimization, the variable λ simply reflects the frequency dependency of the MRCWPT frequency response. The unit matrix $[r]$ of the resonant network is $n * n$ identity matrix, the port normalized impedance matrix $[p]$ is zero except for the power and load port elements, the coupling matrix $[m]$ is a reciprocal matrix of $n * n$, and the other nondiagonal elements represent the coupling between the two resonators. If it is zero, the corresponding two resonators are not coupled.

3. Fully Coupling Matrix Extraction

From (1) we can see that the current vector can be expressed as

$$[I] = -j\,[Z]^{-1}\,[V]\,. \tag{8}$$

Thus, the scattering parameter S of the entire coupling circuit can be expressed as

$$\begin{aligned} S_{21} &= 2\sqrt{Z_{SS}Z_{LL}}\,[I]_n = -2j\sqrt{Z_{SS}Z_{LL}}\,[Z]^{-1}_{SL}\,, \\ S_{11} &= 1 - 2Z_{SS}\,[I]_1 = 1 + 2jZ_{SS}\,[Z]^{-1}_{SS}\,. \end{aligned} \tag{9}$$

We can get from (7) that

$$[A] = -j\left[\widetilde{Z}\right] = [m] - j\,[p] + \lambda\,[r]\,, \tag{10}$$

where the matrix $[A]$ is built from the coupling matrix $[m]$, the source matrix $[p]$, and the resonator matrix $[r]$. It can be shown that, from inverting the $[A]$ matrix, the scattering parameters can be found.

$$\begin{aligned} S_{21} &= -2j\,[A]^{-1}_{SL}\,, \\ S_{11} &= 1 + 2j\,[A]^{-1}_{SS}\,. \end{aligned} \tag{11}$$

The objective function K is uniquely determined by the zero position, the pole position, and the in-band return loss.

$$\begin{aligned} K = &\sum_{i=1}^{n} \left|S_{11}\left(\omega_{zi}\right)\right|^2 + \sum_{i=1}^{p} \left|S_{21}\left(\omega_{pi}\right)\right|^2 \\ &+ \left(\left|S_{11}\left(\omega = -1\right)\right| - \frac{\varepsilon}{\sqrt{1+\varepsilon^2}}\right)^2 \\ &+ \left(\left|S_{11}\left(\omega = 1\right)\right| - \frac{\varepsilon}{\sqrt{1+\varepsilon^2}}\right)^2, \quad (p \le n)\,, \end{aligned} \tag{12}$$

where ω_{pi} is artificially specified quantity and ω_{zi} is a function of ω_{pi}. ω_{zi} and ω_{pi} are the zero and pole of the characteristic function $C_n(\omega)$, respectively. The latter two are used to determine the in-band return loss. When $K = 0$, the target is satisfied and the optimization is finished. Set the following expression:

$$C_n(\omega) = \frac{1}{2}\frac{G_n(\omega) + G'_n(\omega)}{\prod_{i=1}^{n}\left(1 - \omega/\omega_0\right)}, \tag{13}$$

$$G_n(\omega) = \prod_{i=1}^{n}\left[\left(\omega - \frac{1}{\omega_0}\right) + \sqrt{\left(\omega^2 - 1\right)\left(1 - \frac{1}{\omega_0^2}\right)}\right], \tag{14}$$

$$G'_n(\omega) = \prod_{i=1}^{n}\left[\left(\omega - \frac{1}{\omega_0}\right) - \sqrt{\left(\omega^2 - 1\right)\left(1 - \frac{1}{\omega_0^2}\right)}\right], \tag{15}$$

$$G_n(\omega) = U_n(\omega) + V_n(\omega)\,, \tag{16}$$

$$G'_n(\omega) = U_n(\omega) - V_n(\omega)\,, \tag{17}$$

$$U_n(\omega) = u_0 + u_1\omega + u_2\omega^2 + \cdots + u_n\omega^n, \tag{18}$$

$$V_n(\omega) = \sqrt{\omega^2 - 1}\left(v_0 + v_1\omega + v_2\omega^2 + \cdots + v_n\omega^n\right). \tag{19}$$

$G_1(\omega)$ can be obtained as substituting the first pole ω_{p1} into (14), and the values of u_0, u_1, v_0, v_1 are obtained by comparing the coefficients, and then determine $U_1(\omega)$, $V_1(\omega)$.

$$G_n(\omega) = \left[U_{n-1}(\omega) + V_{n-1}(\omega)\right] \cdot \left[\left(\omega - \frac{1}{\omega_0}\right) + \sqrt{(\omega^2 - 1)\left(1 - \frac{1}{\omega_0^2}\right)}\right]. \quad (20)$$

$G_2(\omega)$ can be obtained as substituting the first pole ω_{p2}, and so on, until the N pole is replaced. From formulas (16) and (17), the molecules of $C_n(\omega)$ can be obtained by iteration.

$$\mathrm{NUM}\left[C_n(\omega)\right] = \frac{1}{2}\left[G_n(\omega) + G_n'(\omega)\right] = U_n(\omega). \quad (21)$$

Solving the roots of $U_n(\omega) = 0$ can obtain the N zeros of the characteristic function. The parameters of the objective function can be determined after substituting the zero point, the pole, and the return loss into (12). The relation between generalized coupling matrix $[m]$ and objective function K can be established by the above derivation, and the optimization model of the coupling matrix extraction is shown in formula (22).

$$\begin{aligned}
\min \quad & K \\
& = \sum_{i=1}^{n} \left|S_{11}(\omega_{zi})\right|^2 + \sum_{i=1}^{p} \left|S_{21}(\omega_{pi})\right|^2 \\
& \quad + \left(\left|S_{11}(\omega = -1)\right| - \frac{\varepsilon}{\sqrt{1+\varepsilon^2}}\right)^2 \\
& \quad + \left(\left|S_{11}(\omega = 1)\right| - \frac{\varepsilon}{\sqrt{1+\varepsilon^2}}\right)^2, \quad (p \le n) \\
\text{s.t.} \quad & C_n(\omega) = \frac{1}{2}\frac{G_n(\omega) + G_n'(\omega)}{\prod_{i=1}^{n}(1 - \omega/\omega_0)} \\
& G_n(\omega) \\
& = \prod_{i=1}^{n}\left[\left(\omega - \frac{1}{\omega_0}\right) + \sqrt{(\omega^2 - 1)\left(1 - \frac{1}{\omega_0^2}\right)}\right] \\
& G_n'(\omega) \\
& = \prod_{i=1}^{n}\left[\left(\omega - \frac{1}{\omega_0}\right) - \sqrt{(\omega^2 - 1)\left(1 - \frac{1}{\omega_0^2}\right)}\right].
\end{aligned} \quad (22)$$

4. Impedance Matching Optimization

In order to improve the extraction speed of generalized coupling matrix, a particle swarm optimization algorithm based on simulated annealing is presented. Fitness function can be expressed as follows:

$$\begin{aligned}
\text{fittness} &= G_n(\omega) \\
&= \prod_{i=1}^{n}\left[\left(\omega - \frac{1}{\omega_0}\right) + \sqrt{(\omega^2 - 1)\left(1 - \frac{1}{\omega_0^2}\right)}\right].
\end{aligned} \quad (23)$$

Firstly, the initial population is generated randomly, and a new group of individuals is generated by the basic particle swarm optimization algorithm.

$$\begin{aligned}
V_{i+1} &= w * V_i + c_1 * \mathrm{rand}() * (pbest - x_i) + c_2 \\
&\quad * \mathrm{rand}() * (gbest - x_i) \\
x_{i+1} &= x_i + V_i,
\end{aligned} \quad (24)$$

where *pbest* is the best location of the particle itself and *gbest* is the best location for all particles in the population.

Then, the crossover and the Gaussian mutation operation are carried out independently. Simulated annealing is performed for each individual, and the result is used as an individual in the next generation.

In each evolution, crossover operation selects a specified number of particles into a pool according to crossing probability, which are randomly crossed to produce the same number of children, instead of parents to keep the number of particles unchanged. The position of the child particle is calculated by the weighted sums of the parent particles.

$$\begin{aligned}
\mathrm{child}_1(x) &= p * \mathrm{parent}_1(x) + (1 - p) * \mathrm{parent}_2(x), \\
\mathrm{child}_2(x) &= p * \mathrm{parent}_2(x) + (1 - p) * \mathrm{parent}_1(x),
\end{aligned} \quad (25)$$

where x is the D-dimension position vector and $\mathrm{child}_k(x)$ and $\mathrm{parent}_k(x)$, $k = 1, 2$, respectively, are the location of the child or parent particles. p is a uniform random number vector of D-dimension, with each component in $[0, 1]$ value. The speed of the child particles is given by the following formula:

$$\begin{aligned}
\mathrm{child}_1(v) &= \frac{\mathrm{parent}_1(v) + \mathrm{parent}_2(v)}{\left|\mathrm{parent}_1(v) + \mathrm{parent}_2(v)\right|}\left|\mathrm{parent}_1(v)\right|, \\
\mathrm{child}_2(v) &= \frac{\mathrm{parent}_1(v) + \mathrm{parent}_2(v)}{\left|\mathrm{parent}_1(v) + \mathrm{parent}_2(v)\right|}\left|\mathrm{parent}_2(v)\right|,
\end{aligned} \quad (26)$$

where v is the velocity vector of the D-dimension.

In each evolution, the specified number of particles is selected by mutation operation according to the mutation probability, which was mutated by Gaussian mutation operator, and the mutated particles are used instead of the original particles.

$$\mathrm{mutation}(x) = x * (1 + \mathrm{Gaussian}(\delta)). \quad (27)$$

The implementation of the algorithm is composed of two parts. Firstly, the evolution of the basic particle swarm optimization algorithm (global search) is used to produce a better group, and then the crossover and mutation operations are applied, and the particles are further optimized by simulated annealing (local search). The evolution process is iterated until the termination condition is satisfied. The algorithm flow is as follows:

(1) Initialization parameters.

(2) The population of randomly generated N particles.

(3) Using (24) to manipulate the particles in the population.

Table 1: The system parameters configuration.

Parameters	Values
R_S	50 Ω
R_L	50 Ω
Port coils	
Radius r	100 mm
Number of turns N	1 turn
Resonant coils	
Radius R	100 mm
Number of turns N	5 turns
Resonant frequency f_0	12.85 MHz
Coupling coefficient between resonators $k_{i,i+1}$	0.2
Coupling coefficient between nonadjacent resonators	0

(4) The population generated by (3) select the particle to form the subpopulation by the crossover probability and carries out the following operations to produce a new species population: from the subpopulation randomly selected individuals x_j and x_k according to (25) for cross-operation to produce two new individuals x_j', x_k', calculate the adaptive function value $f(x_j)$, $f(x_k)$, $f(x_j')$, $f(x_k')$; if $\min\{1, \exp(-(f(x_j')) - f(x_j'))/T\} >$ random, then x_j' is a new individual; if $\min\{1, \exp(-(f(x_k')) - f(x_k'))/T\} >$ random, then x_k' is a new individual, where random is a random number on the [0, 1] interval.

(5) The population generated by crossing selects the particle to form the subpopulation by the mutation probability and carries out the following operations to produce a new species population. An individual is selected from the subpopulation to perform a Gaussian mutation operation to produce a new individual x_j', and calculate the adaptive function value $f(x_j)$ and $f(x_j')$; if $\min\{1, \exp(-(f(x_j')) - f(x_j'))/T\} >$ random, then x_j' is a new individual.

(6) If the current optimal individual satisfies the convergence condition, the evolution process ends successfully and returns the global optimal solution.

(7) If the number of evolutions is less than the maximum number of times of evolution, the annealing temperature of the population is modified, and then return to step (3).

5. Simulation Results

In order to optimize the extraction of generalized coupling matrix parameters fast convergence, the initial value should be set close to the actual value. The parameters of the MCRWPTN system are shown in Table 1. The optimized and simulated S parameters are shown in Figures 2–4.

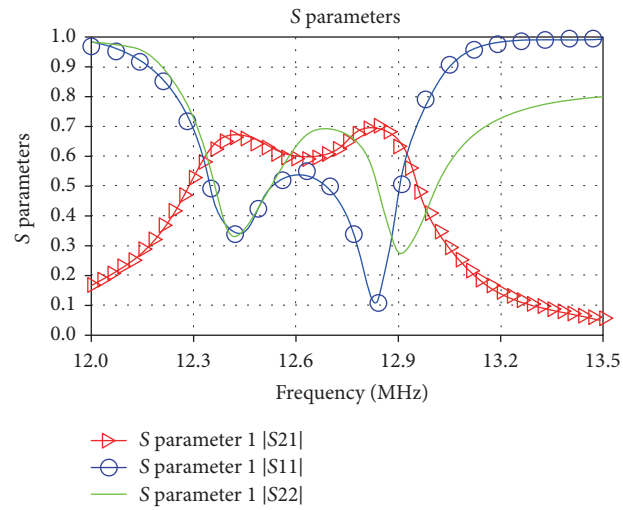

Figure 2: The curves of scattering parameters of WPTN.

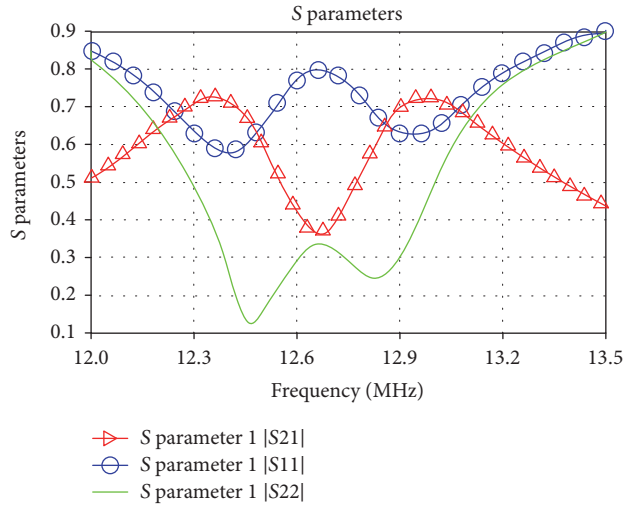

Figure 3: The curves of the scattering parameters of external coupling network of power port.

When the number of ports is $p = 2$, the number of coupling relay coils is $n = 20$, and the system scattering parameter curve is shown in Figures 2–4. These three curves represent the specific distribution of the scattering parameters of the total transmission network and the two transmission subnetworks of the MCRWPTN, respectively, which can reflect the law of the scattering parameters of the system with frequency, where S_{21} is forward transmission coefficient and S_{11} is reflection coefficient of port 1. They can respond to the transmission characteristics of the system, the higher S_{21} is better, and the opposite of S_{11} is as low as possible.

As can be seen from Figure 2, the frequency division of the system has low frequency resonance and high frequency resonance. At the resonant frequency, S_{21} reaches the maximum, and $S_{11} = 0.1$ is the smallest. So the maximum power transmission efficiency is obtained. The response curve

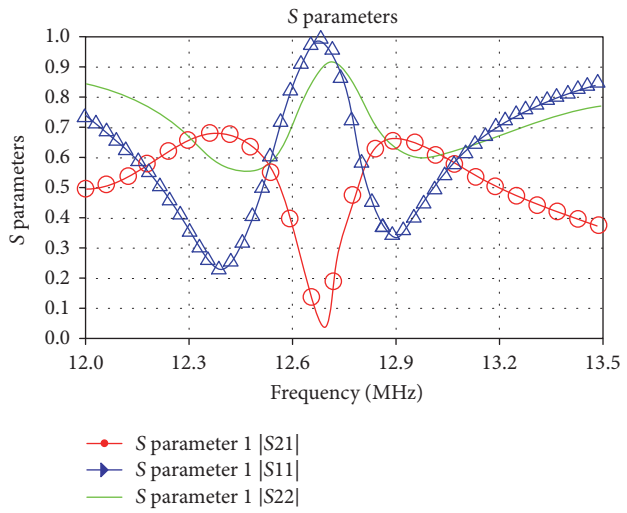

Figure 4: The curves of the scattering parameters of external coupling network of load port.

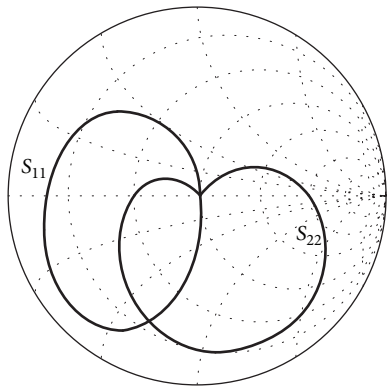

Figure 5: Simulation validation of complex load impedance accommodation.

obtained after optimization is in good agreement with the S parameters obtained from the simulation. From Figures 3 and 4, the existence of external coupling network makes the port impedance match well.

Figure 5 shows the simulated S_{11} and S_{22} responses of the complex load impedance accommodated response measured at the interresonator coupling location $k_{ST} = 0.01$. As shown, the resonance dip of S_{22} response approaches the center of the Smith chart. This indicates that the output impedance of the impedance matching optimized system is the complex conjugate of $Z_p = R_p + jX_p$.

Figure 6 is the modulus value of the reflection coefficient obtained by different algorithms. By comparing the three different algorithms of reflection coefficient magnitude, the particle swarm optimization combined with simulated annealing algorithm is a new type of impedance matching algorithm, and the reflection coefficient tends to zero to achieve impedance matching finally, which is better than the improved particle swarm algorithm in speed.

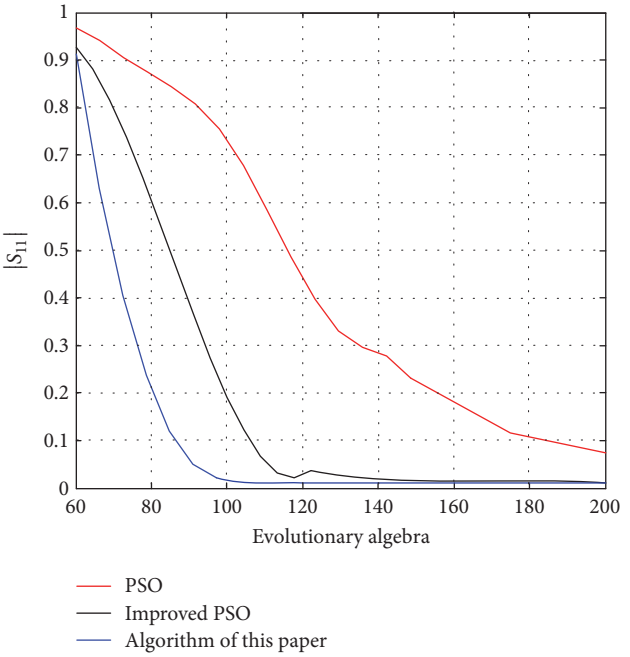

Figure 6: The modulus value of the reflection coefficient obtained by different algorithms.

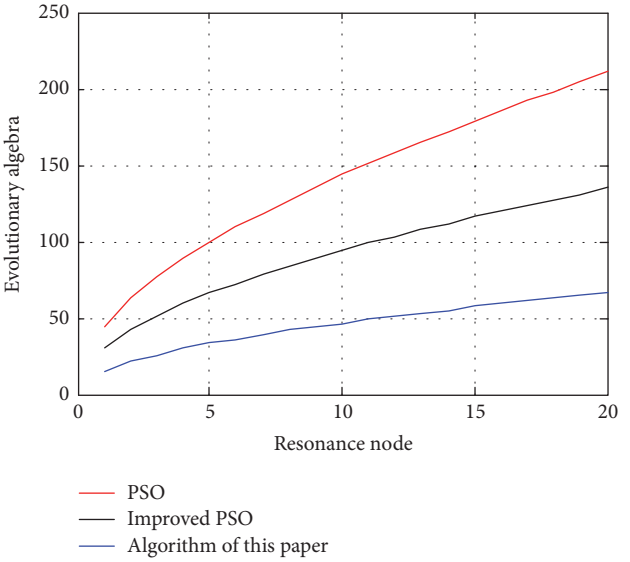

Figure 7: Multicoupled node network optimization.

The relationship between the number of coupled nodes and the number of iterations is shown in Figure 7. As the number of nodes increases, the algorithm is superior to other algorithms and is easy to extend to multirelay MCRWPTN.

6. Conclusion

A fully coupling matrix for multirelay MCRWPTN is proposed and theory to impedance matching optimization algorithm is developed. This combination will emphasize not

only the energy transfer but also the matching speed and scalability. The optimization algorithm combines the ability of the simulated annealing algorithm to jump out of the local optimal solution and the global optimization ability of the particle swarm optimization algorithm, which avoids the shortcomings of falling into the local extreme point and improves the algorithm convergence speed and accuracy. Theoretical results are supported by numerical simulations with impedance matching of the proposed fully coupled matrix and optimization algorithm.

Conflicts of Interest

The authors declare that there are no conflicts of interest regarding the publication of this paper.

References

[1] A. Kurs, A. Karalis, R. Moffatt, J. D. Joannopoulos, P. Fisher, and M. Soljačić, "Wireless power transfer via strongly coupled magnetic resonances," *American Association for the Advancement of Science. Science*, vol. 317, no. 5834, pp. 83–86, 2007.

[2] A. K. RamRakhyani, S. Mirabbasi, and M. Chiao, "Design and optimization of resonance-based efficient wireless power delivery systems for biomedical implants," *IEEE Transactions on Biomedical Circuits and Systems*, vol. 5, no. 1, pp. 48–63, 2011.

[3] A. P. Sample, D. A. Meyer, and J. R. Smith, "Analysis, experimental results, and range adaptation of magnetically coupled resonators for wireless power transfer," *IEEE Transactions on Industrial Electronics*, vol. 58, no. 2, pp. 544–554, 2011.

[4] M. Fu, T. Zhang, C. Ma, and X. Zhu, "Efficiency and optimal loads analysis for multiple-receiver wireless power transfer systems," *IEEE Transactions on Microwave Theory and Techniques*, vol. 63, no. 3, pp. 801–812, 2015.

[5] R. E. Hamam, A. Karalis, J. D. Joannopoulos, and M. Soljačić, "Efficient weakly-radiative wireless energy transfer: an EIT-like approach," *Annals of Physics*, vol. 324, no. 8, pp. 1783–1795, 2009.

[6] M. Meng and M. Kiani, "Design and optimization of ultrasonic wireless power transmission links for millimeter-sized biomedical implants," *IEEE Transactions on Biomedical Circuits and Systems*, vol. 11, no. 1, pp. 98–107, 2016.

[7] G. Monti, L. Tarricone, and M. Mongiardo, "Two-port network approach for a wireless power transfer link using a cascade of inductively coupled resonators," *International Journal of Numerical Modelling: Electronic Networks, Devices and Fields*, p. e2234, 2017.

[8] B. Wang, K. Teo, and S. Yamaguchi, "Flexible and mobile near-field wireless power transfer using an array of resonators," *The Institute of Electronics, Information and Communication Engineers*, pp. 10–16, 2012.

[9] J. Dai and D. C. Ludois, "A Survey of wireless power transfer and a critical comparison of inductive and capacitive coupling for small gap applications," *IEEE Transactions on Power Electronics*, vol. 30, no. 11, pp. 6017–6029, 2015.

[10] S. C. Moon and G.-W. Moon, "Wireless power transfer system with an asymmetric four-coil resonator for electric vehicle battery chargers," *IEEE Transactions on Power Electronics*, vol. 31, no. 10, pp. 6844–6854, 2016.

[11] J. Lee, K. Lee, and D. Cho, "Stability improvement of transmission efficiency based on a relay resonator in a wireless power transfer system," *IEEE Transactions on Power Electronics*, vol. 32, no. 5, pp. 3297–3300, 2017.

[12] J. Kim, D.-H. Kim, and Y.-J. Park, "Free-positioning wireless power transfer to multiple devices using a planar transmitting coil and switchable impedance matching networks," *IEEE Transactions on Microwave Theory and Techniques*, vol. 64, no. 11, pp. 3714–3722, 2016.

[13] X. Huang, Y. Gao, J. Zhou, J. Ma, J. Zhang, and Y. Fang, "Magnetic field design for optimal wireless power transfer to multiple receivers," *IET Power Electronics*, vol. 9, no. 9, pp. 1885–1893, 2016.

[14] S. Kisseleff, I. F. Akyildiz, and W. H. Gerstacker, "Magnetic induction-based simultaneous wireless information and power transfer for single information and multiple power receivers," *IEEE Transactions on Communications*, vol. 65, no. 3, pp. 1396–1410, 2017.

[15] K. E. Koh, T. C. Beh, T. Imura, and Y. Hori, "Impedance matching and power division using impedance inverter for wireless power transfer via magnetic resonant coupling," *IEEE Transactions on Industry Applications*, vol. 50, no. 3, pp. 2061–2070, 2014.

[16] E. Waffenschmidt, "Dynamic resonant matching method for a wireless power transmission receiver," *IEEE Transactions on Power Electronics*, vol. 30, no. 11, pp. 6070–6077, 2015.

[17] G. Monti, L. Corchia, L. Tarricone, and M. Mongiardo, "A network approach for wireless resonant energy links using relay resonators," *IEEE Transactions on Microwave Theory and Techniques*, vol. 64, no. 10, pp. 3271–3279, 2016.

[18] W. X. Zhong, C. Zhang, X. Liu, and S. Y. R. Hui, "A methodology for making a three-coil wireless power transfer system more energy efficient than a two-coil counterpart for extended transfer distance," *IEEE Transactions on Power Electronics*, vol. 30, no. 2, pp. 933–942, 2015.

[19] M. Fu, T. Zhang, X. Zhu, P. C.-K. Luk, and C. Ma, "Compensation of cross coupling in multiple-receiver wireless power transfer systems," *IEEE Transactions on Industrial Informatics*, vol. 12, no. 2, pp. 474–482, 2016.

Hindawi
Mathematical Problems in Engineering
Volume 2017, Article ID 9548407, 9 pages
https://doi.org/10.1155/2017/9548407

Research Article

$\mathscr{H}_\infty$ Filtering for Discrete-Time Nonlinear Singular Systems with Quantization

Yifu Feng,[1] Zhi-Min Li,[2] and Xiao-Heng Chang[3]

[1]*College of Mathematics, Jilin Normal University, Siping, Jilin 136000, China*
[2]*The School of Information Science and Engineering, Wuhan University of Science and Technology, Wuhan, Hubei 430081, China*
[3]*College of Engineering, Bohai University, Jinzhou, Liaoning 121003, China*

Correspondence should be addressed to Xiao-Heng Chang; changxiaoheng@sina.com

Received 25 March 2017; Accepted 9 May 2017; Published 11 June 2017

Academic Editor: Wanquan Liu

This paper investigates the problem of $\mathscr{H}_\infty$ filtering for class discrete-time Lipschitz nonlinear singular systems with measurement quantization. Assume that the system measurement output is quantized by a static, memoryless, and logarithmic quantizer before it is transmitted to the filter, while the quantizer errors can be treated as sector-bound uncertainties. The attention of this paper is focused on the design of a nonlinear quantized $\mathscr{H}_\infty$ filter to mitigate quantization effects and ensure that the filtering error system is admissible (asymptotically stable, regular, and causal), while having a unique solution with a prescribed $\mathscr{H}_\infty$ noise attenuation level. By introducing some slack variables and using the Lyapunov stability theory, some sufficient conditions for the existence of the nonlinear quantized $\mathscr{H}_\infty$ filter are expressed in terms of linear matrix inequalities (LMIs). Finally, a numerical example is presented to demonstrate the effectiveness of the proposed quantized filter design method.

1. Introduction

The study on singular systems (also known as descriptor systems, generalized state-space systems, differential algebraic systems, or implicit systems) has attracted a recurring interest in the past several decades as the singular systems can provide a better description of many physical systems than regular ones such as circuit systems, economic systems, power systems, chemical processes, robotic systems, and networked systems. The problem of stability analysis and controller design for singular systems has achieved many valuable results (see, e.g., [1–7] and references therein). The related problem of robust $\mathscr{H}_\infty$ static output-feedback control for singularly perturbed systems has been addressed in [1]; also the stability, robust stabilization, and $\mathscr{H}_\infty$ control of singular systems with impulsive behavior have been studied in [2]; the problem of observer-based resilient l_2-l_∞ control for singular systems with time-delay has been investigated in [3]; the work in [4] considered the problem of designing stabilizing controllers for singularly perturbed fuzzy systems; by using a new type generalized Lyapunov equation, some new stability conditions for discrete singular systems have been derived in [5]; and [6] investigated the problem state feedback control for uncertain singular systems with time-delay. Due to the fact that the state variables of system are not always available, the problem of state estimation for singular systems has also received considerable attention (see, e.g., [7–17] and references therein). $\mathscr{H}_\infty$ filtering problem for continuous-time linear singular systems has been considered in [8]; in [9], the problem of energy-to-peak filtering for discrete-time linear singular systems has been addressed; $\mathscr{H}_\infty$ unbiased filtering problem for linear descriptor systems has been studied in [10]; the problem of $\mathscr{H}_\infty$ filtering for continuous- and discrete-time singular systems with communication constraints has been investigated in [11] and [12], respectively; the study in [13] considered the problem of robust nonlinear $\mathscr{H}_\infty$ filtering for Lipschitz nonlinear descriptor systems with parametric uncertainties; the problem of robust $\mathscr{H}_\infty$ filter design of uncertain descriptor systems with distributed delays has been studied in [14]; the

paper [15] concerned the problem of generalized nonlinear l_2-l_∞ filtering for discrete-time Markov jump descriptor systems with Lipschitz nonlinearity; the generalized nonlinear $\mathscr{H}_\infty$ filter design problem for discrete-time Lipschitz nonlinear descriptor systems has been considered in [16]; and [17] studied the observer design problem for discrete-time linear descriptor systems which is also applicable to nonlinear descriptor systems with Lipschitz constraints. $\mathscr{H}_\infty$ approach-based fault detection filter design for a continuous-time networked control system and unmanned surface vehicles in network environments has been investigated in [18] and [19], respectively, and some novel filter design criteria have been presented.

On the other hand, due to inherent network-limited bandwidth, quantization effects are unavoidable in practical systems, especially in networked control systems (NCSs); see [20–22] for results in NCSs. As early as 1956, Kalman investigated the effect of quantization in a sampled data control system and pointed out that if a stabilizing controller was quantized using a finite-alphabet quantizer, the feedback system would exhibit limit cycles and chaotic behavior [23]. Over the past several years, significant efforts have been devoted to the study of analysis and synthesis for linear system with quantized feedback [24–29]. The problem of quantized $\mathscr{H}_\infty$ filter design for different systems has been investigated in [30–34]. In [30], the quantized state estimation problem for discrete-time linear systems has been addressed; the work in [31] considered the $\mathscr{H}_\infty$ filtering problem for a class continuous-time polytopic uncertain systems subject to measurement quantization, signal transmission delay, and data packet dropout; the problem of $\mathscr{H}_\infty$ filtering for discrete-time T-S fuzzy systems with measurement quantization and packet dropouts has been studied in [32]; and [33] investigated the problem of $\mathscr{H}_\infty$ filtering for discrete-time polytopic uncertain systems with measurement quantization; in [34], the quantized $\mathscr{H}_\infty$ filtering problem for a class of discrete-time polytopic uncertain systems with packet dropout has been considered. To the best of our knowledge, few attempts have been made on an $\mathscr{H}_\infty$ filter design for singular systems with quantized measurement, especially for the singular systems with Lipschitz nonlinearity, which motivates us for this study.

This paper focuses on the design of $\mathscr{H}_\infty$ filter for a class of discrete-time Lipschitz nonlinear singular systems with measurement quantization. Via introducing auxiliary relaxed variables by Fisher lemma and using the Lyapunov stability theory, some sufficient conditions for the existence of the nonlinear quantized $\mathscr{H}_\infty$ filter are obtained in terms of linear matrix inequalities (LMIs), which can not only ensure that the filtering error system is admissible and has a unique solution but also achieve a prescribed $\mathscr{H}_\infty$ performance. Finally, we will illustrate the effectiveness of our main results by a numerical example.

Notations. The notations that are used throughout this paper are standard. The notation $*$ is used to indicate the terms that can be induced by symmetry. Generally, for a square matrix $\mathscr{A}$, $\mathscr{A}^T$ denotes its transpose and $\mathrm{He}\{\mathscr{A}\}$ denotes $(\mathscr{A} + \mathscr{A}^T)$.

2. Problem Formulation

Consider the following nonlinear discrete-time singular systems described by

$$\begin{aligned} Ex(t+1) &= \mathscr{A}x(t) + \Psi(t, x(t)) + \mathscr{B}w(t), \\ y(t) &= \mathscr{C}x(t) + \mathscr{D}w(t), \\ z(t) &= \mathscr{L}x(t), \end{aligned} \tag{1}$$

where $x(t) \in \mathscr{R}^n$ is the state variable; $y(t) \in \mathscr{R}^l$ is the measurement output; $z(t) \in \mathscr{R}^q$ is the signal to be estimated; $w(t) \in \mathscr{R}^p$ is the noise signal that is assumed to be the arbitrary signal in $l_2[0, \infty)$; the matrix E may be singular, and we shall assume that $\mathrm{rank}(E) = r < n$; the matrices $\mathscr{A}$, $\mathscr{B}$, $\mathscr{C}$, $\mathscr{D}$, and $\mathscr{L}$ are known matrices with appropriate dimensions.

The nonlinear term we consider here is locally Lipschitz with respect to $x(t)$ in a region $\mathscr{D}$ containing the origin; that is,

$$\begin{aligned} &\Psi(0, x(0)) = 0, \\ &\left\|\Psi(t, x_1(t)) - \Psi(t, x_2(t))\right\| \le \mathscr{F}\left\|\Psi(x_1(t) - x_2(t))\right\|, \\ &\qquad \forall x_1(t), x_2(t) \in \mathscr{D}, \end{aligned} \tag{2}$$

where $\mathscr{F}$ denotes the Lipschitz real matrix of $\Psi(t, x(t))$ with appropriate dimension.

For the unforced discrete-time singular system $Ex(t+1) = \mathscr{A}x(t) + \Psi(t, x(t))$, we have the following definition.

Definition 1 (see [9]). The pair $(E, \mathscr{A})$ is said to be regular if there exists a scalar $s \in \mathscr{C}$ such that $\det(E, \mathscr{A}) \neq 0$, the pair $(E, \mathscr{A})$ is said to be causal if $\deg(\det(E, \mathscr{A})) = \mathrm{rank}(E)$, and the pair $(E, \mathscr{A})$ is said to be stable if all the roots of $\det(E, \mathscr{A})$ lie in the interior of unit disk. We call the pair $(E, \mathscr{A})$ admissible if it is regular, causal, and stable, simultaneously. The unforced discrete-time singular system is said to be regular, causal, and stable (asymptotically stable) if the pair $(E, \mathscr{A})$ is admissible.

The designed full-order nonlinear quantized $\mathscr{H}_\infty$ filter is in the form of

$$\begin{aligned} x_f(t+1) &= \mathscr{A}_f x_f(t) + \lambda_1 \Psi\left(t, x_f(t)\right) + \mathscr{B}_f y_q(t), \\ z_f(t) &= \mathscr{C}_f x_f(t) + \mathscr{D}_f y_q(t), \end{aligned} \tag{3}$$

where $x_f(t) \in \mathscr{R}^n$ is the state of the filter and $z_f(t) \in \mathscr{R}^q$ is the output of the filter; the matrices $\mathscr{A}_f$, $\mathscr{B}_f$, $\mathscr{C}_f$, and $\mathscr{D}_f$ are filter matrices with appropriate dimensions to be designed and $y_q(t)$ is the quantized measurement.

Remark 2. Note that the filter we consider here has a standard form, which is convenient for both theoretical analysis and implementation in practical engineering compared to the singular form.

The quantizer we consider is logarithmic static and time-invariant quantizer given in [30]. The set of quantized levels

is described by $U^{(j)} = \{\pm u_i^j, u_i^j = (\rho^j)^i u_0^j,\ i = \pm 1, \pm 2, \ldots\} \cup \{\pm u_0^j\} \cup \{0\},\ u_0^j > 0$ and the quantizer is defined as follows:

$$q_j(y) = \begin{cases} v_i^{(j)} & 0 \le \dfrac{v_i^{(j)}}{\left(1+\delta_j\right)} < y \le \dfrac{v_i^{(j)}}{\left(1-\delta_j\right)} \\ 0 & y = 0 \\ -\mathcal{Q}_j(-y) & y < 0, \end{cases} \tag{4}$$

$$\delta_j = \frac{1-\rho_j}{1+\rho_j}, \quad 0 < \rho_j < 1,\ v_i^{(j)} > 0. \tag{5}$$

Then, by using the sector-bound method described in [30], we can obtain that, for any $y(t)$, $y_q(t) = q(y(t)) = (I + \Delta(t))y(t)$, where $\Delta(t) = \mathrm{diag}\{\Delta_1(t), \Delta_2(t), \ldots, \Delta_f(t)\}$, $|\Delta(t)| \le \delta$.

Combining (1) and (3) and defining $\tilde{x}(t) = [x^T(t), x_f^T(t)]^T$ and $e(t) = z(t) - z_f(t)$, one can obtain the filtering error system as follows:

$$\begin{aligned} \tilde{E}\tilde{x}(t+1) &= \widetilde{\mathscr{A}}\tilde{x}(t) + \mathscr{M}\Phi(t, \tilde{x}(t)) + \widetilde{\mathscr{B}}w(t), \\ e(t) &= \widetilde{\mathscr{C}}\tilde{x}(t) + \widetilde{\mathscr{D}}w(t), \end{aligned} \tag{6}$$

where

$$\begin{aligned} \tilde{E} &= \begin{bmatrix} E & 0 \\ 0 & I \end{bmatrix}, \\ \widetilde{\mathscr{A}} &= \overline{\mathscr{A}} + \Delta\overline{\mathscr{A}} \\ &= \begin{bmatrix} \mathscr{A} & 0 \\ \mathscr{B}_f\mathscr{C} & \mathscr{A}_f \end{bmatrix} + \begin{bmatrix} 0 & 0 \\ \mathscr{B}_f\Delta(t)\mathscr{C} & 0 \end{bmatrix}, \\ \mathscr{M} &= \begin{bmatrix} I & 0 \\ 0 & \lambda_1 \end{bmatrix}, \\ \Phi(t, \tilde{x}(t)) &= \begin{bmatrix} \Psi(t, x(t)) \\ \Psi\left(t, x_f(t)\right) \end{bmatrix}, \\ \widetilde{\mathscr{B}} &= \overline{\mathscr{B}} + \Delta\overline{\mathscr{B}} = \begin{bmatrix} \mathscr{B} \\ \mathscr{B}_f\mathscr{D} \end{bmatrix} + \begin{bmatrix} 0 \\ \mathscr{B}_f\Delta(t)\mathscr{D} \end{bmatrix}, \\ \widetilde{\mathscr{C}} &= \overline{\mathscr{C}} + \Delta\overline{\mathscr{C}} \\ &= \left[\mathscr{L} - \mathscr{D}_f\mathscr{C} \quad -\mathscr{C}_f\right] + \left[-\mathscr{D}_f\Delta(t)\mathscr{C} \quad 0\right], \\ \widetilde{\mathscr{D}} &= \overline{\mathscr{D}} + \Delta\overline{\mathscr{D}} = -\mathscr{D}_f\mathscr{D} - \mathscr{D}_f\Delta(t)\mathscr{D}. \end{aligned} \tag{7}$$

To this end, we aim to design a quantized $\mathscr{H}_\infty$ filter such that the filtering error system (6) satisfies the following requirements.

(R1) The filtering error system (6) is admissible and of a uniquely discrete solution with $w(t) = 0$.

(R2) The filtering error system (6) has a prescribed level γ of $\mathscr{H}_\infty$ noise attenuation; that is, $\sum_{t=0}^{\infty} e^T(t)e(t) < \gamma^2 \sum_{t=0}^{\infty} w^T(t)w(t)$ is satisfied for any nonzero $w(t) \in l_2[0, \infty)$ with the zero initial condition.

To solve the quantized $\mathscr{H}_\infty$ filtering analysis problem of the considered nonlinear singular system, we need the following preliminary results to prove our main results.

Lemma 3 (see [35]). *Let $\xi \in \mathscr{R}^n$, $\mathcal{Q} \in \mathscr{R}^{n\times n}$, and $\mathscr{B} \in \mathscr{R}^{m\times n}$ with $\mathrm{rank}(\mathscr{B}) < n$ and $\mathscr{B}^\perp$ such that $\mathscr{B}\mathscr{B}^\perp = 0$. Then, the following conditions are equivalent:*

(1) $\xi^T\mathcal{Q}\xi < 0,\ \forall \xi \ne 0 : \mathscr{B}\xi = 0$.

(2) $\mathscr{B}^{\perp T}\mathcal{Q}\mathscr{B}^\perp < 0$.

(3) $\exists \mu \in \mathscr{R} : \mathcal{Q} - \mu\mathscr{B}^T\mathscr{B} < 0$.

(4) $\exists \mathcal{X} \in \mathscr{R}^{n\times m} : \mathcal{Q} + \mathcal{X}\mathscr{B} + \mathscr{B}^T\mathcal{X}^T < 0$.

Lemma 4 (see [16]). *System (6) is regular, causal, and of a unique discrete solution, if there exists a matrix $\mathscr{P} = \mathscr{P}^T$ such that the following inequality holds:*

$$\begin{aligned} &\tilde{E}^T\mathscr{P}\tilde{E} \ge 0, \\ &\begin{bmatrix} \widetilde{\mathscr{A}}^T\mathscr{P}\widetilde{\mathscr{A}} - \tilde{E}^T\mathscr{P}\tilde{E} + \widetilde{\mathscr{F}}^T\widetilde{\mathscr{F}} & * \\ \mathscr{M}^T\mathscr{P}\widetilde{\mathscr{A}} & \mathscr{M}^T\mathscr{P}\mathscr{M} - I \end{bmatrix} < 0. \end{aligned} \tag{8}$$

Lemma 5 (see [36]). *For real matrices $\Omega = \Omega^T$, Γ, Λ, and F with appropriate dimensions and $F^TF \le I$. Then, for any scalar $\epsilon > 0$, the following inequality holds:*

$$\Omega + \Gamma F\Lambda + \Lambda^T F^T\Gamma^T \le \Omega + \epsilon^{-1}\Gamma\Gamma^T + \epsilon\Lambda^T\Lambda. \tag{9}$$

3. Main Results

In this section, the quantized $\mathscr{H}_\infty$ filtering problem for nonlinear singular systems will be considered. First, we will give a new $\mathscr{H}_\infty$ performance analysis criterion based on Fisher lemma given in Lemma 3 such that the filtering error system (6) is admissible and of a unique solution with a prescribed $\mathscr{H}_\infty$ performance γ.

Theorem 6. *Let us consider the nonlinear singular system (1) and the quantized filter (3). Then the quantized filtering error system (6) is admissible and of a unique solution with a prescribed $\mathscr{H}_\infty$ performance $\gamma > 0$, if there exist matrix $\mathscr{P} = \mathscr{P}^T = \begin{bmatrix} \mathscr{P}_1 & \mathscr{P}_2 \\ \mathscr{P}_2^T & \mathscr{P}_3 \end{bmatrix}$, $\mathscr{P}_1 > 0$, matrices $\mathscr{G}$ and $\mathscr{N}$, and scalar λ_1 such that the following matrix inequality holds:*

$$\begin{bmatrix} -3\widetilde{E}^T\mathscr{P}\widetilde{E} + \mathrm{He}\left\{\mathscr{N}\widetilde{\mathscr{A}}\right\} + \widetilde{\mathscr{F}}^T\widetilde{\mathscr{F}} & * & * & * & * \\ \mathscr{M}^T\mathscr{N}^T & -I & * & * & * \\ \widetilde{\mathscr{B}}^T\mathscr{N}^T & 0 & -\gamma^2 I & * & * \\ \mathscr{P}\widetilde{\mathscr{A}} - \mathscr{N}^T + \mathscr{G}\widetilde{\mathscr{A}} & \mathscr{P}\mathscr{M} + \mathscr{G}\mathscr{M} & \mathscr{P}\widetilde{\mathscr{B}} + \mathscr{G}\widetilde{\mathscr{B}} & \mathscr{P} - \mathrm{He}\{\mathscr{G}\} & * \\ \widetilde{\mathscr{C}} & 0 & \widetilde{\mathscr{D}} & 0 & -I \end{bmatrix} < 0, \tag{10}$$

where $\widetilde{\mathscr{F}} = \mathrm{diag}\{\mathscr{F}^T\mathscr{F}, \mathscr{F}^T\mathscr{F}\}$.

Proof. Firstly, we shall show the filtering error system is regular and causal with $w(t) = 0$. Equation (10) implies

$$-3\widetilde{E}^T\mathscr{P}\widetilde{E} + \mathscr{N}\widetilde{\mathscr{A}} + \widetilde{\mathscr{A}}^T\mathscr{N}^T + \widetilde{\mathscr{F}}^T\widetilde{\mathscr{F}} < 0. \tag{11}$$

Without loss of generality, we assume that $\widetilde{E} = \begin{bmatrix} I_{n+r} & 0 \\ 0 & 0 \end{bmatrix}$ and $\mathscr{N} = \begin{bmatrix} \mathscr{N}_1 & 0 \\ 0 & \mathscr{K} \end{bmatrix}$, and then (11) can be rewritten as

$$\begin{bmatrix} -3\mathscr{P}_1 + \mathrm{He}\left\{\mathscr{N}_1\mathscr{A}\right\} & * \\ \mathscr{K}\mathscr{B}_f\left(I + \Delta(t)\right)\mathscr{C} & \mathrm{He}\left\{\mathscr{K}\mathscr{A}_f\right\} \end{bmatrix} < 0. \tag{12}$$

Form (12) we have $\mathrm{He}\{\mathscr{K}\mathscr{A}_f\} < 0$ that implies $\mathscr{A}_f$ is nonsingular.

$$\det\left(s\widetilde{E} - \widetilde{\mathscr{A}}\right) = \det\left(sI_{n+r} - \widetilde{\mathscr{A}}\right) \cdot \det\left(-\mathscr{A}_f\right). \tag{13}$$

By choosing nonzero scalar s, we have $\det(s\widetilde{E} - \widetilde{\mathscr{A}}) \neq 0$; that is, $\det(s\widetilde{E} - \widetilde{\mathscr{A}}) \neq 0$. Furthermore, we can obtain

$$\deg\det\left(s\widetilde{E} - \widetilde{\mathscr{A}}\right) = n + r = \mathrm{rank}\,\widetilde{E}. \tag{14}$$

Then, we have that the pair $(\widetilde{E}, \widetilde{\mathscr{A}})$ is regular and causal. Based on Definition 1, we can obtain the fact that filtering error system (6) is regular and causal when condition (10) holds.

Now, by constructing a Lyapunov function as $V(\tilde{x}(t)) = 3\tilde{x}^T(t)\widetilde{E}^T\mathscr{P}\widetilde{E}\tilde{x}(t)$, $\mathscr{P} = \mathscr{P}^T = \begin{bmatrix} \mathscr{P}_1 & \mathscr{P}_2 \\ \mathscr{P}_2^T & \mathscr{P}_3 \end{bmatrix}$, $\mathscr{P}_1 > 0$, we have

$$\begin{aligned} \Delta V(\tilde{x}(t)) &= V(\tilde{x}(t+1)) - V(\tilde{x}(t)) \\ &= \left(\widetilde{\mathscr{A}}\tilde{x}(t) + \mathscr{M}\Phi(t, \tilde{x}(t))\right)^T \mathscr{P}\widetilde{E}\tilde{x}(t+1) \\ &\quad + \tilde{x}^T(t+1)\widetilde{E}^T\mathscr{P}\left(\widetilde{\mathscr{A}}\tilde{x}(t) + \mathscr{M}\Phi(t, \tilde{x}(t))\right) \\ &\quad + \tilde{x}^T(t+1)\widetilde{E}^T\mathscr{P}\widetilde{E}\tilde{x}(t+1) \\ &\quad - 3\tilde{x}^T(t)\widetilde{E}^T\mathscr{P}\widetilde{E}\tilde{x}(t) \\ &\leq \left(\widetilde{\mathscr{A}}\tilde{x}(t) + \mathscr{M}\Phi(t, \tilde{x}(t))\right)^T \mathscr{P}\widetilde{E}\tilde{x}(t+1) \\ &\quad + \tilde{x}^T(t+1)\widetilde{E}^T\mathscr{P}\left(\widetilde{\mathscr{A}}\tilde{x}(t) + \mathscr{M}\Phi(t, \tilde{x}(t))\right) \\ &\quad + \tilde{x}^T(t+1)\widetilde{E}^T\mathscr{P}\widetilde{E}\tilde{x}(t+1) \\ &\quad - 3\tilde{x}^T(t)\widetilde{E}^T\mathscr{P}\widetilde{E}\tilde{x}(t) + \tilde{x}^T(t)\widetilde{\mathscr{F}}^T\widetilde{\mathscr{F}}\tilde{x}(t) \\ &\quad - \Phi^T(t, \tilde{x}(t))\Phi(t, \tilde{x}(t)) = \xi^T(t)\Gamma\xi(t), \end{aligned} \tag{15}$$

where $\xi(t) = \left[\tilde{x}^T(t) \;\; \Phi^T(t, \tilde{x}(t)) \;\; \tilde{x}^T(t+1)\widetilde{E}^T\right]$ and

$$\Gamma = \begin{bmatrix} -3\widetilde{E}^T\mathscr{P}\widetilde{E} + \widetilde{\mathscr{F}}^T\widetilde{\mathscr{F}} & * & * \\ 0 & -I & * \\ \mathscr{P}\widetilde{\mathscr{A}} & \mathscr{P}\mathscr{M} & \mathscr{P} \end{bmatrix}. \tag{16}$$

Form the filtering error system (6), we have

$$\underbrace{\left[\widetilde{\mathscr{A}} \;\; \widetilde{\mathscr{B}} \;\; -I\right]}_{\mathscr{B}}\underbrace{\xi(t)}_{\xi} = 0, \tag{17}$$

and, by using conditions (1) and (4) of Lemma 3 with $\mathscr{X}^T = \left[\mathscr{N}^T \;\; 0 \;\; \mathscr{G}^T\right]^T$, we can obtain $\Gamma < 0$ if and only if (10) is true. Therefore, we have $\Delta V(\tilde{x}(t)) < 0$ for any nonzero $\xi(t)$, and one can infer that the filtering error system (6) is asymptotically stable with $w(t) = 0$.

Next, we will prove that the filtering system (6) is of unique solution. The difference of the Lyapunov function can be rewritten as follows:

$$\begin{aligned} \Delta V(\tilde{x}(t)) &= V(\tilde{x}(t+1)) - V(\tilde{x}(t)) \\ &\leq \left(\widetilde{\mathscr{A}}\tilde{x}(t) + \mathscr{M}\Phi(t, \tilde{x}(t))\right)^T \mathscr{P}\widetilde{E}\tilde{x}(t+1) \\ &\quad + \tilde{x}^T(t+1)\widetilde{E}^T\mathscr{P}\left(\widetilde{\mathscr{A}}\tilde{x}(t) + \mathscr{M}\Phi(t, \tilde{x}(t))\right) \\ &\quad + \tilde{x}^T(t+1)\widetilde{E}^T\mathscr{P}\widetilde{E}\tilde{x}(t+1) - 3\tilde{x}^T(t)\widetilde{E}^T\mathscr{P}\widetilde{E}\tilde{x}(t) \\ &\quad + \tilde{x}^T(t)\widetilde{\mathscr{F}}^T\widetilde{\mathscr{F}}\tilde{x}(t) - \Phi^T(t, \tilde{x}(t))\Phi(t, \tilde{x}(t)) \\ &= 3\left(\widetilde{\mathscr{A}}\tilde{x}(t) + \mathscr{M}\Phi(t, \tilde{x}(t))\right)^T \\ &\quad \cdot \mathscr{P}\left(\widetilde{\mathscr{A}}\tilde{x}(t) + \mathscr{M}\Phi(t, \tilde{x}(t))\right) - 3\tilde{x}^T(t)\widetilde{E}^T\mathscr{P}\widetilde{E}\tilde{x}(t) \\ &\quad + \tilde{x}^T(t)\widetilde{\mathscr{F}}^T\widetilde{\mathscr{F}}\tilde{x}(t) - \Phi^T(t, \tilde{x}(t))\Phi(t, \tilde{x}(t)) \\ &= 3\delta^T(t)\Theta\delta(t), \end{aligned} \tag{18}$$

where $\xi(t) = \left[\tilde{x}^T(t) \;\; \Phi^T(t, \tilde{x}(t))\right]$ and

$$\Theta = \begin{bmatrix} \widetilde{\mathscr{A}}^T\mathscr{P}\widetilde{\mathscr{A}} - \widetilde{E}^T\mathscr{P}\widetilde{E} + \widetilde{\mathscr{F}}^T\widetilde{\mathscr{F}} & * \\ \mathscr{M}^T\mathscr{P}\widetilde{\mathscr{A}} & -I + \mathscr{M}^T\mathscr{P}\mathscr{M} \end{bmatrix}, \tag{19}$$

and then from (10) we can obtain $\Delta V(\tilde{x}(t)) < 0$; that is, $\Theta < 0$. Therefore, based on Lemma 4, we can prove that the filtering error system (6) is of unique solution.

Finally, let us consider the $\mathscr{H}_\infty$ performance of the filtering system (6). For any nonzero $w(t) \in l_2[0, \infty)$ and zero initial condition, we have

$$\begin{aligned}
&\Delta V(\tilde{x}(t)) + e^T(t)e(t) - \gamma^2 w^T(t)w(t) \\
&= \left(\widetilde{\mathscr{A}}\tilde{x}(t) + \mathscr{M}\Phi(t,\tilde{x}(t)) + \widetilde{\mathscr{B}}w(t)\right)^T \\
&\cdot \mathscr{P}\tilde{E}\tilde{x}(t+1) + \tilde{x}^T(t+1) \\
&\cdot \tilde{E}^T\mathscr{P}\left(\widetilde{\mathscr{A}}\tilde{x}(t) + \mathscr{M}\Phi(t,\tilde{x}(t)) + \widetilde{\mathscr{B}}w(t)\right) \\
&+ \tilde{x}^T(t+1)\tilde{E}^T\mathscr{P}\tilde{E}\tilde{x}(t+1) - 3\tilde{x}^T(t)\tilde{E}^T\mathscr{P}\tilde{E}\tilde{x}(t) \\
&+ \left(\widetilde{\mathscr{C}}\tilde{x}(t) + \widetilde{\mathscr{D}}w(t)\right)^T\left(\widetilde{\mathscr{C}}\tilde{x}(t) + \widetilde{\mathscr{D}}w(t)\right) \\
&- \gamma^2 w^T(t)w(t) \\
&\le \left(\widetilde{\mathscr{A}}\tilde{x}(t) + \mathscr{M}\Phi(t,\tilde{x}(t)) + \widetilde{\mathscr{B}}w(t)\right)^T \\
&\cdot \mathscr{P}\tilde{E}\tilde{x}(t+1) + \tilde{x}^T(t+1) \\
&\cdot \tilde{E}^T\mathscr{P}\left(\widetilde{\mathscr{A}}\tilde{x}(t) + \mathscr{M}\Phi(t,\tilde{x}(t)) + \widetilde{\mathscr{B}}w(t)\right) \\
&+ \tilde{x}^T(t+1)\tilde{E}^T\mathscr{P}\tilde{E}\tilde{x}(t+1) - 3\tilde{x}^T(t)\tilde{E}^T\mathscr{P}\tilde{E}\tilde{x}(t) \\
&+ \left(\widetilde{\mathscr{C}}\tilde{x}(t) + \widetilde{\mathscr{D}}w(t)\right)^T\left(\widetilde{\mathscr{C}}\tilde{x}(t) + \widetilde{\mathscr{D}}w(t)\right) \\
&- \gamma^2 w^T(t)w(t) + \tilde{x}^T(t)\widetilde{\mathscr{F}}^T\widetilde{\mathscr{F}}\tilde{x}(t) - \Phi^T(t,\tilde{x}(t)) \\
&\cdot \Phi(t,\tilde{x}(t)) = \eta^T(t)\Lambda\eta(t),
\end{aligned} \tag{20}$$

where $\eta(t) = \left[\tilde{x}^T(t) \;\; \Phi^T(t,\tilde{x}(t)) \;\; \widetilde{w}^T(t) \;\; \tilde{x}^T(t+1)\tilde{E}^T\right]$ and

$$\Lambda = \begin{bmatrix} -3\tilde{E}^T\mathscr{P}\tilde{E} + \widetilde{\mathscr{C}}^T\widetilde{\mathscr{C}} + \widetilde{\mathscr{F}}^T\widetilde{\mathscr{F}} & * & * & * \\ 0 & -I & * & * \\ \widetilde{\mathscr{D}}^T\widetilde{\mathscr{C}} & 0 & -\gamma^2 I + \widetilde{\mathscr{D}}^T\widetilde{\mathscr{D}} & * \\ \mathscr{P}\widetilde{\mathscr{A}} & \mathscr{P}\mathscr{M} & \mathscr{P}\widetilde{\mathscr{B}} & \mathscr{P} \end{bmatrix}. \tag{21}$$

Form the filtering error system (6), we have

$$\underbrace{\left[\widetilde{\mathscr{A}} \;\; \mathscr{M} \;\; \widetilde{\mathscr{B}} \;\; -I\right]}_{\mathscr{B}}\underbrace{\eta(t)}_{\xi} = 0, \tag{22}$$

and, by using conditions (1) and (4) of Lemma 3 with $\mathscr{X} = \left[\mathscr{N} \;\; 0 \;\; 0 \;\; \mathscr{G}\right]$ and Schur complement lemma, we can obtain $\Lambda < 0$ if and only if (10) is true. Then for any $\eta(t) \neq 0$ we have $V(\tilde{x}(t+1)) - V(\tilde{x}(t)) + e^T(t)e(t) - \gamma^2 w^T(t)w(t) < 0$, which implies that $V(\tilde{x}(\infty)) - V(\tilde{x}(0)) + \sum_{t=0}^{\infty} e^T(t)e(t) - \gamma^2\sum_{t=0}^{\infty} w^T(t)w(t) < 0$. Consider the zero initial condition and we obtain $\sum_{t=0}^{\infty} e^T(t)e(t) < \gamma^2\sum_{t=0}^{\infty} w^T(t)w(t)$ for any nonzero $w(t) \in l_2[0, \infty)$. □

Based on the $\mathscr{H}_\infty$ performance analysis criterion given in Theorem 6, we will present a sufficient condition for designing the quantized $\mathscr{H}_\infty$ filter in the form of (3), that is, to determine the filter gain matrices in (3) such that the prescribed $\mathscr{H}_\infty$ performance $\gamma > 0$ is guaranteed for the quantized filtering error system (6).

Theorem 7. *Let us consider the nonlinear singular system (1) and the quantized filter (3). For given quantization density $\rho > 0$, the quantized filtering error system (6) is admissible and of a unique solution with a prescribed $\mathscr{H}_\infty$ performance $\gamma > 0$, if there exist matrices $\mathscr{P}_1 = \mathscr{P}_1^T > 0$, $\mathscr{G}_1$, $\mathscr{G}_2$, $\mathscr{N}_1$, and nonsingular matrix $\mathscr{K}$ and some scalars λ_1, a_1, a_2, a_3, and $\varepsilon > 0$ such that the following matrix inequality holds:*

$$\begin{bmatrix} \Upsilon_{11} & * & * & * & * & * & * & * & * \\ \Upsilon_{21} & -I & * & * & * & * & * & * & * \\ \Upsilon_{31} & 0 & -\gamma^2 I & * & * & * & * & * & * \\ \Upsilon_{41} & \Upsilon_{42} & \Upsilon_{43} & \Upsilon_{44} & * & * & * & * & * \\ \overline{\mathscr{C}} & 0 & \overline{\mathscr{D}} & 0 & -I & * & * & * & * \\ \Upsilon_{61} & 0 & 0 & \Upsilon_{64} & -\overline{\mathscr{D}}_f^T & -\varepsilon I & * & * & * \\ \Upsilon_{71} & 0 & 0 & \Upsilon_{74} & 0 & 0 & -\varepsilon I & * & * \\ \varepsilon\delta\mathscr{H}_2 & 0 & \varepsilon\delta\mathscr{D} & 0 & 0 & 0 & 0 & -\varepsilon I & * \\ \varepsilon\delta\mathscr{H}_2 & 0 & \varepsilon\delta\mathscr{D} & 0 & 0 & 0 & 0 & 0 & -\varepsilon I \end{bmatrix} < 0, \tag{23}$$

where

$$\Upsilon_{11} = \begin{bmatrix} -3E^T\mathscr{P}_1E + \mathrm{He}\{\mathscr{N}_1\mathscr{A}\} + \mathscr{F}^T\mathscr{F} & * \\ \mathscr{K}^TE + \overline{\mathscr{B}}_f\mathscr{C} & \mathrm{He}\{\mathscr{A}_f\} + \mathscr{F}^T\mathscr{F} + a_1\mathscr{K} \end{bmatrix},$$

$$\Upsilon_{21} = \begin{bmatrix} \mathscr{N}_1^T & 0 \\ 0 & \lambda_1^T\mathscr{K}^T \end{bmatrix},$$

$$\Upsilon_{31} = \begin{bmatrix} \mathscr{B}^T\mathscr{N}_1^T & \mathscr{D}^T\overline{\mathscr{B}}_f^T \end{bmatrix},$$

$$\Upsilon_{41} = \begin{bmatrix} \mathscr{P}_1\mathscr{A} + \mathscr{G}_1\mathscr{A} + (1+a_2)\overline{\mathscr{B}}_f\mathscr{C} - \mathscr{N}_1^T & (1+a_2)\overline{\mathscr{A}}_f \\ \mathscr{K}^T\mathscr{A} + \mathscr{G}_2\mathscr{A} + (a_1+a_3)\overline{\mathscr{B}}_f\mathscr{C} & (a_1+a_3)\overline{\mathscr{A}}_f - \mathscr{K}^T \end{bmatrix},$$

$$\Upsilon_{42} = \begin{bmatrix} \mathscr{P}_1 + \mathscr{G}_1 & (a_2+1)\lambda_1\mathscr{K} \\ \mathscr{K}^T + \mathscr{G}_2 & (a_1+a_3)\lambda_1\mathscr{K} - \mathscr{K}^T \end{bmatrix},$$

$$\Upsilon_{43} = \begin{bmatrix} \mathscr{P}_1\mathscr{B} + \mathscr{G}_1\mathscr{B} + (a_2+1)\overline{\mathscr{B}}_f\mathscr{D} \\ \mathscr{K}^T\mathscr{B} + \mathscr{G}_2\mathscr{B} + (a_1+a_3)\overline{\mathscr{B}}_f\mathscr{D} \end{bmatrix},$$

$$\Upsilon_{44} = \begin{bmatrix} \mathscr{P}_1 - \mathrm{He}\{\mathscr{G}_1\} & * \\ \mathscr{K}^T - \mathscr{G}_2 - a_2\mathscr{K}^T & a_1\mathscr{K} - \mathrm{He}\{a_3\mathscr{K}\} \end{bmatrix},$$

$$\Upsilon_{61} = \Upsilon_{71} = \begin{bmatrix} 0 & \overline{\mathscr{B}}_f{}^T \end{bmatrix},$$

$$\Upsilon_{64} = \begin{bmatrix} \overline{\mathscr{B}}_f{}^T & a_1\overline{\mathscr{B}}_f{}^T \end{bmatrix},$$

$$\Upsilon_{74} = \begin{bmatrix} a_2\overline{\mathscr{B}}_f{}^T & a_3\overline{\mathscr{B}}_f{}^T \end{bmatrix}. \tag{24}$$

The $\mathscr{H}_\infty$ filter gain matrices in (3) can be obtained from (23) as $\mathscr{A}_f = \mathscr{K}^{-1}\overline{\mathscr{A}}_f$, $\mathscr{B}_f = \mathscr{K}^{-1}\overline{\mathscr{B}}_f$, $\mathscr{C}_f = \overline{\mathscr{C}}_f$, and $\mathscr{D}_f = \overline{\mathscr{D}}_f$.

Proof. The condition of (10) can be rewritten as follows:

$$\Pi + \mathrm{He}\left\{\Pi_1\frac{\Delta(k)}{\delta}\Pi_2\right\}, \tag{25}$$

where

$$\Pi = \begin{bmatrix} -3\widetilde{E}^T\mathscr{P}\widetilde{E} + \mathrm{He}\left\{\mathscr{N}\overline{\mathscr{A}}\right\} + \widetilde{\mathscr{F}}^T\widetilde{\mathscr{F}} & * & * & * & * \\ \mathscr{M}^T\mathscr{N}^T & -I & * & * & * \\ \overline{\mathscr{B}}^T\mathscr{N}^T & 0 & -\gamma^2 I & * & * \\ \mathscr{P}\overline{\mathscr{A}} - \mathscr{N}^T + \mathscr{G}\overline{\mathscr{A}} & \mathscr{P}\mathscr{M} + \mathscr{G}\mathscr{M} & \mathscr{P}\overline{\mathscr{B}} + \mathscr{G}\overline{\mathscr{B}} & \mathscr{P} - \mathrm{He}\{\mathscr{G}\} & * \\ \overline{\mathscr{C}} & 0 & \overline{\mathscr{D}} & 0 & -I \end{bmatrix}, \tag{26}$$

$$\Pi_1 = \begin{bmatrix} \mathscr{H}_1^T\mathscr{N}^T & 0 & 0 & \mathscr{H}_1^T\mathscr{P}^T & -\mathscr{D}_f^T \\ \mathscr{H}_1^T\mathscr{N}^T & 0 & 0 & \mathscr{H}_1^T\mathscr{G}^T & 0 \end{bmatrix}^T,$$

$$\Pi_2 = \begin{bmatrix} \delta\mathscr{H}_2 & 0 & \delta\mathscr{D} & 0 & 0 \\ \delta\mathscr{H}_2 & 0 & \delta\mathscr{D} & 0 & 0 \end{bmatrix},$$

and $\mathscr{H}_1 = \begin{bmatrix} 0 & \mathscr{B}_f^T \end{bmatrix}^T$ and $\mathscr{H}_2 = \begin{bmatrix} \delta\mathscr{C} & 0 \end{bmatrix}$.

Then, by Lemma 5, we have that there exists a constant scalar $\varepsilon > 0$ such that

$$\begin{bmatrix} \Pi & * \\ \Sigma_1 & \Sigma_2 \end{bmatrix} < 0, \tag{27}$$

where

$$\Sigma_1 = \begin{bmatrix} \mathscr{H}_1^T\mathscr{N}^T & 0 & 0 & \mathscr{H}_1^T\mathscr{P}^T & -\mathscr{D}_f^T \\ \mathscr{H}_1^T\mathscr{N}^T & 0 & 0 & \mathscr{H}_1^T\mathscr{G}^T & 0 \\ \varepsilon\delta\mathscr{H}_2 & 0 & \varepsilon\delta\mathscr{D} & 0 & 0 \\ \varepsilon\delta\mathscr{H}_2 & 0 & \varepsilon\delta\mathscr{D} & 0 & 0 \end{bmatrix},$$

Table 1: The minimum $\mathscr{H}_\infty$ filtering performances $\gamma_{\min}$ under different quantization density ρ.

ρ	0.3	0.4	0.5	0.6	0.7	0.8
δ	0.5385	0.4286	0.3333	0.2500	0.1765	0.1111
$\gamma_{\min}$	0.1951	0.1924	0.1820	0.1586	0.1363	0.1177

$$\Sigma_2 = \begin{bmatrix} -\varepsilon I & * & * & * \\ 0 & -\varepsilon I & * & * \\ 0 & 0 & -\varepsilon I & * \\ 0 & 0 & 0 & -\varepsilon I \end{bmatrix}. \tag{28}$$

We can design the filter if (27) is solvable. Here, assume that the matrix variables involved in (27) have the following form:

$$\{\mathscr{P}, \mathscr{G}, \mathscr{N}\} = \left\{ \begin{bmatrix} \mathscr{P}_1 & * \\ \mathscr{K}^T & a_1 \mathscr{K} \end{bmatrix}, \begin{bmatrix} \mathscr{G}_1 & a_2 \mathscr{K} \\ \mathscr{G}_2 & a_3 \mathscr{K} \end{bmatrix}, \begin{bmatrix} \mathscr{N}_1 & 0 \\ 0 & \mathscr{K} \end{bmatrix} \right\}. \tag{29}$$

With the aforementioned related matrices considered and letting $\overline{\mathscr{A}}_f = \mathscr{K}\mathscr{A}_f$, $\overline{\mathscr{B}}_f = \mathscr{K}\mathscr{B}_f$, $\overline{\mathscr{C}}_f = \mathscr{C}_f$, $\overline{\mathscr{D}}_f = \mathscr{D}_f$, Theorem 7 can be obtained from (27). □

Remark 8. For given a_1, a_2, a_3, and δ, Theorem 7 is strictly LMIs. The quantization error bound δ can be calculated according to the given quantization density ρ by (5) and the optimal values of a_1, a_2, and a_3 can be obtained by using fminsearch function in optimization toolbox of MATLAB (see [34, 37] for more details). Then Theorem 7 can be easily solved with the help of LMI control box in MATLAB [38].

4. A Numerical Example

In this section, a numerical example will be presented to illustrate the effectiveness and applicability of the proposed method. Let us consider the following nonlinear system in form of (1) borrowed from [16]:

$$\begin{bmatrix} 1 & 0 \\ 0 & 0 \end{bmatrix} \begin{bmatrix} x_1(t+1) \\ x_2(t+1) \end{bmatrix} = \begin{bmatrix} -0.5 & 0 \\ 1 & -1 \end{bmatrix} \begin{bmatrix} x_1(t) \\ x_2(t) \end{bmatrix} + \begin{bmatrix} 0.5 \\ -0.5 \end{bmatrix} w(t) + \begin{bmatrix} \frac{1}{\sqrt{10}} \sin(x_1(t)) \\ \frac{1}{\sqrt{10}} \sin(x_2(t)) \end{bmatrix}, \tag{30}$$

$$y(t) = \begin{bmatrix} 0.1 & 0.2 \end{bmatrix} \begin{bmatrix} x_1(t) \\ x_2(t) \end{bmatrix} - w(t),$$

$$z(t) = \begin{bmatrix} 0.2 & -0.1 \end{bmatrix} \begin{bmatrix} x_1(t) \\ x_2(t) \end{bmatrix},$$

and then we have $\mathscr{F} = \left[\begin{smallmatrix} 0.1 & 0 \\ 0 & 0.1 \end{smallmatrix} \right]$ from (2).

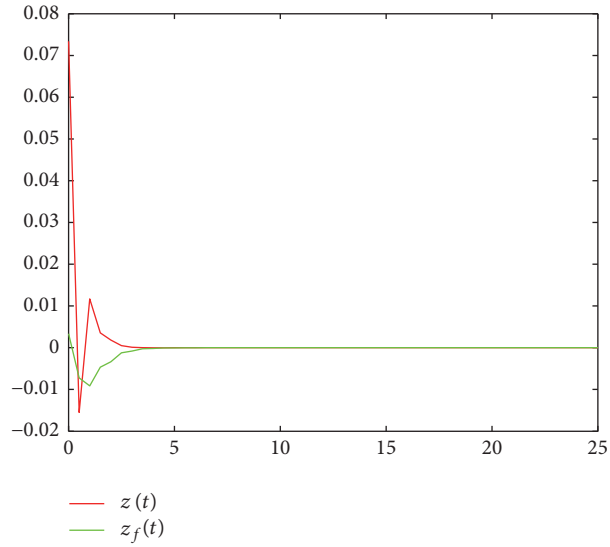

Figure 1: Responses of $z(t)$ and $z_f(t)$.

Table 1 shows the minimum $\mathscr{H}_\infty$ attention level obtained by using Theorem 7 with $a_1 = -1.20$, $a_2 = 0.11$, $a_3 = 3.50$, and $\lambda_1 = 1$, under different quantization density. As expected, we can obtain that $\gamma_{\min}$ increases as the quantization density ρ decreases from this table. Moreover, when $\gamma_{\min} = 0.1820$, the corresponding filter parameters of Theorem 7 can be calculated as follows:

$$\mathscr{A}_f = \begin{bmatrix} 0.2688 & 0.5305 \\ -0.2087 & -0.9779 \end{bmatrix},$$

$$\mathscr{B}_f = \begin{bmatrix} 0.4268 \\ -0.5199 \end{bmatrix} \tag{31}$$

$$\mathscr{C}_f = \begin{bmatrix} 0.0456 & 0.0620 \end{bmatrix},$$

$$\mathscr{D}_f = 0.0114.$$

We assume the external disturbance $w(t) = \sin(t)e^{-2t}$, and the simulation results of signals $z(t)$ and $z_f(t)$ are shown in Figure 1. Figure 2 shows the response of the filtering error $e(t)$. From Figures 1 and 2, we can see that the designed $\mathscr{H}_\infty$ filter is effective.

5. Conclusion

The quantized $\mathscr{H}_\infty$ filtering problem for a class of discrete-time Lipschitz nonlinear singular systems has been addressed in this paper, where the system measurement output is quantized by a static, memoryless, and logarithmic quantizer.

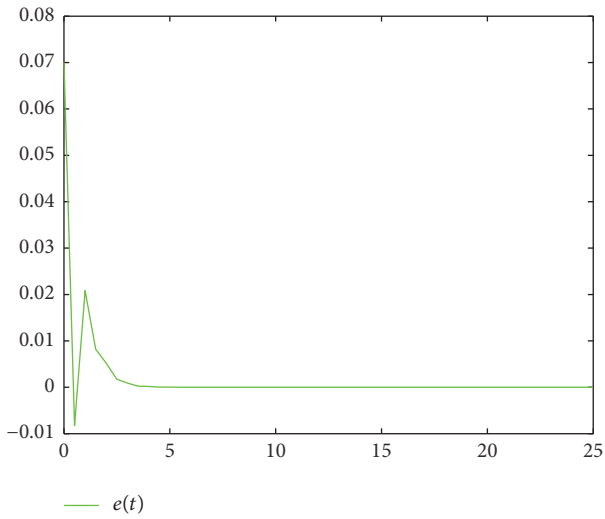

Figure 2: Filtering error $e(t)$.

By introducing some variables and applying Lyapunov stability theory, sufficient conditions for designing the quantized $\mathscr{H}_\infty$ filter are presented in linear matrix inequalities (LMIs), which ensure the quantized filtering error systems to be admissible and has a unique solution with a prescribed $\mathscr{H}_\infty$ performance. A numerical example is given to show the effectiveness of the proposed design method. The results proposed in this paper can be further developed by the novel LMI decoupling approach presented in [39] which has also been used to deal with the $\mathscr{H}_\infty$ filtering problem; see [40] for more details.

Conflicts of Interest

The authors declare that there are no conflicts of interest regarding the publication of this paper.

Acknowledgments

This work was supported in part by the Education Department of Jilin Province, China, under Science and Technology Research Project (Grant no. 20150214).

References

[1] E. Fridman and U. Shaked, "Robust $\mathscr{H}_\infty$ minimum entropy static output–feedback control of singularly perturbed systems," *Automatica. A Journal of IFAC, the International Federation of Automatic Control*, vol. 36, no. 8, pp. 1181–1188, 2000.

[2] J. Yao, Z.-H. Guan, G. Chen, and D. Ho, "Stability, robust stabilization and $\mathscr{H}_\infty$ control of singular–impulsive systems via switching control," *Systems & Control Letters*, vol. 55, no. 11, pp. 879–886, 2006.

[3] L. Li and Y. Jia, "Observer-based resilient $L_2 - L_\infty$ control for singular time–delay systems," *IET Control Theory & Applications*, vol. 3, no. 10, pp. 1351–1362, 2009.

[4] G.-H. Yang and J. Dong, "Control synthesis of singularly perturbed fuzzy systems," *IEEE Transactions on Fuzzy Systems*, vol. 16, no. 3, pp. 615–629, 2008.

[5] Q. L. Zhang, W. Q. Liu, and D. Hill, "A Lyapunov approach to analysis of discrete singular systems," *Systems Control Letters*, vol. 45, no. 3, pp. 237–247, 2002.

[6] H. Gao, S. Zhu, Z. Cheng, and B. Xu, "Delay–ependent state feedback guaranteed cost control for uncertain singular time-delay systems," in *Proceedings of the 44th IEEE Conference on Decision and Control, and the European Control Conference (CDC-ECC '05)*, pp. 4354–4359, Seville, Spain, December 2005.

[7] S. Xu and J. Lam, *Robust Control and Filtering of Singular Systems*, Springer, Berlin, Germany, 2006.

[8] S. Xu, J. Lam, and Y. Zou, "$\mathscr{H}_\infty$ Filtering for Singular Systems," *IEEE Transactions on Automatic Control*, vol. 48, no. 12, pp. 2217–2222, 2003.

[9] Y. Zhou and J. Li, "Energy–to–peak filtering for singular systems: the discrete–time case," *IET Control Theory & Applications*, vol. 2, no. 9, pp. 773–781, 2008.

[10] M. Darouach, "$\mathscr{H}_\infty$ unbiased filtering for linear descriptor systems via LMI," *IEEE Transactions on Automatic Control*, vol. 54, no. 8, pp. 1966–1972, 2009.

[11] R. Lu, Y. Xu, and A. Xue, "$\mathscr{H}_\infty$ filtering for singular systems with communication delays," *Signal Processing*, vol. 90, no. 4, pp. 1240–1248, 2010.

[12] R. Lu, H. Li, and Y. Zhu, "Quantized $\mathscr{H}_\infty$ filtering for singular time–varying delay systems with unreliable communication channel," *Circuits, Systems, and Signal Processing*, vol. 31, no. 2, pp. 521–538, 2012.

[13] M. Abbaszadeh and H. J. Marquez, "A generalized framework for robust nonlinear $\mathscr{H}_\infty$ filtering of Lipschitz descriptor systems with parametric and nonlinear uncertainties," *Automatica*, vol. 48, no. 5, pp. 894–900, 2012.

[14] D. Yue and Q.-L. Han, "Robust $\mathscr{H}_\infty$ filter design of uncertain descriptor systems with discrete and distributed delays," *IEEE Transactions on Signal Processing*, vol. 52, no. 11, pp. 3200–3212, 2004.

[15] L. Li and L. Zhong, "Generalised nonlinear $L_2 - L_\alpha$ filtering of discrete-time Markov jump descriptor systems," *International Journal of Control*, vol. 87, no. 3, pp. 653–664, 2014.

[16] L. Li, Z. Zhang, and J. Xu, "A generalized nonlinear $\mathscr{H}_\infty$ filter design for discrete-time Lipschitz descriptor systems," *Nonlinear Analysis: Real World Applications*, vol. 15, pp. 1–11, 2014.

[17] Z. Wang, Y. Shen, X. Zhang, and Q. Wang, "Observer design for discrete–time descriptor systems: an LMI approach," *Systems and Control Letters*, vol. 61, no. 6, pp. 683–687, 2012.

[18] Y.-L. Wang, P. Shi, C.-C. Lim, and Y. Liu, "Event–Triggered Fault Detection Filter Design for a Continuous–Time Networked Control System," *IEEE Transactions on Cybernetics*, vol. 46, no. 12, pp. 3414–3426, 2016.

[19] Y. Wang and Q. Han, "Network–Based Fault Detection Filter and Controller Coordinated Design for Unmanned Surface Vehicles in Network Environments," *IEEE Transactions on Industrial Informatics*, vol. 12, no. 5, pp. 1753–1765, 2016.

[20] D.-M. Dai, "A fault detection filtering for networked control systems based on balanced reduced–order," *Mathematical Problems in Engineering*, Article ID 673201, 8 pages, 2015.

[21] Y.-L. Wang, T.-B. Wang, and W.-W. Che, "Active–varying sampling–based fault detection filter design for networked control systems," *Mathematical Problems in Engineering*, Article ID 406916, 9 pages, 2014.

[22] Y.-L. Wang and Q.-L. Han, "Quantitative analysis and synthesis for networked control systems with non–uniformly distributed

packet dropouts and interval time–varying sampling periods," *International Journal of Robust and Nonlinear Control*, vol. 25, no. 2, pp. 282–300, 2015.

[23] R. E. Kalman, "Nonlinear aspects of sampled–data control systems," in *Proceedings of the Symposium on Nonlinear Circuit Theory*, NY, New York, USA, 1956.

[24] N. Elia and S. K. Mitter, "Stabilization of linear systems with limited information," *Institute of Electrical and Electronics Engineers. Transactions on Automatic Control*, vol. 46, no. 9, pp. 1384–1400, 2001.

[25] M. Fu and L. Xie, "The sector bound approach to quantized feedback control," *IEEE Transactions on Automatic Control*, vol. 50, no. 11, pp. 1698–1711, 2005.

[26] H. Gao and T. Chen, "A new approach to quantized feedback control systems," *Automatica*, vol. 44, no. 2, pp. 534–542, 2008.

[27] D. Liberzon, "Hybrid feedback stabilization of systems with quantized signals," *Automatica*, vol. 39, no. 9, pp. 1543–1554, 2003.

[28] R. W. Brockett and D. Liberzon, "Quantized feedback stabilization of linear systems," *Institute of Electrical and Electronics Engineers. Transactions on Automatic Control*, vol. 45, no. 7, pp. 1279–1289, 2000.

[29] Q. Ling and M. D. Lemmon, "Stability of quantized control systems under dynamic bit assignment," *IEEE Transactions on Automatic Control*, vol. 50, no. 5, pp. 734–740, 2005.

[30] M. Fu and C. E. de Souza, "State estimation for linear discrete–time systems using quantized measurements," *Automatica*, vol. 45, no. 12, pp. 2937–2945, 2009.

[31] H. Gao and T. Chen, "$\mathscr{H}_\infty$ estimation for uncertain systems with limited communication capacity," *IEEE Transactions on Automatic Control*, vol. 52, no. 11, pp. 2070–2084, 2007.

[32] C. Zhang, G. Feng, H. Gao, and J. Qiu, "$\mathscr{H}_\infty$ filtering for nonlinear discrete–time systems subject to quantization and packet dropouts," *IEEE Transactions on Fuzzy Systems*, vol. 19, no. 2, pp. 353–365, 2011.

[33] K.-Z. Han and X.-H. Chang, "Parameter–dependent robust $\mathscr{H}_\infty$ filter design for uncertain discrete–time systems with quantized measurements," *International Journal of Control, Automation and Systems*, vol. 11, no. 1, pp. 194–199, 2013.

[34] Z.-M. Li, X.-H. Chang, and L. Yu, "Robust quantized $\mathscr{H}_\infty$ filtering for discrete–time uncertain systems with packet dropouts," *Applied Mathematics and Computation*, vol. 275, pp. 361–371, 2016.

[35] S. Boyd, L. El Ghaoui, E. Feron, and V. Balakrishnan, *Linear matrix inequalities in system and control theory*, vol. 15 of *SIAM Studies in Applied Mathematics*, SIAM, Philadelphia, PA, USA, 1994.

[36] I. R. Petersen, "A stabilization algorithm for a class of uncertain linear systems," *Systems & Control Letters*, vol. 8, no. 4, pp. 351–357, 1987.

[37] X.-H. Chang, J. H. Park, and J. Zhou, "Robust static output feedback $\mathscr{H}_\infty$ control design for linear systems with polytopic uncertainties," *Systems & Control Letters*, vol. 85, pp. 23–32, 2015.

[38] P. Gahinet, A. Nemirovski, A. J. Laub, and M. Chilali, *LMI Control Toolbox*, The MathWorks, Massachusetts, MA, USA.

[39] X.-H. Chang and G.-H. Yang, "New results on output feedback $\mathscr{H}_\infty$ control for linear discrete–time systems," *IEEE Transactions on Automatic Control*, vol. 59, no. 5, pp. 1355–1359, 2014.

[40] X.-H. Chang, J. H. Park, and Z. Tang, "New approach to $\mathscr{H}_\infty$ filtering for discrete–time systems with polytopic uncertainties," *Signal Processing*, vol. 113, pp. 147–158, 2015.

Hindawi
Mathematical Problems in Engineering
Volume 2017, Article ID 4840859, 8 pages
https://doi.org/10.1155/2017/4840859

Research Article

Stabilization of Continuous-Time Random Switching Systems via a Fault-Tolerant Controller

Guoliang Wang and Zhiqiang Li

School of Information and Control Engineering, Liaoning Shihua University, Fushun, Liaoning 113001, China

Correspondence should be addressed to Guoliang Wang; gliangwang@aliyun.com

Received 18 February 2017; Accepted 13 March 2017; Published 20 March 2017

Academic Editor: Mohammad D. Aliyu

This paper focuses on the stabilization problem of continuous-time random switching systems via exploiting a fault-tolerant controller, where the dwell time of each subsystem consists of a fixed part and random part. It is known from the traditional design methods that the computational complexity of LMIs related to the quantity of fault combination is very large; particularly system dimension or amount of subsystems is large. In order to reduce the number of the used fault combinations, new sufficient LMI conditions for designing such a controller are established by a robust approach, which are fault-free and could be solved directly. Moreover, the fault-tolerant stabilization realized by a mode-independent controller is considered and suitably applied to a practical case without mode information. Finally, a numerical example is used to demonstrate the effectiveness and superiority of the proposed methods.

1. Introduction

As we know, Markovian jump system (MJS) is a particular kind of hybrid systems, which contains two parts of mechanism. One mechanism is related to system state over time, and another mechanism is named to operation mode and derived from the finite set of discrete time Markov jump parameters. Because of experiencing random characteristics, Markovian jump system is greatly suitable to describe many practical systems whose parameters or structures change abruptly, such as [1–3]. In the past few years, a lot of topics on many kinds of MJSs have been widely studied, such as stability analysis [4–7], stabilization [8–11], H_∞ control and filtering [12–14], output control [15–17], adaptive control [18–20], synchronization [21, 22], and robust control [23–26].

On the other hand, any system is inevitable to have faults in practice. It is necessary and meaningful to study the related problems of system experiencing faults. Fault-tolerant control problem [27–29] is when the faults of actuator, sensor, or internal component occur, the closed-system is still stable and has ideal characteristics. It is known that the classical fault-tolerant control methods may be divided into two categories: passive and active fault-tolerant control methods. Passive fault-tolerant control method is to use a fixed controller which ensures the closed-loop system insensitive to some specific faults. In other words, it could maintain the system stable. Therefore, this strategy is similar to the robust control technique [30, 31]. On the contrary, active fault-tolerant control method needs to reconstruct the controller design and reschedule the control law. In other words, according to the characteristics of expectation, we need to design a new control system after the faults occurred [32, 33]. Compared with the active fault-tolerant control method, the passive fault-tolerant control method does not need the real-time fault information or adjust the structure of controller online. In this sense, it is said that passive fault-tolerant control method is relatively simple to implement. When the underlying system is referred to Markovian jump system, some results about fault-tolerant control were given in [34–36]. By investigating such references, it is seen that the considered problems and studied methods between such cited references and this paper are quite different. Firstly, the considered system is different from the traditional Markovian jump system, where the dwell time considered here consists of a fixed part and random part. Secondly, the fault considered here is described by using a binary structured uncertainty

rather than that simply described by a vector in some existing references. In fact, this structure is more clear to describe the fault. Compared with the traditional methods dealing with the fault, the method to be presented has a better relaxation and is more applicable. Thirdly, but not the last, because of the fault of controller described by a binary structured uncertainty, the quantity of fault combination will be very large and have large computation complexity. Moreover, due to the fixed and random dwell time contained simultaneously, how to make the existence conditions for such a fault-tolerant controller within LMI framework and have a concise form are also necessarily studied. It is said that the abovementioned problems not only are important in theory, but also have practical applications. For example, from [37], it was shown that the helicopter system could be modeled as an Markovian jump system, whose dynamic characteristics are clearly described by a Markov chain with three different states according to airspeeds of 135 (nominal value), 60, and 170 knots. Moreover, the helicopter system is also inevitable to have kinds of faults due to the internal components faults happening or the external environment changing in practice. In order to guarantee it still works when these faults occur, a better and necessary scheme is to design an effective fault-tolerant controller. On the other hand, though the switching of helicopter among such three modes satisfies a Markov process, it is more reasonable that each subsystem is likely to hold for a period of time. In other words, there will be a fixed and random dwell time in each subsystem. Finally, but not the last, it is also important that the desired control method should be with less computation complexity and easily realized. Based on these explanations, it is said that it is significative to design a fault-tolerant controller for Markovian jump systems experiencing forced dwell time and also has practical significance. To the best of our knowledge, very few results are available to design fault-tolerant controller for random switching system. All the facts motivate the current research.

In this paper, the stabilization problem of continuous-time random switching systems closed by a fault-tolerant controller will be studied, whose conditions are presented in terms of LMIs and without any fault. The main contributions of this paper are summarized as follows: (1) A kind of fault-tolerant controller is proposed to stabilize a continuous-time random switching system which contains fixed and random dwell time simultaneously, whose conditions are obtained by exploiting a robust method; (2) the sufficient conditions for the desired controller are presented with LMI forms and fault-free, which could be solved directly; (3) due to the results without any fault, the complexity of computation will be smaller than ones obtained by the traditional methods; (4) because of the given conditions being LMIs, the existence conditions for fault-tolerant controller without any mode operation are obtained easily.

Notation. $\mathbb{R}^n$ denotes the n-dimensional Euclidean space; $\mathbb{R}^{q\times n}$ is the set of all $q \times n$ real matrices. $\|\cdot\|$ refers to the Euclidean vector norm or spectral matrix norm. Ω is the sample space, $\mathscr{F}$ is the σ-algebras of subsets of the sample space, and $\mathbb{P}$ is the probability measure on $\mathscr{F}$. In symmetric block matrices, we use "$*$" as an ellipsis for the terms induced by symmetry, diag$\{\cdots\}$ for a block-diagonal matrix, and $(M)^\star \triangleq M + M^T$.

2. Problem Formulation

Consider a class of switched linear systems defined on a complete probability space $(\Omega, \mathscr{F}, \mathbb{P})$ and described as

$$\dot{x}(t) = A_{\eta(t)}x(t) + B_{\eta(t)}u(t), \tag{1}$$

where $x(t) \in \mathbb{R}^n$ is the system state vector, $u(t) \in \mathbb{R}^q$ indicates the control input vector, and $\eta(t) \in \mathbb{S} \triangleq \{1, 2, \ldots, N\}$ represents the switching signal and determines the current system operation mode. For any $\eta(t) = i \in \mathbb{S}$, $A_{\eta(t)} = A_i$ and $B_{\eta(t)} = B_i$ are known matrices of compatible dimensions. Time instant t_k represents the current operation mode of the system to another operation mode. The parameter $d_i > 0$ represents a fixed dwell time of system (1) with mode i. If the system occurs to interval $[t_k, t_k + d_i)$, where there is no switching, it will surely follow

$$\Pr\left(\eta(t+h) = j \mid \eta(t) = i\right) = \begin{cases} 0, & \text{if } j \neq i \\ 1, & \text{if } j = i, \end{cases} \tag{2}$$

where h represents a very short amount of time and satisfies $\lim_{\Delta t\to 0^+}(o(h)/h) = 0$. For the time interval $[t_k, t_k + d_i)$, if $t \geq t_k + d_i$, at this time the mode switching follows the mode transition probabilities with TRM $\Pi \triangleq (\pi_{ij}) \in \mathbb{R}^{N\times N}$ given by

$$\Pr\left(\eta(t+h) = j \mid \eta(t) = i\right) = \begin{cases} \pi_{ij}h + o(h), & i \neq j \\ 1 + \pi_{ii}h + o(h), & i = j, \end{cases} \tag{3}$$

where $h > 0$, $\pi_{ij} \geq 0$, if $i \neq j$, and $\pi_{ii} = -\sum_{j\neq i}\pi_{ij}$.

In this paper, the designed state feedback controller may have faults, which is referred to be a fault-tolerant controller (FTC) and described by

$$u(t) = \Delta(t)K_{\eta(t)}x(t), \tag{4}$$

where $K_{\eta(t)}$ is the control gain to be determined. The parameter $\Delta(t)$ is a diagonal matrix and used to describe the controller fault happening or not. Its form is defined as

$$\Delta(t) \in \Lambda = \left\{\Delta = \operatorname{diag}\left(\delta_1, \ldots, \delta_q\right) \mid \delta_i \in \{0, 1\}\right\}. \tag{5}$$

Particularly, we could clearly find that $\Delta(t) = I_q$ if there are no faults. It is seen that there are 2^q possible combinations representing the controller faults. Equivalently, Λ has 2^q elements. Then, the resulting closed-loop system is rewritten to be

$$\dot{x}(t) = \overline{A}_{\eta(t)}x(t), \tag{6}$$

where $\overline{A}_{\eta(t)} = A_{\eta(t)} + B_{\eta(t)}\Delta(t)K_{\eta(t)}$.

Remark 1. It is worth mentioning that the fault of controller (4) is described by a binary structured uncertainty. Compared with some existing references [27, 31, 32, 34–36] where the fault is modeled to be a vector, this formulation has a better description and more application scope. However, it is also seen that 2^q possible combinations are included to represent the controller faults. This will make the computation complexity very large; in particular the underlying system is a switching system with N operation modes. Thus, how to reduce the complexity and make the obtained results with concise and easily solvable forms are necessary and meaningful problems.

Lemma 2 (see [4]). *System (1) without any control is stochastically stable if and only if there exists matrix $P_i > 0$, $i \in \mathbb{S}$, such that*

$$A_i^T P_i + P_i A_i + \pi_{ii} P_i + \sum_{j\in\mathbb{S}, j\neq i} \pi_{ij} e^{A_j^T d_j} P_j e^{A_j d_j} < 0. \tag{7}$$

Lemma 3 (see [33]). *Let $T_1 = T_1^T$, T_2, T_3, and T_4 be given matrices with appropriate dimensions, where $\underline{\Delta} = \mathrm{diag}(\underline{\Delta}_1, \ldots, \underline{\Delta}_m)$ and $\overline{\Delta} = \mathrm{diag}(\overline{\Delta}, \ldots, \overline{\Delta}_m)$. Define $T_4^{\min} = I - T_4\underline{\Delta}$, $T_4^{\max} = I - T_4\overline{\Delta}$, where $\det(T_4^{\min}) \neq 0$ and $\det(T_4^{\max}) \neq 0$ should be satisfied. Consider the following inequality*

$$\mathbb{T}(\Delta) = T_1 + \left\{T_2\Delta\left(I - T_4\Delta\right)^{-1} T_3\right\}^{\star} < 0 \tag{8}$$

holds for any $\Delta \in \Lambda$, if there exist matrices S and W such that

$$\left[\begin{array}{c|c} T_1 - T_2\left(\underline{\Delta}S\overline{\Delta}^T\right)^{\star} T_2^T & * \\ \hline T_3 + \left(\underline{T}_4 S\overline{\Delta}^T + \overline{T}_4 S^T\underline{\Delta}^T - W\right)T_2^T & -\left(\underline{T}_4 S\overline{T}_4^T + WT_4^T\right)^{\star} \end{array}\right] < 0, \tag{9}$$

where $S \in \mathbb{R}^{q\times q}$ and $W \in \mathbb{R}^{q\times q}$ satisfied $\Delta W + W^T\Delta^T = 0$.

3. Main Results

Theorem 4. *For given system (1), there exists an FTC (4) such that the resulting close-loop system (6) is stochastically stable, if for given scalars $\gamma_i > 1$ and $\mu_i > 0$, there exist matrices $X_i > 0$, Y_i, and S_i, such that*

$$\begin{bmatrix} \Omega_{i1} & \Omega_{i2} \\ * & \left(-S_i\right)^{\star} \end{bmatrix} \leq 0, \tag{10}$$

$$\begin{bmatrix} \Psi_{i1} & \Psi_{i2} \\ * & \left(-S_i\right)^{\star} \end{bmatrix} \leq 0, \tag{11}$$

$$\begin{bmatrix} \Phi_{i1} & \Phi_{i2} & \Omega_{i2} \\ * & \Phi_{i3} & 0 \\ * & * & -\left(S_i\right)^{\star} \end{bmatrix} < 0, \tag{12}$$

$$X_i \geq \mu_i I, \tag{13}$$

where

$$\begin{aligned} \Omega_{i1} &= \left(A_i X_i\right)^{\star} - \frac{2\ln\gamma_i}{d_i}\mu_i I, \\ \Omega_{i2} &= Y_i^T + B_i S_i^T, \\ \Psi_{i1} &= -\left(A_i X_i\right)^{\star} - \frac{2\ln\gamma_i}{d_i}\mu_i I, \\ \Psi_{i2} &= Y_i^T - B_i S_i^T, \\ \Phi_{i1} &= \left(A_i X_i\right)^{\star} + \pi_{ii} X_i, \\ \Phi_{i3} &= -\mathrm{diag}\left[\mu_1 I, \ldots, \mu_{i-1} I, \mu_{i+1} I, \ldots, \mu_N I\right], \\ \Phi_{i2} &= \left[\gamma_1\sqrt{\pi_{i1}}X_i \ \cdots \ \gamma_{i-1}\sqrt{\pi_{i(i-1)}}X_i \ \ \gamma_{i+1}\sqrt{\pi_{i(i+1)}}X_i \ \cdots \ \gamma_N\sqrt{\pi_{iN}}X_i\right]. \end{aligned} \tag{14}$$

Thus, the gain of controller (4) is computed as

$$K_i = Y_i X_i^{-1}. \tag{15}$$

Proof. Replacing A_i with $\overline{A}_i = A_i + B_i\Delta(t)K_i$ in (7), it is clearly known from Lemma 2 that the resulting closed-loop system is stochastically stable if the following condition is

$$\left(\overline{A}_i^T P_i\right)^{\star} + \pi_{ii} P_i + \sum_{j\in\mathbb{S}, j\neq i} \pi_{ij} e^{\overline{A}_j^T d_j} P_j e^{\overline{A}_j d_j} < 0, \quad \forall i \in \mathbb{S}. \tag{16}$$

It is further guaranteed by

$$\left(\overline{A}_i^T P_i\right)^{\star} + \pi_{ii} P_i + \sum_{j\in\mathbb{S}, j\neq i} \pi_{ij} \left\|e^{\overline{A}_j^T d_j}\right\| \left\|P_j\right\| \left\|e^{\overline{A}_j d_j}\right\| I < 0. \tag{17}$$

For any matrix $A \in \mathbb{R}^{n\times n}$, $\forall t \geq 0$, it is claimed that $\|e^{At}\| \leq e^{\|A\|t}$. Then, it is obtained that

$$\left(\overline{A}_i^T P_i\right)^{\star} + \pi_{ii} P_i + \sum_{j\in\mathbb{S}, j\neq i} \pi_{ij} e^{\|\overline{A}_j^T\| d_j} \left\|P_j\right\| e^{\|\overline{A}_j\| d_j} I < 0. \tag{18}$$

By pre- and postmultiplying (18) with $X_i = P_i^{-1}$, it is get that

$$\left(\overline{A}_i X_i\right)^{\star} + \pi_{ii} X_i + \sum_{j\in\mathbb{S}, j\neq i} \pi_{ij} X_i e^{\|\overline{A}_j^T\| d_j} \left\|X_j^{-1}\right\| e^{\|\overline{A}_j\| d_j} X_i < 0. \tag{19}$$

Based on Lemma 3, it is known that conditions (10), (11), and (12) imply the following conditions, respectively. That is,

$$\Omega_{i1} + \left(B_i \Delta Y_i\right)^{\star} \leq 0, \tag{20}$$

where

$$\left[\begin{array}{c|c} T_1 & T_2 \\ \hline T_3 & T_4 \end{array}\right] = \left[\begin{array}{c|c} \Omega_{i1} & B_i \\ \hline Y_i & 0 \end{array}\right], \tag{21}$$

$$\Psi_{i1} - \left(B_i \Delta Y_i\right)^{\star} \leq 0, \tag{22}$$

where

$$\left[\begin{array}{c|c} T_1 & T_2 \\ \hline T_3 & T_4 \end{array}\right] = \left[\begin{array}{c|c} \Psi_{i1} & -B_i \\ \hline Y_i & 0 \end{array}\right], \qquad \Phi_i + \left(B_i \Delta Y_i\right)^{\star} < 0, \tag{23}$$

where

$$\left[\begin{array}{c|c} T_1 & T_2 \\ \hline T_3 & T_4 \end{array}\right] = \left[\begin{array}{c|c} \Phi_i & B_i \\ \hline Y_i & 0 \end{array}\right], \qquad \Phi_i = \Phi_{i1} + \sum_{j\in\mathbb{S}, j\neq i} \frac{\pi_{ij}\gamma_j^2}{\mu_j} X_i^2. \tag{24}$$

Because of $\Delta = \Delta^T$ in addition to $\underline{\Delta} = 0_{q\times q}$ and $\overline{\Delta} = I_q$, it is concluded that $W = 0_{q\times q}$ and $S_i \in \mathbb{R}^{q\times q}$. Based on (20) and (22), one gets

$$\left\|\left(A_i X_i + B_i \Delta Y_i\right)^{\star}\right\| \leq \frac{2\ln\gamma_i}{d_i}\mu_i. \tag{25}$$

From condition (13), we have

$$X_i^{-1} \leq \mu_i^{-1} I, \tag{26}$$

implying

$$\left\|X_i^{-1}\right\| \leq \mu_i^{-1}. \tag{27}$$

By considering representation (15), (25) is equivalent to

$$\left\|\left(\overline{A}_i X_i\right)^{\star}\right\| \mu_i^{-1} \leq \frac{2\ln\gamma_i}{d_i}. \tag{28}$$

Then, it is obtained that

$$\left\|\left(\overline{A}_i X_i\right)^{\star}\right\| \left\|X_i^{-1}\right\| \leq \left\|\left(\overline{A}_i X_i\right)^{\star}\right\| \mu_i^{-1} \leq \frac{2\ln\gamma_i}{d_i}. \tag{29}$$

It is further derived that

$$\left\|\overline{A}_i\right\| = \left\|\overline{A}_i X_i X_i^{-1}\right\| \leq \left\|\overline{A}_i X_i\right\| \left\|X_i^{-1}\right\| \leq \frac{\ln\gamma_i}{d_i}. \tag{30}$$

Then, we get

$$e^{\|\overline{A}_i\| d_i} \leq \gamma_i. \tag{31}$$

Based on this, condition (19) is guaranteed by

$$\left(\overline{A}_i X_i\right)^{\star} + \pi_{ii} X_i + \sum_{j\in\mathbb{S}, j\neq i} \frac{\pi_{ij}\gamma_j^2}{\mu_j} X_i^2 < 0, \tag{32}$$

which could be implied by condition (12). This completes the proof. □

Remark 5. As for stability problem, [4] firstly presented a necessary and sufficient condition. However, when the system synthesis problems such as stabilization are mentioned, there are few results available. The main reason is that some nonlinear terms will be inevitably encountered, which are not handled easily and directly. From the proof of Theorem 4, such nonlinear terms encountered in condition (7) have been done suitably. Though the large quantity of fault combination, fixed, and random dwell time are included, sufficient existence conditions for fault-tolerant controller (4) are given in terms of LMIs, which are more general than ones in [38]. Moreover, the established conditions are fault-free. In other words, instead of 2^q combinations involved, only two special cases of no fault and all fault are taken into account, which are fewer than ones in [39–41]. Based on these facts, it is said that the conditions given in this theorem have small computation complexity and could be solved directly and easily.

From Theorem 4, it is seen that the desired controller (4) is mode-dependent and needs its operation mode available online. It is very known that this assumption will be limited in some practical applications. In order to deal with the general condition, a mode-independent controller is usually designed and described as

$$u(t) = \Delta(t) K x(t), \tag{33}$$

where K is the common control gain to be determined.

Theorem 6. *For given system (1), there exists a mode-independent FTC (33) such that the resulting system is stochastically stable, if for given scalars $\gamma_i > 1$, and $\mu_i > 0$, there exist matrices $X_i > 0$, G, Y, and S_i satisfying (13) and*

$$\begin{bmatrix} \Omega_{i1} & \Xi_i & \widehat{\Omega}_{i2} \\ * & (-G)^{\star} & Y^T \\ * & * & (-S_i)^{\star} \end{bmatrix} \leq 0, \tag{34}$$

$$\begin{bmatrix} \Psi_{i1} & \Xi_i & \widehat{\Psi}_{i2} \\ * & (-G)^{\star} & Y^T \\ * & * & (-S_i)^{\star} \end{bmatrix} \leq 0, \tag{35}$$

$$\begin{bmatrix} \Phi_{i1} & \Xi_i & \widehat{\Omega}_{i2} & \Phi_{i2} \\ * & (-G)^{\star} & Y^T & 0 \\ * & * & (-S_i)^{\star} & 0 \\ * & * & * & \Phi_{i3} \end{bmatrix} < 0, \tag{36}$$

where

$$\widehat{\Omega}_{i2} = Y^T + B_i S_i^T,$$
$$\widehat{\Psi}_{i2} = Y^T - B_i S_i^T, \tag{37}$$
$$\Xi_i = X_i - G^T.$$

The other variables are given in Theorem 4. Then, the gain of controller (33) is computed by

$$K = YG^{-1}. \tag{38}$$

Proof. Similar to the proof of Theorem 4, it is concluded that conditions (34)–(36) could imply

$$\begin{bmatrix} \Omega_{i1} & \Xi_i \\ * & (-G)^\star \end{bmatrix} + \left(\begin{bmatrix} B_i \\ 0 \end{bmatrix} \Delta \begin{bmatrix} Y & Y \end{bmatrix} \right)^\star \le 0, \tag{39}$$

where

$$\left[\begin{array}{c|c} T_1 & T_2 \\ \hline T_3 & T_4 \end{array}\right] = \left[\begin{array}{cc|c} \Omega_{i1} & \Xi_i & B_i \\ * & (-G)^\star & 0 \\ \hline Y & Y & 0 \end{array}\right], \tag{40}$$

$$\begin{bmatrix} \Psi_{i1} & \Xi_i \\ * & (-G)^\star \end{bmatrix} + \left(\begin{bmatrix} -B_i \\ 0 \end{bmatrix} \Delta \begin{bmatrix} Y & Y \end{bmatrix} \right)^\star \le 0, \tag{41}$$

where

$$\left[\begin{array}{c|c} T_1 & T_2 \\ \hline T_3 & T_4 \end{array}\right] = \left[\begin{array}{cc|c} \Psi_{i1} & \Xi_i & -B_i \\ * & (-G)^\star & 0 \\ \hline Y & Y & 0 \end{array}\right], \tag{42}$$

$$\begin{bmatrix} \Phi_{i1} & \Xi_i & \Phi_{i2} \\ * & (-G)^\star & 0 \\ * & * & \Phi_{i3} \end{bmatrix} + \left(\begin{bmatrix} B_i \\ 0 \\ 0 \end{bmatrix} \Delta \begin{bmatrix} Y & Y & 0 \end{bmatrix} \right)^\star < 0, \tag{43}$$

where

$$\left[\begin{array}{c|c} T_1 & T_2 \\ \hline T_3 & T_4 \end{array}\right] = \left[\begin{array}{ccc|c} \Phi_{i1} & \Xi_i & \Phi_{i2} & B_i \\ * & (-G)^\star & 0 & 0 \\ * & * & \Phi_{i3} & 0 \\ \hline Y & Y & 0 & 0 \end{array}\right]. \tag{44}$$

Without loss of generality, we only consider (43) in detail. By using Lemma 3 and the Schur complement lemma, it is got that the following condition

$$\begin{bmatrix} \Phi_i + \left(B_i \Delta Y\right)^\star & \Xi_i + B_i \Delta Y \\ * & (-G)^\star \end{bmatrix} < 0 \tag{45}$$

is guaranteed by condition (43). Moreover, it is concluded from (36) that matrix G is nonsingular. Based on representation (38), it is claimed that

$$\widehat{\Phi}_i + \sum_{j \in \mathbb{S}, j \ne i} \frac{\pi_{ij} \gamma_j^2}{\mu_j} X_i^2 < 0, \tag{46}$$

where

$$\widehat{\Phi}_i = \left(A_i X_i + B_i \Delta Y_i\right)^\star + \pi_{ii} X_i \tag{47}$$

is implied by pre- and postmultiplying both sides of (45) with

$$\begin{bmatrix} I & B_i \Delta K \end{bmatrix} \tag{48}$$

and its transpose, respectively. The next is similar to the proof of (32). On the other hand, as for conditions (39) and (41), it is concluded that they can imply conditions (20) and (22) by pre- and postmultiplying both sides with $\begin{bmatrix} I & B_i \Delta K \end{bmatrix}$ and $\begin{bmatrix} I & -B_i \Delta K \end{bmatrix}$, respectively. The next steps are similar to the ones in Theorem 4. This completes the proof. □

Remark 7. In order to deal with the mode-independent control problem, a simple and direct way is to select a common Lyapunov function for all modes. Though the gain of controller or filter could be get without any mode information, the choice of mode-independent Lyapunov function usually brings larger conservatism, which may make the design of mode-independent controller fail. In this case, a better way is to make the requirements of mode-independent controller and mode-dependent Lyapunov function be satisfied simultaneously. From Theorem 6, it is seen that such requirements could be satisfied well by letting mode-dependent matrix X_i and common matrix G. In other words, the conservatism of the obtained results could be reduced, while the goal of mode-independent control could also be achieved.

4. Numerical Examples

Example 1. Consider a continuous-time random switching system of form (1) with $\eta(t) \in \mathbb{S} = \{1, 2\}$, whose parameters are described as follows:

$$A_1 = \begin{bmatrix} -1.5 & 0.1 \\ -1 & -2 \end{bmatrix},$$
$$B_1 = \begin{bmatrix} -1 & 0.3 \\ 0.4 & 1 \end{bmatrix},$$
$$A_2 = \begin{bmatrix} -2.1 & 0 \\ 0.2 & -2.5 \end{bmatrix}, \tag{49}$$
$$B_2 = \begin{bmatrix} 0.1 & -0.2 \\ 0.5 & -2 \end{bmatrix}.$$

The transition rate matrix is given as

$$\Pi = \begin{bmatrix} -1.2 & 1.2 \\ 0.5 & -0.5 \end{bmatrix}. \tag{50}$$

Without loss of generality, the fixed dwell time of such two subsystems is assumed to be $d_1 = 0.1$ and $d_2 = 0.2$, respectively. As for this example, one could design a stabilizing controller by solving a set of LMIs. In this section, we will compare two types of controller: the standard mode-dependent controller ("S" as the subscript, "i" as the superscript) and

Table 1: Stability analysis of system closed by two types of controllers.

Δ	Combinations (1, 2, 3, 4)			
δ_1	0	0	1	1
δ_2	0	1	0	1
K_S^i	s	u	u	s
K_{FTS}^i	s	s	s	s

the mode-dependent fault-tolerant controller ("FTC" as the subscript, "i" as the superscript). Particularly, the existence conditions of such two controllers are both LMIs, which are described in conditions (20), (22), (23), and (25) with $\Delta = I_q$ and conditions in Theorem 4, respectively. By Theorem 4 with $\gamma_1 = 1.6$, $\gamma_2 = 2$, $\mu_1 = 0.1$, and $\mu_2 = 0.3$, we have the gains of the mode-dependent fault-tolerant controller (4) computed as

$$K_{FTC}^1 = \begin{bmatrix} 0.8033 & -0.0584 \\ -0.1135 & 0.1752 \end{bmatrix},$$
$$K_{FTC}^2 = \begin{bmatrix} -4.1769 & -0.9585 \\ -0.9030 & -0.2501 \end{bmatrix}. \quad (51)$$

The gains of standard mode-dependent controller are given as

$$K_S^1 = \begin{bmatrix} -277.9190 & -724.2014 \\ -786.8851 & 247.5663 \end{bmatrix},$$
$$K_S^2 = \begin{bmatrix} -4.7291 & -1.1025 \\ -1.1025 & -0.3494 \end{bmatrix}, \quad (52)$$

which are similar to the ones in [38]. After applying the above controllers, respectively, the stability effects of the resulting closed-loop system are given in Table 1. Here, four types of fault combinations are contained in Δ. In this table, "s" represents the stable closed-loop system, while "u" denotes that the closed-loop system is unstable. Since the above standard mode-dependent controller is without considering faults, the resulting closed-loop system will be unstable for two types of fault combinations. To the contrary, the resulting system closed by the designed mode-dependent fault-tolerant controller (FTC) is always stable. Moreover, though the existence conditions for the desired fault-tolerant controller are within LMI framework, only two special cases of complete fault and no fault are taken into account. Instead of four types of fault combinations involved such as [39–41], the complexity of computation could be reduced; particularly system dimension n or amount of subsystems N is large. Even for a simple case that system dimension $n = 2$ and number of subsystems $N = 2$, there will be 4 fault combinations, where the amount of LMIs is 8. In other words, the amount of the fault combinations or system dimension n in addition to quantity of operation mode N has a very large influence on the complexity of the calculation. Under the initial condition $x_0 = [1 \ \ -1]^T$, the state response of the resulting closed-loop system by the standard mode-dependent controller is given

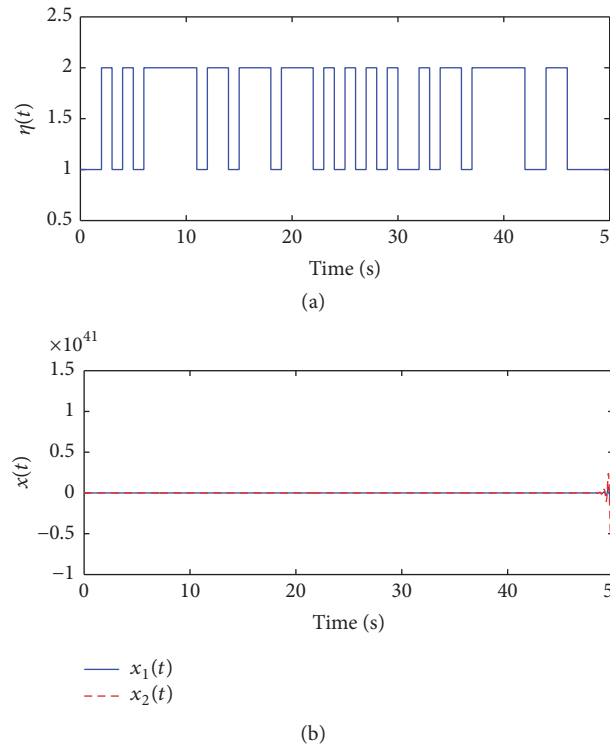

Figure 1: Simulation of system closed by mode-dependent controller.

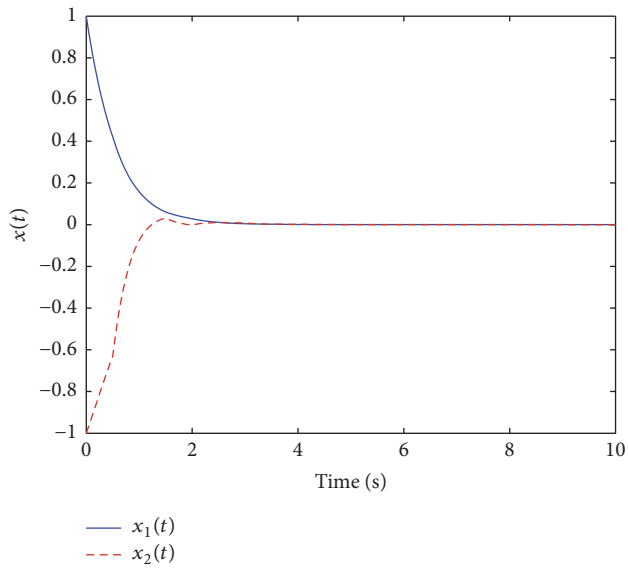

Figure 2: State response of system closed by mode-dependent FTC.

in Figure 1(b), while Figure 1(a) is simulation of operation mode. From this simulation, it is said that the fault of controller plays a negative effect to system and could make the system unstable. To the contrary, after applying the above mode-dependent fault-tolerant controller, one could get the state response given in Figure 2. It is obvious that the resulting closed-loop system is stable though there are faults in the desired controller. Moreover, when system mode is

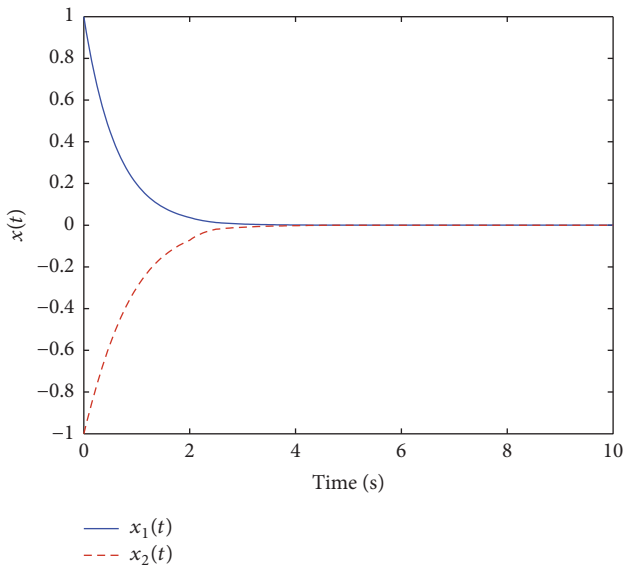

FIGURE 3: The curves of system closed by mode-independent FTC.

unavailable, a kind of mode-independent fault-tolerant controller (33) could be designed by Theorem 6, and its gain is computed as

$$K_{\mathrm{FTC}} = \begin{bmatrix} 0.2595 & 0.0459 \\ 0.0616 & 0.0422 \end{bmatrix}. \tag{53}$$

The corresponding matrices of Lyapunov function are computed as

$$X_1 = P_1^{-1} = \begin{bmatrix} 0.1549 & -0.0125 \\ -0.0125 & 0.1738 \end{bmatrix},$$
$$X_2 = P_2^{-1} = \begin{bmatrix} 0.3185 & -0.0054 \\ -0.0054 & 0.3450 \end{bmatrix}. \tag{54}$$

It is seen that the obtained controller is mode-independent, while the corresponding Lyapunov function is mode-dependent. Because of this, without selecting a common Lyapunov function, the solvable set of mode-independent controller will be larger. Thus, the results will be less conservative than the ones obtained by mode-independent Lyapunov functions. Under the same fault combinations and the initial condition, we could obtain the state response of the resulting closed-loop system given in Figure 3 and stable too. Based on these simulations, it is said that our methods based on fault-tolerant controller are superior to ones without considering faults.

5. Conclusions

In this paper, the stabilization problem of continuous-time random switching systems has been realized by a fault-tolerant controller, where both fixed and random dwell time are included. Based on the robust method, sufficient conditions for both mode-dependent and mode-independent controllers are established in terms of LMIs, which are also fault-free. Because of all the results without fault information, they are with smaller computation complexity. Compared with the ones obtained by the traditional approaches, the given conditions have fewer LMIs and could be solved easily and directly. Finally, an example has been used to demonstrate the effectiveness and superiority of the proposed methods.

Conflicts of Interest

The authors declare that there are no conflicts of interest regarding the publication of this paper.

Acknowledgments

This work was supported by the National Natural Science Foundation of China under Grants 61374043 and 61473140, the Program for Liaoning Excellent Talents in University under Grant LJQ2013040, and the Natural Science Foundation of Liaoning Province under Grant 2014020106.

References

[1] E.-K. Boukas, *Control of Singular Systems with rAndom Abrupt Changes*, Communications and Control Engineering Series, Springer, Berlin, Germany, 2008.

[2] S.-L. Kong and Z.-S. Zhang, "Optimal control of stochastic system with Markovian jumping and multiplicative noises," *IEEE Transactions on Automatic Control*, vol. 38, no. 7, pp. 1113–1118, 2012.

[3] W. Li and Z. Wu, "Output tracking of stochastic high-order nonlinear systems with Markovian switching," *IEEE Transactions on Automatic Control*, vol. 58, no. 6, pp. 1585–1590, 2013.

[4] J. Xiong, J. Lam, Z. Shu, and X. Mao, "Stability analysis of continuous-time switched systems with a random switching signal," *IEEE Transactions on Automatic Control*, vol. 59, no. 1, pp. 180–186, 2014.

[5] J. Xia, C. Sun, X. Teng, and H. Zhang, "Delay-segment-dependent robust stability for uncertain discrete stochastic Markovian jumping systems with interval time delay," *International Journal of Systems Science*, vol. 45, no. 3, pp. 271–282, 2014.

[6] R. Rakkiyappan, S. Lakshmanan, R. Sivasamy, and C. P. Lim, "Leakage-delay-dependent stability analysis of Markovian jumping linear systems with time-varying delays and nonlinear perturbations," *Applied Mathematical Modelling. Simulation and Computation for Engineering and Environmental Systems*, vol. 40, no. 7-8, pp. 5026–5043, 2016.

[7] Y. Ding and H. Liu, "Stability analysis of continuous-time Markovian jump time-delay systems with time-varying transition rates," *Journal of the Franklin Institute*, vol. 353, no. 11, pp. 2418–2430, 2016.

[8] B. Y. Park, N. K. Kwon, and P. Park, "Stabilization of Markovian jump systems with incomplete knowledge of transition probabilities and input quantization," *Journal of the Franklin Institute*, vol. 352, no. 10, pp. 4354–4365, 2015.

[9] G. Wang, Q. Zhang, and C. Yang, "Stabilization of singular Markovian jump systems with time-varying switchings," *Information Sciences*, vol. 297, pp. 254–270, 2015.

[10] G. Wang, "Mode-independent control of singular Markovian jump systems: a stochastic optimization viewpoint," *Applied Mathematics and Computation*, vol. 286, pp. 155–170, 2016.

[11] Z. Chen and Q. Huang, "Globally exponential stability and stabilization of interconnected Markovian jump system with mode-dependent delays," *International Journal of Systems Science. Principles and Applications of Systems and Integration*, vol. 47, no. 1, pp. 14–31, 2016.

[12] S. Xu, J. Lam, and X. Mao, "Delay-dependent H_∞ control and filtering for uncertain Markovian jump systems with time-varying delays," *IEEE Transactions on Circuits and Systems I: Regular Papers*, vol. 54, no. 9, pp. 2070–2077, 2007.

[13] G. Wang, P. Zhang, and Q. Zhang, "A generalized robust H_∞ filtering for singular Markovian jump systems and its applications," *International Journal of Robust and Nonlinear Control*, vol. 24, no. 18, pp. 3491–3507, 2014.

[14] C. X. Guan, Z. Y. Fei, Z. C. Li, and Y. L. Xu, "Improved H_∞ filter design for discrete-time Markovian jump systems with time-varying delay," *Journal of the Franklin Institute*, vol. 353, no. 16, pp. 4156–4175, 2016.

[15] L. Wu, X. Su, and P. Shi, "Output feedback control of markovian jump repeated scalar nonlinear systems," *IEEE Transactions on Automatic Control*, vol. 59, no. 1, pp. 199–204, 2014.

[16] R. Yang, G.-P. Liu, P. Shi, C. Thomas, and M. V. Basin, "Predictive output feedback control for networked control systems," *IEEE Transactions on Industrial Electronics*, vol. 61, no. 1, pp. 512–520, 2014.

[17] Y. Wei, J. Qiu, and S. Fu, "Mode-dependent nonrational output feedback control for continuous-time semi-Markovian jump systems with time-varying delay," *Nonlinear Analysis: Hybrid Systems*, vol. 16, pp. 52–71, 2015.

[18] H. Fan, B. Liu, W. Wang, and C. Wen, "Adaptive fault-tolerant stabilization for nonlinear systems with Markovian jumping actuator failures and stochastic noises," *Automatica*, vol. 51, pp. 200–209, 2015.

[19] M. Liu, D. W. Ho, and P. Shi, "Adaptive fault-tolerant compensation control for Markovian jump systems with mismatched external disturbance," *Automatica*, vol. 58, pp. 5–14, 2015.

[20] H. Li, P. Shi, D. Yao, and L. Wu, "Observer-based adaptive sliding mode control for nonlinear Markovian jump systems," *Automatica*, vol. 64, pp. 133–142, 2016.

[21] R. Rakkiyappan, A. Chandrasekar, J. H. Park, and O. M. Kwon, "Exponential synchronization criteria for Markovian jumping neural networks with time-varying delays and sampled-data control," *Nonlinear Analysis. Hybrid Systems*, vol. 14, pp. 16–37, 2014.

[22] H. Shen, J. H. Park, Z.-G. Wu, and Z. Zhang, "Finite-time H∞ synchronization for complex networks with semi-Markov jump topology," *Communications in Nonlinear Science and Numerical Simulation*, vol. 24, no. 1–3, pp. 40–51, 2015.

[23] G. Wang and Q. Zhang, "Robust control of uncertain singular stochastic systems with Markovian switching via proportional-derivative state feedback," *IET Control Theory & Applications*, vol. 6, no. 8, pp. 1089–1096, 2012.

[24] P. Shi, Y. Yin, F. Liu, and J. Zhang, "Robust control on saturated Markov jump systems with missing information," *Information Sciences*, vol. 265, pp. 123–138, 2014.

[25] H. Yang, H. Li, F. Sun, and Y. Yuan, "Robust control for Markovian jump delta operator systems with actuator saturation," *European Journal of Control*, vol. 20, no. 4, pp. 207–215, 2014.

[26] Q. Zhou, D. Yao, J. Wang, and C. Wu, "Robust control of uncertain semi-Markovian jump systems using sliding mode control method," *Applied Mathematics and Computation*, vol. 286, pp. 72–87, 2016.

[27] X. Zhang, T. Parisini, and M. M. Polycarpou, "Adaptive fault-tolerant control of nonlinear uncertain systems: an information-based diagnostic approach," *IEEE Transactions on Automatic Control*, vol. 49, no. 8, pp. 1259–1274, 2004.

[28] H. Alwi and C. Edwards, "Fault tolerant control using sliding modes with on-line control allocation," *Automatica*, vol. 44, no. 7, pp. 1859–1866, 2008.

[29] Q. Yang, S. S. Ge, and Y. Sun, "Adaptive actuator fault tolerant control for uncertain nonlinear systems with multiple actuators," *Automatica*, vol. 60, pp. 92–99, 2015.

[30] H. Niemann and J. Stoustrup, "Passive fault tolerant control of a double inverted pendulum—a case study," *Control Engineering Practice*, vol. 13, no. 8, pp. 1047–1059, 2005.

[31] M. Benosman and K. Y. Lum, "Passive actuators' fault tolerant control for affine nonlinear systems," *IEEE Transactions on Control Systems Technology*, vol. 18, no. 1, pp. 152–163, 2010.

[32] F. Shi and R. J. Patton, "Fault estimation and active fault tolerant control for linear parameter varying descriptor systems," *International Journal of Robust and Nonlinear Control*, vol. 25, no. 5, pp. 689–706, 2015.

[33] F. R. Segundo Sevilla, I. M. Jaimoukha, B. Chaudhuri, and P. Korba, "A semidefinite relaxation procedure for fault-tolerant observer design," *IEEE Transactions on Automatic Control*, vol. 60, no. 12, pp. 3332–3337, 2015.

[34] M. Liu, X. B. Cao, and P. S. Shi, "Fault estimation and tolerant control for fuzzy stochastic systems," *IEEE Transactions on Fuzzy Systems*, vol. 21, no. 2, pp. 221–229, 2013.

[35] H. Li, H. Gao, P. Shi, and X. Zhao, "Fault-tolerant control of Markovian jump stochastic systems via the augmented sliding mode observer approach," *Automatica*, vol. 50, no. 7, pp. 1825–1834, 2014.

[36] L. Chen, X. Huang, and S. Fu, "Observer-based sensor fault-tolerant control for semi-Markovian jump systems," *Nonlinear Analysis. Hybrid Systems*, vol. 22, pp. 161–177, 2016.

[37] D. P. De Farias, J. C. Geromel, J. B. R. Do Val, and O. L. V. Costa, "Output feedback control of Markov jump linear systems in continuous-time," *IEEE Transactions on Automatic Control*, vol. 45, no. 5, pp. 944–949, 2000.

[38] G. Wang, Q. Zhang, C. Yang, and C. Su, "Stabilization of continuous-time randomly switched systems via the LMI approach," *Applied Mathematics and Computation*, vol. 266, pp. 527–538, 2015.

[39] M. Staroswiecki, G. Hoblos, and A. Aitouche, "Sensor network design for fault tolerant estimation," *International Journal of Adaptive Control and Signal Processing*, vol. 18, no. 1, pp. 55–72, 2004.

[40] M. Cattafi, M. Gavanelli, M. Nonato, S. Alvisi, and M. Franchini, "Optimal placement of valves in a water distribution network with CLP(FD)," *Theory and Practice of Logic Programming*, vol. 11, no. 4-5, pp. 731–747, 2011.

[41] S. Alvisi, M. Franchini, M. Gavanelli, and M. Nonato, "Near-optimal scheduling of device activation in water distribution systems to reduce the impact of a contamination event," *Journal of Hydroinformatics*, vol. 14, no. 2, pp. 345–365, 2012.

Hindawi
Mathematical Problems in Engineering
Volume 2017, Article ID 7057628, 13 pages
https://doi.org/10.1155/2017/7057628

Research Article

Disordered Stabilization of Stochastic Delay Systems: The Disorder-Dependent Approach

Guoliang Wang and Hongyang Cai

School of Information and Control Engineering, Liaoning Shihua University, Fushun, Liaoning 113001, China

Correspondence should be addressed to Guoliang Wang; gliangwang@aliyun.com

Received 20 December 2016; Accepted 16 February 2017; Published 20 March 2017

Academic Editor: Sabri Arik

In this paper, a general stabilization problem of stochastic delay systems is realized by a disordered controller and studied by exploiting the disorder-dependent approach. Different from the traditional results, the stabilizing controller here experiences a disorder between control gains and system states. Firstly, the above disorder is described by the robust method, whose probability distribution is embodied by a Markov process with two modes. Based on this description, a kind of disordered controller having special uncertainties and depending on a Markov process is proposed. Then, by exploiting a disorder-dependent Lyapunov functional, two respective conditions for the existence of such a disordered controller are provided with LMIs. Moreover, the presented results are further extended to a general case that the corresponding transition rate matrix of the disordered controller has uncertainties. Finally, a numerical example is exploited to demonstrate the effectiveness and superiority of the proposed methods.

1. Introduction

It is very known that time delay is commonly encountered in variously practical dynamical systems, such as chemical systems, heating systems, biological systems, networked control systems (NCSs), and telecommunication and economic systems. Due to the presence of time delay in such practical systems, many negative effects, for example, oscillation, instability, and poor performance, could be caused. Motivated by these facts, various research topics of time-delayed systems have been considered. By investigating the existing results, it is found that they are mainly classified into two classes: delay-dependent and delay-independent ones. Because of delay-dependent results making use of the information on the length of delays, they are less conservative than delay-independent ones, especially when time delay is small. During the past decades, many important results on all kinds of delay systems have emerged, such as stability analysis [1–9], stabilization [10–18], dissipativity analysis [19] and dissipative and passive control [20–22], output control [23, 24], H_∞ control and filtering [25–34], state estimation [35–37], synchronization [38–40], slide control [41, 42], and positivity analysis [43]. It is said that the more information about time delay is used, the less conservative results will be obtained. In order to achieve this aim, some methods or techniques applied to improved Lyapunov functionals are proposed and used, such as slack variable method [1, 5, 11], Jensen inequality algorithm [2, 4, 12], delay decomposition technique [3, 15, 26], and stochastic approach [13, 14, 17, 27], where the other results or methods can be found in the existing large references.

By investigating the most results on the system synthesis in the literature, it is seen that there were few references to consider the disordering problem. The motivation of disordering problem usually comes from the data transmitted through the shared communication networks. It is a phenomenon that the transmitted data arriving at the destination is usually out of order [44] and usually complicates its analysis and synthesis. During the past years, very few results were considered on this issue. Some new interesting and challenging problems could also been introduced. In [45], some LMI conditions were presented by exploiting a packet disordering compensation method. Based on transforming the underlying system into a discrete-time system with multistep delays, the stability and H_∞ control problems of NCSs with packet disordering were considered in [46, 47], while

some less conservative results were given in [48]. Recently, a kind of packet reordering method based on the average dwell-time method was proposed in [49]. By investigating such references, it will be seen that the considered problems and studied methods between these references and this paper are quite different. Firstly, the considered systems between these references and this paper are different. The originally considered systems of such references are ones without any time delay, while there is time delay in our considered systems. Secondly, the places of disordering happening are different. In the above references, the disordering only exists in system states transmitted through networks, while the disordering to be considered in this paper takes place between system states and control gains. A suitable model to describe such problems correctly should be established firstly. Thirdly, but not the last, even if a suitable model is presented, how to make the existence conditions of the desired controller with solvable forms is also necessary studied. To our best knowledge, very few results are available to design a disordered controller for delay systems. All the facts motivate the current research.

In this paper, the general stabilization for a class of stochastic delay systems closed a disordered controller is studied by a disorder-dependent approach. The main contributions of this paper are summarized as follows: (1) a kind of stabilizing controller experiencing a disorder between control gains and system states is proposed. Not only is the disorder described by the robust method but also its probability distribution is expressed by a Markov process with two modes; (2) based on the established model of disordered controller, two different sufficient conditions for such a controller are presented with LMI forms, where a disorder-dependent approach in terms of depending on the Markov process is exploited; it was also shown by a numerical example that the conservatism of above conditions is not constant and should be considered on the concrete situations; (3) because of all the results being LMIs, they are further extended to another general case that the TRM describing the disorder has uncertainties.

Notation. $\mathbb{R}^n$ denotes the n-dimensional Euclidean space. $\mathbb{R}^{m\times n}$ is the set of all $m \times n$ real matrices. $\mathscr{E}[\cdot]$ means the mathematical expectation of $[\cdot]$. $\|\cdot\|$ refers to the Euclidean vector norm or spectral matrix norm. In symmetric block matrices, we use "$*$" as an ellipsis for the terms induced by symmetry, diag$\{\cdots\}$ for a block-diagonal matrix, and $(M)^\star \triangleq M + M^T$.

2. Problem Formulation

Consider a kind of stochastic delay systems described as

$$\begin{aligned} dx(t) &= \left[Ax(t) + A_\tau x(t-\tau) + Bu(t)\right]dt \\ &\quad + \left[Cx(t) + C_\tau x(t-\tau) + Du(t)\right]d\omega(t) \\ x(t) &= \phi(t),\ t \in [-\tau, 0], \end{aligned} \tag{1}$$

where $x(t) \in \mathbb{R}^n$ is the system state, $u(t) \in \mathbb{R}^m$ is the control input, and $\omega(t)$ is a one-dimensional Brownian motion or Wiener process. Matrices A, A_τ, B, C, C_τ, and D are known matrices of compatible dimension. Time delay τ satisfies $\tau \geq 0$. $\phi(t)$ is a continuous function and defined from $[-\tau, 0]$ to $\mathbb{R}^n$.

As we know, the traditional state feedback controllers for delay systems are commonly described as follows:

$$u_1(t) = \overline{K}x(t), \tag{2}$$

$$u_2(t) = \overline{K}_\tau x(t-\tau), \tag{3}$$

$$u_3(t) = Kx(t) + K_\tau x(t-\tau), \tag{4}$$

where $\overline{K}$, $\overline{K}_\tau$, K, and K_τ are control gains to be determined. It is said that controller (4) compared to (2) and (3) is more general and has some advantages in terms of being less conservatism. The main reason is both delay and nondelay states are taken into account. However, it is said that the action of controller (4) needs an assumption that the control gains and theirs related states should be available in a right sequence. Unfortunately, due to some practice constraints, this assumption may be very hard satisfied. In this paper, a kind of controller experiencing disordering phenomenon is proposed and described by

$$u(t) = \begin{cases} Kx(t) + K_\tau x(t-\tau), & \text{no disordering} \\ K_\tau x(t) + Kx(t-\tau), & \text{disordering occurring.} \end{cases} \tag{5}$$

It is rewritten to be

$$\begin{aligned} u(t) &= \left(\overline{K} + \Delta\overline{K}(\eta_t)\right)x(t) \\ &\quad + \left(\overline{K}_\tau + \Delta\overline{K}_\tau(\eta_t)\right)x(t-\tau), \end{aligned} \tag{6}$$

where $\overline{K} = (1/2)(K + K_\tau)$ and $\overline{K}_\tau = (1/2)(K_\tau - K)$. Particularly, the process $\{\eta_t,\ t \geq 0\}$ introduced here is a Markov process having two modes and assumed to take values in a finite set $\mathbb{S} \triangleq \{1, 2\}$. Its transition rate matrix (TRM) $\Pi \triangleq (\pi_{ij}) \in \mathbb{R}^{2\times 2}$ is given by

$$\Pr\left(\eta_{t+\Delta t} = j \mid \eta_t = i\right) = \begin{cases} \pi_{ij}\Delta t + o(\Delta t), & i \neq j \\ 1 + \pi_{ii}\Delta t + o(\Delta t), & i = j, \end{cases} \tag{7}$$

where $\Delta t > 0$, $\pi_{ij} \geq 0$, if $i \neq j$, and $\pi_{ii} = -\sum_{j\neq i}\pi_{ij}$. Here, the gain fluctuations are selected to be

$$\begin{aligned} &\Delta\overline{K}(\eta_t) \\ &= \begin{cases} \frac{1}{2}(K - K_\tau), & \text{if } \eta_t = 1 \text{ or no disordering} \\ \frac{1}{2}(K_\tau - K), & \text{if } \eta_t = 2 \text{ or disordering occurring} \end{cases} \\ &\Delta\overline{K}_\tau(\eta_t) \\ &= \begin{cases} \frac{1}{2}(K + K_\tau), & \text{if } \eta_t = 1 \text{ or no disordering} \\ \frac{1}{2}(3K - K_\tau), & \text{if } \eta_t = 2 \text{ or disordering occurring.} \end{cases} \end{aligned} \tag{8}$$

Applying controller (6) to system (1), we get

$$\begin{aligned} dx(t) &= \left[\left(\overline{A} + B\Delta\overline{K}(\eta_t)\right)x(t)\right. \\ &\quad \left. + \left(\overline{A}_\tau + B\Delta\overline{K}_\tau(\eta_t)\right)x(t-\tau)\right]dt \\ &\quad + \left[\left(\overline{C} + D\Delta\overline{K}(\eta_t)\right)x(t)\right. \\ &\quad \left. + \left(\overline{C}_\tau + D\Delta\overline{K}_\tau(\eta_t)\right)x(t-\tau)\right]d\omega(t) \\ x(t) &= \phi(t),\ \eta_t = \eta_0,\ \forall t \in [-\tau, 0], \end{aligned} \tag{9}$$

where

$$\begin{aligned} \overline{A} &= A + B\overline{K}, \\ \overline{A}_\tau &= A_\tau + B\overline{K}_\tau \\ \overline{C} &= C + D\overline{K}, \\ \overline{C}_\tau &= C_\tau + D\overline{K}_\tau. \end{aligned} \tag{10}$$

In this paper, the gain fluctuations $\Delta\overline{K}(\eta_t)$ and $\Delta\overline{K}_\tau(\eta_t)$ with forms (8) satisfy

$$\begin{aligned} \Delta\overline{K}^T(\eta_t)\Delta\overline{K}(\eta_t) &\le W, \\ \Delta\overline{K}_\tau^T(\eta_t)\Delta\overline{K}_\tau(\eta_t) &\le W_\tau(\eta_t), \end{aligned} \tag{11}$$

where W and $W_\tau(\eta_t)$ are positive-definite matrix to be determined.

Remark 1. Different from the traditional stabilization methods of delay systems that no disorder occurs in controllers, controller (5) has a disordering phenomenon between control gains and system states. Based on the robust method, the controller with disorder is transformed into a controller with special uncertainties. Moreover, the probabilities of nondisorder and disorder happening are described by a Markov process with two operation modes. It is seen that the proposed model (6) with conditions (8) and (11) is fundamental in the disorder-dependent approach.

Remark 2. It is said that disordered controller (5) not only is important in theory but also has the practical significance. From [44], it is known that disordering is usually encountered in practice especially in NCSs. This phenomenon makes the system analysis and synthesis very complicated. In order to deal with this practical problem, some methods have been proposed in [45–48]. Though such results are useful in studying this problem, more generally practical problem about disordering could be proposed. By investigating these references, it is seen that there is no delay in the originally considered systems. More importantly, the place of disorder occurring only exists in system states transmitted through networks. From [14, 50], it is seen that not only system state but also operation mode of controller could be transmitted through networks and suffer the effect of network. Based on these facts, it is said that the proposed model for controller having a disorder between control gain and system state is seen to be a meaningful extension of the existing results and will play important roles in the developments of theory and applications.

Definition 3. System (9) is said to be stochastically stable, if there exists a constant $M(x_0, \eta_0)$ such that

$$\mathscr{E}\left\{\int_0^\infty \|x(t)\|^2 dt \mid x_0, \eta_0\right\} \le M(x_0, \eta_0). \tag{12}$$

Lemma 4. *Let A, D, L, W, and F be real matrices of appropriate dimensions such that $W > 0$ and $F^TF \le I$. Then, for any $\varepsilon > 0$ such that $W - \varepsilon DD^T > 0$,*

$$\begin{aligned} &(A + DFL)^T W^{-1}(A + DFL) \\ &\quad \le A^T\left(W - \varepsilon DD^T\right)^{-1}A + \varepsilon^{-1}L^TL. \end{aligned} \tag{13}$$

3. Main Results

Theorem 5. *Given stochastic delay system (1), there is disordered controller (5) such that the resulting closed-loop system (9) is stochastically stable, if given positive scalars $\varepsilon_i > 0$, there exist matrices $X_i > 0$, $\overline{Q}_i > 0$, $\overline{Q} > 0$, $\overline{W} > 0$, $\overline{W}_{\tau i} > 0$, G, Y, and Y_τ, such that the following LMIs hold for all $i \in \mathbb{S}$:*

$$\begin{bmatrix} \Theta_{i1} & \Theta_{i2} & \Lambda_{i2} & \Lambda_{i3} & X_i & \tau^{1/2}X_i & \bar{\varepsilon}_i X_i & \Phi_i \\ * & \Theta_{i3} & 0 & \Lambda_{i3} & 0 & 0 & 0 & 0 \\ * & * & \Theta_{i4} & \Lambda_{i4} & 0 & 0 & 0 & 0 \\ * & * & * & \Theta_{i5} & 0 & 0 & 0 & 0 \\ * & * & * & * & \Theta_{i6} & 0 & 0 & 0 \\ * & * & * & * & * & \Theta_{i7} & 0 & 0 \\ * & * & * & * & * & * & \Theta_{i8} & 0 \\ * & * & * & * & * & * & * & \Gamma_i \end{bmatrix} < 0 \tag{14}$$

$$\sum_{j=1}^{2}\pi_{ij}\overline{Q}_j \le \overline{Q} \tag{15}$$

$$\begin{bmatrix} -\overline{W}_{\tau i} & \overline{Y}_i^T \\ * & -I \end{bmatrix} \le 0 \tag{16}$$

$$\begin{bmatrix} -\overline{W} & Y^T - Y_\tau^T \\ * & -I \end{bmatrix} \le 0, \tag{17}$$

where

$$\begin{aligned} \Theta_{i1} &= (\Lambda_{i1})^\star + \pi_{ii}X_i + 2BB^T, \\ \Theta_{i2} &= \Lambda_{i1} + X_i - G^T, \\ \Theta_{i3} &= (-G)^\star, \end{aligned}$$

$$
\begin{aligned}
\Theta_{i4} &= -\overline{Q}_i + \overline{\varepsilon}_i^2 \overline{W}_{\tau i},\\
\Theta_{i5} &= -\left(X_i - \varepsilon_i \widetilde{D}\widetilde{D}^T\right),\\
\Theta_{i6} &= \Theta_{i3} + \overline{Q}_i,\\
\Theta_{i7} &= \Theta_{i3} + \overline{Q},\\
\Theta_{i8} &= \Theta_{i3} + \overline{W},\\
\Lambda_{i1} &= AG + B\left(Y + Y_\tau\right),\\
\Lambda_{i2} &= A_\tau G + B\left(Y_\tau - Y\right),\\
\Lambda_{i3} &= G^T C^T + \left(Y + Y_\tau\right)^T D^T,\\
\Lambda_{i4} &= G^T C_\tau^T + \left(Y_\tau - Y\right)^T D^T,\\
\Phi_1 &= \sqrt{\pi_{12}} X_1,\\
\Phi_2 &= \sqrt{\pi_{21}} X_2,\\
\Gamma_1 &= -X_2,\\
\Gamma_2 &= -X_1,\\
\overline{\varepsilon}_i &= \left(1 + \varepsilon_i^{-1}\right)^{1/2},\\
\overline{Y}_1 &= Y + Y_\tau,\\
\overline{Y}_2 &= 3Y - Y_\tau.
\end{aligned}
\tag{18}
$$

Then, the gains of disordered controller with form (5) or (6) are obtained by

$$
\begin{aligned}
K &= 2YG^{-1},\\
K_\tau &= 2Y_\tau G^{-1}.
\end{aligned}
\tag{19}
$$

Proof. Choose a stochastic Lyapunov functional for the closed-loop system (9) as

$$
\begin{aligned}
V\left(x_t, \eta_t\right) &= x^T(t) P\left(\eta_t\right) x(t)\\
&\quad + \int_{t-\tau}^{t} x^T(s) Q\left(\eta_t\right) x(s)\, ds\\
&\quad + \int_{-\tau}^{0}\int_{t+\theta}^{t} x^T(s) Q x(s)\, ds.
\end{aligned}
\tag{20}
$$

Let $\mathscr{L}$ be the weak infinitesimal generator of random process $\{x_t, \eta_t\}$ for each $\eta_t = i \in \mathbb{S}$; it is defined as

$$
\begin{aligned}
&\mathscr{L}V\left(x_t, t, i\right)\\
&\quad = \lim_{\Delta t \to 0^+} \frac{1}{\Delta t}\left\{\mathscr{E}\left[V\left(x_{t+\Delta t}, \eta_{t+\Delta t}, t + \Delta t\right) \mid x_t, \eta_t = i\right]\right.\\
&\quad \left. - V\left(x_t, i, t\right)\right\}.
\end{aligned}
\tag{21}
$$

Then, based on condition (11) and Lemma 4, it is obtained that

$$
\begin{aligned}
&\mathscr{L}V\left(x_t, t, i\right) = x^T(t)\left(P_i\overline{A}\right)^\star x(t) + x^T(t)\\
&\cdot \sum_{j=1}^{2} \pi_{ij} P_j x(t) + 2x^T(t) P_i \overline{A}_\tau x(t-\tau) + 2x^T(t)\\
&\cdot P_i B \Delta\overline{K}_i x(t) + 2x^T(t) P_i B \Delta\overline{K}_{\tau i} x(t-\tau)\\
&+ \left[\left(\overline{C} + D\Delta\overline{K}_i\right) x(t) + \left(\overline{C}_\tau + D\Delta\overline{K}_{\tau i}\right) x(t-\tau)\right]^T\\
&\times P_i \left[\left(\overline{C} + D\Delta\overline{K}_i\right) x(t) + \left(\overline{C}_\tau + D\Delta\overline{K}_{\tau i}\right) x(t-\tau)\right]\\
&+ x^T(t) Q_i x(t) - x^T(t-\tau) Q_i x(t-\tau)\\
&+ \int_{t-\tau}^{t} x^T(s) \sum_{j=1}^{N} \pi_{ij} Q_j x(s)\, ds + \tau x^T(t) Q x(t)\\
&- \int_{t-\tau}^{t} x^T(s) Q x(s)\, ds = x^T(t)\\
&\cdot \left[\left(P_i\overline{A}\right)^\star + \sum_{j=1}^{2} \pi_{ij} P_j + Q_i + \tau Q\right] x(t) + 2x^T(t)\\
&\cdot P_i \overline{A}_\tau x(t-\tau) + 2x^T(t) P_i B \Delta\overline{K}_i x(t) + 2x^T(t)\\
&\cdot P_i B \Delta\overline{K}_{\tau i} x(t-\tau)\\
&+ \left[\left(\overline{C} + D\Delta\overline{K}_i\right) x(t) + \left(\overline{C}_\tau + D\Delta\overline{K}_{\tau i}\right) x(t-\tau)\right]^T\\
&\times P_i \left[\left(\overline{C} + D\Delta\overline{K}_i\right) x(t) + \left(\overline{C}_\tau + D\Delta\overline{K}_{\tau i}\right) x(t-\tau)\right]\\
&- x^T(t-\tau) Q_i x(t-\tau)\\
&+ \int_{t-\tau}^{t} x^T(s) \left(\sum_{j=1}^{N} \pi_{ij} Q_j - Q\right) x(s)\, ds = \xi^T(t)\\
&\cdot \left[\left(\widetilde{C} + \widetilde{D}\Delta\widetilde{K}_i\right)^T P_i \left(\widetilde{C} + \widetilde{D}\Delta\widetilde{K}_i\right) + \Omega_i\right] \xi(t)\\
&+ 2x^T(t) P_i B \Delta\overline{K}_i x(t) + 2x^T(t) P_i B \Delta\overline{K}_{\tau i} x(t-\tau)\\
&+ \int_{t-\tau}^{t} x^T(s) \left(\sum_{j=1}^{2} \pi_{ij} Q_j - Q\right) x(s)\, ds \le \xi^T(t)\\
&\cdot \left[\widetilde{C}^T \left(P_i^{-1} - \varepsilon_i \widetilde{D}\widetilde{D}^T\right)^{-1} \widetilde{C} + \varepsilon_i^{-1} \widetilde{W} + \Omega_i\right] \xi(t)\\
&+ \xi^T(t) \begin{bmatrix} 2P_i B B^T P_i + W & 0\\ * & W_{\tau i} \end{bmatrix} \xi(t)\\
&+ \int_{t-\tau}^{t} x^T(s) \left(\sum_{j=1}^{2} \pi_{ij} Q_j - Q\right) x(s)\, ds < 0,
\end{aligned}
\tag{22}
$$

where

$$\xi(t) = \begin{bmatrix} x(t) \\ x(t-\tau) \end{bmatrix},$$

$$\Omega_i = \begin{bmatrix} \Omega_{i1} & P_i\overline{A}_\tau \\ * & -Q_i \end{bmatrix},$$

$$\widetilde{C} = \begin{bmatrix} \overline{C} & \overline{C}_\tau \end{bmatrix},$$

$$\widetilde{D} = \begin{bmatrix} D & D \end{bmatrix},$$

$$\Delta\widetilde{K}_i = \begin{bmatrix} \Delta\overline{K}_i & 0 \\ * & \Delta\overline{K}_{\tau i} \end{bmatrix}, \tag{23}$$

$$\widetilde{W} = \begin{bmatrix} W & 0 \\ * & W_{\tau i} \end{bmatrix},$$

$$\Omega_{i1} = \left(P_i\overline{A}\right)^\star + \sum_{j=1}^{N}\pi_{ij}P_j + Q_i + \tau Q.$$

From condition (11), it is implied by

$$\widetilde{C}^T\left(P_i^{-1} - \varepsilon_i\widetilde{D}\widetilde{D}^T\right)^{-1}\widetilde{C} + \widetilde{\Omega}_i < 0, \tag{24}$$

which is equivalent to

$$\begin{bmatrix} \widetilde{\Omega}_i & \widetilde{C}^T \\ * & -\left(P_i^{-1} - \varepsilon_i\widetilde{D}\widetilde{D}^T\right) \end{bmatrix} < 0, \tag{25}$$

$$\sum_{j=1}^{2}\pi_{ij}Q_j \le Q, \tag{26}$$

where

$$\widetilde{\Omega}_i = \begin{bmatrix} \widetilde{\Omega}_{i1} & P_i\overline{A}_\tau \\ * & -Q_i + \overline{\varepsilon}_i^2 W_{\tau i} \end{bmatrix},$$

$$\widetilde{\Omega}_{i1} = \left(P_i\overline{A}\right)^\star + \sum_{j=1}^{2}\pi_{ij}P_j + Q_i + \tau Q + 2P_iBB^TP_i + \overline{\varepsilon}_i^2 W. \tag{27}$$

From (14), one concludes that G is nonsingular. Then, it is known that condition (25) is equivalent to

$$\begin{bmatrix} \widehat{\Omega}_{i1} & \overline{A}_\tau G & X_i\overline{C}^T \\ * & -\overline{Q}_i + \overline{\varepsilon}_i^2\overline{W}_{\tau i} & G^T\overline{C}_\tau^T \\ * & * & -\left(X_i - \varepsilon_i\widetilde{D}\widetilde{D}^T\right) \end{bmatrix} < 0, \tag{28}$$

where

$$\begin{aligned} \widehat{\Omega}_{i1} &= \left(\overline{A}X_i\right)^\star + \sum_{j=1}^{2}\pi_{ij}X_iP_jX_i + X_iQ_iX_i + \tau X_iQX_i \\ &\quad + 2BB^T + \overline{\varepsilon}_i^2 X_iWX_i, \\ X_i &= P_i^{-1}, \\ \overline{Q}_i &= G^TQ_iG, \\ \overline{W} &= G^TWG, \\ \overline{W}_{\tau i} &= G^TW_{\tau i}G, \end{aligned} \tag{29}$$

which is obtained by pre- and postmultiplying both sides of (25) with $\mathrm{diag}\{X_i, G^T, I\}$ and its transpose, respectively. Moreover, it is further implied by

$$\begin{bmatrix} \check{\Omega}_{i1} & \check{\Omega}_{i2} & \overline{A}_\tau G & G^T\overline{C}^T \\ * & \Theta_{i3} & 0 & G^T\overline{C}^T \\ * & * & -\overline{Q}_i + \overline{\varepsilon}_i^2\overline{W}_{\tau i} & G^T\overline{C}_\tau^T \\ * & * & * & -\left(X_i - \varepsilon_i\widetilde{D}\widetilde{D}^T\right) \end{bmatrix} < 0, \tag{30}$$

where

$$\begin{aligned} \check{\Omega}_{i1} &= \left(\overline{A}G\right)^\star + \sum_{j=1}^{2}\pi_{ij}X_iP_jX_i + X_iQ_iX_i + \tau X_iQX_i \\ &\quad + 2BB^T + \overline{\varepsilon}_i^2 X_iWX_i, \\ \check{\Omega}_{i2} &= \overline{A}G + X_i - G^T, \\ \Theta_{i3} &= (-G)^\star, \end{aligned} \tag{31}$$

via pre- and postmultiplying it with the following matrix

$$\begin{bmatrix} I & \overline{A} & 0 & 0 \\ 0 & 0 & I & 0 \\ 0 & \overline{C} & 0 & I \end{bmatrix} \tag{32}$$

and its transpose. Taking into the representation (19), condition (30) is equivalent to

$$\begin{bmatrix} \Theta_{i1} & \Theta_{i2} & \Lambda_{i2} & \Lambda_{i3} & X_i & \tau^{1/2}X_i & \overline{\varepsilon}_iX_i & \Phi_i \\ * & \Theta_{i3} & 0 & \Lambda_{i3} & 0 & 0 & 0 & 0 \\ * & * & \Theta_{i4} & \Lambda_{i4} & 0 & 0 & 0 & 0 \\ * & * & * & \Theta_{i5} & 0 & 0 & 0 & 0 \\ * & * & * & * & -Q_i^{-1} & 0 & 0 & 0 \\ * & * & * & * & * & -Q^{-1} & 0 & 0 \\ * & * & * & * & * & * & -W^{-1} & 0 \\ * & * & * & * & * & * & * & \Gamma_i \end{bmatrix} < 0. \tag{33}$$

As for $-Q_i^{-1}$, based on representation $\overline{Q}_i = G^T Q_i G$, it is known that

$$-Q_i^{-1} = -G\left(G^T Q_i G\right)^{-1} G^T \le \Theta_{i3} + \overline{Q}_i, \tag{34}$$

while $-Q^{-1}$ and $-W^{-1}$ can be done similarly with representation $\overline{Q} = G^T Q G$ and $\overline{W} = G^T W G$. Based on (34), we have (14) implying (33). As for condition (26), based on the above representations, it is claimed that it is equivalent to (15). Moreover, from the proof of this theorem, it is seen that condition (11) is important, which is equivalent to

$$\begin{bmatrix} -W & \left(\Delta\overline{K}\left(\eta_t\right)\right)^T \\ * & -I \end{bmatrix} \le 0, \tag{35}$$

or

$$\begin{bmatrix} -W_{\tau i} & \left(\Delta\overline{K}_\tau\left(\eta_t\right)\right)^T \\ * & -I \end{bmatrix} \le 0. \tag{36}$$

Because of $\overline{W} = G^T W G$ and considering representation (19), it is obvious that either of them is equivalent to (16) and (17). This completes the proof. □

Remark 6. Based on the disordered controller (6), a stochastic Lyapunov functional depending on system mode η_t is exploited. It is different from the traditional methods in which a single or common Lyapunov functional is used. Because of the Markov process coming from the disorder, the adopted Lyapunov functional is said to be disorder-dependent, which could reduce the conservatism of common or disorder-independent Lyapunov functional. It is worth mentioning that the introduced stochastic Lyapunov functional (20) is not unique, which could be replaced by others similarly. In addition, the existing improved techniques such as slack variable method, Jensen inequality approach, and delay decomposition technique may be used in the process of controller design.

Theorem 7. *Given stochastic delay system (1), there is disordered controller (5) such that the resulting closed-loop system (9) is stochastically stable, if given positive scalars $\beta_i > 0$, there exist matrices $X_i > 0$, $\overline{Q}_i > 0$, $\overline{Q} > 0$, $\overline{W} > 0$, $\overline{W}_{\tau i} > 0$, G, Y, and Y_τ satisfying conditions (15), (16), (17), and*

$$\begin{bmatrix} \Theta_{i1} & \Theta_{i2} & \Lambda_{i2} & \overline{\Lambda}_{i3} & X_i & \tau^{1/2}X_i & \overline{\beta}_i X_i & \Phi_i \\ * & \Theta_{i3} & 0 & \overline{\Lambda}_{i3} & 0 & 0 & 0 & 0 \\ * & * & \overline{\Theta}_{i4} & \overline{\Lambda}_{i4} & 0 & 0 & 0 & 0 \\ * & * & * & -X_i & 0 & 0 & 0 & 0 \\ * & * & * & * & \Theta_{i6} & 0 & 0 & 0 \\ * & * & * & * & * & \Theta_{i7} & 0 & 0 \\ * & * & * & * & * & * & \Theta_{i8} & 0 \\ * & * & * & * & * & * & * & \Gamma_i \end{bmatrix} < 0, \tag{37}$$

$$\begin{bmatrix} -\beta_i I & D^T \\ * & -X_i \end{bmatrix} \le 0, \tag{38}$$

where

$$\begin{aligned} \overline{\Theta}_{i4} &= -\overline{Q}_i + \overline{\beta}_i^2 \overline{W}_{\tau i}, \\ \overline{\Lambda}_{i3} &= \sqrt{2}\Lambda_{i3}, \\ \overline{\Lambda}_{i4} &= \sqrt{2}\Lambda_{i4}, \\ \overline{\beta}_i &= \left(1 + 4\beta_i\right)^{1/2}. \end{aligned} \tag{39}$$

The other symbols are given in Theorem 5. Then, the gains of controller (5) are computed by (19).

Proof. Choosing the same Lyapunov functional (20), similar to the computation of (22), it is obtained that

$$\begin{aligned} \mathscr{L}V\left(x_t, t, i\right) &= x^T(t)\left[\left(P_i\overline{A}\right)^* + \sum_{j=1}^{2}\pi_{ij}P_j + Q_i + \tau Q\right] \\ &\cdot x(t) + 2x^T(t)P_i\overline{A}_\tau x(t-\tau) + 2x^T(t) \\ &\cdot P_i B\Delta\overline{K}_i x(t) + 2x^T(t)P_i B\Delta\overline{K}_{\tau i}x(t-\tau) + \xi^T(t) \\ &\cdot \left(\widetilde{C} + \widetilde{D}\Delta\widetilde{K}_i\right)^T P_i\left(\widetilde{C} + \widetilde{D}\Delta\widetilde{K}_i\right)\xi^T(t) - x^T(t-\tau) \\ &\cdot Q_i x(t-\tau) + \int_{t-\tau}^{t} x^T(s)\left(\sum_{j=1}^{N}\pi_{ij}Q_j - Q\right)x(s)\,ds \\ &= \xi^T(t)\left[\Omega_i + \widetilde{C}^T P_i\widetilde{C} + 2\widetilde{C}^T P_i\widetilde{D}\Delta\widetilde{K}_i\right. \\ &\left. + \Delta\widetilde{K}_i^T\widetilde{D}^T P_i\widetilde{D}\Delta\widetilde{K}_i\right]\xi(t) + 2x^T(t)P_i B\Delta\overline{K}_i x(t) \\ &+ 2x^T(t)P_i B\Delta\overline{K}_{\tau i}x(t-\tau) \\ &+ \int_{t-\tau}^{t} x^T(s)\left(\sum_{j=1}^{2}\pi_{ij}Q_j - Q\right)x(s)\,ds \le \xi^T(t) \\ &\cdot \left[\Omega_i + \operatorname{diag}\left\{2P_i BB^T P_i + W, W_{\tau i}\right\} + \widetilde{C}^T P_i\widetilde{C}\right. \\ &\left. + 2\widetilde{C}^T P_i\widetilde{D}\Delta\widetilde{K}_i + \Delta\widetilde{K}_i^T\widetilde{D}^T P_i\widetilde{D}\Delta\widetilde{K}_i\right]\xi(t) \\ &+ \int_{t-\tau}^{t} x^T(s)\left(\sum_{j=1}^{2}\pi_{ij}Q_j - Q\right)x(s)\,ds < 0 \end{aligned} \tag{40}$$

which is guaranteed by

$$\begin{aligned} \Omega_i + \operatorname{diag}\left\{2P_i BB^T P_i + W, W_{\tau i}\right\} + \widetilde{C}^T P_i\widetilde{C} \\ + 2\widetilde{C}^T P_i\widetilde{D}\Delta\widetilde{K}_i + \Delta\widetilde{K}_i^T\widetilde{D}^T P_i\widetilde{D}\Delta\widetilde{K}_i < 0, \end{aligned} \tag{41}$$

and condition (26). From the representations of $\widetilde{C}$, $\widetilde{D}$, and $\Delta\widetilde{K}_i$ and the following condition

$$-\beta_i I + D^T P_i D \le 0, \tag{42}$$

condition (41) is guaranteed by

$$\begin{aligned}
&\Omega_i + \operatorname{diag}\left\{2P_iBB^TP_i + W, W_{\tau i}\right\} + 2\widetilde{C}^TP_i\widetilde{C} \\
&\quad + 2\Delta\widetilde{K}_i^T\widetilde{D}^TP_i\widetilde{D}\Delta\widetilde{K}_i \le \Omega_i \\
&\quad + \operatorname{diag}\left\{2P_iBB^TP_i + W, W_{\tau i}\right\} + 2\widetilde{C}^TP_i\widetilde{C} \\
&\quad + 2\Delta\widetilde{K}_i^T\widehat{I}^TD^TP_iD\widehat{I}\Delta\widetilde{K}_i \le \Omega_i \\
&\quad + \operatorname{diag}\left\{2P_iBB^TP_i + W, W_{\tau i}\right\} + 2\widetilde{C}^TP_i\widetilde{C} \\
&\quad + 2\beta_i\Delta\widetilde{K}_i^T\widehat{I}^T\widehat{I}\Delta\widetilde{K}_i \le \Omega_i \\
&\quad + \operatorname{diag}\left\{2P_iBB^TP_i + \overline{\beta}_i^2W, \overline{\beta}_i^2W_{\tau i}\right\} + 2\widetilde{C}^TP_i\widetilde{C} < 0,
\end{aligned} \tag{43}$$

where $\widehat{I} = [I \;\; I]$ and $\overline{\beta}_i = (1 + 4\beta_i)^{1/2}$. Similar to the proof of (28) implying (25), it is obtained that condition (43) is guaranteed by

$$\begin{bmatrix}
\breve{\Omega}_{i1} & \overline{A}_\tau G & \sqrt{2}X_i\overline{C}^T \\
* & -\overline{Q}_i + \overline{\beta}_i^2\overline{W}_{\tau i} & \sqrt{2}G^T\overline{C}_\tau^T \\
* & * & -X_i
\end{bmatrix} < 0, \tag{44}$$

where

$$\begin{aligned}
\breve{\Omega}_{i1} &= \left(\overline{A}X_i\right)^\star + \sum_{j=1}^{2}\pi_{ij}X_iP_jX_i + X_iQ_iX_i + \tau X_iQX_i \\
&\quad + 2BB^T + \overline{\beta}_i^2X_iWX_i.
\end{aligned} \tag{45}$$

The next process is similar to the process of (28) guaranteed by condition (14), which is omitted here. As for condition (42), it is known that it is equivalent to (38). Similar to the proof of Theorem 5, conditions (11) and (34) are also needed. This completes the proof. □

Remark 8. From the forms of Theorems 5 and 7, one cannot conclude which one is less conservative. However, in the following numerical example, it is seen that sometimes the former theorem is less conservative, while sometimes the latter one has less conservatism. Thus, it is concluded that it is impossible to claim that either of them is less conservative and should be considered in the concrete situations.

From the established result, it is seen that TRM Π related to disorder is assumed to be exact. However, due to many practical situations in practice, it is impossible or high cost to get it exactly. Instead, it has admissible uncertainty $\Delta\widetilde{\Pi} \triangleq (\Delta\widetilde{\pi}_{ij})$ and is described as

$$\begin{aligned}
\Pi &= \widetilde{\Pi} + \Delta\widetilde{\Pi} \\
\text{with } &\left|\Delta\widetilde{\pi}_{ij}\right| \le \epsilon_{ij}, \quad \epsilon_{ij} \ge 0, \;\; j \ne i.
\end{aligned} \tag{46}$$

In (46), TRM $\widetilde{\Pi} \triangleq (\widetilde{\pi}_{ij})$ is the known constant estimation of Π with $\widetilde{\pi}_{ij}$ satisfying (7). It is assumed that $\Delta\widetilde{\pi}_{ij}$, $j \ne i$, takes any value in $[-\epsilon_{ij}, \epsilon_{ij}]$. Then, it is concluded that $|\Delta\widetilde{\pi}_{ii}| \le -\epsilon_{ii}$, where $\epsilon_{ii} \triangleq -\epsilon_{ij}$, $\alpha_{ij} \triangleq \widetilde{\pi}_{ij} - \epsilon_{ij}$, and $\alpha_{ii} \triangleq -\alpha_{ij}$, $\forall j \ne i$.

Theorem 9. *Given stochastic delay system (1), there is disordered controller (5) such that the resulting closed-loop system (9) is stochastically stable over uncertainty (46), if given positive scalars $\varepsilon_i > 0$, if there exist matrices $X_i > 0$, $\overline{Q}_i > 0$, $\overline{Q} > 0$, $\overline{W}_i > 0$, $\overline{W}_{\tau i} > 0$, $T_i > 0$, $S_i > 0$, $M_i = M_i^T$, $V_i = V_i^T$, Y, and Y_τ satisfying conditions (16), (17), and*

$$\begin{bmatrix}
\overline{\Theta}_{i1} & \Theta_{i2} & \Lambda_{i2} & \Lambda_{i3} & X_i & \tau^{1/2}X_i & \bar{\varepsilon}_iX_i & \overline{\Phi}_i & M_i \\
* & \Theta_{i3} & 0 & \Lambda_{i3} & 0 & 0 & 0 & 0 & 0 \\
* & * & \Theta_{i4} & \Lambda_{i4} & 0 & 0 & 0 & 0 & 0 \\
* & * & * & \Theta_{i5} & 0 & 0 & 0 & 0 & 0 \\
* & * & * & * & \Theta_{i6} & 0 & 0 & 0 & 0 \\
* & * & * & * & * & \Theta_{i7} & 0 & 0 & 0 \\
* & * & * & * & * & * & \Theta_{i8} & 0 & 0 \\
* & * & * & * & * & * & * & \Gamma_i & 0 \\
* & * & * & * & * & * & * & * & -T_i
\end{bmatrix} < 0, \tag{47}$$

$$\begin{bmatrix}
\Theta_{i9} & V_i \\
* & -S_i
\end{bmatrix} < 0, \tag{48}$$

$$\begin{bmatrix}
-X_i - M_i & X_i \\
* & -X_j
\end{bmatrix} \le 0, \quad j \ne i \tag{49}$$

$$\overline{Q}_j - \overline{Q}_i - V_i < 0, \quad j \ne i, \tag{50}$$

where

$$\begin{aligned}
\overline{\Theta}_{i1} &= \left(\Lambda_{i1}\right)^\star + \alpha_{ii}X_i + 2BB^T - \epsilon_{ii}M_i + 0.25\epsilon_{ii}^2T_i, \\
\overline{\Phi}_1 &= \sqrt{\alpha_{12}}X_1, \\
\overline{\Phi}_2 &= \sqrt{\alpha_{21}}X_2, \\
\Theta_{i9} &= -\overline{Q} - \epsilon_{ii}V_i + 0.25\epsilon_{ii}^2S_i + \sum_{j=1}^{2}\alpha_{ij}\overline{Q}_j.
\end{aligned} \tag{51}$$

The other symbols are given in Theorem 5. Then, the gains of controller (5) can be get by (19).

Proof. From the proof of Theorem 5, it is seen that only some terms are related to uncertainty (46), which are referred to be (26) and (30), respectively. As for $\breve{\Omega}_{i1}$ in (30), it is equivalent to

$$\begin{aligned}
&\left(\overline{A}G\right)^\star + X_iQ_iX_i + \tau X_iQX_i + 2BB^T + \bar{\varepsilon}_i^2X_iWX_i \\
&\quad + \sum_{j=1}^{2}\left(\widetilde{\pi}_{ij} + \Delta\widetilde{\pi}_{ij}\right)X_iP_jX_i - \sum_{j=1}^{2}\epsilon_{ij}X_iP_jX_i \\
&\quad + \sum_{j=1}^{2}\epsilon_{ij}X_iP_jX_i - \sum_{j=1}^{2}\left(\Delta\widetilde{\pi}_{ij} + \epsilon_{ij}\right)M_i
\end{aligned}$$

$$= \left(\overline{A}G\right)^{*} + X_i Q_i X_i + \tau X_i Q X_i + 2BB^T + \bar{\varepsilon}_i^2 X_i W X_i + \sum_{j=1}^{2} \alpha_{ij} X_i P_j X_i - \left(\Delta\tilde{\pi}_{ii} + \epsilon_{ii}\right) M_i + \sum_{j\neq i} \left(\Delta\tilde{\pi}_{ij} + \epsilon_{ij}\right)\left(X_i P_j X_i - X_i - M_i\right), \tag{52}$$

where $M_i = M_i^T$, which is guaranteed by

$$\left(\overline{A}G\right)^{*} + X_i Q_i X_i + \tau X_i Q X_i + 2BB^T + \bar{\varepsilon}_i^2 X_i W X_i + \sum_{j=1}^{2} \alpha_{ij} X_i P_j X_i - \left(\Delta\tilde{\pi}_{ii} + \epsilon_{ii}\right) M_i < 0, \tag{53}$$

$$\sum_{j\neq i} \left(\Delta\tilde{\pi}_{ij} + \epsilon_{ij}\right)\left(X_i P_j X_i - X_i - M_i\right) \leq 0. \tag{54}$$

For any $T_i > 0$, it is concluded that

$$-\Delta\tilde{\pi}_{ii} M_i \leq 0.25\epsilon_{ii}^2 T_i + M_i T_i^{-1} M_i. \tag{55}$$

Based on conditions (54) and (55), (52) is implied by

$$\left(\overline{A}G\right)^{*} + X_i Q_i X_i + \tau X_i Q X_i + 2BB^T + \bar{\varepsilon}_i^2 X_i W X_i + \sum_{j=1}^{2} \alpha_{ij} X_i P_j X_i - \epsilon_{ii} M_i + 0.25\epsilon_{ii}^2 T_i + M_i T_i^{-1} M_i < 0, \quad X_i P_j X_i - X_i - M_i \leq 0, \tag{56}$$

where the latter one is equivalent to (49). Then, based on the proof of Theorem 5, it is concluded that conditions (47) and (49) imply (30) with Π replaced by (46), where $\overline{Q}_i = G^T Q_i G$, $\overline{Q} = G^T Q G$, and $\overline{W} = G^T W G$. As for condition (15), similar to the method of (52), it is equivalent to

$$-\overline{Q} - \epsilon_{ii} V_i + \sum_{j=1}^{2} \alpha_{ij} \overline{Q}_j - \Delta\tilde{\pi}_{ii} V_i + \sum_{j\neq i} \left(\Delta\tilde{\pi}_{ij} + \epsilon_{ij}\right)\left(\overline{Q}_j - \overline{Q}_i - V_i\right) \leq 0 \tag{57}$$

with $V_i = V_i^T$. It is further guaranteed by

$$-\overline{Q} - \epsilon_{ii} V_i + 0.25\epsilon_{ii}^2 S_i + \sum_{j=1}^{2} \alpha_{ij} \overline{Q}_j + V_i S_i^{-1} V_i < 0, \quad \sum_{j\neq i} \left(\Delta\tilde{\pi}_{ij} + \epsilon_{ij}\right)\left(\overline{Q}_j - \overline{Q}_i - V_i\right) \leq 0, \tag{58}$$

which are implied by (48) and (50). This completes the proof. □

Theorem 10. *Given stochastic delay system (1), there is disordered controller (5) such that the resulting closed-loop system (9) is stochastically stable over uncertainty (46), if given positive scalars $\beta_i > 0$, there exist matrices $X_i > 0$, $\overline{Q}_i > 0$, $\overline{Q} > 0$, $\overline{W_i} > 0$, $\overline{W}_{\tau i} > 0$, $T_i > 0$, $S_i > 0$, $M_i = M_i^T$, $V_i = V_i^T$, Y, and Y_τ satisfying conditions (16), (17), (38), (48), (49), (50), and*

$$\begin{bmatrix} \overline{\Theta}_{i1} & \Theta_{i2} & \Lambda_{i2} & \overline{\Lambda}_{i3} & X_i & \tau^{1/2} X_i & \overline{\beta}_i X_i & \overline{\Phi}_i & M_i \\ * & \Theta_{i3} & 0 & \overline{\Lambda}_{i3} & 0 & 0 & 0 & 0 & 0 \\ * & * & \overline{\Theta}_{i4} & \overline{\Lambda}_{i4} & 0 & 0 & 0 & 0 & 0 \\ * & * & * & -X_i & 0 & 0 & 0 & 0 & 0 \\ * & * & * & * & \Theta_{i6} & 0 & 0 & 0 & 0 \\ * & * & * & * & * & \Theta_{i7} & 0 & 0 & 0 \\ * & * & * & * & * & * & \Theta_{i8} & 0 & 0 \\ * & * & * & * & * & * & * & \Gamma_i & 0 \\ * & * & * & * & * & * & * & * & -T_i \end{bmatrix} < 0, \tag{59}$$

where symbols are given in Theorems 5–9. Then the gain of controller (5) can be get by (19).

Proof. Similar to the proof of Theorem 9, its proof could be obtained and is omitted. This completes the proof. □

4. Numerical Examples

Example 1. Consider a stochastic delay system (1) with parameters as follows:

$$A = \begin{bmatrix} -2 & -0.6 \\ 0.5 & -1 \end{bmatrix}, \quad A_\tau = \begin{bmatrix} -0.4 & -0.1 \\ 0 & -0.5 \end{bmatrix}, \quad B = \begin{bmatrix} -1 \\ 1 \end{bmatrix}, \quad C = \begin{bmatrix} -0.4 & 0 \\ 0.2 & -0.1 \end{bmatrix}, \quad C_\tau = \begin{bmatrix} -0.3 & 0 \\ 0.2 & -0.1 \end{bmatrix}, \quad D = \begin{bmatrix} 0 \\ 0.2 \end{bmatrix}. \tag{60}$$

Firstly, by the traditional methods such as [10–12, 15, 17] where no disorder between control gains and system states happens, one can design controller (4) by exploiting a disorder-independent Lyapunov functional $V(x_t) = x^T(t)Px(t) + \int_{t-\tau}^{t} x^T(s)Qx(s)ds$. Here, it should be pointed out that the above selected Lyapunov functional is without

Table 1: The correlation between $\tau_{\max}$ and ε_2 with given different ε_1.

$\varepsilon_1 = 2$ & $\varepsilon_2 =$	0.221	0.3	0.5	1	2	5
$\tau_{\max}$	0.002	0.760	1.559	2.092	2.312	2.425
$\varepsilon_1 = 11$ & $\varepsilon_2 =$	0.221	0.3	0.5	1	2	5
$\tau_{\max}$	0.005	0.950	1.759	2.306	2.547	2.677
$\varepsilon_1 = 20$ & $\varepsilon_2 =$	0.221	0.3	0.5	1	2	5
$\tau_{\max}$	0.002	0.760	1.559	2.092	2.312	2.425

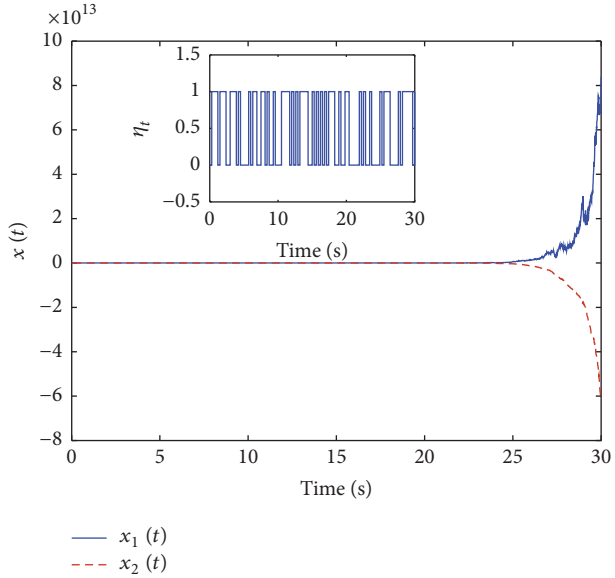

Figure 1: The curves of the resulting system via controller experiencing disorder.

loss of generality. Its form given here is determined by the one exploited in (20). In other words, in order to make some comparisons in this example, they should be coincident. On the other hand, based on the existing methods where some improved Lyapunov functionals or some techniques are used to deal with delay systems, less conservative results could be obtained. Thus, if either of the Lyapunov functionals referred to cases (4) and (5), respectively, is selected to be an improved form or some techniques are exploited, the other one should be done similarly. Based on these illustrations, it is said that the comparisons between controllers (4) and (5) based on similar Lyapunov functionals and similar techniques are without loss of generality. Then, the corresponding gains of controller (4) are computed as

$$K = \begin{bmatrix} -0.2600 & 0.0923 \end{bmatrix}, \quad K_\tau = \begin{bmatrix} -2.0000 & 1.0000 \end{bmatrix}, \tag{61}$$

where delay is $\tau = 0.3$. When the above desired controller experiences a disorder between control gains and system states, without loss of generality, the TRM of such a disorder is described as

$$\Pi = \begin{bmatrix} -0.4 & 0.4 \\ 0.6 & -0.6 \end{bmatrix}. \tag{62}$$

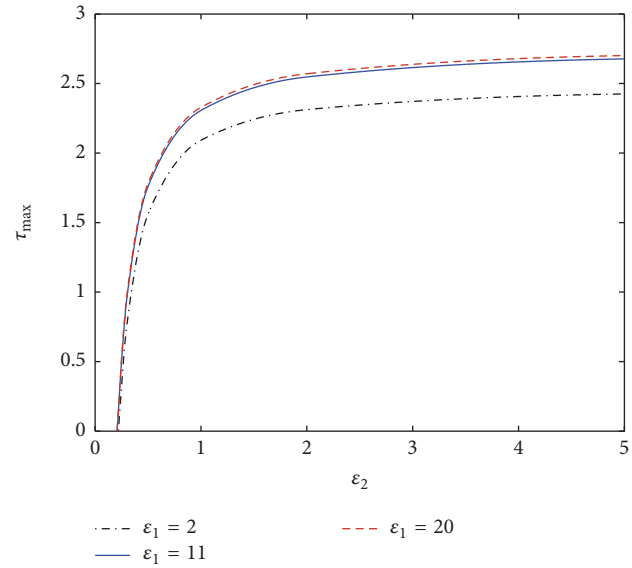

Figure 2: The simulation of correlation between $\tau_{\max}$ and ε_2.

Its simulation is given in the smaller subgraph of Figure 1. Under the initial condition $x_0 = \begin{bmatrix} 1 & -1 \end{bmatrix}^T$, the state response of the resulting closed-loop system is presented in the larger subgraph of Figure 1, which is obviously stable. It is claimed that such a disorder plays a negative effect and could make the resulting closed-loop system unstable. Thus, it is necessary and important to consider such a disorder problem. Under the same TRM and letting $\varepsilon_1 = 11$ and $\varepsilon_2 = 2$, we could have the gains of controller (5) with disorders (8) obtained by Theorem 5 and given as

$$K = \begin{bmatrix} -0.0396 & -0.0289 \end{bmatrix}, \quad K_\tau = \begin{bmatrix} -0.1443 & -0.0454 \end{bmatrix}. \tag{63}$$

However, when the parameters of Theorem 7 are selected to be $\beta_1 = 11$ and $\beta_2 = 2$, respectively, it is known that there is no solution to controller (5). In this case, it is said that Theorem 5 is less conservative. However, when the above parameters are chosen to be $\varepsilon_1 = 0.2$ ($\beta_2 = 0.2$) and $\varepsilon_2 = 0.1$ ($\beta_1 = 0.1$), it is concluded that there is no solution to Theorem 5, while the gains of controller (5) can be gotten by Theorem 7 and given as

$$K = \begin{bmatrix} -0.0083 & -0.0128 \end{bmatrix}, \quad K_\tau = \begin{bmatrix} -0.0650 & -0.0258 \end{bmatrix}. \tag{64}$$

As for this case, it is obtained that Theorem 5 has less conservatism. Thus, it is claimed that which one of such two theorems is less conservative is not constant and should be considered in the concrete situations. In order to further demonstrate this conclusion, more additional comparisons are done in Tables 1 and 2, where $\tau_{\max}$ denotes the allowable upper bound of τ. Moreover, the simulations of such comparisons given in the above tables are further demonstrated in Figures 2 and 3, which are used to show the statements about the conservatism of Theorems 5 and 7 vividly. For a given parameter

Table 2: The correlation between $\tau_{\max}$ and β_2 with given different β_1.

$\beta_1 = 0.2$ & $\beta_2 =$	0.001	0.005	0.01	0.05	0.1	0.3	0.5	0.749
$\tau_{\max}$	1.498	1.493	1.488	1.444	1.385	1.061	0.614	0.001
$\beta_1 = 0.3$ & $\beta_2 =$	0.001	0.005	0.01	0.05	0.1	0.3	0.5	0.694
$\tau_{\max}$	1.196	1.192	1.188	1.149	1.099	0.844	0.452	0.001
$\beta_1 = 0.5$ & $\beta_2 =$	0.001	0.005	0.01	0.05	0.1	0.3	0.5	0.527
$\tau_{\max}$	0.578	0.575	0.571	0.539	0.497	0.305	0.044	0.0001

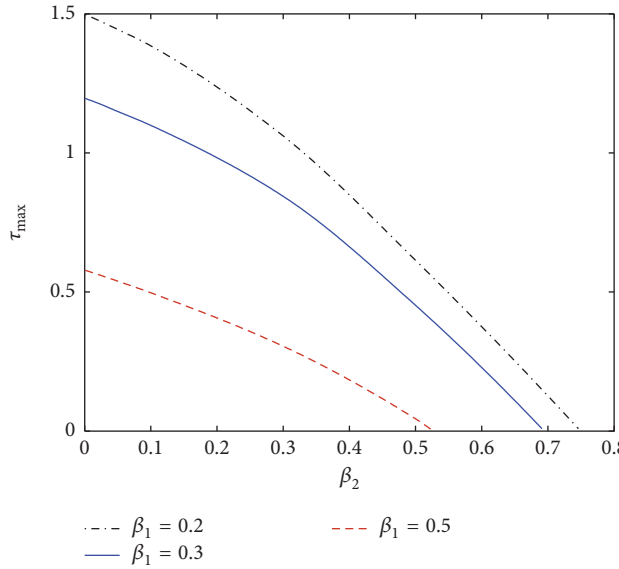

Figure 3: The simulation of correlation between $\tau_{\max}$ and β_2.

ε_1, it is known from Figure 2 that larger ε_2 will result in less conservative results in terms of larger $\tau_{\max}$. In addition, it is also seen that smaller ε_1 will lead to less conservative results with larger $\tau_{\max}$. To the contrary, from Figure 3, it is found that, for a given parameter β_1, larger β_2 will make the results more conservative in terms of smaller $\tau_{\max}$. Moreover, there is an inverse phenomenon about the correlation between $\tau_{\max}$ and β_1. From these simulations, it is claimed that the effects of parameters ε_i and β_i, $i = 1, 2$, are different, which are contrary. More importantly, based on the curves of such figures in addition to considering the correlation between the upper and lower bounds, it is known that there is a cross section of Figures 2 and 3. In other words, it is concluded that sometimes Theorem 5 is less conservative, while sometimes Theorem 7 is less conservative. Based on these facts, it is said that the conservatism of such theorems is not deterministic, and their applications should be considered in the concrete situations. In addition, even there is uncertainty (46) in Π, such as

$$\widetilde{\Pi} = \begin{bmatrix} -0.4 & 0.4 \\ 0.6 & -0.6 \end{bmatrix} \tag{65}$$

with $\Delta\widetilde{\Pi} = (\Delta\widetilde{\pi}_{ij})$ satisfying $\Delta\widetilde{\pi}_{ij} \le \epsilon_{ij} = 0.3\widetilde{\pi}_{ij}$, $\forall i, j \in \mathbb{S}$, and $i \ne j$; we can also design effective stabilizing controllers with form (5). Firstly, based on Theorem 9 with $\varepsilon_1 = 11$ and $\varepsilon_2 = 2$, we have the gains of disordered controller (5) computed as

$$\begin{aligned} K &= \begin{bmatrix} -0.0065 & -0.0027 \end{bmatrix}, \\ K_\tau &= \begin{bmatrix} -0.0180 & -0.0053 \end{bmatrix}. \end{aligned} \tag{66}$$

On the other hand, based on Theorem 7 with $\beta_1 = 0.2$ and $\beta_2 = 0.1$, the corresponding gains are given by

$$\begin{aligned} K &= \begin{bmatrix} -0.0030 & -0.0045 \end{bmatrix}, \\ K_\tau &= \begin{bmatrix} -0.0268 & -0.0101 \end{bmatrix}. \end{aligned} \tag{67}$$

Under the same initial condition, after applying the above desired controllers, respectively, we have the state response of the resulting closed-loop systems illustrated in Figure 4. There, the upper subgraph is simulation of the resulting systems obtained by Theorem 9, while the under one is gotten by Theorem 10. It is found that all the states of the resulting systems are stable. Based on these simulations, it is seen that both the desired controllers are useful; even TRM Π experiences uncertainties.

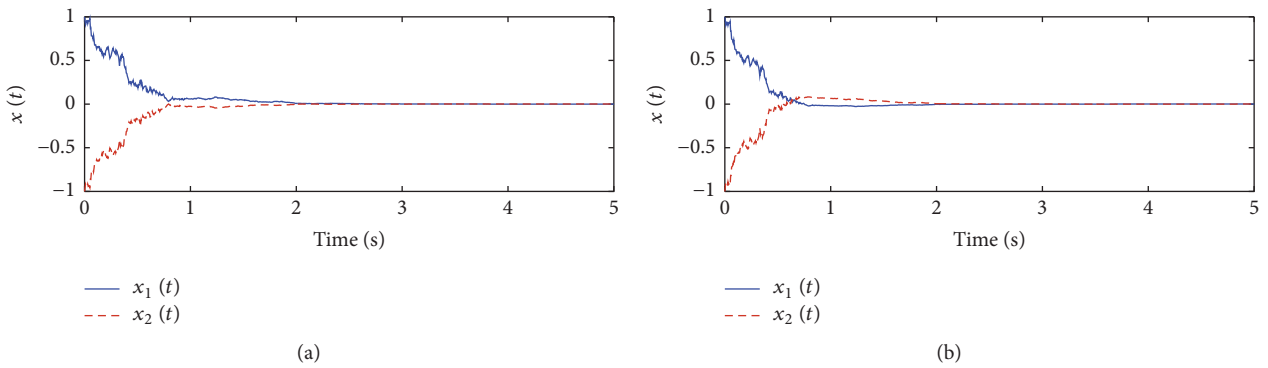

Figure 4: The state responses of the resulting system with uncertain TRM.

5. Conclusions

In this paper, the general stabilization for stochastic delay systems closed by a disordered controller has been studied by a disorder-dependent approach. Firstly, a kind of disordered controller whose control gains and system states experience a disorder has been proposed. Based on the robust method and exploiting a Markov process, the above controller is transformed to be a controller having special uncertainties and depending on a Markov process with two modes. Several sufficient LMI conditions for the desired controller are obtained by using the disorder-dependent Lyapunov functional. In addition, more applications about the TRM of the described disorder having uncertainties have been considered too. Finally, a numerical example has been used to demonstrate the effectiveness of the proposed methods.

Disclosure

A preliminary version of this work first appeared at the 29th Chinese Control and Decision Conference, Chongqing, China.

Competing Interests

The authors declare that there is no conflict of interests regarding the publication of this paper.

Acknowledgments

This work was supported by the National Natural Science Foundation of China under Grants 61104066, 61374043, and 61473140, the China Postdoctoral Science Foundation funded project under Grant 2012M521086, the Program for Liaoning Excellent Talents in University under Grant LJQ2013040, and the Natural Science Foundation of Liaoning Province under Grant 2014020106.

References

[1] Y. He, Q. G. Wang, C. Lin, and M. Wu, "Delay-range-dependent stability for systems with time-varying delay," *Automatica*, vol. 43, no. 2, pp. 371–376, 2007.

[2] X. Jiang and Q. L. Han, "New stability criteria for linear systems with interval time-varying delay," *Automatica*, vol. 44, no. 10, pp. 2680–2685, 2008.

[3] D. Yue, E. Tian, Y. Zhang, and C. Peng, "Delay-distribution-dependent robust stability of uncertain systems with time-varying delay," *International Journal of Robust and Nonlinear Control*, vol. 19, no. 4, pp. 377–393, 2009.

[4] H. Y. Shao, "New delay-dependent stability criteria for systems with interval delay," *Automatica*, vol. 45, no. 3, pp. 744–749, 2009.

[5] H. Shao and Q. L. Han, "New stability criteria for linear discrete-time systems with interval-like time-varying delays," *IEEE Transactions on Automatic Control*, vol. 56, no. 3, pp. 619–625, 2011.

[6] B. Song, J. H. Park, Z. G. Wu, and X. Li, "New results on delay-dependent stability analysis and stabilization for stochastic time-delay systems," *International Journal of Robust and Nonlinear Control*, vol. 24, no. 16, pp. 2546–2559, 2014.

[7] J. Xia, C. Sun, X. Teng, and H. Zhang, "Delay-segment-dependent robust stability for uncertain discrete stochastic Markovian jumping systems with interval time delay," *International Journal of Systems Science*, vol. 45, no. 3, pp. 271–282, 2014.

[8] S. Xu, J. Lam, B. Zhang, and Y. Zou, "A new result on the delay-dependent stability of discrete systems with time-varying delays," *International Journal of Robust and Nonlinear Control*, vol. 24, no. 16, pp. 2512–2521, 2014.

[9] G. Wang, Q. Zhang, and C. Yang, "Exponential stability of stochastic singular delay systems with general Markovian switchings," *International Journal of Robust and Nonlinear Control*, vol. 25, no. 17, pp. 3478–3494, 2015.

[10] L. Zhang, Y. Shi, T. Chen, and B. Huang, "A new method for stabilization of networked control systems with random delays," *IEEE Transactions on Automatic Control*, vol. 50, no. 8, pp. 1177–1181, 2005.

[11] H. Gao, T. Chen, and J. Lam, "A new delay system approach to network-based control," *Automatica*, vol. 44, no. 1, pp. 39–52, 2008.

[12] X. Jiang, Q.-L. Han, S. Liu, and A. Xue, "A new H_∞ stabilization criterion for networked control systems," *IEEE Transactions on Automatic Control*, vol. 53, no. 4, pp. 1025–1032, 2008.

[13] D. Huang and S. K. Nguang, "State feedback control of uncertain networked control systems with random time delays," *IEEE Transactions on Automatic Control*, vol. 53, no. 3, pp. 829–834, 2008.

[14] M. Liu, D. W. Ho, and Y. Niu, "Stabilization of Markovian jump linear system over networks with random communication delay," *Automatica*, vol. 45, no. 2, pp. 416–421, 2009.

[15] D. Yue, E. Tian, Z. Wang, and J. Lam, "Stabilization of systems with probabilistic interval input delays and its applications to networked control systems," *IEEE Transactions on Systems, Man, and Cybernetics Part A:Systems and Humans*, vol. 39, no. 4, pp. 939–945, 2009.

[16] S. Ma and C. Zhang, "Robust stability and H_∞ control for uncertain discrete Markovian jump singular systems with mode-dependent time-delay," *International Journal of Robust and Nonlinear Control*, vol. 19, no. 9, pp. 965–985, 2009.

[17] G. L. Wang and Q. L. Zhang, "Stabilization of linear systems with time-varying delays," *International Journal of Robust and Nonlinear Control*, vol. 23, no. 14, pp. 1581–1596, 2013.

[18] Z. Zhang, Z. Zhang, H. Zhang, B. Zheng, and H. R. Karimi, "Finite-time stability analysis and stabilization for linear discrete-time system with time-varying delay," *Journal of the Franklin Institute*, vol. 351, no. 6, pp. 3457–3476, 2014.

[19] M. S. Mahmoud and A. A. Saif, "Dissipativity analysis and design for uncertain Markovian jump systems with time-varying delays," *Applied Mathematics and Computation*, vol. 219, no. 18, pp. 9681–9695, 2013.

[20] G. Wang, Q. Zhang, and C. Yang, "Dissipative control for singular Markovian jump systems with time delay," *Optimal Control Applications & Methods*, vol. 33, no. 4, pp. 415–432, 2012.

[21] B. Zhu, Q. Zhang, and C. Chang, "Delay-dependent dissipative control for a class of non-linear system via Takagi-Sugeno fuzzy descriptor model with time delay," *IET Control Theory & Applications*, vol. 8, no. 7, pp. 451–461, 2014.

[22] Z. Wu, P. Shi, Z. Shu, H. Su, and R. Lu, "Passivity-based asynchronous control for Markov jump systems," *IEEE Transactions on Automatic Control*, pp. 1–1, 2016.

[23] J. Zhang, J. Lam, and Y. Xia, "Output feedback delay compensation control for networked control systems with random delays," *Information Sciences*, vol. 265, pp. 154–166, 2014.

[24] L. Liu, X. D. Zhao, B. Niu, H.-Q. Wang, and X.-J. Xie, "Global output-feedback stabilisation of switched stochastic non-linear time-delay systems under arbitrary switchings," *IET Control Theory and Applications*, vol. 9, no. 2, pp. 283–292, 2015.

[25] H. Shen, S. Xu, X. Song, and Y. Chu, "Delay-dependent H_∞ filtering for stochastic systems with Markovian switching and mixed mode-dependent delays," *Nonlinear Analysis: Hybrid Systems*, vol. 4, no. 1, pp. 122–133, 2010.

[26] H. N. Wu, J. W. Wang, and P. Shi, "A delay decomposition approach to L_2–L_∞ filter design for stochastic systems with time-varying delay," *Automatica*, vol. 47, no. 7, pp. 1482–1488, 2011.

[27] G. Wang and C. Su, "Delay-distribution-dependent H_∞ filtering for linear systems with stochastic time-varying delays," *Journal of the Franklin Institute*, vol. 350, no. 2, pp. 358–377, 2013.

[28] C. Y. Han, H. S. Zhang, and M. Y. Fu, "Optimal filtering for networked systems with Markovian communication delays," *Automatica*, vol. 49, no. 10, pp. 3097–3104, 2013.

[29] M. S. Mahmoud and Z. Xiang, "Quantized H_∞ filter design of interconnected continuous-time delay systems," *Optimal Control Applications & Methods*, vol. 35, no. 1, pp. 41–60, 2014.

[30] Z. G. Wu, P. Shi, H. Su, and J. Chu, "A delay decomposition approach to L_2–L_∞ filter design for stochastic systems with time-varying delay," *Automatica*, vol. 50, no. 1, pp. 180–186, 2014.

[31] G. Wang, H. Bo, and Q. Zhang, "H_∞ filtering for time-delayed singular Markovian jump systems with time-varying switching: a quantized method," *Signal Processing*, vol. 109, pp. 14–24, 2015.

[32] G. Wang and S. Xu, "Robust H_∞ filtering for singular time-delayed systems with uncertain Markovian switching probabilities," *International Journal of Robust and Nonlinear Control*, vol. 25, no. 3, pp. 376–393, 2015.

[33] Y. Ma and H. Chen, "Reliable finite-time H_∞ filtering for discrete time-delay systems with Markovian jump and randomly occurring nonlinearities," *Applied Mathematics and Computation*, vol. 268, pp. 897–915, 2015.

[34] H. Shen, Z. G. Wu, and J. H. Park, "Reliable mixed passive and H_∞ filtering for semi-Markov jump systems with randomly occurring uncertainties and sensor failures," *International Journal of Robust and Nonlinear Control*, vol. 25, no. 17, pp. 3231–3251, 2015.

[35] H. Gao, Z. Fei, J. Lam, and B. Du, "Further results on exponential estimates of markovian jump systems with mode-dependent time-varying delays," *IEEE Transactions on Automatic Control*, vol. 56, no. 1, pp. 223–229, 2011.

[36] G. Wang and Q. Zhang, "Adaptive state estimation for stochastic delay systems with state-dependent Markovian switching," *IET Control Theory & Applications*, vol. 6, no. 6, pp. 822–828, 2012.

[37] H. Shen, Y. Zhu, L. Zhang, and J. H. Park, "Extended dissipative state estimation for markov jump neural networks with unreliable links," *IEEE Transactions on Neural Networks and Learning Systems*, vol. 28, no. 2, pp. 346–358, 2016.

[38] Z. G. Wu, P. Shi, H. Y. Su, and J. Chu, "Stochastic synchronization of markovian jump neural networks with time-varying delay using sampled-data," *IEEE Transactions on Cybernetics*, vol. 43, no. 6, pp. 1796–1806, 2013.

[39] L. Li, D. W. Ho, and J. Lu, "A unified approach to practical consensus with quantized data and time delay," *IEEE Transactions on Circuits and Systems. I. Regular Papers*, vol. 60, no. 10, pp. 2668–2678, 2013.

[40] H. Shen, J. H. Park, Z. G. Wu, and Z. Zhang, "Finite-time H_∞ synchronization for complex networks with semi-Markov jump topology," *Communications in Nonlinear Science and Numerical Simulation*, vol. 24, no. 1-3, pp. 40–51, 2015.

[41] H. Li, P. Shi, D. Yao, and L. Wu, "Observer-based adaptive sliding mode control for nonlinear Markovian jump systems," *Automatica*, vol. 64, pp. 133–142, 2016.

[42] H. Li, P. Shi, and D. Yao, "Adaptive sliding mode control of markov jump nonlinear systems with actuator faults," *IEEE Transactions on Automatic Control*, 2016.

[43] Y. Zhang, Q. Zhang, T. Tanaka, and X. G. Yan, "Positivity of continuous-time descriptor systems with time delays," *IEEE Transactions on Automatic Control*, vol. 59, no. 11, pp. 3093–3097, 2014.

[44] J. C. R. Bennett, C. Partridge, and N. Shectman, "Packet reordering is not pathological network behavior," *IEEE/ACM Transactions on Networking*, vol. 7, no. 6, pp. 789–798, 1999.

[45] Y. L. Wang and G. H. Yang, "H_∞ control of networked control systems with time delay and packet disordering," *IET Control Theory & Applications*, vol. 1, no. 5, pp. 1344–1354, 2007.

[46] J. N. Li, Q. L. Zhang, and M. Cai, "Modelling and robust stability of networked control systems with packet reordering and long delay," *International Journal of Control*, vol. 82, no. 10, pp. 1773–1785, 2009.

[47] J. N. Li, Q. L. Zhang, Y. L. Wang, and M. Cai, "H_∞ control of networked control systems with packet disordering," *IET Control Theory & Applications*, vol. 3, no. 11, pp. 1463–1475, 2009.

[48] A. D. Liu, L. Yu, and W.-A. Zhang, "H_∞ control for network-based systems with time-varying delay and packet disordering," *Journal of the Franklin Institute*, vol. 348, no. 5, pp. 917–932, 2011.

[49] A. Liu, W. Zhang, L. Yu, S. Liu, and M. Z. Chen, "New results on stabilization of networked control systems with packet disordering," *Automatica*, vol. 52, pp. 255–259, 2015.

[50] J. Xiong and J. Lam, "Stabilization of discrete-time Markovian jump linear systems via time-delayed controllers," *Automatica*, vol. 42, no. 5, pp. 747–753, 2006.